PATHOGENICITY OF ISOLATES OF *BEAUVERIA BASSIANA* TO THE BANANA WEEVIL *COSMOPOLITES SORDIDUS*

C. A. Omukoko[1,2], K. N. Maniania[2], J. M Wesonga[3], E. M. Kahangi[4] and L. S Wamocho[5]

[1,3,4,5]Department of Horticulture Jomo Kenyatta University of Agriculture and Technology, Kenya

[2]International Centre of Insect Physiology and Ecology (ICIPE), Kenya

E-mail:

Abstract

Bananas constitute a major staple food crop for millions of people in developing countries, providing energy as well as important vitamins and minerals. It's production in Kenya has been on the decline due to, among other factors, pests and disease of which the banana weevil, *Cosmopolites sordidus,* is the most important. The aim of this study was to screen ten isolates of the entomopathogenic fungus *Beauveria bassiana* for pathogencity against *C.sordidus.* Twenty weevils were inoculated with the fungus by dipping them into a fungal suspension containing $1x10^8$ conidia ml^{-1} for 11 seconds. The suspension was then drained out and pieces of banana corm introduced as food for the weevils. All the ten isolates of *B. bassiana* tested were found to be pathogenic to adult banana weevil causing mortalities of between 20-50% by 40 days post exposure. ICIPE 273 was the most pathogenic isolate killing 50% of adults, followed by M313 at 36% and M207 at 30%. Isolates KE300, M221, ICIPE 50, M573, M618, M470 and ICIPE 279 killed less than 30% of the weevils, ICIPE 279 was the least pathogenic isolate to the adult *C. sordidus* killing 6% of the inoculated weevils. The dead weevils were incubated in sterile moist filter papers in Petri dishes for two weeks and fungal mycelia was observed on the surface of the weevils starting from intersegmental junctions. Mortality caused by fungus was confirmed by microscopic examination. Since isolate ICIPE 273 has reasonable pathogenicity to *C. sordidus* and field/screenhouse studies are recommended to validate the findings.

Key words: biocontrol, entomopathogens, pest management

1.0 Introduction

Banana (*Musa sapientum, M. acuminata*) constitutes a major staple food crop for millions of people in developing countries providing energy as well as important vitamins and minerals. Majority of producers are small-scale farmers growing the crop either for home consumption or for local markets as a source of income for rural people (Karamura, 1998). This crop is also considered a key component of sustainable agricultural systems in densely populated rainfall zones. On steep slopes, bananas reduce soil erosion and are a principal source of mulch for maintaining and improving soil fertility (Akello, 2008).

Banana production in Kenya has been declining due to environmental stresses, declining soil fertility, poor crop management as well as lack of clean planting material (Seshu *et al.,* 1998).Pest and disease pressures have also increased, reducing the life span of banana orchards (ISAAA, 1996). Important banana diseases include black Sigatoka caused by the fungus *Mycosphaerella fijiensis* and fusarium wilt caused by *Fusarium oxysporum* f.sp. *cubense* (Seshu *et al.,* 1998).

Out of about 200 insect pests reported to attack banana, the most important is the banana weevil, *Cosmopolites sordidus* (Germar) (Godonou *et al.,* 2000). The other pests of economic importance are the parasitic nematodes (*Radopholus similis, Pratylenchus spp. and Helicotylenchus multicinctus*). Both the weevil and nematode infestation interfere with nutrient uptake and transport resulting in slow growth, reduced fruit filling and susceptibility to wind lodging hence the need to device control measures for sustainable banana production (Gold *et al.,* 2003).

The yield losses associated with the banana weevil range from 40% to 100% in severe infestations (Seshu *et al.,* 1998). Banana weevil attack in newly-planted banana stands can lead to poor crop establishment. In established fields, weevil damage can result in plant loss due to snapping and toppling, lower bunch weight, mat die-out and shortened plantation life (Gold *et al.,* 2003).

Chemical pesticides, have been used extensively for the control of *C. sordidus* but environmental pollution and widespread resistance to these pesticides have developed in most parts of the world (Allard *et al.,*1991).The most commonly used cultural control methods include the use of clean planting material, crop hygiene, agronomic practices to improve plant vigor and tolerance to weevil attack. Application of these methods have labour requirements and adoption by resource poor subsistence farmers is often limited (Nankinga *et al.,* 1998).

There is need therefore to develop safer and cheaper control alternatives that can be used to complement existing control methods (Nankinga *et al.,* 1998). Entomopathogenic fungi have been used successfully to control various agricultural pests (Kaaya and Hassan 2000), including banana weevils (Gold *et al*.,

2003). *Beauveria bassiana* has for instance been researched extensively as an alternative means for controlling the banana weevil (Nankinga *et al*., 1994). Isolates often perform well in short -term laboratory bioassays causing high mortality of >90.0% within 2 weeks but field applications do not perform well (Kaaya *et al*., 1993; Nankinga *et al*., 1994, 1999;Godonou *et al*., 2000).

Laboratory pathogenicity tests using different strains of *Beauveria bassiana* in Uganda, (Nankinga *et al.,* 1994) and in West Africa (Godonou *et al.,* 2000) produced 50%-100% mortality in banana weevil adults in 14 days (Magara *et al.,* 2004). The aim of this study was therefore to assess the pathogenicity of ten *Beauveria bassiana* isolates to the banana weevil, *C. sordidus.*

2.0 Materials and Methods

2.1 Trapping of Banana Weevils

Adult banana weevils were obtained from naturally infested banana plants in Kenya Agriculture Research Institute banana farm in Mwea, Central Kenya. Split pseudostem (approximately 45cm) traps were used to attract and capture adults of banana weevil in the field that was infested with weevils. The two half cylinders were placed flat (cut) surface down, on either side of the plant. Pseudostem used for the traps were obtained from freshly harvested plants. Traps were left in place for three days before examination of weevils. Weevils were collected in 10litre plastic buckets. The weevils were then transferred in plastic buckets at room temperature (27 ± 2^{o}C) in the laboratory for one week before being used in the experiments. The covers of the containers were perforated for ventilation. Banana suckers of susceptible variety were cut into small pieces and corm tissue placed in the containers and used as food for the weevils.

2.2 Fungal Isolates Used in the Study

The following ten isolates of *Beauveria bassiana* were used in the bioassays: ICIPE 273, ICIPE 279, ICIPE 50, M470, KE300, M313, M207, M573, M618 and M221. They were obtained from the International Centre for Insect Physiology and Ecology, (*icipe*'s) Arthropod Germplasm Centre, Duduville, Nairobi, Kenya. The original cultures were stored at –85^{o}C in 10% sterile glycerol. Details of the date of isolation, host and site where the isolates were sampled are presented in Table 1.

Table 1: Date of isolation, substrate and sampling site for Beauveria bassiana isolates used in the study

Isolates	Year of Isolation	Host/Substrate	Locality /Country
ICIPE 273	2006	Soil	Mbita/Kenya
ICIPE 279	2005	Coleopteran larvae	Kericho/Kenya
M573	2005	Soil	Mauritius
KE 300	2007	Hymenoptera	Taita hills/Kenya
M221	2005	Soil	Mauritius
M618	2005	Soil	Mauritius
M313	2005	Soil	Mauritius
M207	2005	Soil	Mauritius
ICIPE 50	1996	*Rhipicephalus appendiculatus*	Rusinga island/Kenya
M470	2005	Soil	Mauritius

2.3 Culturing the *Beauveria bassiana*

The fungal isolates had been stored at –85^{o}C in 10% sterile glycerol in the germplasm at *icipe*.They were then transferred to a deep freezer at -4 ^{o}C for 12 hours before being placed in a refrigerator at 5- 10 ^{o}C for 4 hours. Sabouraud Dextrose Agar (SDA) was prepared using the standard procedure, antibiotic chloramphenical added and dispensed into 90 mm Petri dishes and left to solidify. The fungal isolates were then cultured on Sabouraud Dextrose Agar (SDA) for three weeks for sporulation in an incubator at 26°C and 70 % relative humidity for 21 days to allow for sporulation to take place (Inglis *et al.,* 1996).

2.4 Inoculum Preparation

Conidia were gently scrapped from Petri dishes and suspended in sterile 10 ml of 0.01% Tween-20. The suspension was then transferred with a sterile pasteur pipette into 20 ml sterile universal bottles with glass beads. For counting the spores a dilution of x100 was prepared by removing 0.1ml using a pasteur pipette from 10 ml sterile distilled water with Tween-20.0.1 ml was picked from the stock solution and added into the diluent. Vortexing was done for three minutes. Conidial density for each strain was then estimated by placing 0.1 ml on the improved Neubauer haemocytometer and counting the spores. For a concentration of 1 x 10^{8} the concentration formula was used. The spores counted from x100 dilution were multiplied by a constant 2.5 x 10^{5} and x 100. This gives the spores in the standard 1 x 10^{8}. From the standard concentration C_1V_1 and C_2V_2 the number of spores needed for each isolate were then calculated.

2.5 Spore Germination Test

Sabouraud Dextrose Agar was prepared as described above and dispensed into 90 mm diameter petri dishes. A conidial suspension with a concentration of $3x10^6$ conidia ml^{-1} was prepared. The viability of conidia was determined by spread plating 0.1 ml of conidial suspension *B. bassiana* on SDA plates using a sterile glass rod. For each of the ten isolates, three 90 mm Petri dishes were prepared and incubated at 27 ± 2 °C for 16 hours. The culture was then fixed using a few drops of lactophenol cotton blue, cover slips were placed over four sections of the Petri dish with germinated spores. Conidial germination was assessed by counting a total of 100 spores, i.e the number of conidia that germinated plus those that had not germinated in four different fields under a dissecting microscope. Conidial germination was characterized by germ tube development and these were categorized as viable conidia while the non-germinated conidia that lacked the germ tube were categorized as non-viable. The germination test is important since it indicates which isolates are viable and therefore can be used in the experiment. Percentage conidial germination was determined by counting 100 spores for each plate. Four replicates were used for each plate, the percentage germination was then calculated as: (viable conidia/total conidia) x100

2.6 Inoculation of Weevils with *Beauveria bassiana*

Weevils were inoculated by dipping them into 20 ml fungal suspension with a conidia concentration of 10^8 conidia ml^{-1} for 11 seconds. The suspension was then drained off and weevils were transferred to plastic containers. Banana corms were then placed in the plastic containers as food for the weevils and placed in the laboratory in a dark room. Control weevils used as a check were dipped in sterile distilled water containing 0.01% Tween 20. Mortality of the weevils was recorded every 3days for 40 days. The experiment consisted of five replicates for ICIPE 279, M573, ICIPE 273 and KE300, and four replicates for ICIPE 50, M470, M207, M618, M221 and M313.

Figure 1: Banana weevils infected with Beauveria bassiana and introduced into plastic containers with banana corm.

To assess fungus induced mortality, dead weevils were surface-sterilized in 2% sodium hypochlorite, 70% alcohol and rinsed twice with sterilized water for 15 seconds before placing them in clean petri dishes with moist sterile filter papers. Dead insects were monitored for fungal growth for two weeks and observations recorded. Only dead insects with fungal growth were considered to have been killed by the fungus.

2.7 Statistical Analysis

All data for mortality was analysed with analysis of variance using the PROC GLM of SAS statistical software and the treatment means were separated using Student-Newman-Keuls (SNK) (SAS version 9.1).

3.0 Results

3.1 Conidial Germination Experiment

In germination tests 81.2-92.7% of spores germinated, for all *B. bassiana* isolates 16 h after exposure on SDA media. There was no significant difference (P=0.37) in percentage conidial germination among the isolates. However there were slight differences among the isolates in germination M 313 and ICIPE 273 gave the best germination of spores (92 %), followed by M470, M207, ICIPE 50 (87 % - 89 %).The rest ICIPE 279, M573, KE 300, M 221 and M618 had germination percent that ranged between (81.3 %-86.6 %).These results are shown in Table 2.

Table 2: Beauveria bassiana isolates used in the study and their % germination SDA

Isolates	% Germination ± SE
ICIPE 273	92.2 ± 3.2
ICIPE 279	86.8 ± 4.5
M573	85.4 ± 3.7
KE 300	86.6 ± 3.5
M221	82.3 ± 3.7
M618	81.3 ± 3.5
M313	92.7 ± 2.1
M207	88.0 ± 2.6
ICIPE 50	87.3 ± 2.6
M470	89.0 ± 2.4

3.2 Pathogenicity Test

All the ten isolates of *Beauveria bassiana* were pathogenic to the adult *Cosmopolites sordidus,* causing mortalities varying from 20-50% by 40 days post-exposure . ICIPE 273 killed 50% of adults followed by M313 36% and M207 30% (Figure 2). The rest KE 300, M 221, ICIPE 50, M573, M 618, M 470 and ICIPE 279

killed < 30% of the inoculated weevils. Isolate ICIPE 279 was the least pathogenic to *C. sordidus* causing only 6% mortality.

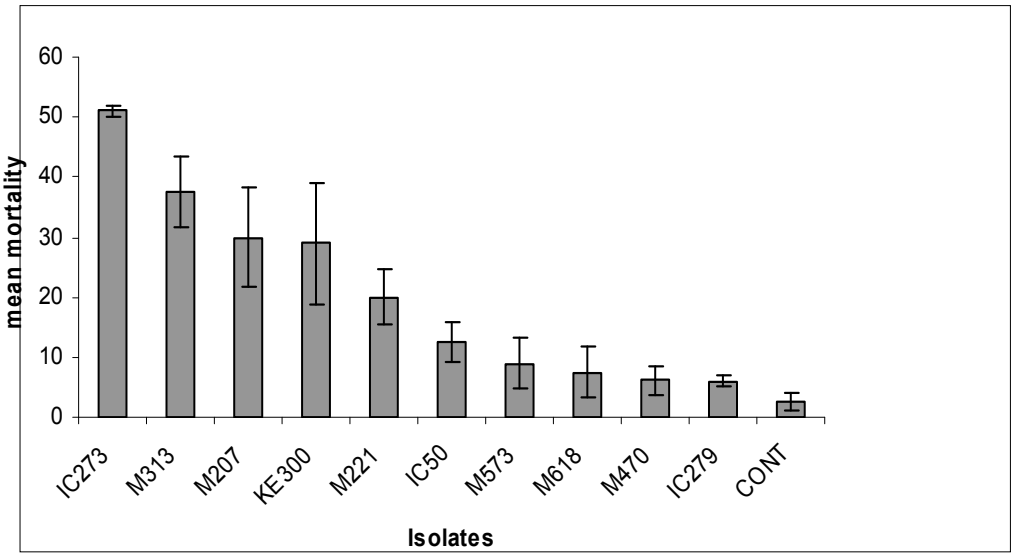

Figure 2: Mortalities in adult weevils inoculated with 10 isolates of Beauveria bassiana 40 days post exposure.

Incubation of the dead weevils in humidified chambers resulted in development of mycelia on the surface of the cadaver, starting from the intersegmental junctions of the body and legs (Figure 2). No fungi grew on dead weevils in the controls since they died due to other causes apart from the fungus.

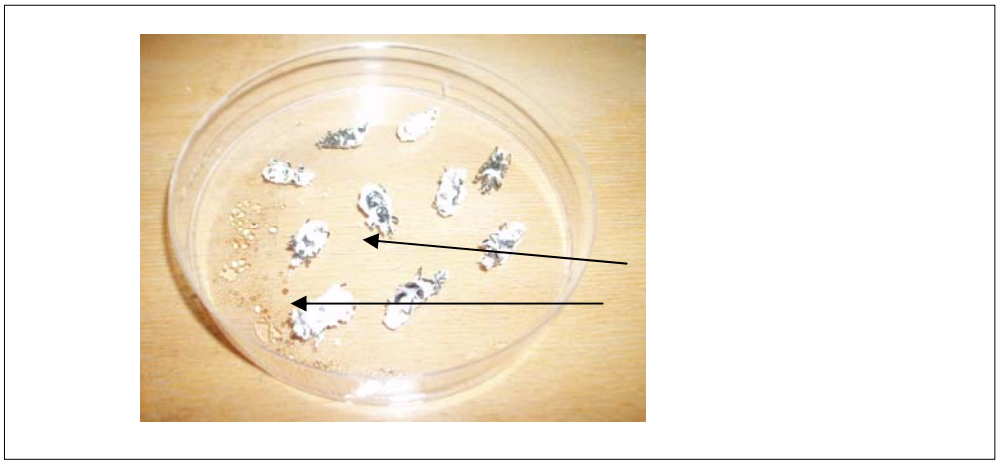

Plate 1: Adult C. sordidus infected with B. bassiana. Notice fungal growth at intersegmental junctions (arrows)

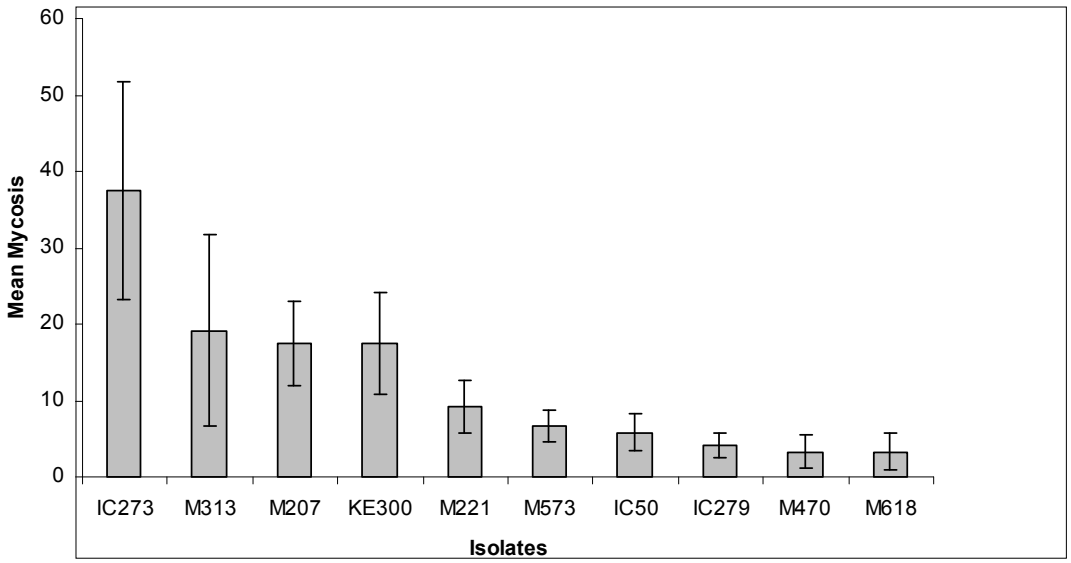

Figure 3: Percent Mean mycosis of adult banana weevils infected with different isolates of B. bassiana

ICIPE 273 had over 38% mycosis on the dead insects, while M313, M207, KE 300, had between 18% - 19% mycosis. All the other isolates had mycosis that ranged between 5 % -10% mycosis. No fungi grew on dead weevils in the controls.

4.0 Discussion

Laboratory pathogenicity studies indicate that *B. bassiana* isolate ICIPE 273 isolated from soil in Mbita, Kenya gave better results among the tested isolates since it gave 50% mortality when a standard concentration of 1 x 10^8 for 11 seconds was used. This is acceptable for entomopathogens when used as biological control agents since reduction of the pest population by 50% and above is usually targetted. The level of effectiveness obtained in our study compares favourably with those of Nankinga *et al.* (1994), Pena *et al.* (1991) and Godonou *et al.* (2000). Isolates from Mauritius M313 had mortality of 36% while M207 had 30% which was comparatively low. For all the tested isolates, dead insects kept in humidified chambers developed surface mycelia. Mortality caused by *B. bassiana* was confirmed by microscopic examination of the dead banana weevils.

5.0 Conclusions

All isolates of *Beauveria bassiana* tested were pathogenic to banana weevils causing mortalities of 20% to 50% with the best isolates being ICIPE 273, M313 and M207.The rest KE 300, M221, ICIPE 50, M470, M618, M573 and ICIPE 279 killed less than 20% of the banana weevils with ICIPE 279 being the least pathogenic to the adult banana weevil *Cosmopolites sordidus*.

6.0 Recommendations

ICIPE 273 has reasonable pathogenicity to *C.sordidus* and field/screenhouse studies are recommended to validate the findings.

Acknowledgements

The authors would like to express their sincere gratitude to Ms Elizabeth Ouna for technical assistance, Mr.Njinjo and Mr. Ngare from KARI-Mwea for providing the banana weevils that were used in this study.

References

Allard B. G., Nankinga C. and Latigo, O.M. (1991). The potential of indigenous Fungal pathogens as a component of Integrated management of banana weevil in Uganda **In**: G. S.Gold and B.Gemill (eds) Biological and integrated control of highland banana and plantain, pests and diseases of a research coordination meeting. Cotonou Benin 12-14 November 1991.

Akello J. (2008). *Beauveria bassiana* Balsamo (Vuillemin) as an endophyte to control the Banana weevil**,** *Cosmopolites sordidus* (Germar) MSc Thesis ,Department of Crop science, Faculty of Agriculture , Makerere University , Uganda, pp 123.

Godonou I., Green K. R., Oduro K. A., Lomer C. J. and Afreh-Nuamah (2000). Field Evaluation of Selected Formulations of *Beauveria Bassiana* for the Management of Banana Weevil(*Cosmopolites sordidus*) On Plantain(Musa spp., AAB Group) Biocontrol Science and Technology, **10,** pp 779-788.

Gold C. S., Nankinga C., Niere B. and Godonou I. (2003). IPM of banana weevil in Africa with emphasis on microbial control. **In:** Neuenschwander, P., Borgemeister, C. and Langewaid, J. (eds) Biological Control in IPM Systems in Africa. CAB International, Wallingford, pp 243-257.

Kaaya G. P. and Hassan S. (2000). Entomogenous fungi as promising biopesticides for tick control. Experimental and Applied Acarology**, 24,** pp 913–926.

Kaaya G. P, Seshu-Reddy K. V., Kokwaro E. D. and Munyinyi D. M. (1993). Pathogenicity of *Beauveria bassiana,Metarhizium anisopliae* and *Serratia marcescens* to banana Weevil *Cosmopolites sordidus* Biocontrol science and Technology journal, **3**, pp 177-187.

Karamura E. B. (1998). Importance of Banana in Sub-Saharan Africa pp 5-11
In*:* Gold C.S., Karamura E. B. and Sikora R. A. (eds). Mobilizing IPM for sustainable banana production in Africa, Proceedings of a workshop on banana IPM held in Nelspruit, South Africa, 23-28, November, 1998, INIBAP, Montpellier, France. Available: www.inibap.org. Accessed: 4/05/06.

Inglis G.D., Johnson D.L. and Goettel M.S.(1996). Bioassay Method Used to test the efficacy of *Beauveria bassiana* against Grasshoppers. Journal of Invertebrate Pathology, **67**, pp 312-315.

ISAAA (1996). International Service for the Acquisition of Agri-biotech Applications (ISAAA) Annual Report. 1996. Available: http:// www.isaaa.org.Accessed: 4/05/06

Magara C., Nankinga C., Gold C., Kyamanywa S., Ragama S., Tushemereirwe W., Moore D. and Gowen S. (2004). Efficacy of *Beauveria bassiana* substrates and formulations for the control of banana weevil.Uganda Journal of Agricultural Sciences, **9,** pp 908-913.

Nankinga C. M., Latigo-Ogenga W. M., Allard B.G. and Ogwang J. (1994). Potential of *Beauveria bassiana* for control of banana weevils in Uganda.African crop science conference proceedings, **1**, pp 300-302.

Nankinga C. M., Moore D., Bridge P. and Gowen S. (1998). Recent advances in microbial control of banana weevil pp 73- 83 **In:** Frison, Gold, C. S., Karamura, E. B. and Sikora, R. H. (Eds.), Mobilizing IPM for sustainable banana production in Africa. INIBAP, Montpellier, France.

Nankinga C. M. (1999). Characterization of Entomopathogenic Fungi and Evaluation of Delivery Systems of *Beauvaria bassiana* for the Biological Control of the Banana Weevil, *Cosmopolites sordidus*. Ph.D. Thesis, University of Reading, London, UK. pp 276.

Pena J. E., Duncan R. and Martin R. (1991). Biological control of *Cosmopolites sordidus* in Florida pp 124-139 **In:** G. S. Gold and B. Gemill (eds) Biological and integrated control of highland banana and plantain, pests and diseases of a research coordination meeting. Cotonou Benin 12-14 November 1991.

Seshu R. V., Ngode L., Ssenyonga J. W., Wabule M., Onyango M., Adede T. O. and Ngoze S. (1998). Management of pests and diseases of banana in Kenya. **In**: Gold C. S., Karamura, E. B. and Sikora, R. A. ***(eds)***. Mobilizing IPM for sustainable banana production in Africa, Proceedings of a workshop on banana IPM held in Nelspruit, South Africa, 23-28, November 1998 INIBAP, Montpellier, France, pp 215. Available: www.inibap.org Accessed: 13/05/06.

Appendix

Pathogenicity mortality

Source	**DF**	**Sum of Squares**	**Mean Square**	**F Value**	**Pr > F**
Treatment	10	11242.91	1124.29	9.46	<.0001
Error	37	4398.75	118.88		
Corrected Total	47	15641.66			

Pathogenicity mycoses

Source	**DF**	**Sum of Squares**	**Mean Square**	**F Value**	**Pr > F**
Treatment	9	6278.75	697.63	2.47	0.020
Error	50	14145.83	282.91		
Corrected Total	59	20424.58			

EFFECTS OF SUBSTITUTING SKIMMED MILK POWDER WITH MODIFIED STARCH IN YOGHURT PRODUCTION

E. M. Okoth[1], P. K. Kinyanjui[2], J. N. Kinyuru[3] and F. O. Juma[4]
[1, 2, 3] Department of Food Science and Technology, Jomo Kenyatta University of Agriculture and Technology, Kenya
[4]Corn Products International, Kenya
E-mail:

Abstract
Rheological properties of yoghurt are known to be influenced by several factors during processing including the milk composition, additives, the type of culture (ropy or non ropy), heat treatment and mechanical processes it undergoes after fermentation. The objective of this study was to determine the most appropriate levels of modified starch that could be added in the yoghurt without noticeably altering the keeping quality and consumer acceptability of the yoghurt. A stirred type of yoghurt was developed using modified corn starch as a stabiliser to variably replace skimmed milk powder (partially or in totally) while maintaining the same quality and consumer acceptability on the yoghurt product. Different formulations were made and their quality characteristics studied using the 3% skimmed milk powder sample as the control. The results showed that the modified corn starch addition did not affect the gelation process, texture, fermentation time and the desired pH end point. Two sample formulations were identified as the most comparable to the control in terms of viscosity, taste, mouth-feel and general acceptability. These were the 0.5% modified corn starch alone and 0.5% modified corn starch with 1% skimmed milk powder. These reduced the cost of production per litre by 22% and 13% respectively. The samples were stable for three consecutive weeks in all the desirable yoghurt quality parameters tested including consumer acceptability. In conclusion, the application of modified starch at the level of 0.4% was found to have the most significant reduction in cost of production while having the least effect on the keeping quality and consumer acceptability of the yoghurt.

Key words: Yoghurt, starch, quality, acceptability, cost

1.0 Introduction

Yoghurt is a milk product made by a fermentation process of fresh milk using lactic acid starter culture containing *Streptococcus thermophillus* and *Lactobacillus delbrukii ssp. bulgaris* to give a pH value of 3.8-4.6 (Tamine, 2002; Michelle *et al.*, 2005). Yoghurt can be regarded as a concentrated dispersion of particles in serum. Its total viscosity is given by the following formula $\eta = \eta_s \times f(\emptyset)$, where η is the total viscosity of the system, η_s is the serum viscosity of the aqueous phase and $f(\emptyset)$ is the function of the particle volume and their interactions in the matrix system (Marie *et al*., 2006). These factors contribute to desirable textural attributes of yoghurt. Rheological properties of yoghurt are known to be influenced by several factors during processing, the milk constituency itself (protein content, additives), the type of culture (ropy or non ropy), heat treatment and mechanical processes it undergoes after fermentation. The mechanical processes include stirring, pumping through pipes and filling which exposes it to shear resulting in a viscosity decrease.

Rheological and stability properties of yoghurt can be modified by fortifying the milk with dairy – based ingredients, non-dairy ingredients or a combination of both prior to heat treatment and acidification (Oh *et al*., 2006). Non-dairy additives like polysaccharides such as starches can be used in yoghurt in conjunction with dairy ingredients or on their own to modify the rheological properties. Yoghurts made from different starches exhibit different rates of viscosity e.g. wheat starch showed highest shear consistency compared to other varieties (Keogh and O'Kennedy, 1998). Changes in the native structures of both milk proteins and starch occur upon heat treatment above their relevant critical temperatures during pasteurization. The heat treatment of milk at temperatures above 70^{o}C results in denaturation of the whey proteins (Anema and McKenna, 1996). These denatured whey proteins can undergo a complex series of aggregation reactions with other denatured whey proteins and with the casein micelles (Anema and Li, 2003). In contrast, starch 'gelatinize' when heated in the presence of water, with the critical temperature dependent on the type of starch.

Starch gelatinisation encompasses disruption of the granular structure, swelling and hydration, and solubilization of starch molecules. Swelling is accompanied by leaching of granule constituents, mostly amylose, and the formation of a three dimensional network in the serum. The swelling that develops in such a mixed system of milk and starch during heat treatment may lead to different rheological characteristics in the final yoghurt gel and consequently in the stirred yoghurt product compared to that made from milk alone (Narpinder *et al*., 2003). The swelling property of starch is depended on its amylopectin content, amylose acts both as a diluent and inhibitor of swelling (Tester and Morrison, 1990). Starch exhibits unique viscosity behavior with change in temperature, concentration and shear rate (Nurul *et al*., 1999). Starch behavior in a system like that one of yoghurt, will also depend on their physical and chemical characteristics, such as mean granule size distribution, amylase/amylopectin ratio and mineral content.

Rheological characteristics of casein gels depend on the number and strength of the bonds between the casein particles, on its structure and the special distribution of the strands making up these particles (Roefs *et al*., 1990). Heating milk at a temperature above 80^{o}C produces gels with elastic modulus (G') of up to 450 Pa. In gels the resistance against deformation is proportional to the number of contact points per cross-section of the network. Cross-linking/bridging of denatured whey proteins in the gel has been postulated to be responsible for this high G' modulus of the network (Lucey *et al*., 1998). Large deformation/destructive tests of yoghurt with and without starch provide information on properties that may be related to the consistency of yoghurt gel during consumption. They also provide information on the resistance of the gel to processes such as stirring, pumping and other shearing operations which are used in production of stirred yoghurt (Ronnegard *et al*., 1993).

Addition of starch, a low cost polysaccharide to milk prior to heat treatment and acidification/fermentation modifies the properties of the acid gels (Decourcelle *et al*., 2004; Keogh and O'Kennedy, 1998; Wong *et al*., 2007). This includes thickening and gelling properties. Starch is the most widely used additive in the food industry for this purpose (Basim *et al*., 2004). It is used in yoghurt to increase its viscosity, improve its mouth-feel, and prevent syneresis. It also helps keep the fruit uniformity mixed in the yoghurt where applicable. Starch granules imbibe water and swell to many times their original size, resulting in increased viscosity of the solution (Gaston *et al*., 2007). It is one of the most frequently used thickening agents in yoghurt production due to its processing ease and low cost when compared to other hydrocolloids (Foss, 2000). Certain additives such as flavourings or fruit concentrates tend to reduce the consistency of the product which, therefore, generally needs some stabilization with products like starch (Ramaswamy and Basak, 1992). In practice, milk-based proteins such as skimmed milk powder, whey proteins and caseins are often used in yoghurt to improve its viscosity and stability. However starch gives a cheaper product than these milk based additives. Further, modified starch is not widely used in Kenya though it is expected to have a better output as compared to the non-modified starch commonly used in yoghurt production by some dairy industry players in Kenya. The aim of this research was therefore to develop a shelf stable, low cost and acceptable modified starch stabilised yoghurt, with a sufficient shelf life and thereby reduce the cost of stirred yoghurt production without compromising quality and customer acceptability.

2.0 Materials and Methods

2.1 Yoghurt Production Raw Materials

The fresh milk of acceptable organoleptic and microbial quality was obtained from a local supplier. Sucrose used was obtained from a local wholesaler in a shop outside Jomo Kenyatta University of Agriculture and Technology. The starter culture used was obtained from Chr Hansen (YFL 811®) through an appointed agent (Pradip Enterprises) in Nairobi, Kenya. This is a thermophillic yoghurt starter culture with *Streptococcus thermophilus* and *Lactobacillus bulgaricus* micro-organisms. The skimmed milk was obtained from New Kenya Cooperative Creameries (NKCC) which contained 3.2% moisture. The modified corn starch used (Snow-Flake R 6704®™), was obtained from Corn Products International (Kenya Office) produced by Corn Products Brazil. The modified starch contained 14% moisture and had a pH of 4.5. The liquid milk used in the yoghurt making was first analysed to ascertain its composition. The same milk was used for all the formulations in a given batch. On average the fresh milk used contained 3.9% butter fat, 0.15% titratable acidity, 12.63% total solids, 8.73% solids non-fat, pH of 6.7 and a density of 1.029%.

2.2. Yoghurt Formulation and Production

Yoghurt was processed as shown in the flow chart below (Figure 1). The milk used in yoghurt production was analysed to ascertain its composition to allow batch to batch comparisons. Yoghurt-milk with 3% skimmed milk powder was used as the reference sample. The modified starch and skimmed milk powder were mixed with sugar prior to addition to the milk as shown in Figure 1. The same batch of skimmed milk powder, sugar and modified corn starch were used to allow comparisons from batch to batch. The milk was heated to 40ºC and the mix added. The samples were then pasteurized at 90^{o}C for 30 minutes in a boiling pan. The milk was then cooled to 45ºC and inoculated with 0.02% thermophilic lactic acid starter culture. It was stirred for about 30 seconds for complete dissolution and equal distribution of the culture granules in the milk. The milk was incubated at 45^{o}C for 5 hours until a firm curd was formed at the top and a pH of 4.1 - 4.4 was obtained. This was then aged at 10ºC overnight to allow for cooling. The curd was broken by swirling 40 times with a hand stirrer to form a smooth homogeneous product. It was then stored under refrigeration at a temperature of 8ºC for further analysis and storage stability tests.

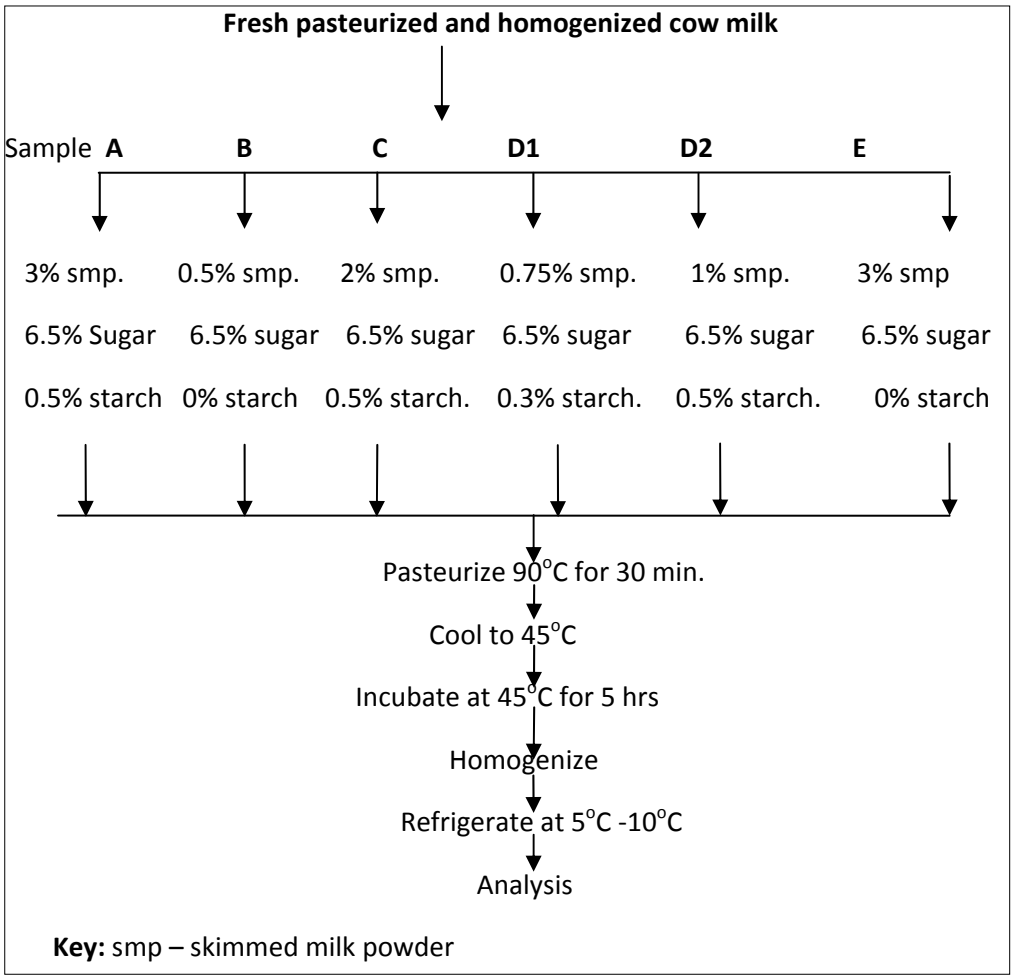

Figure 1: Standard flow chart for yoghurt processing

2.3 Analysis

2.3.1 Visual Observation

The stirred yoghurt was poured on a black plate which had been tilted at angle of 30˚ to allow it to flow (Lucey and Singh, 1998). Observations were made on consistency and body texture, to determine if the addition of starch had any observable effect on these parameters, for example, flaking.

2.3.2 Viscosity

2.3.2.1 Yoghurt Viscosity

The viscosity was measured using an imitation of a modified Ford cup (Posthumus funnel), (Galesloot, 1958) with a diameter of 12.5 cm at the top, diameter of 1.5 cm at the exit opening and a length of 13 cm as shown in Figure 2 below. The measurements were taken at 8°C. To monitor the change of viscosity with shear, 500 ml samples were poured through the funnel twenty times consecutively. The

temperature was maintained at 8°C by keeping the samples under ice bath. The funnel was also dipped in ice water for 2 minutes after every five measurement to maintain this temperature. The viscosity is given by the time taken for a given amount of yoghurt to flow through the funnel in seconds. The longer it takes, the more viscous the yoghurt becomes.

Figure 2: 'Posthumus funnel apparatus'

The viscosity was also measured using Brookfield viscometer model BM type (Keogh and O'Kennedy, 1998). Three readings from each sample were taken and an average recorded. The readings were taken at 10ºC, the temperature at which yoghurt is consumed. The speed of the spindle used was adjusted according to the thickness of each sample. In this case, the specification combination used was speed 12 (revolutions per second) and spindle number 4. To get the final viscosity in centipoises, a factor of 500 was used to multiply the figure obtained.

2.3.3 Sensory Evaluation

The six samples coded A, B, C, D_1, D_2 and E were presented to a 15-member consumer panel drawn from the staff and students community of the Food Science Department of Jomo Kenyatta University. The yoghurt samples were tasted and rated using a 7 point hedonic scale; 1-dislike it very much to 7-like it very much. The parameters scored were viscosity, mouth-feel, taste, general perception and acceptability (Keogh and O'Kennedy, 1998)

2.3.4 Storage Stability Tests

The samples were kept under refrigeration (8°C). Viscosity, pH, visual appearance and organoleptic changes were monitored for a period of three weeks (Keogh and O'Kennedy, 1998).

2.3.4 Yoghurt Costing

The costing of all yoghurt samples was done. This was to determine the cost implication of substituting skimmed milk powder with starch. However, only the direct materials used were considered and the other indirect cost like labour, power and overheads were left out since they were assumed to be uniform for all the samples, hence not included in the costing. The cost of the milk used was Ksh.

40.00 per litre, the skimmed powder was Ksh. 500.00 per kilogram, the sugar was Ksh. 90.00 per kilogram and the modified starch was Ksh 250.00 per kilogram.

3.0 Results

3.1 General

3.1.1. Acidification

The pH obtained for all the samples at the end of the fermentation/incubation period of 5 hours ranged between 4.1 and 4.3 as shown in Table 1. The final pH attained by the different yoghurt formulations was almost similar. The fermentation times were also not affected by the addition of modified starch as they had all attained the requisite acidity level after being subjected to similar fermentation times.

3.1.2 Visual Appearance

The texture and grain of all the samples obtained were found to be smooth and fine respectively. This can be seen in the pictorial image (Figure 3). These were acceptable visual quality parameters. On the basis of texture and grain, one could not differentiate the yoghurt samples which contained starch from those which did not contain any starch. This showed that the modified starch was completely soluble in the milk, thus giving smooth, viscous yoghurt. The samples containing starch gave the same visual appearance of consistency as those that had milk powder.

3.2 Viscosity

3.2.1 Viscosity by Brookfield Viscometer

Samples A (3% skimmed milk powder plus 0.5% modified starch) and C (2% milk powder plus 0.5% modified starch) were most viscous/thick, registering a viscosity of 8080η and 7600η respectively as shown in Figure 4. These were significantly different from the control sample E (3% skimmed milk powder) which had a viscosity value of 4750η. Sample B had a viscosity of 5000η which was comparable to the Control sample E (4750η)

3.2.2 Viscosity by Posthumus Funnel Method

Sample A registered most time which is an indication that this was the most viscous (thick) sample followed by sample C as shown in Figure 5. It was found to support the results obtained by using the Brookfield viscometer. The mean time taken to run samples B (15.5 sec) and D_2 (15.1 sec) were comparable (not significantly different) from the control sample E (16.3 sec). Sample B had 0.5% corn starch and no skimmed milk powder, while sample D_2 had 0.5% corn starch and only 1% skimmed milk powder. Sample D_1 registered the least mean time in seconds. This is also an indication that the viscosity was the lowest of all. In this sample, 0.75 % skimmed milk powder and 0.3% starch were used.

3.2.3 Effect Of Handling on Viscosity Using the Posthumous Cup Method

During handling and packing of yoghurt, there is a decrease in viscosity which can be simulated by passing the yoghurt through the posthumous cup twenty times to determine the effect of handling on the yoghurts viscosity where the results in Figure 6 were obtained. Sample A had the most viscous / thick product with a rum time of 45 mean seconds. This was in agreement with the results obtained on determining the viscosity by Brookfield viscometer. It was followed by sample E (control sample) with a run time of 33 seconds. Samples B, C, D_2, had a similar run times. However sample D_2 had a similar run time from the 7^{th} run to the 20^{th} run with that of sample E (control). This indicates that sample D_2 was most comparable in retained viscosity to the control (E). This also agrees with the results obtained in the determination of viscosity by the Brookfield viscometer and by the use of the Posthumus cup and also to the results of Lucey and Singh (1998). However, sample B was still cheaper than C since it had corn starch only as a stabilizer while sample C had both 0.5% starch and 1% skimmed milk Powder.

3.3 Sensory Evaluation

Sample E which was the yoghurt made with skimmed milk powder alone was ranked the highest on all the parameters as shown in Figure 7. It was not significantly different from sample D_2 on all the parameters tested ($p \leq 0.05$). It was not significantly different from C on viscosity/consistence ($p \leq 0.05$), not significantly different from sample A on mouth-feel and taste ($p \leq 0.05$). Sample D_1 scored the least on mouth-feel and taste. This is because it was least viscous. It had low starch (0.3%) and skimmed milk powder 0.7%.

3.4 Keeping Quality

After storing the samples for three weeks, all the products were found to be smooth and homogeneous on pouring. There was no wheying off or syneresis. There were no off flavours detected, thus fit for consumption**.** The results (Figure 8) exhibited different patterns on viscosity change on storage for the different samples. Samples A, B, C and E showed a decrease in their viscosity from week 1 to week 2 and then an increased past week 2 onwards. This shows stabilization and aging of starch on long storage which lead to increase of viscosity after two weeks of storage. For D_1, its viscosity increased from week 1 to week 2 then showed a decrease after the second week. This could be explained by the fact that the sample did not have the optimum solids and therefore during the time of stirring on determining the viscosity, the yoghurt network system collapsed easily. Viscosity change on sample D_2 recorded increase through all the three weeks. This is a sign of a stable yoghurt system as a result of sufficient solid present. Thus when starch is used for stabilization the product should be given a few days for its viscosity to age and stabilize. The pH recoded a stable pattern too in the three weeks of storage. Samples A, B, C, D_1 and D_2 had an average pH of 4.2 throughout the three weeks of storage period. Sample E had a higher pH initially (pH 4.3) and

went up slightly to 4.4 for the next two weeks. The pH was stable over the storage period and was within the expected range as documented in other studies (Lucey and Singh, 1998).

3.5 Cost of Production

The results obtained on costing the yoghurt samples showed a distinct price difference between samples as shown in Figure 9. Sample A was the most expensive product costing Ksh. 57.20 per liter. This was not significantly different from the control sample E which was costing Ksh. 55.30 per liter. Both were significantly different from samples B, D_1 and D_2, which were costing Ksh. 42.80, 45.80 and 47.60 per liter respectively. Samples B and D_2 were samples most acceptable and comparable to the control sample E in most of the quality parameters tested. When their price was calculated, they were found to be lower by Ksh. 12.50 and Ksh. 7.7 per liter respectively as compared with sample E. This translated to a cost cut of 22% for producing yoghurt sample B and 13% for producing yoghurt sample D_2.

3.6 Model of the Effect of the Modified Starch on Viscosity

On analysis of the viscosity results obtained using the SPSS software package, the effects of the starch was found to be very significant at 5% level of significance with a significance of 0.042. It was also noted that the skimmed milk powder had a significant effect at the 5% level of significance with a significance level of 0.048. This implied that the starch had a greater effect on the viscosity than the skimmed milk powder. Further analysis was carried out to determine the various β to fit in the equation:

$\eta = \beta_1 x_1 + \beta_2 x_2 + \beta_3$

where;

η = total viscosity

$\beta_{1=}$ effect of skimmed milk powder coefficient

$x_{1=}$ percentage of milk powder added

$\beta_{2=}$ effect of starch coefficient

$x_{2=}$ percentage of starch added

$\beta_{3=}$ the y-intercept coefficient.

From the SPSS output,

$\beta_1 = 1227$

$\beta_2 = 6701$

$\beta_3 = 1092.5$

Therefore,

$\eta = 1227x_1 + 6701x_2 + 1092.5$

where: η = total viscosity;

x_1 = percent skimmed milk powder content;

x_2 = percent starch content

4.0 Discussion

During fermentation, the ingredients added have different effects, some of which include the increase or decrease of the fermentation times and the final pH attained. The pH range attained by the yoghurts in this study (Table 3) was in agreement with the results of yoghurt fermentation in other studies (Lucey and Singh, 1998; Oh *et al*., 2006), which established it to be between 3.8 and 4.6. This was the first indication that addition of corn starch as a stabilizer did not affect the fermentation process both in fermentation time and final pH attained. This is a very important criteria since an increase in processing times means an increase in cost of production (Oh *et al*., 2006).

From visual observation, one could not differentiate between the yoghurt samples which contained starch from those which did not contain any starch. This showed that the starch grains were completely solubilized in the milk, thus giving smooth, viscous yoghurts. This was as a result of the starch granules embedding in the continuous protein network during the milk heating process before the fermentation commenced (Oh *et al*., 2006). This then led to an increase in the concentration of the protein net work due the increase in size of the gelatinized starch granules leading to the formation of large protein particles which gave a thick consistency (Lucey and Singh, 1998; Roefs *et al*., 1990). The thick consistency might also have been enhanced by the higher serum viscosity as a result of starch constituents leaching out during starch gelatinization, which increased the viscosity of the aqueous phase and consequently a thick smooth consistency/appearance as visually seen (Narpinder *et al*., 2003 ; Oh *et al*., 2006).

These yoghurts on being subjected to further analysis by the use of a Brookfield viscometer showed similar results. Based on the results obtained, it was observed that it is possible to make yoghurt of acceptable viscosity incorporating modified starch only at the rate of 0.5% without adding any skimmed milk powder. It was also established that it is possible to make yoghurt with as reduced skimmed milk powder content such as 1% instead of 3%, while substituting the milk powder with 0.5% modified starch.

In determination of the viscosity by the use of a Posthumus cup, sample D_1 registered the least mean time in seconds. This is an indication that the viscosity was the lowest of all. This showed that the stabilizer amounts (0.3% modified starch) used were not effective or were too low to give the desired viscosity (Lucey and Singh, 1998). In this sample, 0.75 % skimmed milk powder and 0.3% starch were used. This indicated that the amount of corn starch required to produce a comparable product in viscosity to that of reference/control (E) aught to be not less than 0.5%. These results are in agreement with those obtained by the use of a Brookfield viscometer.

As earlier mentioned, yoghurt handling has a viscosity reducing effect on the yoghurt. However this reduction is dependent of the yoghurt ingredients. In general, a trend of decrease of posthumus mean seconds was observed in all the samples as the number of runs increased. This was brought about by the strong deformation of the gel particles in elongational flow during the repeated flow tests. It led to large deformation, break-up and pressing out of the gel particles, leading to a decrease in apparent viscosity thus recording less time in each subsequent run.

The results are in agreement with those obtained by Galesloot *et al*. (1958), who found that the flow time decreased with an increasing number of times that the sample of yoghurt passed through the funnel. The Posthumus results from the different tests showed that the samples exhibited shear thinning behaviour, as indicated by the reduced time on subsequent run which is in agreement with the findings of Alistair (1995). However Sample D_2 with 1% skimmed milk powder and 0.5% corn starch stabilizer was most comparable to the reference sample (E). This further confirmed that it was possible to produce a high quality stirred yoghurt product with starch as the only thickener and completely eliminating the use of skimmed milk powder. This confirmed the findings obtained by Ramaswamy and Basak (1992). On subjecting the different yoghurts to production costs analysis, the difference realized in monetary terms was 22% per liter for sample B and that of 13% per liter for sample D_2 which would translate to huge profits in a long term mass production. All this has been achieved without compromising the quality and consumer acceptability of the yoghurt which confirms the results obtained from other studies albeit with non-modified starches (Decourcelle *et al*., 2004; Keogh *et al*., 1998; Oh *et al*., 2007).

5.0 Conclusion and Recommendations

By substituting skimmed milk powder with modified corn starch, it was possible to cut the cost of producing stirred yoghurt product by as much as 22% without compromising its quality and consumer acceptability.

It is recommended that the results obtained should be implemented to produce this high quality and profitable yoghurt. This ought to be done in phases with the

first phase involving its production hand in hand with the control (3% skimmed milk powder) then gradually be made alone as the acceptability of the wider market is assessed.

Acknowledgements
We wish to thank the Department of Food Science and Technology, JKUAT and Corn Products International, Kenya for availing the resources required for the successful completion of this study.

References

Alistair M. S. (1995). Food Polysaccharides and their applications. TX553. P65F66 95-15184. pp 1-123.

Anema, S. G. and Li, Y. M (2003). Association of denatured whey proteins in with the casein micelles in heated reconstituted skimmed milk and its effect on casein micelle size. Journal of Dairy Research, **70**, pp 73-83.

Anema, S. G. and McKenna, A. B. (1996). Reaction kinetics of thermal denaturation of whey proteins in heated reconstituted whole milk. Journal of Agriculture and Food chemistry**, 44**, pp 422-428.

Ares G., Goncalvez D., Perez C., Reolon G., Segura N., Lema P., Gambaro, A. (2007). Influence of gelatine and starch on the instrumental and sensory texture of stirred yoghurt. International journal of Dairy Technology, **4**, pp 263-269.

Basim A., Hazim M., and Ammar E. (2004). Rheology of starch–milk–sugar systems: effect of starch concentration, sugar type and milk fat content. Journal of food engineering, **64**, pp 207-212.

Foss J. W. (2000). How processing affects Starch Selection for yoghurt. Bridgewater, NJ: National starch and Chemical Company.

Galesloot T. E. (1958). Investigations concerning the consistency of yoghurt. Netherlands Milk and Dairy Journal, **12**, pp 130-161 (summary pp. 161-165)

Koegh M. K. and O'Kenedy B. T (1998). Rheology of stirred yoghurt as affected by added milk fat, protein and hydrocolloids. Journal of Food Science, **63**, pp 108-112

Lucey J. A. and Singh H. (1998). Formation and physical properties of acid milk gels: a review. Food Research International, **13**, pp 529-542.

Narpinder S., Jaspreet S., Lovedeep K., Navdeep S. S. and Balmeet S. G., (2003). Morphological, thermal and rheological properties of starches from different botanical sources. Food chemistry, **81**, pp 218-231.

Narpnder S., Lovedeep K., Kawaljit S. S, Jagdeep K., and Katsuyoshi N. (2006). Relationship between physicochemical, morphological, thermal, rheological properties of rice starches. Food hydrocolloids, **20**, pp 532-542.

Nuruli M., and Azemi B. M. (1990). Rheological behaviour of sago (Metroxylon sagu) starch pastes. Food chemistry, **64**, pp 501-505.

Oh H.E., Anema S. G, Wong M., Pinder D. N., and Hemar Y. (2006). Effect of potato starch addition on the acid gelation of milk. International Dairy Journal, **17**, pp 808-815.

Rasmaswamy H. S., and Basak S. (1992). Pectin and raspberry concentrate effects on the rheology of stirred yoghurt. Journal of Dairy Science, **81**, pp 1525-153.

Roefs S. P. F. M., de Groot-Mostert A. E. A. and van Vliet T. (1990). Structure of acid casein gels. 1. Formation and model of gel network. Colloidal and surfaces **50**, pp 141-159.

Ronnegard E. and Dejmek P. (1993). Development and breakdown of structure in yoghurt studied by oscillatory rheological measurements. Lalt73, pp 371-379.

Tamine A. Y. (2002). Fermented milks a historical food with modern application. A review. European Journal of clinical nutrition, **56**, S2-S15.

Teggatz J. A. and Morris H. A. (1990). Changes in the rheology and microstructure of the ropy yoghurt during shearing. Food Structure, **9**, pp 133-138.

Tester R. F. and Morrison W. R. (1990). Swelling and gelatinization of cereal starches. Cereal chemistry, **67**, pp 558-563.

Waistra P., Wouters J. T., and Geurts T. J. (2006). Dairy science and Technology, Second edition, CRC Press. pp 15, 169-172, 290-291,450-451, 567-568.

Appendix

Table 1: pH of the milk at the beginning of fermentation and that of the end

Samples	A	B	C	D_1	D_2	E
PH (start)	6.5	6.5	6.5	6.5	6.5	6.5
pH (end)	4.2	4.3	4.2	4.1	4.3	4.3

Figure 3: Photographs of the six stirred yoghurt gels on black plate

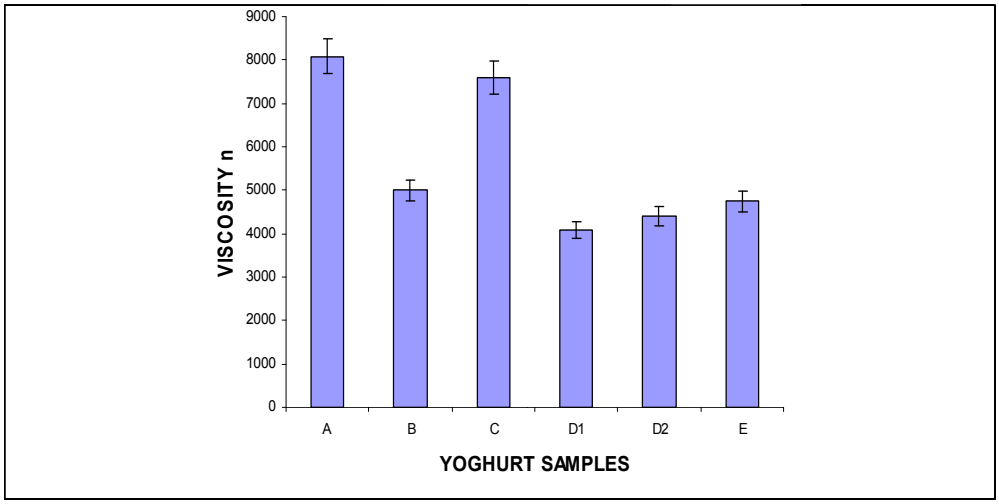

Figure 4: Effect of corn starch addition on yoghurt viscosity

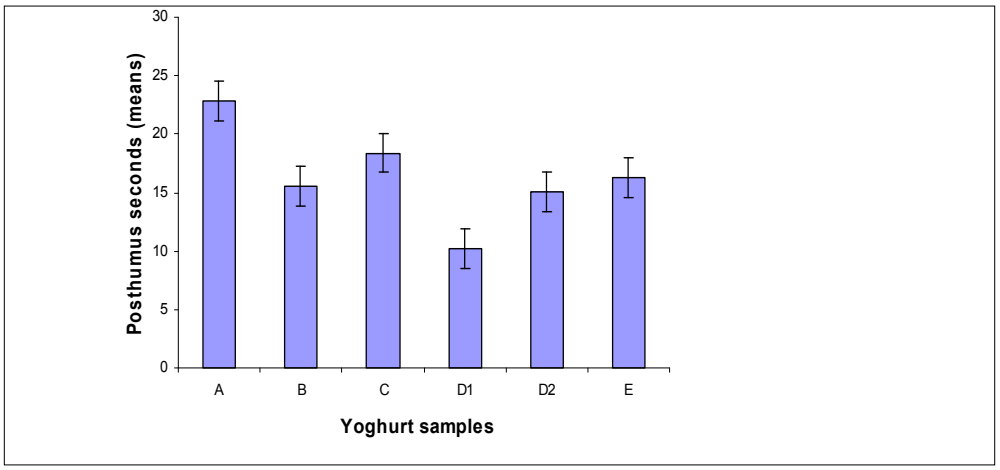

Figure 5: Posthumus mean seconds as an indication of yoghurt viscosity

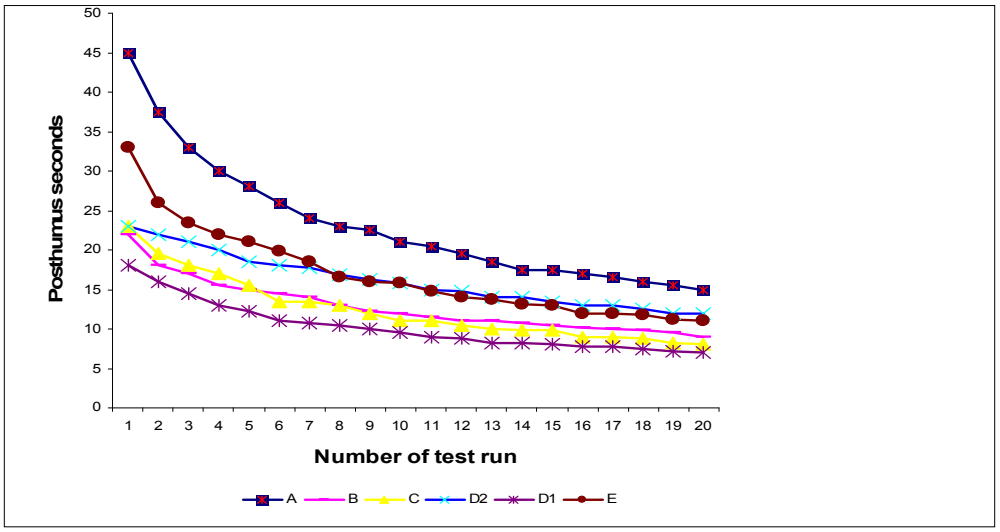

Figure 6: Posthumus Seconds 20X run curves

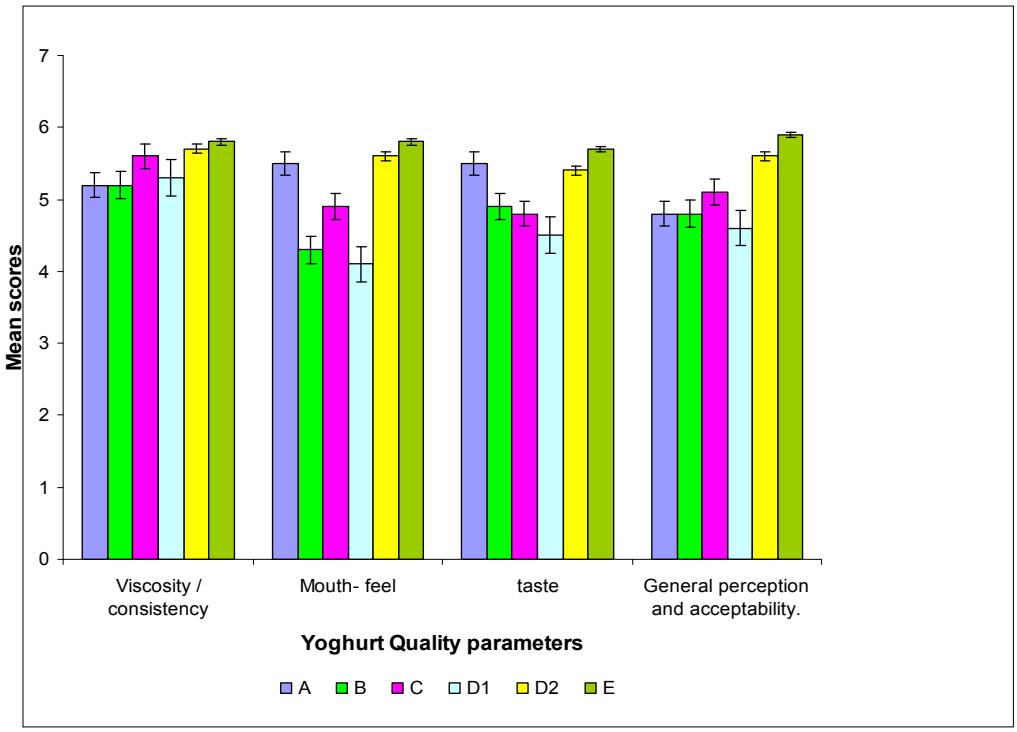

Figure 7: Sensory evaluation results of the six samples.

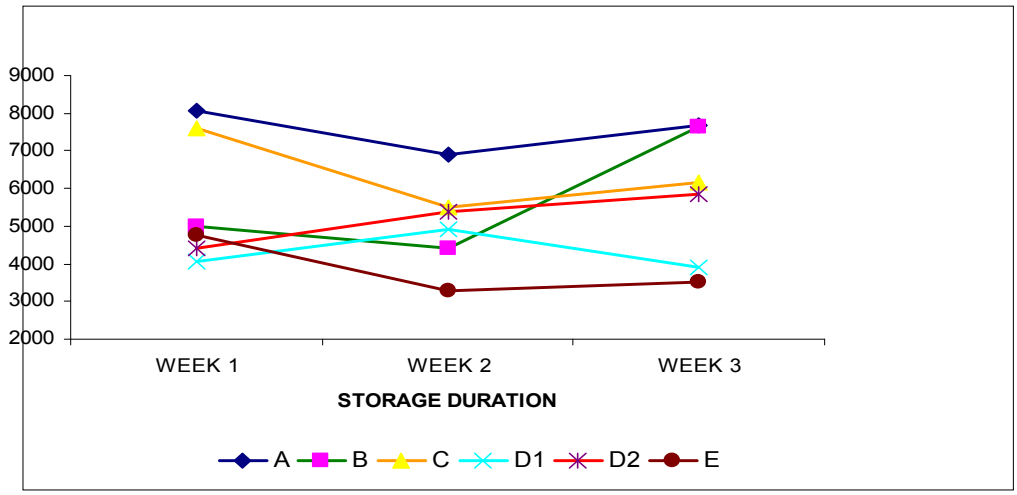

Figure 8: Viscosity change within 21 days of storage

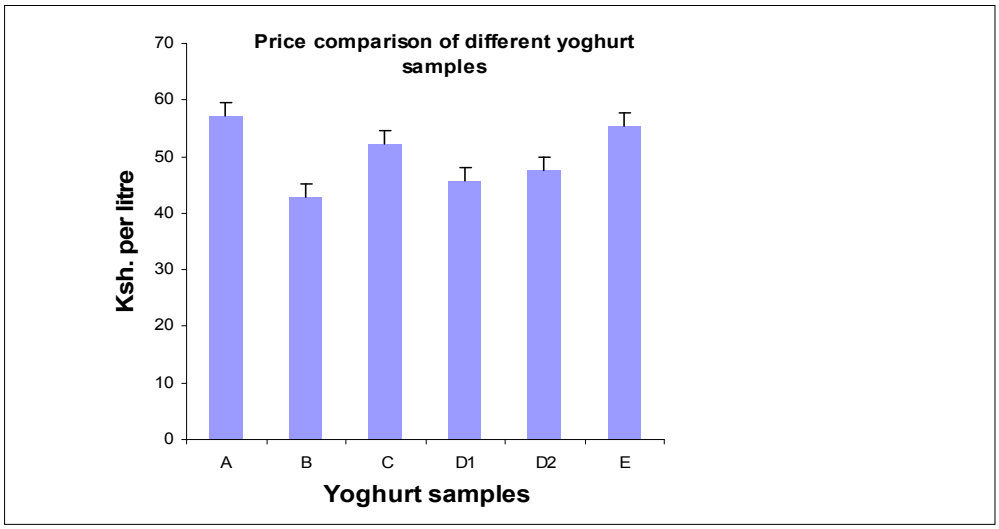

Figure 9: Cost comparison of producing different yoghurt samples

LEAF STOMATA CONDUCTANCE, LEAF WATER POTENTIAL AND SOIL WATER STATUS IN *PANICUM MAXIMUM* JACQ. IN DISTURBED AND NON-DISTURBED MICROSITES IN A SEMI-ARID ECOSYSTEM IN KENYA

E. K. Maranga[1] D. Nassiuma[2] and J. I. Kinyamario[3]

[1]Department of Natural Resources, Egerton University, Kenya
[2]Kabarak University, Kabarak, Kenya
[3]School of Biological Sciences, University of Nairobi, Kenya
Email:

ABSTRACT

Tropical semi-arid ecosystems are intricate ecosystems characterized by alternating dry-wet cycles. The question of how trees and grasses coexist under a considerable range of environmental and management conditions has been referred to as the "savanna problem" The practical significance of understanding the dynamics of natural ecosystems in relation to disturbances induced by herbivory, changing land use patterns or climate change is increasingly being recognized. Natural resource conservationists, range managers, and other custodians of natural resources require concrete information bases for land use policy formulations and as a means of regulating land use systems for sustainable resource use and development. An experiment using a randomised complete block design was set up to measure the effects of induced disturbances on ecosystem components and concomitant plant physiological responses. Analysis of variance techniques were used to determine the presence or absence of significant treatment effects. Disturbed micro-sites (manipulated treatments where *Acacia tortilis* trees were removed) demonstrated contrasting results compared to the non-disturbed micro-sites (*Acacia tortilis* trees left intact).The disturbed sites had less average moisture content in the 10cm soil profile (14.4%) than the non-disturbed sites(18.8%). *Panicum maximum* had an average stomata conductance of a magnitude of 0.65cms^{-1}(270mmolm^{-2} s^{-1}) for the disturbed microsites and 0.75cms^{-1}(312mmolm^{-2}s^{-1}) for the non-disturbed sites. There were no significant treatment effects in transpiration rates and leaf water potential of *Panicum maximum* in the disturbed and non-disturbed sites. This analysis demonstrates that long term changes in microenvironmental conditions of soil and plant water status due to tree removal is likely to cause shifts in botanical composition of graminoid species with direct implications on nitrogen sequestration, species biodiversity, and productivity.

Key words: *Panicum maximum*, semi-arid ecosystems, soil water status, stomata conductance, tree-grass interactions, micro-environmental fluxes

1.0 INTRODUCTION

Tropical semi-arid ecosystems are intricate ecosystems characterized by alternating dry-wet cycles (Maranga *et al*. 1983; Kinyamario *et al.*1995; Higgins *et al*. 2000; Ludwig *et al*. 2004; Tietjen and Jeltsch 2007 and Muthuri *et al.* 2009). The question of how trees and grasses coexist under a considerable range of environmental and management conditions has been referred to as the "savanna problem" (Sarmentio 1984). Trees may influence microenvironmental conditions of temperature, light distribution, wind regimes, soil and water status (Maranga *et al*. 1983; Anderson *et al*. 2001 and Ludwig *et al.* 2004). Maranga *et al*. (1983) and Kinyamario *et al*. (1995) found that *Panicum maximum* predominantly occurred under the extended canopies of *Acacia tortilis* trees in Kenya. This influence of trees on the distribution of understorey grasses was explained in terms of improved water status beneath their canopies. Light energy interception by tree canopies reduced evapotranspiration, however, the reduction of rainfall due to interception was compensated by reduced water loss due to the presence of the canopy shade. Specialized habitats beneath tree canopies may explain the special mix of graminoid species associated with these microsites (Belsky *et al*. 1989; Ludwig *et al.* 2001, Anderson *et al*. 2001, Ludwig *et al.* 2004, Otieno *et al*.2005).

The effect of trees on microenvironmental fluxes of water, light and temperature of understorey species have been studied in situations involving intact isolated trees with distinct "within canopy" and "outside canopy" microsites (Maranga *et al*. 1983; Belsky 1990, 1994; Kinyamario *et al.* 1995; Le Roux *et al.* 1995; Scholes and Archer 1997; Ludwig *et al.* 2004;Tietjen and Jeltsch 2007). Although these studies have adduced evidence that suggested that light intensity had both negative and positive effects on graminoid understorey productivity, it is not clear how increased light intensity (full sun) and evapotranspiration rates would impact the soil and plant water status of shade adapted plants in situations where trees are removed to give way to alternative land uses as is the case in Kenyan semi-arid ecosystems.

The present study was designed to establish the dynamics of soil and plant water status of understorey species associated with selective removal of trees.

2.0 MATERIAL AND METHODS

2.1 Study Sites

The study was conducted in a semi-arid ecosystem in south central Kenya on the Kenya Agricultural Research Institute (KARI), National Range Research Centre, Kiboko (NRRC). The research station facility covers about 25,000 ha and lies between latitude 2^0 20'S and longitude 37^0 50' E with an elevation of approximately 1000m above sea level.

The study sites were approximately 10 kilometers away from the station headquarters. These were at Muuni and Four Corners area. The salient floristic and

physiognomic attributes of the vegetation include scattered overstorey trees of *Acacia tortilis* with large umbrella shaped canopies. *Acacia tortilis* trees often reached a height of 5metres with canopy diameters exceeding 10metres. The dominant grasses were *Panicum maximum* (beneath the canopy of *Acacia tortilis* trees) and *Chloris roxburghiana*, *Themeda triandra*, *Digitaria macroblephora*, *Cenchrus ciliaris* found in the sunny habitats. Interspersed with *Acacia tortilis* were isolated bushes comprising of *Commiphora riparia*, *Commiphora_africana*, *Acacia senegal*, *Acacia mellifera*, *Grewia bicolor* and *Duosperma* species. Bimodal rainfall regime is typical of the study area. The meteorological data used in this study was obtained from Makindu and Spray Race weather stations within the Kiboko station facility and about 3 kilometres away from the study sites.

Well-defined precipitation periods include the long rainfall season from March to May and the short rains from October to December. These wet periods are interrupted by a short dry season between June and September. The mean annual rainfall for Makindu Weather Station about 3 kilometres from the study locations is 600mm (based on 70 years of rainfall data). Ambient air temperatures range from 28.6^0C (mean maximum) to 16.5^0C (mean minimum). The lowest temperatures occur in July (8.8^0C) and the highest in February (36.1^0C). Relative humidity varies between 78% at 0600 GMT and 47% at 1200 GMT. Soils are acri-rhodic ferralsols, deep and reasonably well drained (Michieka and Van der Pouw, (1977)). Significant water stress during the dry season coupled with tree felling and herbivory characterizes the ecological dynamics of the study sites.

2.2 Field Experimentation

Field studies were conducted on four micro-sites with replicates located at Muuni and Four Corners areas in the southern part of Kiboko National Range Research Station land facility. Two of these micro-sites represented treatments (undisturbed microsites) where *Panicum maximum* coexisted with *Acacia tortilis* beneath the canopies of these trees. *Acacia tortilis* were removed in the other two micro-sites to simulate conditions in the sun (disturbed microsites). Here *Panicum maximum* was exposed to conditions under full sun.

Insitu measurements of leaf transpiration, ambient air temperature, leaf temperature and relative humidity were taken on fully expanded leaves of *Panicum maximum* by means of a Li-Cor LI-1600 steady state porometer. Data from these measurements were used in the calculation of stomata conductance as described by Long and Hällgren 1985. Six leaf samples from each sampling location in the disturbed and non disturbed sites were identified for porometric measurements.

After insitu measurements were taken, leaves were immediately cut and their water potential measured with a pressure chamber (PMS Instrument Company,

Corvallis, Oregon, USA) as described by Scholander, *et al.* 1964. Measurements were carried out once or twice a week between 1100hrs and 1400hrs for a period including one short rainfall season and long rainfall season. The period of measurements spanned the time frame including November 2002 to mid December 2002. Data collection ceased after mid December because of the short dry season and recommenced with the onset of the long rainfall season in April 2003 and continued up to June 2003. Leaf stomata conductance (Sc) was calculated using the equation of Long and Hällgren 1985 as follows:

$$Sc = E/Ls\ (L_T - W_O) \quad \text{.....(i)}$$

Where E = transpiration in m mol m^{-2} s^{-1} ,

Ls =Saturation vapour pressure, that is, mole fraction of water vapour at saturation,

$Log_{10} Ls = 0.02604T + 0.82488$ (Rosenberg, 1974),

Where T = ambient air temperature (^{0}C),

L_T = Leaf chamber temperature assuming its leaf is saturated with water vapour at the actual leaf temperature,

W_O = mole fraction of water vapour at the leaf chamber outlet (mol mol^{-1}).

Soil moisture samples were obtained at short term intervals with frequencies running between 3 days and 14 days. Sampling for soil moisture commenced with the onset of the short rains. The initial samples were taken on 18th of November for the short rains and 24th of April for the long rains. Sampling was stopped when differences in soil moisture content ceased with progressive drying around 13th of December for the short rains and 9th of June for the long rains. Soil moisture status was determined gravimetrically by drying samples in the oven at 105^{0}C for 24hours. The difference between the field weights and the oven dry weights constituted the moisture content of the samples (AOAC, 1975).

A randomized complete block research design was used in this experiment. The study was replicated twice. Treatments comprised of microsites with intact *Acacia tortilis* canopy environments (undisturbed microsites) and where these trees had been removed to expose *Panicum_maximum* to the full sun (disturbed microsites), and time. Analysis of variance was conducted on leaf water potential, transpiration, leaf stomatal conductance and soil moisture content using analysis of variance methods (Little and Hills 1975). Duncan Multiple Range Test was used in separating means that were statistically different at $p \leq 0.05$.

3.0 Results

3.1 Rainfall

The rainfall distribution in the study sites that influenced the soil moisture supplies is shown in Fig 1. Relatively higher rainfall amounts were recorded for the study sites (Makindu and Spray Race) in the short rainfall season (October - December) compared to the long rainfall season (March - May). The highest rainfall amounts were received in the second week of December with single rainfall events contributing more than 100mm. The seasonal rainfall totals received at the Makindu Weather Station near the study experimental plots for the short rainfall season and long rainfall seasons during the study period (2002-2003) were 257mm and 112mm respectively. There were no rains in January and February.

3.2 Soil Moisture

Seasonal trends of soil moisture distributions in the (average values of soil moisture for each sampled date and sampling depth) 10cm and 30cm soil profiles (Fig 2a and 2b) reflect the pattern of soil moisture replenishment through rainfall.

The onset of the short rainfall season was associated with considerable soil moisture infilling in both the disturbed and non-disturbed microsites. However, there was a slight but conspicuous increase in wetting intensity between November and December in the non-disturbed microsites compared to the disturbed microsites in the 10cm and 30cm soil depths. Mean soil moisture content calculated from pooled seasonal data for each profile and associated Duncan Multiple Range Test in the disturbed and non-disturbed areas (76 observations for all sampled dates in the disturbed sites and 25observations for the non-disturbed sites) are shown in Table 1c. Statistical parameters for seasonal soil moisture data are depicted in Table 1a.

In the second wetting phase (April-May) and beginning of the drying cycle (mid-June) differences in soil moisture between microsites in the surface layers were less apparent. In the deep soil profiles (90cm) the seasonal course of moisture distribution (Fig 2c) during the short rainfall season indicated that non-disturbed microsites were drier than the disturbed microsites (Table 1a).

3.3 Leaf Water Potential (Ψ_l)

Progressive increase in soil dryness in the disturbed and non-disturbed microsites was occasioned by increase in divergence in leaf water potential of *Panicum maximum* in these microsites. On 21st January (short dry phase) the leaf water potential of *Panicum maximum* in the non-disturbed microsites was -1.5MPa whereas in disturbed microsites, it was -2.2MPa. At the peak of the short dry season around 7th and 14th February, *Panicum maximum* in the non-disturbed microsites exhibited a leaf water potential of

-6.3 MPa whereas in the disturbed microsites, it reached -7.0 MPa (Fig 3). The leaf water potential means in the contrasting microsites were not significantly different ($p \leq 0.05$) (see Table1c).

3.4 Transpiration

The highest transpiration rates were recorded for *Panicum maximum* (Figs. 4and 5) in the disturbed microsites (full sunlight). In the course of the dry period, mean transpiration values for *Panicum maximum* (4.2mmol H_2O m^{-2} s^{-1}) in the non-disturbed microsites remained relatively higher compared to those of *Panicum maximum* (4.0mmol H_2O m^{-2} s^{-1}) in the disturbed microsites. Statistical parameters for transpiration data are depicted in Table 1b. Transpiration means in the disturbed and non disturbed microsites were, however, not significantly different at $p \leq 0.05$.

3.5 Leaf Stomata Conductance

Variations in leaf stomatal conductance in *Panicum maximum* in disturbed and non-disturbed microsites were similar to those of transpiration rates (Figs.4a, 4b, 5a and 5b). Leaf stomata conductance increased during the wet phases and decreased with the advancement of the dry season in the contrasting microsites. Mean leaf stomata conductance of 0.75cms^{-1} (312 mmolm^{-2} s$^{-1)}$ was recorded in *Panicum maximum* in the non-disturbed microsites whereas *Panicum maximum* in the disturbed microsites registered a mean value of 0.65cms^{-1} (270 mmolm^{-2} s^{-1}.) Leaf stomata conductance means in the contrasting microsites were significantly different ($p \leq 0.05$). Standard errors for seasonal leaf stomata conductance data and other relevant statistical parameters are shown in Table 1b.

PET refers to potential evapotranspiration

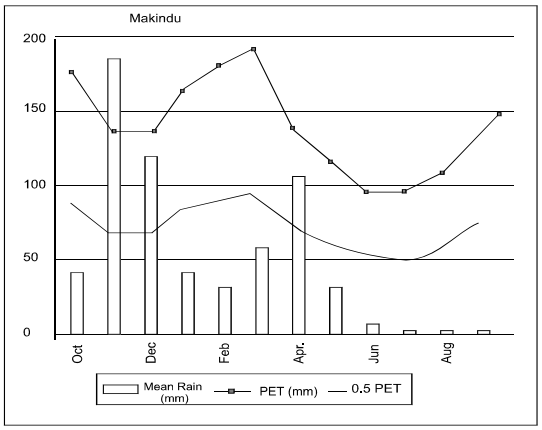

Fig.1a :Water balance of the study locations, National Range Research Centre, Kiboko

Source:Adapted from Gichuki, (2000).

Table 1a: Summary of averages (M) and standard errors (SE) of moisture content (%) at 10cm (SM1), 30cm (SM2) and 90cm (SM3) soil depths in disturbed and non-disturbed microsites during the Nov-Dec.2002 and April-June 2003growth cycle at the Muuni study site, KARI, Kiboko, Kenya

Date	Disturbed Microsite						Non-Disturbed Microsite					
	SM1		SM2		SM3		SM1		SM2		SM3	
	M	SE	M	SE	M	SE	M	SE	M	SE	M	SE
18/11/02	18.5	5.5347	10.7	3.1275	10.1	3.1171	35.8	8.0500	22.7	0.8500	22.6	4.1000
29/11/02	19.9	7.9146	7.5	2.4044	14.2	3.5327	17.0	3.0000	18.6	3.5999	10.4	1.3000
13/12/02	37.4	2.0895	36.3	2.9091	34.2	2.8634	49.1	8.4430	45.2	4.3444	40.1	5.6888
24/04/03	14.1	2.0436	12.3	1.6711	8.8	0.6052	20.4	3.6500	13.7	3.6500	9.4	3.3500
08/05/03	15.1	1.3960	14.9	0.8593	14.3	1.3561	16.5	0.7929	13.7	0.6500	15.7	0.8071
22/05/03	10.2	1.1482	10.8	0.9373	13.7	0.5582	9.2	0.8500	10.9	0.2828	13.1	0.9000
28/05/03	11.5	0.6731	12.3	1.1734	9.7	2.0642	14.8	1.5513	12.1	1.2223	11.4	0.4898
06/06/03	11.9	0.2788	10.0	1.8857	13.1	0.4618	10.1	0.6499	11.7	1.6499	11.4	0.6499
09/06/03	10.5	0.6753	11.0	0.5404	11.5	1.9539	11.6	3.3843	9.8	0.1999	11.3	0.0999
17/06/03	11.3	0.4314	10.9	0.5056	11.3	0.8582	8.4	1.6499	9.7	0.3000	14.0	3.9500

Table 1b. Summary of averages (M), standard deviations(SD) and standard errors(SE) of transpiration rates(TS) mmol H_2O m^{-2} s^{-1} and stomatal conductance (SC) cms^{-1} of Panicum maximum at the Muuni study site,KARI, Kiboko, Kenya

Date	DISTURBED MICROSITE						NON-DISTURBED MICROSITE					
	TS			SC			TS			SC		
	M	SD	SE	M	SD	SE	M	SD	SE	M	SD	SE
19/12/02	11.9	0.44	0.1258	1.3	0.13	0.0368	10.2	0.50	0.1462	1.5	0.31	0.0900
23/12/02	7.4	1.61	0.6569									
23/01/03							3.4	2.50	0.7219	0.6	0.53	0.1530
24/01/03	1.1	1.36	0.5146	0.2	0.30	0.1150	4.9	1.73	0.4619	0.8	0.48	0.1292
04/02/03	0.5	0.35	0.1025	0.1	0.05	0.0131	0.6	0.32	0.0927	0.1	0.03	0.0091
10/02/03	0.8	0.39	0.1585	0.1	0.03	0.0105	0.5	0.18	0.0519	0.0	0.01	0.0037
23/04/03	0.3	0.24	0.0767	1.0	0.03	0.0084	0.6	0.43	0.1229	0.1	0.07	0.0019
09/05/03	0.9	0.82	0.2365	0.1	0.12	0.0033						
14/05/03	4.2	1.48	0.4260	0.5	0.20	0.0589	7.2	1.41	0.4058	0.8	0.17	0.0478
23/05/03	7.3	1.27	0.3661	1.2	0.29	0.0845	8.2	0.73	0.2102	1.2	0.18	0.0505
29/05/03	10.3	1.53	0.4429	1.6	0.24	0.0700	8.0	0.56	0.1614	1.4	0.08	0.0243
06/06/03	9.2	1.50	0.4342	1.7	0.30	0.0874	8.3	0.98	0.2834	1.2	0.11	0.0316
09/06/03	7.0	0.27	0.0788	1.5	0.12	0.0356	6.9	0.30	0.0873	1.5	0.09	0.0255
13/06/03	7.7	2.12	0.6133	0.0	0.30	0.0879	8.5	0.46	0.1341	1.4	0.13	0.0385

Table 1c: *Physiological responses of Panicum maximum as influenced by the environmental conditions in the disturbed and non-disturbed microsites*

Variable	Disturbed microsite	Non-disturbed microsite
Air temperature(C^0)	617	587 Duncan= Duncan Multiple Range Test
N	30.8	29.0
Mean	a	b $p \leq 0.05$
Duncan		
		587 Means followed with the same letter
Leaf temperature	617	29.6 are not significantly different
N	31.9	b
Mean	a	
Duncan		
Soil moisture (%)	76	25
10cm soil depth	14.4	18.8
N	a	b
Mean		
Duncan		
Soil moisture (%)	76	25
30cm soil depth	14.7	15.1
N	a	a
Mean		
Duncan		
Soil moisture(%)	76	26
90cm soil depth	13.8	14.1
N	a	a
Mean		
Duncan		
Transpiration($mmolH_2Om^{-2}s^{-1}$)	617	587
N	4.47	4.61
Mean	a	a
Duncan		
Leaf stomata conductance		
($mmolm^{-2}s^{-1}$)	617	587
N	270	312
Mean	a	b
Duncan		
Leaf water potential(MPa)		
N		
Mean	1122	1018
Duncan	-2.3	-2.26
	a	a

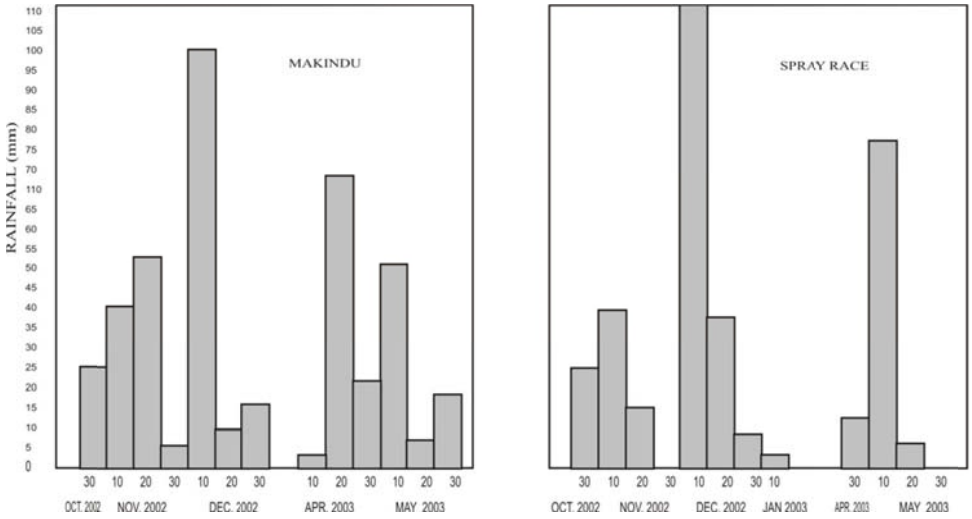

Fig.1b Rainfall distribution in the study area during the study period (2002 – 2003) for Makindu Meteorological Station and Spray Race within the Study sites

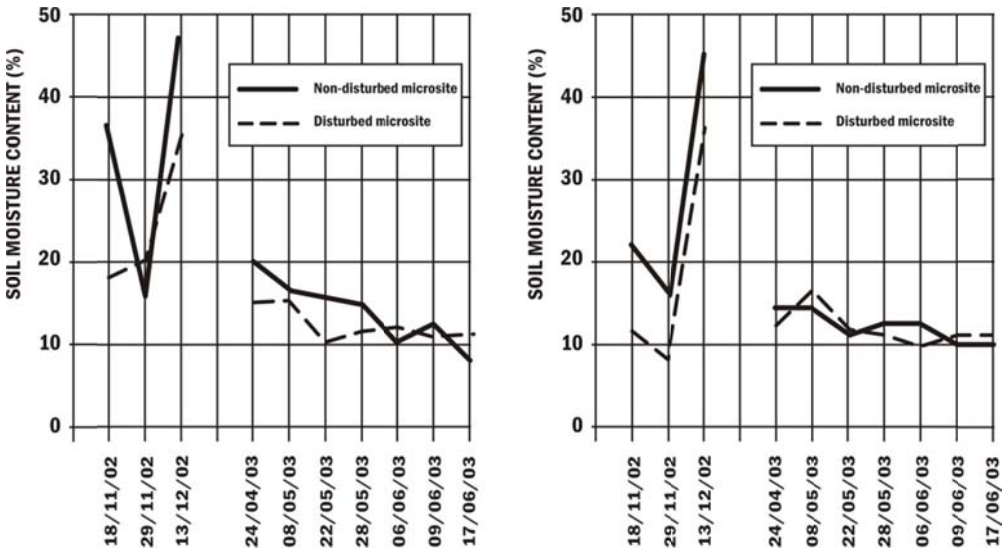

ıre d
ırbed :m
sites at)2
e Nov- cle
ıe 2003
ıuni study
/a

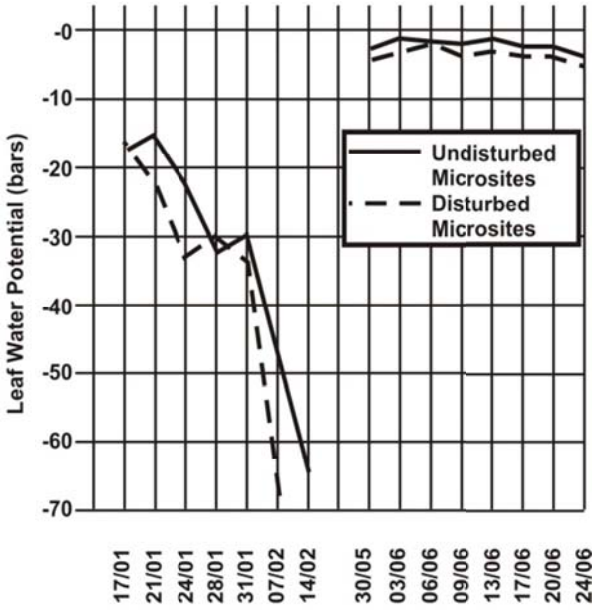

Fig 2c : Gravimetric soil moisture distribution in the disturbed microsites and undisturbed microsites at 90 cm depth during the Nov-Dec. 2002 and April-June 2003 growth cycle at the Muuni

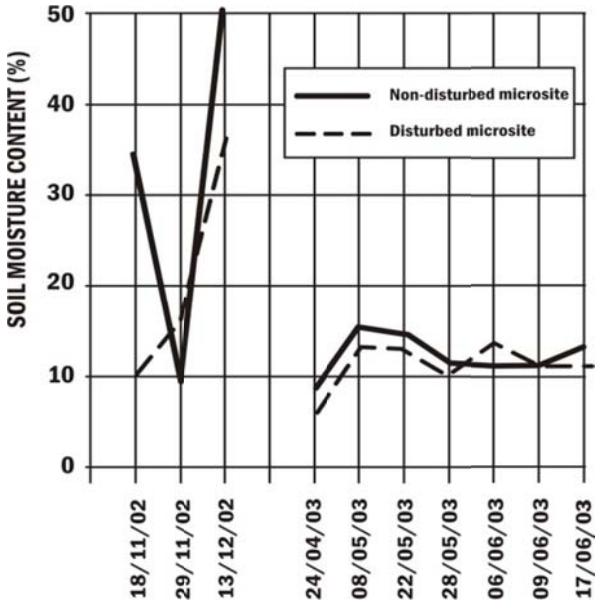

Fig 3 : Leaf water potential in the disturbed and undisturbed microsites forPanicum maximum at the Muuni study Site, KARI, Kiboko, Kenya

4.0 DISCUSSION

Temporal patterns of soil moisture, leaf water status, leaf stomatal conductance and transpiration suggested the presence of shifts in environmental conditions in the disturbed and non-disturbed microsites that were superimposed on physiological responses of *Panicum maximum*. Similarities in soil wetting patterns in the contrasting microsites in the course of the bi-modal wet-dry cycle were clearly reflected in patterns of leaf stomatal conductance, leaf water potential and transpiration rates. This illustrates the role of synergistic mechanisms in the environmental modulation of plant physiological responses. Davies and Kozlowski (1974), Kinyamario *et al.* (1995) and Ludwig *et al*. (2004) reported that differences in light energy regimes were responsible for differences in diffusive resistance and transpiration rates. In this study, significant differences in soil water status in the shallow soil profiles (10-30cm) may be attributed to differential heating and consequent evapotranspiration variations in the contrasting microsites. Higher transpiration rates were associated with lower diffusive resistance recorded in *Panicum maximum* in the disturbed microsites (full sunlight). Higher leaf stomata conductance was observed in *Panicum maximum* in non-disturbed microsites.

A coupling of soil moisture availability with leaf water potential was clearly evident in this study. The phase of intense soil moisture - infilling (November-December) was associated with smaller divergence in leaf water potential in *Panicum maximum* in the disturbed and non-disturbed microsites. The coupling of soil moisture with leaf water potential is due to the fact that the level of tissue hydration determines cell turgidity, which is in turn dependent on soil moisture availability (Kramer 1983). Higher leaf water potential in *Panicum maximum* in the non-disturbed microsites in the course of the early part of the dry season may be due to lower vapour pressure deficits irrespective of the highest transpiration rates recorded at this time at the diurnal level. These findings are in agreement with the evidence adduced by Drake *et al.* (1970) and Maranga (2007) that plants growing in wet environments exhibited high transpiration rates. Mwangi *et al.* (1999) found that transpiration was related directly to the air vapour pressure deficit and stomata conductance to water vapour. Evidence was also adduced in this study that suggested a strong coupling of soil moisture availability with transpiration in *Panicum maximum* in the contrasting microsites. This relationship suggested the significance of soil profile moisture availability and profile partitioning in relation to the use of water by shallow rooted graminoid species. This was indicated by the achievement of maximum transpiration rates early in the day during the wet season when moisture was non-limiting compared to the dry phase when the wetting front moved away from the zone of maximum density. Differences in the seasonal soil moisture cycle in the contrasting microsites meant that the relatively stable soil moisture supply into the dry phase for the non-disturbed microsites

permitted. *Panicum maximum* to remain physiologically active over a longer period compared to *Panicum maximum* in the disturbed microsites. A detailed study of the implications of the extension of physiological activity into the dry season in the non-disturbed microsites in relation to net CO_2 assimilation rates is the subject of another technical paper to be considered for publication in this series.

4.0 CONCLUSION AND RECOMMENDATIONS

Evidence from this study that demonstrated:

(i) That there was a significant difference in soil moisture status in the contrasting microsites suggested that tree removal in semi-arid environments may accelerate soil dryness with consequent negative effects on plant water status and physiological processes that control productivity.

(ii) That there was a significant difference in the stomata conductance of *Panicummaximum* in the disturbed and non-disturbed microsites suggested that tree removal had a negative impact on the water relations of *Panicum maximum.* Continuous exposure of *Panicum maximum* to full sun under conditions of limited soil moisture availability is likely to cause tissue dehydration with consequent implications on CO_2 uptake carbohydrate metabolism and plant productivity.

(iii) Efforts to arrest indiscriminate tree removal and overexploitation of tree resources in the semi- arid ecosystems are critical in the dynamics of soil and plant water resources that regulate tree- grass co-existence and productivity.

References

Anderson L. J., Brumbaugh M. S and Jackson R. B. (2001). Water and tree nderstorey interactions: A natural experiment in a savanna with oak wilt. Ecology, **82**, pp 33-49

AOAC (1975). Association of official analytical Chemists, Official methods of Analysis, 12th Edition, Washington D. C. U.S.A.

Belsky A. J., Amundson R. G., Duxbury J. M., Riha S. J., Ali A.R. and Mwonga S. M. (1989). The effects of trees on their physical, chemical and biological environments in a semi arid savanna in Kenya. Journal of Applied Ecology, **26**, pp 1005-1024.

Belsky A. J. (1990). Tree/ grass relations in East African savannas: a comparison ofexisting models. Journal of Biogeography, **17**, pp 483-489.

Belsky, A. J. (1994). Influences of trees on savanna productivity: tests of shade nutrients and tree-grass composition. Ecology, **75**, pp 922-932.

Davies W. G. and Kozlowski T. T. (1974). Stomatal responses of five woody angiosperms to light intensity and humidity Canadian Journal of Botany, **52**, pp 1525-1534.

Drake B. G., Rasche K. and Salisbury F. B. (1970). Temperature and transpiration resistance of Xanthium leaves as affected by air temperature, humidity and windspeed. Plant physiology, **46**, pp 324-330.

Gichuki F. N.(2000). Makueni District Profile: rainfall variability, 1950-1997; policy requirements for farmer investment in semi-arid Africa: Kenya series, Drylands research paper, working paper 2, **17**; Market Square, Crewkeme England

Higgins S. I., Bond W. J. and Trollope W.S.W.(2000). Fire, resprouting and variability: A recipe for grass-tree co-existence in savanna.. Journal of Ecology, **88**, pp 213-229.

Kinyamario, J.I., Trlica, M.J. and Njoka, T.J. (1995). Influence of tree shade on plant water status, gas exchange and water use efficiency of Panicum

maximum Jacq. and Themeda triandra Forsk. In a Kenya savanna. African Journal of Ecology, **33**, pp 114-123.

Kramer P. J. (1983). Water Relations of Plants. Academic Press Inc. (London) Ltd.

Little, T.M. and Hills, F.J. (1975). Statistical methods in agricultural research. University of California, Davis.

Long S. P. and Hällgren J-E. (1985). Measurement of CO2 assimilation by plants in the field and in the laboratory, In: Techniques in Bioproductivity and photosynthesis. (Eds. J. Coombs, D.O. Hall, S.P. Long and J.M.O. Scurlock). Pergamon Press, Oxford.

Le Roux X., Bariac T. and Mariotti A. (1995). Spatial partitioning of the soil water resource between grass and shrub components in a West African humid

wig F., de Kroon H., Prins H. H. T and Berendse F. (2001). The effect of nutrients and shade on tree-grass interactions on an East African savanna. Journal of Vegetation Science, **12,** pp 579-588.

Ludwig F., de Kroon, H., Berendse F. and Prins H. H. T. (2004). The influence of savanna trees on nutrient, water and light availability and the understorey vegetation. Plant Ecology 170: pp 93-105 Kluwer Academic Publishers. Printed in Netherlands.

Maranga E. K., Trlica M. J. and Smeins F. (1983). Water relations of Panicum maximum and Digitaria macroblephara on a semi arid Rangeland in Kenya. E. Afr. Agric. For. J., **48**, pp 74-80.

Maranga E. K. (2007). Effects of Acacia tortilis trees on the ecophysiology of graminoid herbaceous species in Makueni District, Kenya. Ph.D thesis, Egerton University, Njoro, Kenya.

Michieka D.O and B. J. A. Van der Pouw, (eds.), Soil and vegetation of the Kiboko Range Research Station. Semi detailed soil report No. 53, Draft edition, Kenya Soil Survey, NAL, Ministry of Agriculture, Nairobi, Kenya (1977).

Muthuri C. W., Ong C. K. Craigon J., Mati B. M., Ngumi V. W. and Black C. R. (2009).

Gas exchange and water use efficiency of trees and maize in agroforestry systems in arid Kenya. Agriculture, Ecosystems, and Environment, vol. 129, **4**, pp 497-507.

Mwangi M. T., Kinyamario J. I and Van Speybroeck D. (1999). Photosynthesis and related physiological processes in two mangrove species Rhizophora mucronata and Ceriops tagal at Gazi bay, Kenya. African Journal of Ecology, **37**, pp 180-193.

Otieno D. O. Schmidt N. W. T., Kinyamario J. I. and Tenhunen J. (2005). Responses of Acacia tortilis and Acacia xanthophloea to seasonal changes in soil water availability in the savanna region of Kenya. Journal of Arid Environments, **62**, pp 377-400

Rosenberg N. J. (1974).Microclimate. The Biological environment. A Wiley Intersience Publication, John Wiley and sons, New York, Chichester, Brisbane, Toronto.

Sarmentio G. (1984). The ecology of Neotropical Savannas. Harvard University Press, Cambridge, M.A

Scholander P. F., Hammel H. T., Hemmingsen E.A. and Bradstreet E.D. (1964). Hydrostatic pressure and osmotic potential in leaves of mangroves and some other plants. National Academy of science, **52**, pp 119-125.

Scholes R. J. and Archer S. R. (1997). Tree- grass interactions in savannas. Annual Review of Ecology and systematics, **28**, pp 517-544.

Tietjen B. and Jeltsch F. (2007). Semi-arid grazing systems and climate change: a survey of present modeling potential and future needs. Journal of Applied ecology, **44**, pp 425-434.

HIV STATUS DISCLOSURE AND ARV ADHERENCE AMONG PATIENTS ATTENDING JOMO KENYATTA UNIVERSITY COMPREHENSIVE CARE CLINIC

M.W. Mutugi[1], L. W. Kanga'ra[2], A. M'Mene[3] and L. W. Ndahi[4]

[1] Zoology Department, Jomo Kenyatta University of Agriculture and Technology, Nairobi, Kenya

[2, 4] Institute of Tropical Medicine and Infectious Diseases, Jomo Kenyatta University of Agriculture and Technology

[3]Jomo Kenyatta University of Agriculture and Technology Hospital

E-mail:

Abstract

Although Anti Retroviral Therapy (ART) is the single most important management of HIV infection, success in decreasing viral load depends on adherence to a strict regimen that requires taking the prescribed drugs daily at the specified times. Failure to daily intake of Anti Retrovirals (ARV) not only prevents treatment failure but may also lead to viral development of resistance to the drugs. The fact that HIV is mainly sexually transmitted means that it is associated with socially unaccepted practices such as premarital and extramarital as well as multiple sexual partners. Fear of such stigma related to these practices may thus prevent HIV status disclosure and deny the patient social support that may be important in management of the disease in general and adherence to ART in particular. This study was carried out in a three month period among 89 HIV positive patients attending Jomo Kenyatta University Hospital' comprehensive care clinic (CCC). A questionnaire was administered to the patients to investigate their knowledge regarding adherence and determine any association between disclosure of HIV and adherence. Their socio-demographic characteristics were also documented and related to adherence levels. The results indicate that although patients were aware of the importance of taking their medications on time, the adherence rate of 76% is below the recommended 95% optimum required for viral suppression to undetectable levels. Those that had disclosed their status were more likely to be adherent than those that had not as indicated by a statistical correlation between disclosure adherence ($P > 0.9$). This study recommends that psychosocial support of HIV positive patients should emphasize disclosure as a strategy for increasing adherence to the required optimum levels.

Key words: HIV, ART, ARV, disclosure, adherence

1.0 Introduction

The first case of HIV in Kenya was identified in 1984 and since then the infection levels has risen to the current estimate of 1.4 million. The latest Kenya AIDS Indicator Survey (KAIS, 2008) that sampled 18,000 adults aged 15-64 in 10,000 households throughout the country found that the prevalence of HIV infection is 7.4%. The survey indicated that there were more females infected compared to males (8.7 and 5.6 % respectively) with the most vulnerable group being females between the ages of 15-34. This is unlike a previous survey (KDHS, 2003), this study showed that there were high infection levels among older people (50-64).

There is stigma attached to HIV infection particularly due to its sexual transmission and association with moral issues such as casual, premarital and extramarital sex. In addition, this stigma is further exacerbated by the historical association of HIV infection to homosexuality, a sexual preference that is considered abnormal and repugnant among many African societies. Thus an HIV positive person will often be the subject of gossip either labelled as a homosexual or a person without moral uprightness thus face discrimination and possible exclusion in the community on account of perceived sexual habits.

The effect of this stigma is a barrier to HIV testing and when tested fear of disclosure of positive infection status. Such a situation dictates that when HIV positive patients are on ARVs, they take their medication privately away from prying eyes and may impact on adherence resulting in delay in taking their medication or even skipping them altogether.

Although it is estimated that one in every 25 Kenyans are infected, only four out of every five of these know their status (KAIS, 2008). Of those that know, Anti Retroviral Therapy (ART) is available to 190,000 of them in over 500 sites that are government or privately sponsored. The Ministry of health however supports all these sites by availing counselling, testing and Anti Retrovirals (ARV) services.

ARVs suppress viral replication resulting in lowered viral loads and a dramatic improvement in morbidity and mortality (Palella *et al*, 1998). The fact that ARVs do not eliminate the virus means that ART is a lifelong commitment with the accompanying challenges of adherence to stringent drug regimens. Adherence to ART is an essential element of successful HIV treatment. There are several forms of non- adherence ranging from not observing intervals between doses, missing one or several doses to missing whole days of treatment altogether. Adherence has been shown to vary not just between individuals, but also in the same individual over time, thus making adherence a dynamic rather than a static characteristic of an individual (Amberbir *et al*, 2008. Most people will exhibit low adherence at some time during this extended therapy (Nischal *et al*, 2005). Non-adherence does not only result in symptomatic progression of infection but may also lead to

treatment failure, development of viral resistance and need to resort to more expensive and toxic drugs (Bangsberg *et al*, 2006).

In order to achieve levels of HIV adherence required to suppress viral replication, it is important to investigate and understand factors associated with adherence. This study thus set out to investigate the relationship between disclosure of HIV positive status and adherence with the hypothesis that there is a positive correlation between the two.

2.0 Materials and Methods

This study was a survey conducted at Jomo Kenyatta University of Agriculture and Technology (JKUAT) hospital based at Juja, Kenya. The hospital is a Ministry of Health ART site providing HIV prevention and control services to staff, students and the general Juja community. The study was part of the project entitled "Care and Support: Scaling up ART use and Adherence" that among other function provides psychosocial care and support to People Living with HIV/AIDS. A questionnaire (annex 1) was administered to all consenting Clients on ART attending the CCC for three months of May-July 2008. Data was collected pertaining to their socio-economic status, period since testing, reason for testing, onset of ART as well as information on disclosure and adherence. In order to ensure privacy, all the data was coded to ensure that information could not be traced to the respondents.

Adherence levels were calculated as: no of doses taken in last 7 days / no of doses supposed to be taken in same period x 100. Data was analysed using to provide descriptive statistics and correlation between disclosure and adherence.

3.0 Results

3.1 Socio-Demographic Characteristics

Eighty nine (89) patients on ART answered the questionnaire. Of these, 72% were females and 28 % males (Figure 1) with over two thirds (70%) of them aged between the ages of 30 and 50 (Figure 2). Fifty two percent (52%) of them were married, 31% single, 7% widowed and the rest either divorced or cohabiting with a partner (Figure 3). In terms of education, 48% had either had some or completed primary education; 31% some secondary education while the rest had completed secondary education (Figure 4). Almost half of the respondents (41%) were business people; 14 and 10 % respectively in permanent or contract employment and the rest reported that they were in casual employment or did not work (24 and10 % respectively).

In respect to living arrangement, 72% of the respondents were family people living with spouse and children in the same house while another 17% lived with their

parents. As shown in Figure 5, the rest either lived with their siblings, members of their extended family or with friends, co-workers or employer.

3.2 HIV Status and Disclosure

Figure 6 shows that over 55% of the patients had been diagnosed to be HIV positive within the last two years and 72% had started on ART within that same two-year period. Fifty four percent of the respondents knew their HIV status for reasons cited for testing was being sick while 35% went for VCT and another 7% were tested during their visit to the ante natal clinic.

Eighty percent of the respondents reported that they had disclosed their HIV status to a person they lived with such as spouse, children, parents or sibling (Figure 7). Of these disclosures, 62% were male. One third of the married women had not disclosed their HIV status to their spouses while all the married males reported that they had disclosed their HIV positive status to their wives. In addition, all the widowed men had disclosed their status to their children while only 63% of the widowed women had done so. The majority of those that had not disclosed had only been tested within the last one year (92%). There was however no statistical significant relationship between disclosure and all socio-demographic characteristics investigated ($P>0.05$).

3.3 Adherence to ARV Regimen

All the respondents stated that it was important to take ARVs as directed the major benefit quoted being improved health (41%). Others were more specific and reported that adherence to treatment reduced viral loads (14%), “was effective” (10%) helped patients to “live longer” (7%) and also prevents development of resistance (7%). Other reasons given were ARVs improved immunity, “assist” and “give strength”. Three percent (3%) said that they did not know the exact reason (Figure 8). This knowledge however did not translate to practice for only 76% of the patients reported that they had taken their drugs in the last seven days as instructed. Of the 24% that missed their doses, 80% were female with 17% reporting having missed one or two doses and the rest (7%) three or more doses. All of those who reported to have missed their medication had been on ART for less than a year. There was no apparent relationship between adherence and age, marital status, occupation or education.

In that same seven day period, 45% reported they had been more than 6 hours late in taking their medication on more than one or two occasions, 24% had been late three or four times and 3% over five times. Twenty seven (27%) however reported that in the last seven days they had taken their medication as expected and were not late for more than an hour. Among those who were late, there were more females (73%) than males. The majority attributed this lateness to forgetting and travelling (35 and 28% respectively). Other reasons given were, lack of food,

presence of visitors, being busy, being involved in accidents, civil unrest to tardiness in acquiring refills.

3.4 Disclosure of HIV Status and Adherence ARV Regimen

Many of the respondents (64%) said that there was a relationship between disclosure of HIV status and adherence. The role of the person one disclosed to was of reminding (73%) and monitoring (19%) ARV use. Thirteen percent of the respondents, evenly divided among the sexes, said there was no relationship between disclosure and adherence while 23% said they did not know. All those who said they did not know of a relationship between the disclosure of status and adherence had not completed primary school. It is interesting to note that only 70% however said that the role of assisting with adherence was played by a housemate who most likely knew their HIV status.

Statistical analysis showed that there was positive correlation between disclosure and adherence both in terms of taking the required dose (P= 0.945) and taking it on time (P= 0.972). These associations were irrespective of all socio-demographic characteristics.

4.0 Discussion and Conclusions

The ART 76% adherence level reported in this study is below optimum adherence of 95% that has been shown to achieve a sustained plasma drug concentration that will inhibit viral replication to below detectable levels in 80% of individuals (WHO, 2006). Decreased adherence leads to decreased viral suppression with 70% adherence resulting in viral suppression at only 33% (Nischal *et al*, 2005).

The level observed in this study is similar to a self-reporting study in India which showed that 80% of patients had not missed a single dose in the last seven days (Sarna *et al*, 2008) as well as 77% adherence reported in several studies in sub-Saharan African (Mills *et al*, 2006). These results are however much higher than those reported in a study in Tanzanian where adherence was only at 21% (Irunde *et al*, 2005).

Forgetting and traveling cited as reasons for poor adherence in our study are the same as those cited in the Indian study (Sarna *et al*, 2008). A study in South Africa however also included social barriers to adherence such as non-disclosure, lack of family support and fear of stigma (Dahab *et al*, 2008). The reasons are similar to those in the current study where patients who had disclosed their status to family or friends that they lived with had higher adherence levels than those who had not.

In the current study, most patients referred to a apparent effect of ARV in terms of improved health, being effective and able to reduce the virus load. This is

expected as almost half of them had been tested within the previous two years when they were sick and had been initiated to ARV use within the same period. This suggests that they had already progressed to symptomatic infection by the time they were tested and after ARV use, they had experienced significant change in their health status. In addition, patients knew the importance for adherence to ART regimen although this knowledge did not translate to actual practice. In the adherence study done in Tanzania, however some patients were not knowledgeable on ART nor well informed about consequences of suboptimal levels of adherence. This may have been due to patient or medical staff factors such as cost of traveling to the clinic, lack of food, lack of confidentiality in the clinics, long waiting periods at the clinics and shortages of medicines. Low staff motivation, inadequate training and work overload are other factors that may have lead to poor adherence (Irunde *et al*, 2005). The fact that the current study is in an ART outlet in University hospital setting that has a psychosocial support component my have mitigated the factors cited in the Tanzanian study. Indeed one of the reasons cited by patients in preferring the JKUAT site to neighboring district hospitals is the confidentiality and privacy that the University set-up provides as well as the comparatively lower patient numbers.

The fact that over 90% of the respondents in this study who had not disclosed their status had been tested within the previous one year period suggests that it takes a while for patients who have tested positive to accept the diagnosis enough to disclose their status to family or friends. A study in Ethiopia also found a correlation between disclosure and time length of time post diagnosis (Deride *et al* 2008). Our study showed that although patients did not think there is a correlation between disclosure and adherence to ART, patients who have disclosed their HIV status were reminded to take their medication on time and were thus more adherent to the ART regimen. In addition, the study showed that males were more likely to have disclosed their HIV status which contradicts commonly held beliefs that males are more “secretive” and women more open concerning private matters such as HIV infection. Studies in South Africa have shown conflicting results with one associating males with disclosure (Skogmar *et al* 2006) and another with non-disclosure (Olley *et al* 2004). The fact that adherence was higher in males than females also contradicts myths that men are averse to taking drugs.

As in self-reporting studies, this study has limitations of respondent, recall and societal bias that may have influenced the results. We thus recommend a further study involving a larger number of patients and more objective methods of determining adherence. However in view of these preliminary findings, HIV positive patients should be encouraged to disclose their status to a trusted person who will act as a “treatment buddy” and monitor ARV adherence. Disclosure should thus be a crucial component integrated in counselling during regular

hospital visits as well as all psychosocial support programmes not just to increase adherence levels but also reduce stigma attached to HIV infection.

Acknowledgement

We wish to acknowledge Columbia University's ICAP program who supported the project entitled "Care and Support: Scaling up ART use and Adherence" without which this work would not have been possible.

References

Amberbir M., Woldemichael K., Getachew S., Girma B. and Deribe K. **(**2008) Predictors of adherence to antiretroviral the pay among HIV-infected persons: a prospective study in Southwest Ethiopia. *BMC Public Health*, **8**, pp 265.

Bangsberg D. R. Acosta E. P. Gupta R. Guzman D. Riley E. D. Harrigan P. R. Parkin N. Deeks S.G. (2006) Adherence-resistance relationships for protease and non-nucleoside reverse transcriptase inhibitors explained by virological fitness. *AIDS*. 20**, 2,** pp 223

Dahab M., Charalambous S., H. R., Fielding K., Kielmann K. Churchyard G. J. and Grant A. D.(2008). "That is why I stopped the ART": Patients' & providers' perspectives on barriers to and enablers of HIV treatment adherence in a South African workplace programme. *BMC Public Health,* **8**, pp 63.

Deribe K., Woldemichael K., Wondafrash M., Haile A**.** and Amberbir M. (2008). Disclosure experience and associated factors among HIV positive men and women clinical service users in southwest Ethiopia *BMC Public Health* 2008, **8,** pp 81.

Irunde H., Temu F., Maridadi J. and Comoro C. (2005). A study on antiretroviral adherence in Tanzania: a pre-intervention perspective, In WHO "From access to adherence: the challenges of antiretroviral treatment". Studies from Botswana, Tanzania and Uganda." Editors: Hardon A., Davey S., Gerrits T., Hodgkin C., Irunde H., Kgatlwane J., Kinsman J., Nakiyemba A., Laing R., Mills E. J., Nachega J. B., Buchan I., Orbinski J., Attaran A., Singh S., Rachlis B., Wu P., Cooper C., Thabane L., Wilson K., Guyatt G. H., Bangsberg D.R. (2006). Adherence to Antiretroviral Therapy in Sub-Saharan Africa and North America: a meta-analysis . *JAMA,* **296**, pp 679-690

Kenya AIDS Indicator Survey, 2008 National AIDS and STI control Programme (NASCOP), Ministry of Health, Kenya.

Kenya Demographic and Health Survey, (2003) Central Bureau of Statistics (CBS), Ministry of Planning, Kenya.

Nischal K. C., Khopkar U. and Saple D. G. (2005). Improving adherence to antiretroviral therapy. Indian Journal Dermatology Venereology and Leprosy, **71**, pp 316-320.

Olley B. O., Seedat S., Stein D. J.(2004). Self-Disclosure of HIV Serostatus in Recently Diagnosed Patients with HIV in South Africa. *African Journal of Reproductive Health* 2004, **8,** pp71-76.

Palella F. J., Delaney K. M., Moorman A. C., Loveless M. O., Furher J. Statten G.A. Aschman D. J. and Holmberg S. D. (1998). Declining morbidity and mortality among patients with advanced human immunodeficiency virus infection. *The New England Journal of Medicine*, **338**(**13**), pp 853-60.

Sarna A., Pujari S., Sengar A., Garg R., Gupta I. and Van Dam J. (2008). Adherence to antiretroviral therapy and its determinants amongst HIV patients in India. *Indian Journal Medical Research,* **127**, pp 28-36.

Skogmar S. Shakely D lans M. Danell J. Andersson R. Tshandu N Ode'n A. Roberts S. Francois Venter WD: (2006) Effect of antiretroviral treatment and counseling on disclosure of HIV-serostatus in Johannesburg, South Africa**.** *AIDS Care*, **18,** pp 725-730.

World Health Organization. (2006). Antiretroviral therapy for HIV infection in adults and adolescents: Recommendations for a public health approach. Revisions.

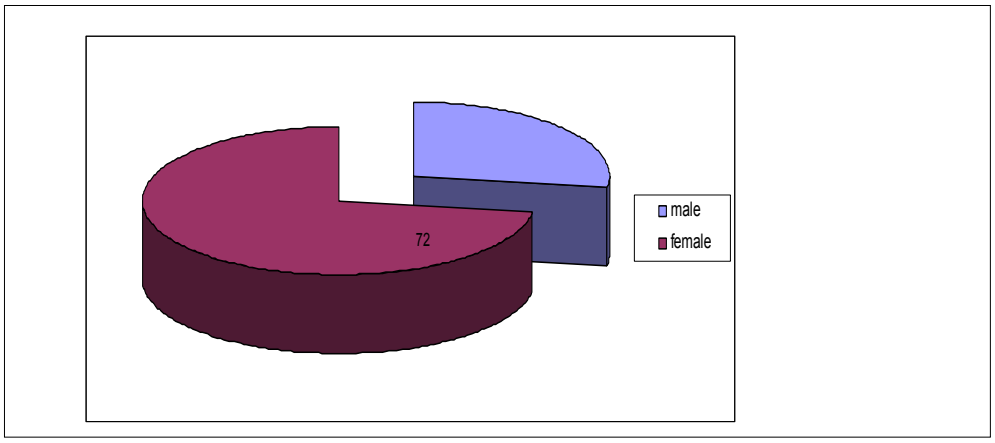

Figure 1: Sex distribution of the respondents

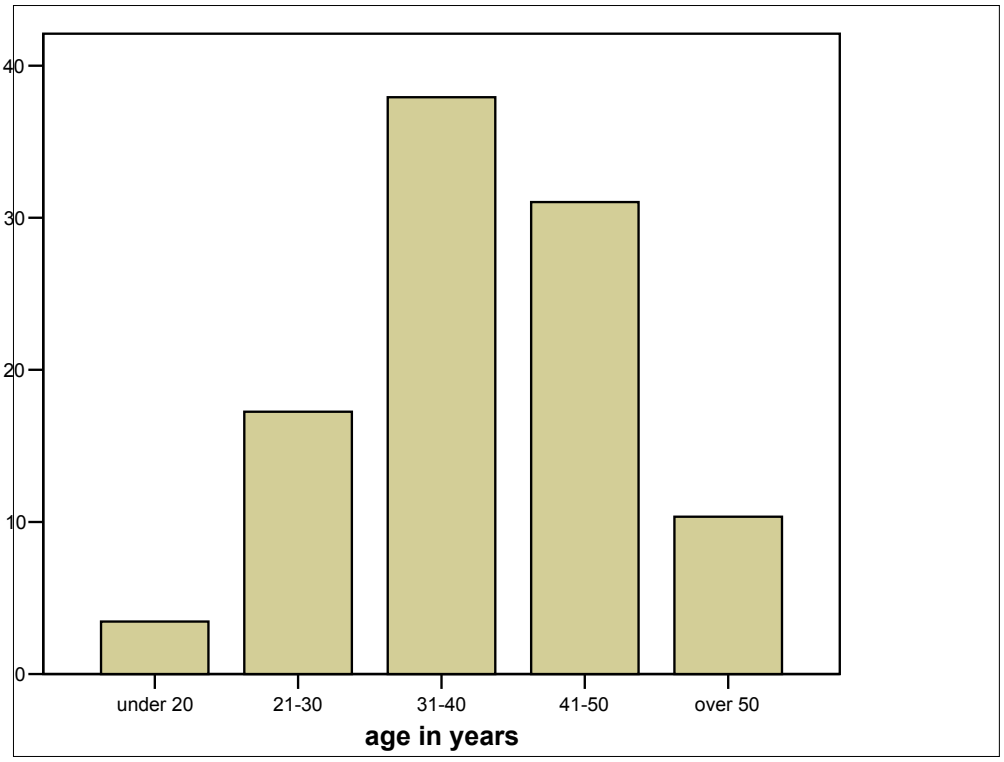

Figure 2: Age distribution of the respondents

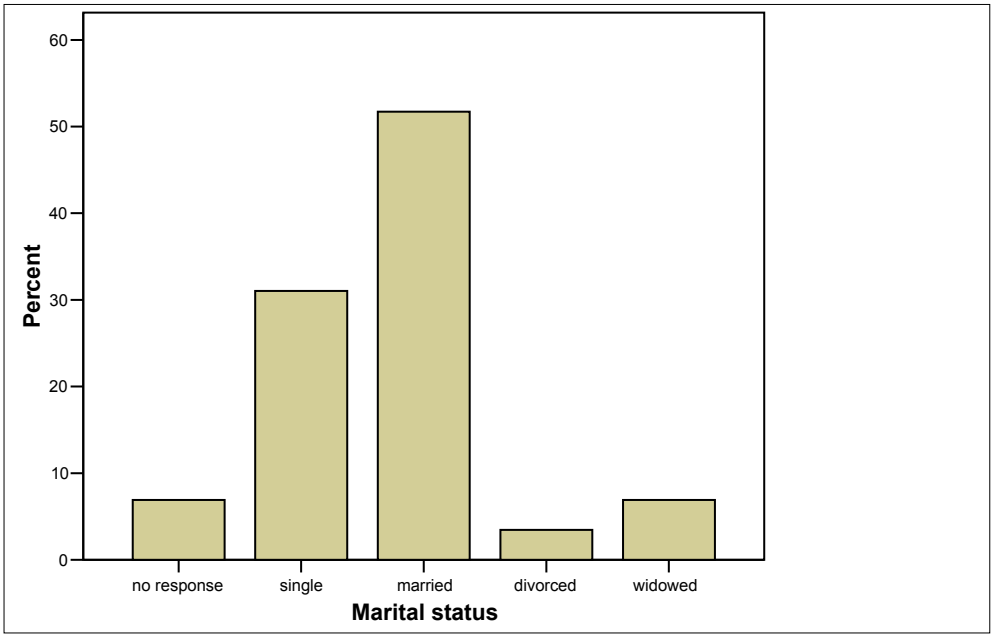

Figure 3: Marital status of the respondents

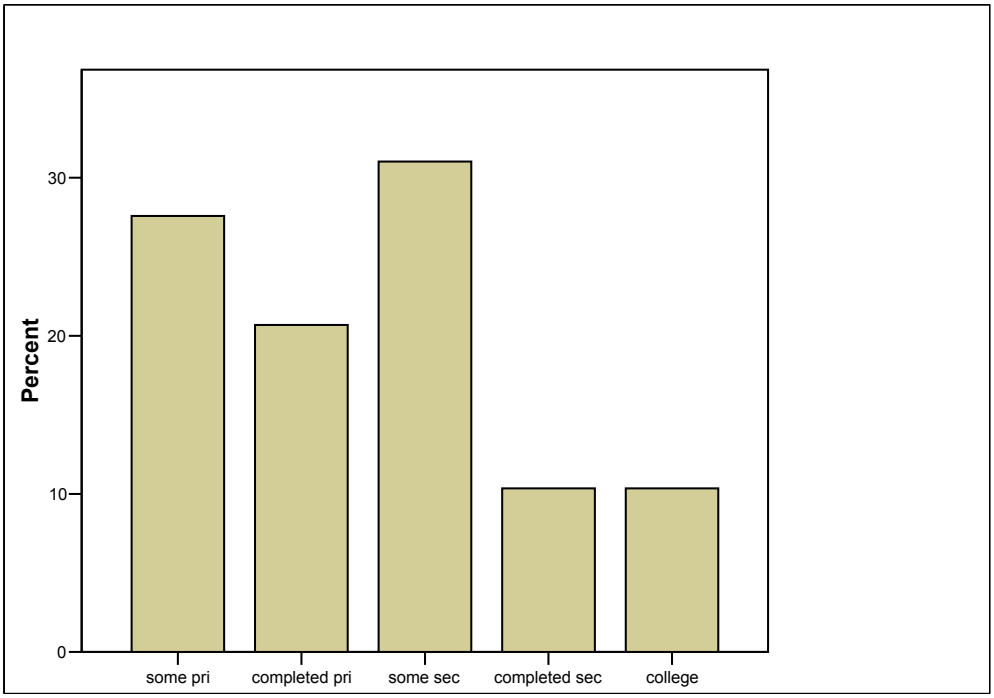

Figure 4: Educational status of the respondents

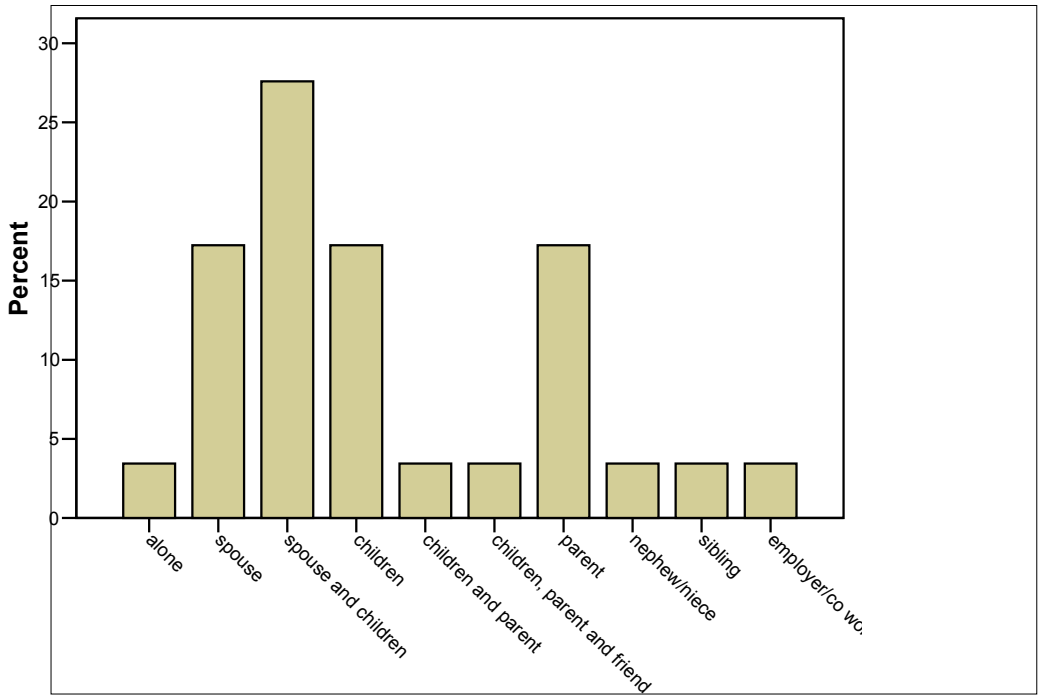

Figure 5: Living arrangement of the respondents.

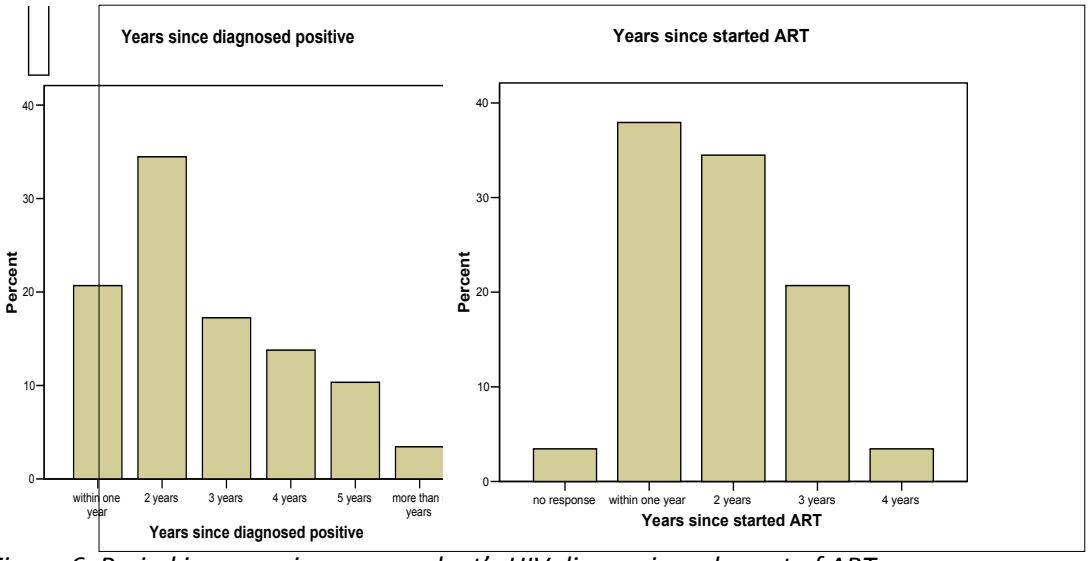

Figure 6: Period in years since respondent's HIV diagnosis and onset of ART

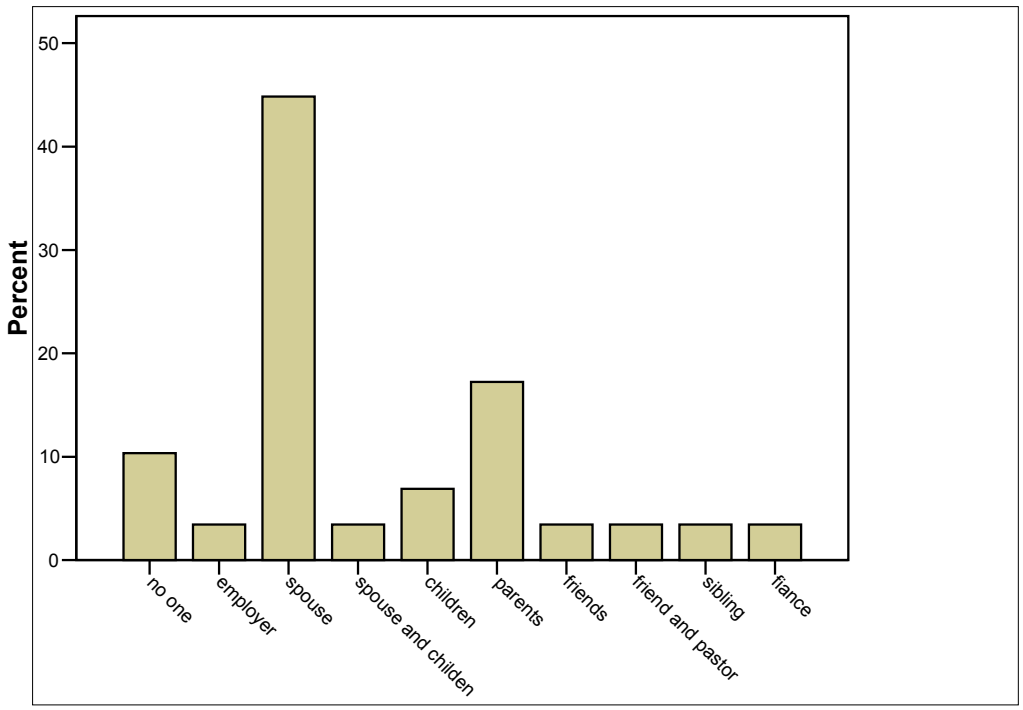

Figure 7: To whom the respondent had disclosed positive HIV status to

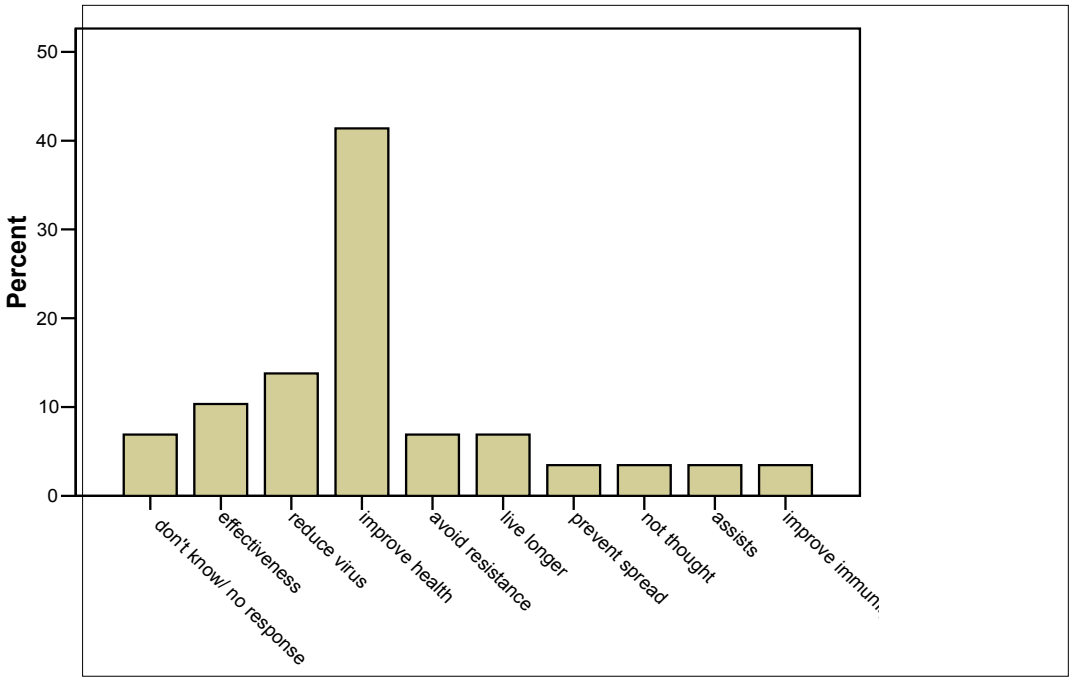

Figure 8: Why respondents think adherence to recommended ART regime is important

Annex 1

ADHERENCE QUESTIONNAIRE

1. Sex

Male ☐ Female ☐

2. Marital Status

Single ☐ Cohabiting ☐ Married ☐ Divorced ☐ Widowed ☐

3. Age

Under 20 ☐ 21-30 ☐ 31-40 ☐ 41-50 ☐ Over 50 ☐

4. Educational Status

Some primary ☐ Completed pri. ☐ Some sec. ☐ Completed sec. ☐ College ☐

5. Occupation

Fulltime ☐ contract ☐ Casual ☐ Business ☐ did not work ☐

6. Who lives with you in the same house?

Spouse ☐ Children ☐ Parent ☐ Friend ☐ nephew/niece ☐ *sibling* ☐ *co-workers employers* ☐

7. When were you diagnosed HIV positive?_____

<1 yr **1-2** **2-3** **3-4** **>5** **>10**

8. What was your reason for testing?

Sick ☐ ANC ☐ VCT ☐ Job ☐ Other ☐

9. When did you start ART (month/year)? _____

10. Have you disclosed your status to anybody?

Yes ☐ No ☐

11. Who have you disclosed to?

Health ☐ Spouse ☐ Children ☐ Parents ☐ Friend ☐ nephew/ niece ☐ workmates ☐ *sibling* ☐ *fiancé* ☐ *employer* ☐ *pastor/religious leader* ☐ worker ☐

12. Do people you live with know your status?

Yes ☐ No ☐

13. In the last 7 days have you taken your medicines as expected?

Yes ☐ No ☐

14. Of the last 14 doses (7 days) how many times have you missed your medication?

None ☐ 1-2 ☐ 3-4 ☐ 5 or more ☐

15. Why did you miss your medication?

_____

16. Of the last 14 doses (7 days) how many times were you late for more than 6 hours in taking your medication?

None ☐ 1-2 ☐ 3-4 ☐ 5 or more ☐

17. Why were late in taking your medication?

_____

18. Do the people you live with assist in adherence? Yes ☐ No ☐

19. Is there a relationship between disclosure and adherence?

Yes ☐ No ☐

20. If yes what is it?

_____

21. Why do you think adherence is important?

_____

VOLTAGE STABILITY ANALYSIS USING A MODIFIED CONTINUATION LOAD FLOW AND OPTIMAL CAPACITOR BANK PLACEMENT

C. M. Muriithi, L. M. Ngoo, G. N. Nyakoe and S. N. Njoroge
Department of Electrical and Electronics Engineering, Jomo Kenyatta University of Agriculture and Technology, Kenya
E-mail: cmmuriithi@eng.jkuat.ac.ke

Abstract
This paper addresses the rising problem of identifying the voltage stability limits of load buses in a power system and how to optimally place capacitor banks for voltage stability improvement. This paper uses the concept of the continuation power flow analysis used in voltage stability analysis. It uses the modified continuation load flow to plot the PV curves of a load bus with an aggregate induction motor load. Neuro-fuzzy techniques have been used to model the induction motor load which represents an industrial load. In the subsequent predictor-corrector stages, the induction motors are increased to depict increment in loading. Different motor ratings are used in the investigations. The process starts at some base values of the system and leading to the critical point. Further the reduced Jacobian is used to strategically locate the capacitor banks in the power system so as to effect maximum voltage improvement. In case study, illustrative examples with the IEEE 30 bus system are shown. The results indicate that the modified continuation load flow captures the active and reactive power consumption of the induction motors revealing cases which could lead to voltage instability. In general, the larger rated aggregated induction motors posed a greater voltage instability risk by demanding more reactive power at lower voltages compared the equivalent lower rated aggregated induction motors. In all, manipulation of the reduced Jacobian identified the optimal placement of capacitor banks for voltage stability improvement.

Key words: Continuation load flow, induction motors, voltage stability, neuro-fuzzy

1.0 Introduction

Modern power systems are becoming more complex and heavily loaded. The issue of voltage stability has thus raised serious concerns both in planning and operation of these systems. Moreover, a significant number of power system failures have been attributed to voltage instability (Kundur; 1994). Thus, it is becoming more and more important to develop Voltage Stability Analysis tools in our current Energy Management Systems. (Sivaramakrishnan *et al,* 2009)

The determination of the security margin is a key problem to be solved in voltage stability analysis. Closely related to this is the load model used in the analysis. It has been a common practice to use static loads, but for better estimation of security margins more accurate load models are being researched. It is revealed in (Ricardo *et al* 2002) that modeling industrial loads as motors allows better analysis of the system behavior and improves the ability to reveal voltage stability problems. In (Muriithi *et al.,* 2009), the conventional load flow algorithm has been modified to incorporate a neuro fuzzy model of an induction motor load (IM), which updates the reactive power and slip during each iteration. In this modification the reactive power of the IM load which is a function of its voltage is accurately estimated, which is not the case in the conventional load flow solution (Sadaat, 2002). This model is incorporated in the modified continuation load flow.
In the present power systems, it is a common to use capacitor banks for reactive power compensation in order to sustain continuous power system reliability. However, the use of these components is very expensive, much more for developing nations which face a myriad of other power system challenges. It is therefore paramount to strategically place capacitor banks in buses that will effect the greatest improvement it the overall voltage profile. In (Kundur, 1994) the reduced Jacobian is derived for V-Q sensitivity analysis. The continuation load flow using static load models and a simple manipulation of the reduced Jacobian has been used to determine the suitable bus for capacitor placement over a range of operating points. (Sivaramakrishnan *et al.,* 2009)

This paper demonstrates how the neuro-fuzzy model of the induction motor can be incorporated in the continuation load flow. Further, different induction motor ratings are used to plot the PV and QV curves. The results indicate that though the PV curves have almost similar maximum loading, the QV curves are different for various motor ratings. This is because large induction motors consume less reactive power at base values, but as loading continues, the consumption increases drastically leading to stressed buses in terms of voltage stability. During the continuation power flow, the buses evaluated as optimal for capacitor placement are determined.

The paper is organised as follows. Section 1 served as an Introduction. In section 2, we discuss the Mathematical Formulation, section 3, a case study using the IEEE 30 bus system is demonstrated; section 4, we outline the conclusions.

2.0 Mathematical Formulation

2.1 The Continuation Load Flow Algorithm

The method of continuation power flow (Kundur;1994, Venkataramana; 2006) is dealt with in brief in this section. The conventional power flow equations based on the Newton-Raphson (NR) method for a particular bus *i* are reformulated to contain a load parameter λ.

Let ***F*** be used to denote the whole set of equations, the problem can be expressed as

$$F(\underline{\partial},\underline{V},\lambda)=0$$
$$0\le\lambda\le\lambda_{critical} \quad \ldots\ldots (1)$$

where $\underline{\delta}$ represents the vector of bus voltage angles and $\underline{V}$ represents the vector of bus voltage magnitudes.

The starting solution, also known as the base case solution, is determined from the conventional load flow solution. The subsequent solutions are sought over a range of *λ.* The dimension of F is $2n_1 + n_2$, where n_1 and n_2 are the number of *P-Q* and *P-V* buses respectively.

From the base case solution, subsequent solutions are obtained using a predictor-corrector scheme at different load levels. The corrector is a slightly modified NR power flow, while the predictor is discussed below.

Based on the starting solution, (*λ = 0*), a prediction of the next solution can be made by taking an appropriately sized step in a direction tangent to the solution path. The first step in the predictor stage is to determine the tangent vector. To obtain this, the derivative of both sides of the power flow equations is taken (2) and factorized (3).

$$d[F(\underline{\delta},\underline{V},\lambda)]=F_{\underline{g}}d\underline{\delta}+F_{\underline{y}}d\underline{V}+F_{\lambda}d\lambda=\underline{0} \quad \ldots\ldots (2)$$

$$\begin{vmatrix}F_{\delta} & F_{V} & F_{\lambda}\end{vmatrix}\begin{vmatrix}d\underline{\delta}\\ d\underline{V}\\ d\lambda\end{vmatrix}=\underline{0} \quad \ldots\ldots (3)$$

The resulting equation (3) is simply the conventional Jacobian derived in subsequent iterations of the NR method. The only difference is that there is an additional column (F_{λ}). The right hand side of the equation is the tangent vector to be calculated. In order to obtain a unique solution for the vector tangent, an additional equation is added. This is accomplished by choosing a non-zero

magnitude for one of the components of the tangent vector, resulting in equation (4).

$$\begin{vmatrix} \underline{F}_{\underline{\delta}} & \underline{F}_{\underline{V}} & \underline{F}_{\lambda} \\ & \underline{e}_k & \end{vmatrix} \begin{vmatrix} \underline{t} \end{vmatrix} = \begin{vmatrix} \underline{0} \\ \pm 1 \end{vmatrix} \quad \text{.....(4)}$$

Where $\underline{e}_k$ is an appropriately dimensioned row vector with all elements equal to zero except the k^{th}, which equals one. By choosing k correctly, and letting $t_k = \pm 1$ imposes a non-zero norm on the tangent vector. This guarantees that the augmented Jacobian will be non-singular at the critical point and enables the solution to be achieved over the entire range of λ. Having obtained the tangent vector, the prediction for the next solution is made in accordance with equation (5).

$$\begin{vmatrix} \underline{\delta}^* \\ \underline{V}^* \\ \lambda^* \end{vmatrix} = \begin{vmatrix} \underline{\delta} \\ \underline{V} \\ \lambda \end{vmatrix} + \sigma \begin{vmatrix} d\underline{\delta} \\ d\underline{V} \\ d\lambda \end{vmatrix} \quad \text{.....(5)}$$

where "*" is the predicted solution for a subsequent value of λ, while σ is a scalar that designates the step size.

2.2 Incorporating The Continuation Load Flow to Neuro-Fuzzy Model of an Induction Motor Load

Having briefly load at the continuation load flow, we now consider the introduction of an induction motor load into its algorithm.

In the base case solution, the induction motor load is determined from the base scheduled active power at the *P-Q* bus with an induction motor load. Based on this power, the number of motors to be aggregated is determined by dividing the scheduled power with the horse power rating of the induction motor being investigated.

During the subsequent operating points ($\lambda \neq 0$) the motor load change is brought about by a change in the load parameter λ as per the equation (6).

$$P_{Li} = P_{i0} + \lambda(K_{Li} S_{\Delta base} \cos\psi_i) \quad \text{.....(6)}$$

where;

P_{Li0}, Q_{Li0} – original load at bus *i*, active and reactive respectively.

K_{Li} - multiplier to designate the rate of load change at bus *i* as λ changes.

ψ_i - power factor angle of load change at bus i.

$S_{\Delta base}$ - a given quantity of apparent power which is chosen to provide appropriate scaling of λ.

Based on the newly updated scheduled power, the number of motors to be aggregated in the induction motor load is again determined as previously mentioned.

The motors are then aggregated using appropriate formulas well elaborated in (Pillay et al; 1997). Figure 1 shows the equivalent circuit of the aggregated induction motor load.

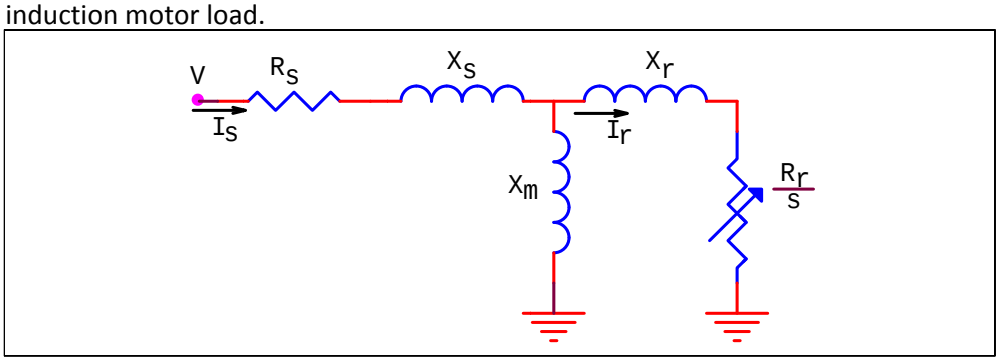

Figure 1: Per Phase equivalent circuit (squirrel-cage)

The slip curves derived at different load bus voltages for the aggregated induction motor are shown in Figure 2. Also show is the mechanical power as a function of the slip.

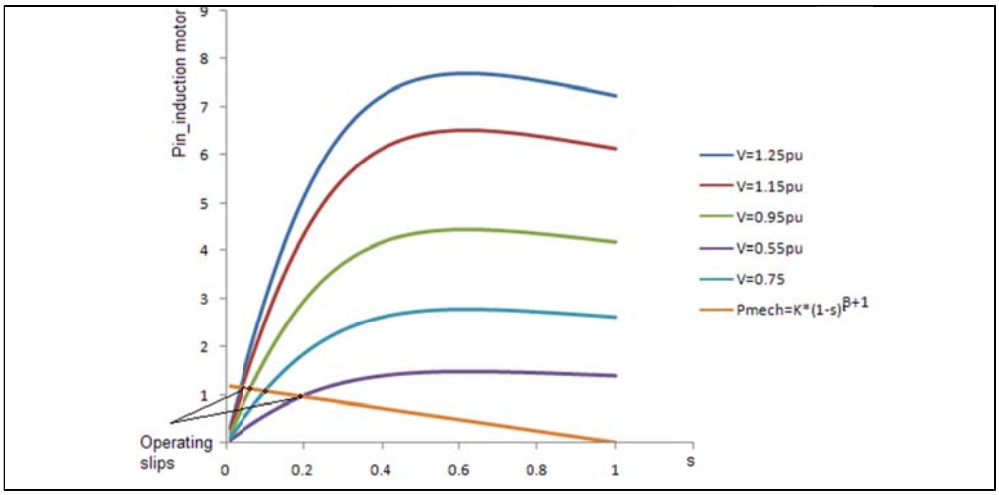

Figure 2. Electrical and Mechnical Power Slip Curves

To get neuro-fuzzy model of an induction motor load, the power balance equation (7) at the operating slips which is non-linear is solved to get the operating slip at each voltage.

$$P_{elect} - P_{mech} = 0 \quad \text{.....(7)}$$

The operating slip is used to calculate the active and reactive power consumed at the load bus at each voltage . The Artificial Neuro Fuzzy Inference System is used to model the induction motor load. This is achieved by mapping the active and reactive power at operating slips to the respective voltages. The algorithm for creating the neuro-fuzzy model of the induction motor as detailed in (Muriithi et al; 2009) is summarized in Figure A1 in the appendix.

The neuro-fuzzy model of the induction motor is stored and is used to update the active and reactive powers during the iterative process of the corrector stage at each subsequent operating point.

2.3 The Reduced Jacobian Technique for Optimal Capacitor Bank Placement

The technique is carried out by a simple manipulation of the elements of the reduced Jacobian. The reduced Jacobian (Kundur; 1994) is formulated from the Jacobian of the NR load flow. A brief description of the formulation of the reduced Jacobian is given below.

The NR method aids to develop the linearized equation (8).

$$\begin{bmatrix} \Delta P \\ \Delta Q \end{bmatrix} = \begin{bmatrix} J_1 & J_2 \\ J_3 & J_4 \end{bmatrix} \begin{bmatrix} \Delta\Theta \\ \Delta V \end{bmatrix} \quad \text{.....(8)}$$

where

P and *Q* are the active and reactive power injections respectively,
V and θ are voltage magnitudes and bus angles, respectively,
Δ*P* and Δ*Q* is the active and reactive power mismatches respectively,
Δθ and Δ*V* is the change in bus angle and bus voltage magnitude respectively.

The reduced Jacobian assumes that there is no change in the active load. Thus by substituting ΔP = 0 into (8), we get

$$J_1\Delta\Theta + J_2\Delta V = 0 \quad \text{..... (9)}$$

$$J_3\Delta\Theta + J_4\Delta V = \Delta Q \quad \text{.....(10)}$$

By appropriate mathematical manipulations we get

$$\Delta Q = (J_4 - J_3 J_1^{-1} J_2)\Delta V \quad \text{.....(11)}$$

$$\Delta Q = J_R \Delta V \quad \text{.....(12)}$$

$$\Delta V = J_R^{-1} \Delta Q \quad \text{.....(13)}$$

where J_R is reduced Jacobian.

Equation (13) describes the relationship of change in the voltage magnitude Δ*V* the in terms of reactive power mismatch Δ*Q* (Sivaramakrishnan et al; 2009). In this case, Δ*Q* models a vector change in reactive power, while Δ*V* represents the resulting vector of change in the voltage magnitude.

From matrix algebra, it can be shown that the elements in each column of the inverse matrix J_R^{-1} can be made to represent the change in voltage of every load bus for a given injection of reactive power into the bus corresponding to that column (Sivaramakrishnan et al; 2009). This can be done by invoking the superposition theorem for equal reactive power injection in all the load buses. The summation of the elements of column *i* of J_R^{-1} is carried out during each stage of

the reactive power injection to a bus *i*. The sum represents the total system voltage improvement ΔV_{totali} due to the injection at the bus *i.*

The column that results in maximum ΔV_{totali} due to the injection of reactive power is deemed as the appropriate bus index to place the capacitor banks.

$$bus_i : \Delta V_{total_i} = \max\left\{\Delta V_{total_1}, \Delta V_{total_2}, \Delta V_{total_3}\right\} \quad \text{.....(14)}$$

2.4 Case Study – IEEE 30 Bus System

2.5 System Model

We used the IEEE 30 bus system shown in Figure A2 in the Appendix, for the case study. The load bus data and line data are given in Table A1 and 2 respectively in the Appendix.

3.0 Simulation Results and Discussion

3.1 The Modified Continuation Load Flow

The continuation load flow was carried out using the IEEE 30 bus system. The algorithm was based on the equations formulated in section 2. Bus 26 was selected as the industrial load whose induction motors were increased to depict increment in loading. Based on (Pillay, 1997) the aggregate motor model and parameters were obtained from individual motors whose parameters are shown in Table A3 as found in (Franklin et al., 1997, Aree, 2006).

The number of induction motors to be aggregated was calculated from the scheduled active power at the predicted operating point at each step of the continuation load flow. Based on the aggregate motor parameters obtained, the IM load was then modeled using Artificial Neuro Fuzzy inference system as described in section 2 using the algorithm in Figure A1. The Neuro fuzzy model of the induction motor was then used in the predictor-corrector stages of the solution. This process was conducted until all the operating points were calculated.

Figure 3 shows the PV curves for the industrial load, while Figure 4 shows the QV curves for the same load bus.

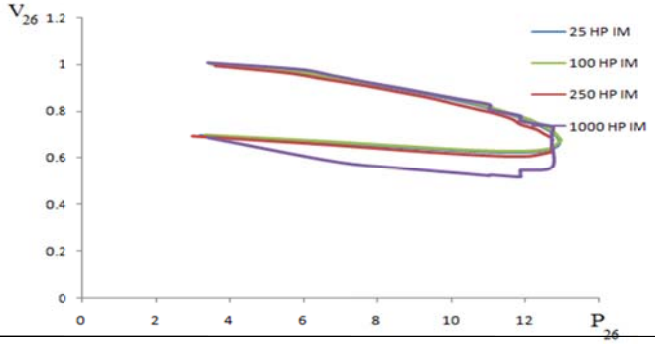

Figure 3: PV curve for bus 26 with different induction motor ratings

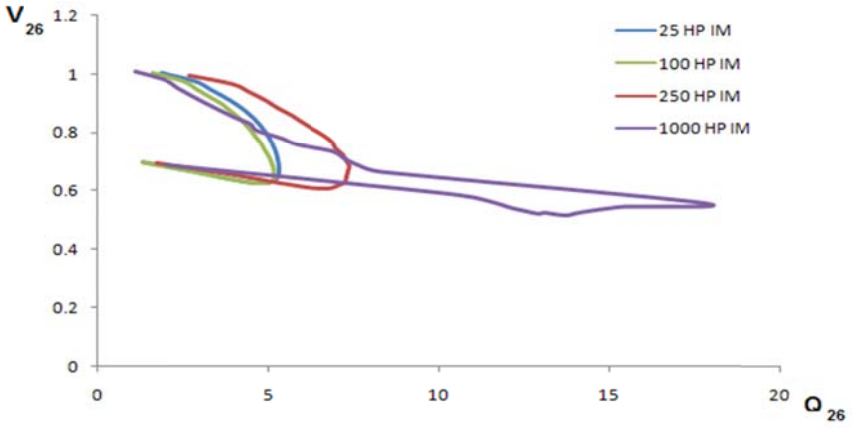

Figure 4: QV curve for bus 26 with different induction motor ratings

3.2 Optimal Capacitor Bank Placement

Based on the reduced Jacobian technique the optimal bus to place a capacitor bank was determined as shown in Figure 5.

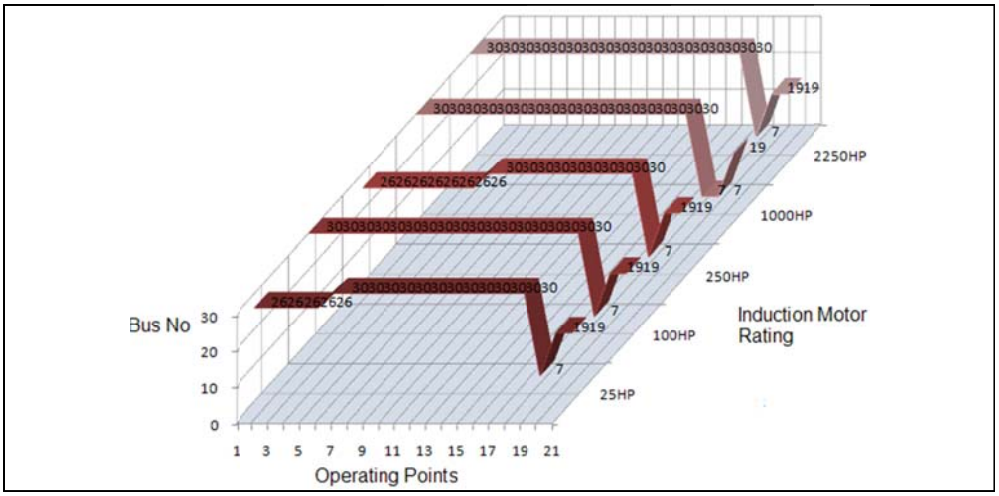

Figure 5: Optimal capacitor bank placement over operating points range

4.0 Conclusion

The modified continuation load flow with a neuro-fuzzy induction motor clearly shows that though the PV curves have almost similar maximum operating points, the QV curves are significantly different for different motors. This is because an induction motor load indicated that larger motors operate at low slips in normal rated operations, and hence consume less reactive power. But as the operating points move towards the critical loading and lower voltages, the larger motors drew more reactive power and hence posed as a greater threat to voltage stability of a system compared to their smaller counter parts. Thus depending on the induction motor ratings connected to a particular industrial load, the voltage stability risk is different.

The smoothness of the PV curve is distorted when large motors are added to depict increment in loading. This is because while in the normal continuation load flow, load increment is performed in small steps, in this modified algorithm, the increment is depicted by the individual horse power ratings of the induction motors being aggregated. Smaller increments lead to a smooth curve, while the large motor ratings are bound to distort that smoothness.

The reduced Jacobian technique successfully allocated the optimal bus for capacitor placement at each of the operating points plotted by the continuation power flow. This is important since it identifies the bus (buses) to place capacitor banks for effective voltage recovery for a particular operating point given a particular industrial load.

References

Aree P. (2006). *Load flow solution with induction motor*, Songklanakarin J. Sci. Technol., (28), **1** , pp 157-168.

Franklin D. C., Morelato A. (1994). *Improving Dynamic Aggregation of Induction Motor Models*, IEEE Transactions on Power Systems., **9**, pp. 1934-194.

Kundur P. (1994). *Power System Stability and Control*, McGraw-Hill, pp. 959-1022.

Muriithi C. M., Ngoo L. M., Nyakoe GN (2009). *Load Flow Analysis With A Neuro-Fuzzy Model Of An Induction Motor Load*, IEEE AFRICON.

Pillay P., Sabur S., M. A., Haq M. M. (1997). A Model for Induction Motor Aggregation for Power System Studies. Electrical Power Syst. Res. pp 225-228.

Ricardo M. H., Nelson M., Julio C. R. F., Antonio C. B. M., Herminio J. C. P. P and Sandoval C. Jr (2002). Impact of Induction motor Loads into Voltage Stability Margins of Large Systems –Rio Area Analysis, VIII SEPOPE.

Sadaat Hadi (2002). Power System Analysis, McGraw-Hill pp. 691.

Sivaramakrishnan R. Amit J. Ramamoorty M. Ashok V (2009). A Methodology for Selective Localization of Capacitor Banks for Power Systems, Third International Conference on Power Systems, Kharagpur, pp 318.

Venkataramana A. (2006). Lowa State University, Computational techniques for voltage stability assessment and control, Springer, pp 51-115

Appendix

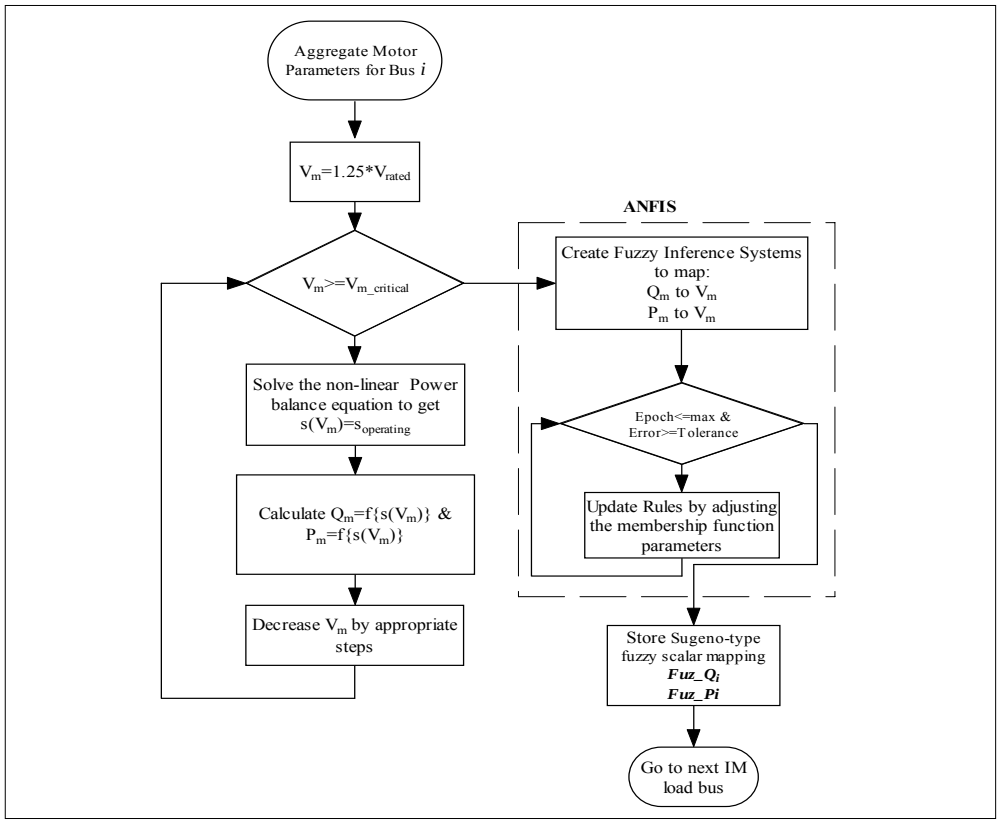

Figure A1: Algorithm for creating the neuro-fuzzy model of the induction motor

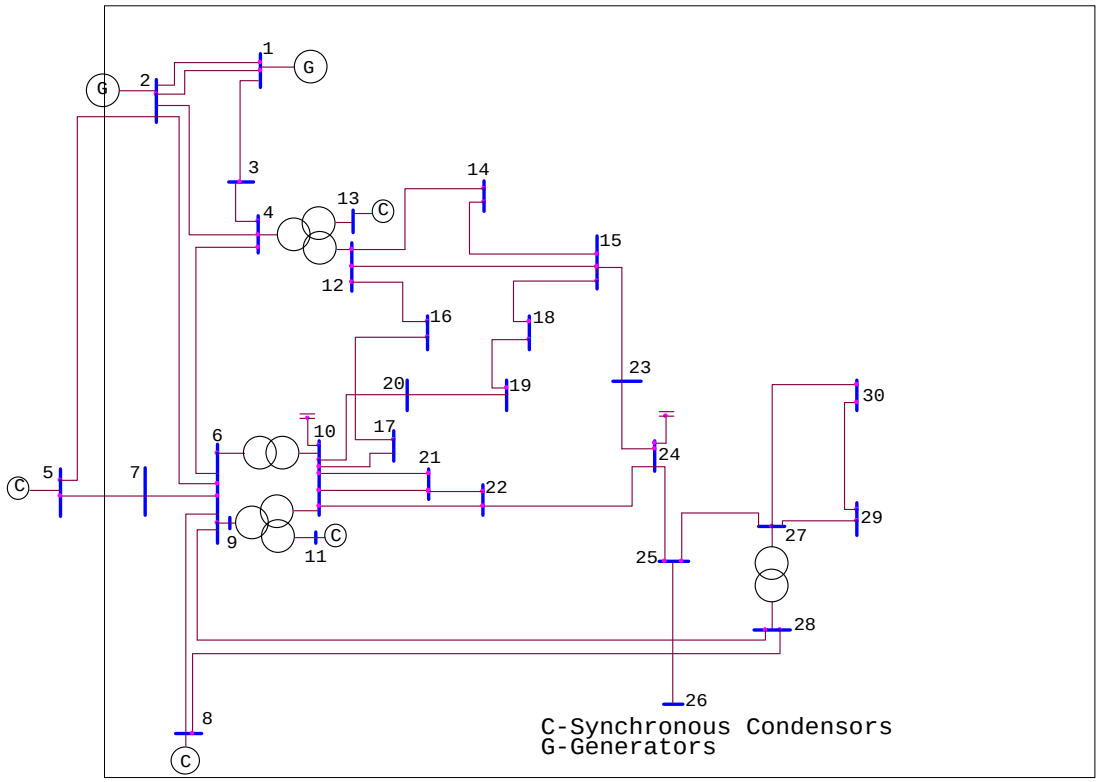

Figure A2: IEEE 30-bus system

Table A1: IEEE 30 Bus system Load Bus Data

Bus No	Load MW	MVAr
2	21.7	12.7
3	2.4	1.2
4	7.6	1.6
5	94.2	19
7	22.8	10.9
8	30	30
10	5.8	2
12	11.2	7.5
14	6.2	1.6
15	8.2	2.5
16	3.5	1.8
17	9	5.8
18	3.2	0.9
19	9.5	3.4
20	2.2	0.7
21	17.5	11.2
23	3.2	1.6
24	8.7	6.7
26	3.5	2.3
29	2.4	0.9
30	10.6	1.9

Table A2: IEEE 30 Bus system Line Data

Bus No	Bus No	R pu	X pu	B/2 pu	Transformer tap setting
1	3	0.0452	0.1852	0.0204	1
2	4	0.057	0.1737	0.0184	1
3	4	0.0132	0.0379	0.0042	1
2	5	0.0472	0.1983	0.0209	1
2	6	0.0581	0.1763	0.0187	1
4	6	0.0119	0.0414	0.0045	1
5	7	0.046	0.116	0.0102	1
6	7	0.0267	0.082	0.0085	1

Table A2: Cont'd

Bus No	**Bus No**	**R** pu	**X** pu	**B/2** pu	**Transformer tap setting**
6	8	0.012	0.042	0.0045	1
6	9	0	0.208	0	0.978
6	10	0	0.556	0	0.969
9	11	0	0.208	0	1
9	10	0	0.11	0	1
4	12	0	0.256	0	0.932
12	13	0	0.14	0	1
12	14	0.1231	0.2559	0	1
12	15	0.0662	0.1304	0	1
12	16	0.0945	0.1987	0	1
15	18	0.1073	0.2185	0	1
18	19	0.0639	0.1292	0	1
19	20	0.034	0.068	0	1
10	20	0.0936	0.209	0	1
10	17	0.0324	0.0845	0	1
10	21	0.0348	0.0749	0	1
10	22	0.0727	0.1499	0	1
21	22	0.0116	0.0236	0	1
15	23	0.1	0.202	0	1
22	24	0.115	0.179	0	1
23	24	0.132	0.27	0	1
23	24	0.132	0.27	0	1
24	25	0.1885	0.3292	0	1
25	26	0.2544	0.38	0	1
25	27	0.1093	0.2087	0	1
28	27	0	0.396	0	0.968
27	29	0.2198	0.4153	0	1
27	30	0.3202	0.6027	0	1
27	30	0.3202	0.6027	0	1
29	30	0.2399	0.4533	0	1
8	28	0.0636	0.2	0.0214	1
6	28	0.0169	0.0599	0.065	1
14	15	0.221	0.1997	0	1
16	17	0.0824	0.1923	0	1

Table A3. Induction motor parameters based on individual Horse Powers (HP) (f=60Hz)

HP	Rs	Rr	Xs	Xr	Xm
25	0.0219	0.0472	0.0498	0.0498	1.9504
100	0.0109	0.0472	0.0532	0.0532	2.5121
250	0.0241	0.0141	0.0864	0.864	3.0263
1000	0.0158	0.0104	0.0851	0.0851	7.6343

MODELING FLUID FLOW IN OPEN CHANNEL WITH CIRCULAR CROSS-SECTION

M. N. Kinyanjui, D. P. Tsombe, J. K. Kwanza and K. Gaterere
Department of Pure and Applied Mathematics, Jomo Kenyatta University of Agriculture and Technology, Kenya
E-mail:

Abstract
Flow in a closed conduit is regarded as open channel flow, if it has a free surface. This study considers unsteady non-uniform open channel flow in a closed conduit with circular cross-section. We investigate the effects of the flow depth, the cross section area of flow, channel radius, slope of the channel, roughness coefficient and energy coefficient on the flow velocity as well as the depth at which flow velocity is maximum. The Saint-Venant partial differential equations of continuity and momentum governing free surface flow in open channels are highly nonlinear and therefore do not have analytical solutions. The Finite Difference Approximation method is used to solve these equations because of its accuracy, stability and convergence. The results are presented graphically. It is established that for a given flow area, the velocity of flow increases with increasing depth and that the velocity is maximum slightly below the free surface. Moreover, increase in the slope of the channel and energy coefficient leads to an increase in flow velocity whereas increase in roughness coefficient, flow depth, radius of the conduit and area of flow leads to a decrease in flow velocity.

Key words: open-channel flow, free surface, saint-venant equation, finite difference method

Nomenclature

Symbol	*Quantity*
V	Mean velocity of flow (m/s)
L	Length of the channel (m)
g	Acceleration due to gravity (ms^{-2})
Q	Discharge (m^3s^{-1})
A	Cross- sectional area of flow (m^2)
n	The Manning coefficient of roughness ($sm^{-1/3}$)
S_o	Slope of the channel bottom
S_f	Friction slope
P	Wetted perimeter of the channel cross section (m)
T	Top width of the free surface (m)
y	Depth of the flow (m)
t	Time (s)
q	Lateral/uniform inflow (m^2s^{-1})
R	Hydraulic Radius (m)
x	Distance along the main flow direction (m).
Fr	Froude number (dimensionless)
Re	Reynolds number (dimensionless)
D	Hydraulic depth (m)
v	Kinematic viscosity (m^2/s)
α	Energy coefficient
r	Channel radius (m)

1.0 Introduction

Water flows more rapidly on a steeper slope, but for a constant slope, the velocity reaches a steady value when the gravitational force is equal to the resistance to flow. Over the years, man has endeavoured to direct water to the desired areas

such as farms, where it is used for irrigation. He has also tried to draw water from storage sites such as reservoirs, dams and lakes. To achieve this objective, he has constructed open channels which are physical systems in which water flows with a free surface.

The cross-section of these channels may be open or closed at the top. The structures with closed tops are referred to as closed conduits while those with open tops are called *open channels*. This study focuses on open channel flow in a closed conduit with circular cross-section. The findings of this study will go a long way in providing reference for designers of open channel projects and guidelines for the hydraulic analysis and design of open channel flows. In addition, it will provide an understanding into the propagation of flood wave in natural rivers, originating from torrential rains or of breaking of a control structure.
Open channel flow is a familiar sight, whether in a natural channel like that of a river, or an artificial channel like that of an irrigation ditch. Its flow is a complex when everything is considered, especially with the variability of natural channels, but in many cases the major features can be expressed in terms of only a few variables, whose behavior can be described adequately by a simple theory. The principal forces at work are those of inertia, gravity and viscosity, each of which plays an important role.

Open channels have been a subject of study for a long time. The Chézy equation is one of the earliest procedures developed in 1768 by a French Engineer, Henderson. The development of this equation was based on the dimensional analysis of the friction equation under the assumption that the condition of flow is uniform. Chézy's formula did not provide results that satisfied engineers. The Swiss engineers Ganguillet E. and Kutter W. R. in 1869 showed that much better results could be obtained if the constant C depended on R, S_o and a constant n that was characteristic of the roughness of the channel.

A more practical procedure was presented in 1889 by the Irish engineer Manning R., Chow (1959). Studies in open channel flows have to take into account the coefficient of roughness, called the *Manning coefficient.* The Manning coefficient takes into account the bed materials, degree of channel irregularity, variation in shape and size of the channel and relative effect of channel obstruction, vegetation growing in the channel and meandering, Chadwick (1993). This makes the Manning equation more desirable for the design of open channels.

Akbari G. and Firoozi B. (2010) investigated two different numerical methods, namely; Preissmann and Lax diffusive schemes for numerical solution of Saint-Venant equations that govern the propagation of flood wave, in natural rivers, with the objective of the better understanding of this propagation process. The

results showed that the hydraulic parameters play an important role in the flood wave propagation.

Moshirvaziri S. *et al* (2010) examined numerically, the nature of pollutant connectivity between unsealed forest roads and adjacent nearby streams in terms of spatial and temporal patterns of runoff generation, erosion, and sediment transport with an aim of improving our ability to scale-up the impacts of forest roads on catchment water quality in future works. They considered the relative effects of rainfall intensity and duration, surface roughness, infiltration rate, sediment detachment and transport with an objective of identifying the dominant processes and parameters that affect the degree of pollutant connectivity between roads and streams.

Kwanza, J. K. *et al*. (2007) analyzed the effects of channel width, slope of the channel and lateral discharge on fluid velocity and channel discharge for both rectangular and trapezoidal channels. They noted that the discharge increases as the specified parameters are varied upwards. Chagas and Souza (2005) sought to provide solution of Saint Venant's Equation to study flood in rivers through Numerical Methods. They used a discretization, for the equations that governs the propagation of a flood wave, in natural rivers, with the objective of a better understanding of this propagation process. Their results showed that the hydraulic parameters play an important role in the propagation of a flood wave.

Khan A. A. (2000) studied open channel flow over an initially dry bed with the aim of better understanding of flow over islands during rising flood stage, flow downstream of the hydraulic structures (such as dams and gates) during intermittent release of water, and flood wave, either due to natural causes or sudden failure of a hydraulic structure, over an initially dry bed. Tuitoek and Hicks (2001) modeled unsteady flow in compound channels with an aim of controlling floods.

2.0 Mathematical Formulation

The basic equations that describe unsteady one-dimensional fluid flow in an open channel are the Saint Venant equations, which consist of continuity and momentum equations. In the development of the mathematical model, some simplifications are made: the flow is considered one-dimensional, the distribution the pressure in the vertical is a hydrostatic one, the fluid considered is water. The fluid is assumed incompressible and homogeneous. Thus for prismatic channels of arbitrary shape, the model equation, which consists of the continuity and momentum equation, is defined as:

$$\frac{\partial Q}{\partial x} + \frac{\partial A}{\partial t} = q \qquad (1)$$

$$\frac{\partial V}{\partial t} + \alpha V \frac{\partial V}{\partial x} + g \frac{\partial y}{\partial x} = g(S_o - S_f) \quad (2)$$

Given the velocity, the discharge (Q) is calculated as the product of velocity and cross-sectional area

$$Q = AV \quad (3)$$

Substituting equation (3) in equation (1) above and then differentiating partially w.r.t x yields:

$$V \frac{\partial A}{\partial x} + A \frac{\partial V}{\partial x} + \frac{\partial A}{\partial t} - q = 0 \quad (4)$$

The flow area is assumed to be a known function of the depth; therefore derivatives of A may be expressed in terms of y as:

$$\frac{\partial A}{\partial x} = \frac{dA}{dy}\frac{\partial y}{\partial x} = T \frac{\partial y}{\partial x} \quad (5)$$

$$\frac{\partial A}{\partial t} = \frac{dA}{dy}\frac{\partial y}{\partial t} = T \frac{\partial y}{\partial t} \quad (6)$$

In this discussion, it is assumed that T is as determined by Franz (1982)

$$T = \frac{dA}{dy} \quad (7)$$

Substituting equations (5) and (6) in equation (4) yields:

$$\frac{\partial y}{\partial t} + \frac{A}{T}\frac{\partial V}{\partial x} + V \frac{\partial y}{\partial x} - \frac{q}{T} = 0 \quad (8)$$

3.0 Method of solution

The objective of this paper is to investigate the effects of the various flow parameters on the velocity profiles of a fluid flow in an open channel with circular cross section area as shown in figure A below

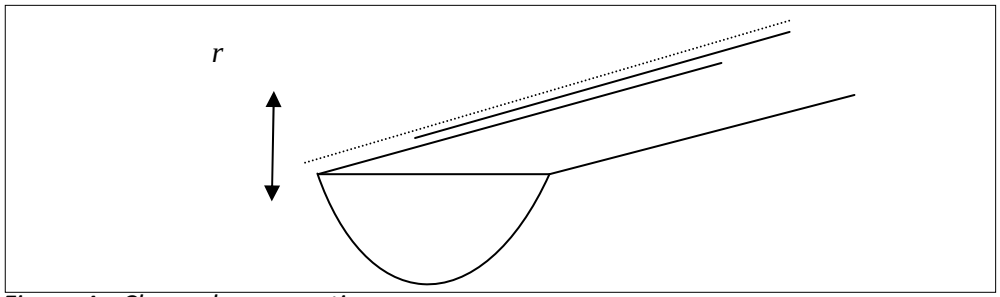

Figure A: Channel cross section

An analysis of the effects of the various parameters on the flow velocity has been carried out. The equations governing the flow considered in the problem are non-linear and therefore to obtain their solutions, an efficient finite difference scheme was developed. The mesh used in the problem considered in this work is divided uniformly.

Equations (2) and (8) are non-linear first order partial differential equations of the hyperbolic type. It is not possible to solve these equations analytically thus the finite difference method is used to obtain approximate solutions. In this technique, the numerical solution of equations (2) and (8) is approximated at a discrete number of points arranged to form a rectangular grid. This rectangular grid is obtained by dividing the (x, t) plane into a network of rectangles of sides Δx and Δt. The nodes or mesh points or grid points of the network occur at the intersections of straight lines drawn parallel to the x and t axes. We are assuming the grid size is uniform along each axis. For brevity, we will call the $i\Delta x$ grid point i and the $(i + 1)\Delta x$ grid point $i + 1$. For the time axis, we will call $j\Delta t$ grid point j and the $(j + 1)\Delta t$ grid point $j + 1$. To refer to different variables at these grid points, we use the number of the spatial grid and that of the time grid as the first and second subscript respectively. We denote the known time level by j and the unknown time level by $j + 1$. The primary difficulty with explicit finite difference techniques is the problem of numerically unstable solutions. The partial derivatives in the equations are replaced by their corresponding finite difference approximations. However, Viessman *et al*. (1972) noted that more stable solutions can be obtained if a diffusing difference approximation is used. Using this scheme, equations (8) and (2) become:

$$\frac{y(i,j+1) - 0.5(y(i-1,j) + y(i+1,j))}{\Delta t} + \frac{A}{T}\frac{V(i+1,j) - V(i-1,j)}{2\Delta x} + V(i,j)\frac{y(i+1.j) - y(i-1,j)}{2\Delta x} - \frac{q}{T} = 0 \quad (9)$$

$$\frac{V(i,j+1) - 0.5\big(V(i-1,j) + V(i+1,j)\big)}{\Delta t} + \alpha V(i,j)\frac{V(i+1,j) - V(i-1,j)}{2\Delta x} + g\frac{y(i+1,j) - y(i-1,j)}{2\Delta x} - g\left(S_0 - \frac{S_f(i-1,j) + S_f(i+1,j)}{2}\right) = 0 \quad (10)$$

From equation (9)

$$y(i,j+1) = 0.5[y(i-1,j) + y(i+1,j)] - \Delta t\left\{\frac{A}{T}\frac{V(i+1,j) - V(i-1,j)}{2\Delta x} + V(i,j)\frac{y(i+1,j) - y(i-1,j)}{2\Delta x} - \frac{q}{T}\right\} \quad (11)$$

In the computation of unsteady flow, it is usually assumed that the friction slope S_f can be estimated from either the Manning or Chezy resistance equations. The Manning resistance equation is as follows:

$$S_f = \frac{n^2 V^2}{R^{4/3}} \quad (12)$$

Substituting equation (12) in equation (10), it is possible to find

$$V(i,j+1) = 0.5[V(i-1,j) + V(i+1,j)] - \Delta t\left\{\alpha V(i,j)\frac{V(i+1,j) - V(i-1,j)}{2\Delta x} + g\frac{y(i+1,j) - y(i-1,j)}{2\Delta x} - g\left[S_0 - \frac{n^2}{2R^{4/3}}\left(V^2(i-1,j) + V^2(i+1,j)\right)\right]\right\} \quad (13)$$

In equations (11) and (13), the index i refers to spatial points whereas the index j refers to time. The consecutive terms of depth and velocities $y_{i,j+1}$ and $V_{i,j+1}$ respectively are computed by equations (11) and (13) subject to the initial and boundary conditions

$$V(x,0) = 10\,, \quad y(x,0) = 0.5 \quad \text{for all } x > 0 \quad (14)$$

$$V(0,t) = 10\,, \quad y(0,t) = 0.5 \quad \text{for all } t > 0 \quad (15)$$

$$V(x_l,t) = 10\,, \quad y(x_l,t) = 0.5 \quad \text{for all } t > 0 \quad (16)$$

The computations are performed using small values of Δt. In our research, we set $\Delta t = 0.0012$ *and* $\Delta x = 0.1$. From equation (11), the depth y at the end of the time step $\Delta t, y_{i,j+1}$ $i = 1,2,3,\ldots,40$ is computed in terms of velocities and depths at points on earlier time step. Similarly, $V_{i,j+1}$ is also to be computed from equation (13). The procedure repeated till $j = 50$.

4.0 Discussion of the Results

From figure 1, we observe that for a fixed flow area the flow velocity increases with increase in depth from the bottom of the channel to the free stream and that maximum velocity occurs just below the free surface. The free surface occurs at a depth of 0.5m and the velocity of the fluid layer at this depth is 10m/s. It is also observed that maximum velocity occurs just below the free surface, at a depth of about 0.38m.

The flow velocity in a channel section varies from one point to another due to shear stress at the bottom and at the sides of the channel. The velocity is not maximum at the free surface mainly due to surface tension caused by the strong cohesive forces between the liquid molecules. In the bulk of the liquid, each molecule is pulled equally in every direction by neighboring liquid molecules, resulting in a net force of zero. The molecules at the free surface do not have other molecules surrounding them entirely and are therefore pulled inwards. This creates some internal pressure and forces liquid surfaces to contract to the minima leading to a reduction in velocity at the free stream. On the other hand, both the atmospheric pressure and gravity acting in a direction that is perpendicular to the free surface creates some internal pressure causing the contraction of the liquid surface. This contraction lowers the movement of the fluid particles at the free surface resulting in reduced velocities. In addition, the wind blowing over the free surface also affects the velocity in the free stream due to frictional resistance particularly when wind blows over the free surface at high velocities and in the opposite direction to the main direction of flow.

From figure 2, we observe that a reduction in the slope from 0.02 m/m to 0.004 m/m leads to a decrease in the flow velocity as shown from curve I to curve II. An increase in the cross sectional area of flow from 0.6144 m^2 to 1.5712 m^2 results to a decrease in the flow velocity from curve I to curve III.

Manning's velocity formula shows a direct relationship between flow velocity and the slope. Thus a decrease in slope results in a decrease in the flow velocity. An increase in the cross-sectional area of flow leads to an increase in the wetted perimeter. A large wetted perimeter results in high shear stresses at the sides of the channel which results in a reduction in the flow velocity.

From figure 3, we observe that increasing the radius from 1 m to 3 m results in a decrease in the flow velocity from curve I to curve II. Moreover, an increase in the roughness coefficient from 0.012 to 0.029 also results in a reduction in the flow velocity as shown from curve I to curve III.

An increase in the radius results in an increase in the wetted perimeter because the fluid will spread more in the conduit. A large wetted perimeter will result in large shear stresses at the sides of the channel and therefore the flow velocity will

be reduced. An increase in the roughness coefficient results in large shear stresses at the sides of the channel. This means that the motion of fluid particles at or near the surface of the conduit will be reduced. The velocity of the neighbouring molecules will also be lowered due to constant bombardment with the slow moving molecules leading to an overall reduction in the flow velocity.

From figure 4, we observe that an increase in the energy coefficient from 1 to 2 leads to an increase in the flow velocity from curve I to curve II. In addition, an increase in the flow depth from 0.5m to 1m results in a reduction in the flow velocity from curve I to curve III.

An increase in the energy of the fluid results in the molecules attaining high energy which leads to more random motion. This random motion causes constant bombardment between the fluid particles resulting in an increase in velocities of the molecules and in general, of the fluid. The increase in flow depth leads to an increase in the wetted perimeter. This leads to large shear stresses at the sides of the channel and therefore the flow velocity will be reduced.

5.0 Conclusion

The various flow parameters were varied, one at a time while holding the other parameters constant. This was repeated for all the flow parameters and the results presented graphically. It was established that for a fixed flow area, the flow velocity increases with increase in depth from the bottom of the channel to the free stream and that maximum velocity occurs just below the free surface. Reduction in the slope leads to a decrease in the flow velocity. An increase in the cross sectional area of flow results in a decrease in the flow velocity.
An increase in the radius of the conduit results in a reduction of the flow velocity. This is because, as the radius is increased, so is the wetted perimeter as the fluid spreads more in the conduit. Moreover, an increase in the roughness coefficient results in a decrease in the flow velocity due to large shear stresses at the sides of the channel.

An increase in the energy coefficient leads to an increase in the flow velocity due to an increase in the energy of the fluid resulting in an increase in the molecular energy which leads to more random motion. Finally, an increase in the flow depth results in a reduction in the flow velocity. The increase in flow depth leads to an increase in the wetted perimeter resulting in large shear stresses at the sides of the channel with an effect of reduced velocities.

References

Akbari G., Firoozi B. Implicit and Explicit Numerical Solution of Saint-Venant Equations for Simulating Flood Wave in Natural Rivers. *5th National Congress on Civil Engineering*. May 4-6, 2010, Ferdowsi University of Mashhad, Mashhad, Iran.

Chadwick A. and Morfet J. (1993). *Hydraulics in Civil Engineering and Environmental Engineering*, Chapman & Hall, pp. 187-200.

Chagas Patricia and Souza Raimundo. Solution of Saint Venant's Equation to Study Flood in Rivers, through Numerical Methods. Paper_1 *Conf AGU Hydrology Days* 2005. Mar7-Mar 9, 2005.

Chow V. T. (1959). *Open-Channel Hydraulics.* McGraw Hill. New York.

Franz D. D. (1982). Tabular representation of cross-sectional elements. Proceedings of the American Society of Civil Engineers. *Journal of the Hydraulics Division*. **108** no. HY10, pp. 1070-1081.

French R.H. (1985). Open-Channel Hydraulics. Mc-Graw Hill, Inc. New York.

Ganguillet E., and Kutter, W.R. (1869). Versuch zur Augstellung einer neuen allgeneinen Furmel für die gleichformige Bewegung des Wassers in Canalen und Flussen. *Zeitschrift des Osterrichischen Ingenieur – und Architecten-Vereines*,**21**, (1), pp 6-25 and (2), pp 46-59. Translated into English by: Hering, R. and Trautwine, J.C. (1888 and 1891). *A General Formula for the Uniform Flow of Water in Rivers and Other Channels*. New York, NY: John Wiley & Sons.

Khan Abdul A. Modeling flow over an initially dry bed. *Journal of Hydraulic Research*., **38**, 2000, NO. 5.

Kwanza J. K., Kinyanjui M. and Nkoroi, J.M. (2007). *Modeling fluid flow in rectangular and trapezoidal open channels*. Advances and Applications in Fluid Mechanics., **2**, pp. 149-158.

Moshirvaziri S., Sheridan G., Lane P., Jones O. Modelling connectivity between pollutant source areas and streams.
http://www.iemss.org/iemss2010/index.php?n=Main.Proceedings.

Trautwine J. C. *The Civil Engineer's Pocket-Book* (Philadelphia: Wm. Butter & Co., 1888). pp. 236-281. Kutter's formula, together with much practical information.

Tuitoek D. K. and Hicks F. E. (2001). Modelling of unsteady flow in compound channels. *African Journal Civil Engineering*, **4**, pp. 45-53.

Viessman W., Jr., Knapp J. W., Lewis G. L., and Harbaugh T. E., Introduction to hydrology, 2nd ed., Harper & Row, New York, 1972.

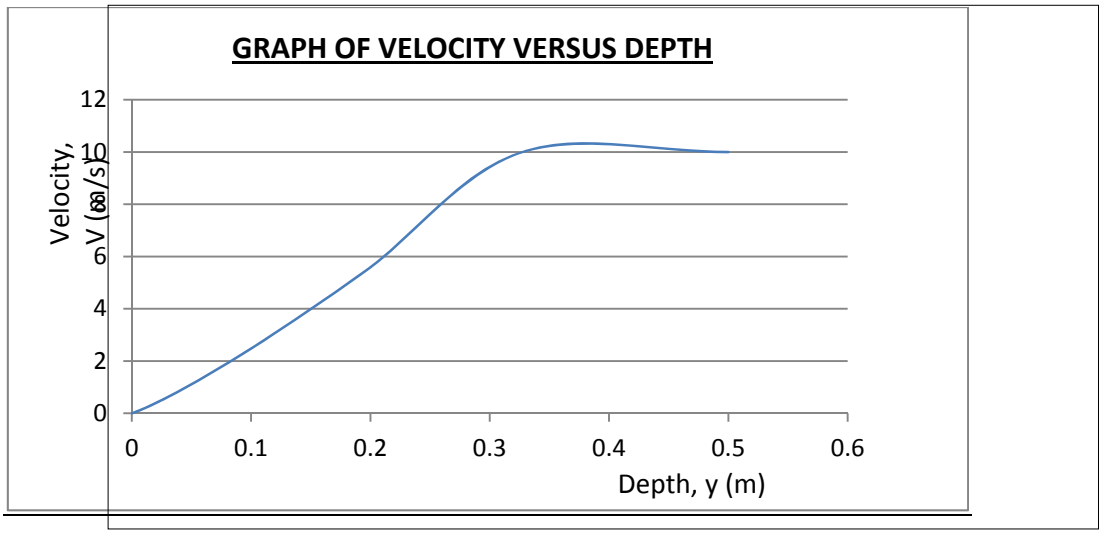

Figure 1: Velocity profiles for A = 0.6144, S_o =0.02, r = 1, n = 0.012, α = 1, P = 2.0947

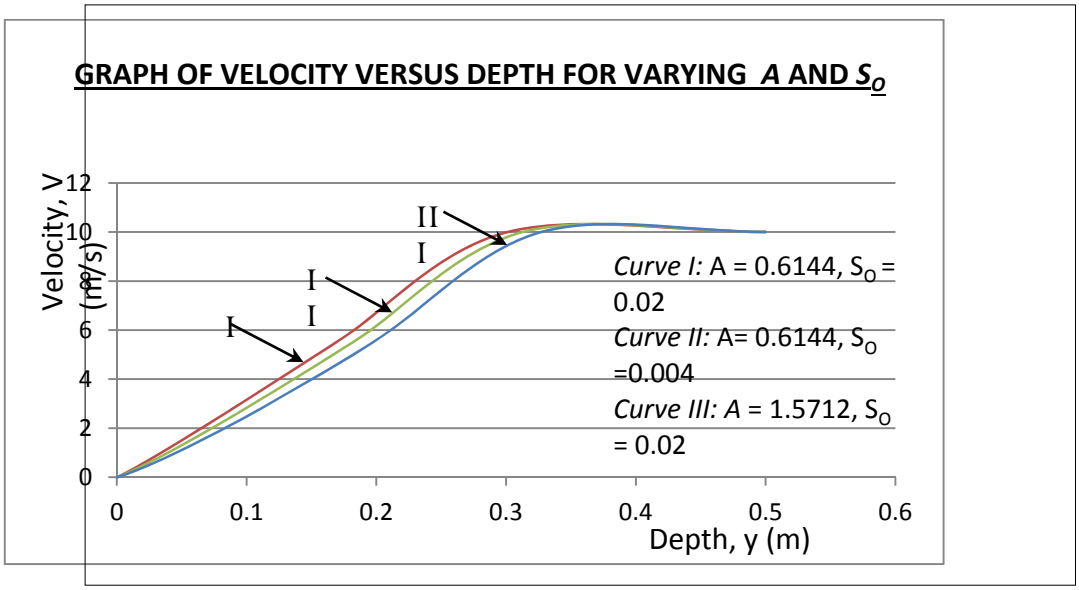

Figure 2: Velocity profiles for r = 1, n = 0.012, α = 1, P = 2.0947

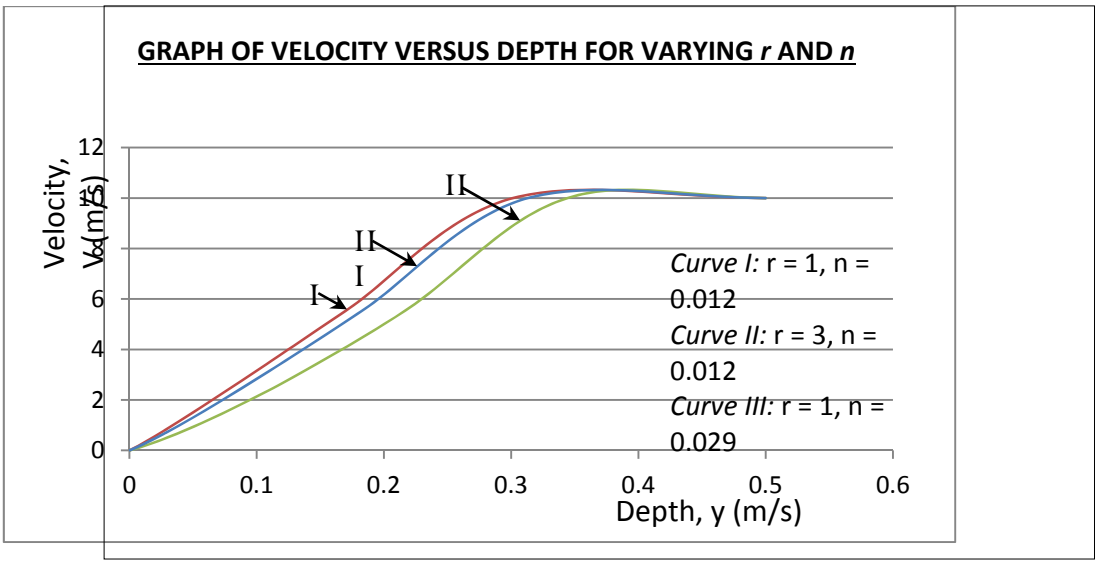

Figure 3: Velocity profiles for A = 0.6144, S_o =0.02, α = 1, P = 2.0947

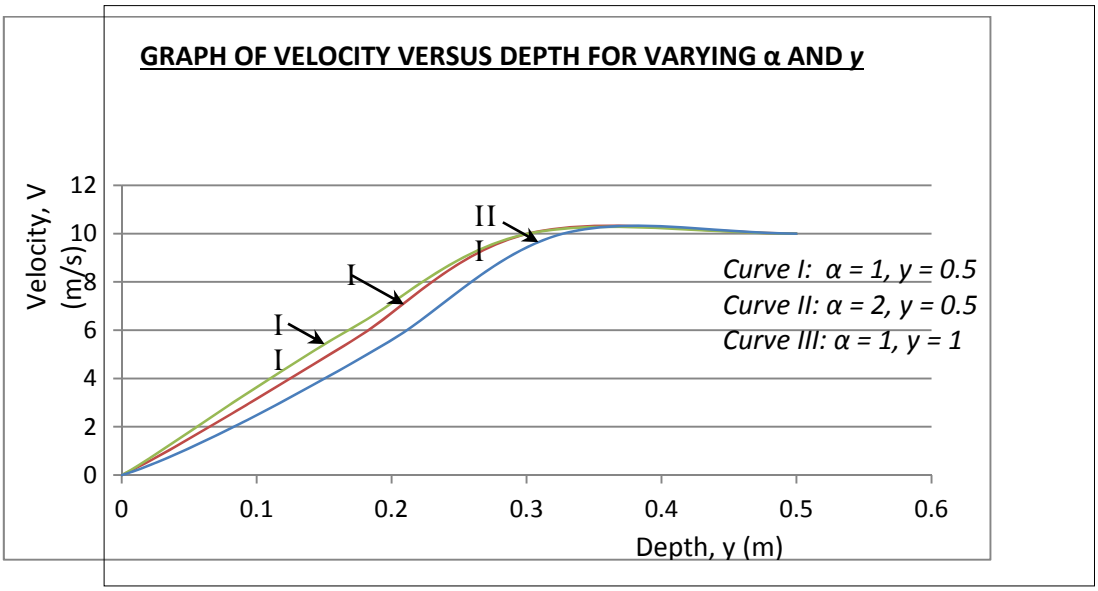

Figure 4: Velocity profiles for A = 0.6144, S_o =0.02, r = 1, n = 0.012

APPLICATION OF THE GEOLOGICAL STREAMFLOW AND MUSKINGUM CUNGE MODELS IN THE YALA RIVER BASIN, KENYA

V. M. Kiluva[1], F. Mutua[2], S. K. Makhanu[3] and B. T. I. Ong'or[4]
[1] Centre for Disaster Management and Humanitarian Assistance, Masinde Muliro University of Science and Technology
[2] Department of Meteorology, University of Nairobi
[3, 4]Department of Civil and Structural Engineering, Masinde Muliro University of Science and Technology
Email: mvmwikali@gmail.com

Abstract
The nature of surface runoff and its effects in the watershed can be represented by the application of hydrologic and hydraulic models. In this study, the Geological Streamflow Model (GeoSFM) and the Muskingum Cunge (M-C) model were used to model the hydrologic processes of the Yala river network. The objective was to develop a flood early warning system to mitigate potential flood hazard risk exposed to the downstream inhabitants. Historical hydro-metric datasets of 1975-2005 were used for calibration, verification and streamflow routing based on a split record analysis. For the runoff generation, rainfall and evaporation datasets were provided by the Kenya Meteorological Department while for model calibration and verification, streamflow was obtained from Water Resources Management Authority. To determine the hydrologic connectivity, the 30 meters by 30 meters Digital Elevation Model was obtained from the International Centre for Research in Agro-forestry. The Digital Soil Map of the World developed by Food and Agricultural Organisation and the Global Land Cover data of the United States Geological Survey were used for model parameterisation. The soil moisture accounting and routing method transferred water through the subsurface, overland and river phases. The percentage of the correlation coefficient (R^2% value) was used to determine model performance. The GeoSFM modeled streamflow at the Bondo streamflow gauging station, coded 1FG02 where during the calibration and verification phases, streamflow was modeled at R^2 value of 80.6% and 87.3% respectively. The M-C model routed streamflow from 1FG02 to the Kadenge streamflow gauging station, coded 1FG03 at R^2 value of 90.8%, Muskingum K value of 2.76 hours and Muskingum X value of 0.4609. The extreme value analysis done on the modeled streamflow portrayed a unique behaviour of the system when compared to the ideal system model that should mimic the real world. It was concluded that the GeoSFM and M-C models were hence useful tools for flood mitigation by issuing flood early warning messages defined by peak streamflow and flood wave travel time.

Key words: Flood, Yala River, geological streamflow model, muskingum cunge model.

1.0 Introduction

There is a continued exposure to flood risk in the western region of Kenya (Berhane, 2005). This calls for a concerted effort to provide flood mitigation measures in form of flood warning systems. The streamflow in the Yala river causes serious flooding conditions downstream as was established by UNEP (2004). This is more so because there is no contingency protection and drainage options for any excess waters which may originate from within the Yala river (Ogallo et al., 2004). An analysis done by NBCBN-RE (2004a, b and c) showed that changes in land use and/or climate have enhanced the frequency and magnitude of flooding. Some existing land use practices enhance flooding such as the Dominion Farms Limited project located at the Yala swamp.

Rainfall run-off modeling (Todini, 1978; Wang, 1996 and Seki, 1989) is the hydrologic process of generating flood early warning systems for flood management at river catchment scale. Rainfall runoff modeling from a watershed is of vital importance as the output is required for water resources planning and management. Numerical models of watershed hydrology are designed to answer the question, 'what happens to the rain?' at a level of detail depending on the problem at hand and are employed in a wide spectrum of areas ranging from watershed management to engineering design (Chow *et al.,* 1988; 1994). A numerical model is a hypothesis and has to be calibrated for the catchment under study (Kiluva, 2007 and Kiluva *et al.,* 2007).

Rainfall run-off modeling involves estimation of the magnitude of streamflow at various locations in a watershed resulting from a given precipitation input. The hydrologic cycle is the basic concept onto which flood modeling is derived and it comprises of all the physical processes that affect the movement of water in its various forms. The main processes include interception, water storage in the subsurface, lakes, reservoirs, infiltration, percolation, evaporation and transpiration. Due to the complexity of the real hydrologic system, the analysis is performed using hydrologic models, which are an approximation of the reality. The input and output of the model are measurable hydrological variables and the model structure is a set of equations that relate the inputs and outputs.

The complexity of any watershed compels one to use simplification and abstraction while conducting the study. Depending on which problem is being dealt with, sub-areas of the watershed are determined with regard to the contents and spatial relations that are considered as relevant in each case. If a modeler is only interested in particular objects in the system, for instance the Yala river basin, this selection leads to the first simplification. If the selected attributes of these objects are regarded to be significant, for instance the hydrology, this implies further abstractions (Young, 2001). This way the modeler gets from reality to a

model which sufficiently describes the objects of interest in a way specific to the problem (such as flooding).

The GeoSFM has a universal applicability and success in modeling floods in Africa and the world at large. The GeoSFM which is a semi-distributed model incorporates the physical features of the catchment by ingesting geospatial and soils datasets of the study area (Kiluva *et al.,* 2010). Most catchments are ungauged and thus a methodology to compute the flood wave propagation down a river reach or through a reservoir is required. An example of a simple and most popular hydrologic flood routing technique used in natural channels is the physically based M-C flood routing method (Gorbrecht and Brunner, 1991a; 1991b and Todini, 2007).

Great works in the area of rainfall runoff modeling have been done under the auspices of the Capacity Building and Networking of the Nile countries: Flow Regime from International Experimental and Network Data (FRIEND) by Bashar *et al.,* (2006), Mutua and Kadwan, (2006) and Mutua *et al.,* (2006). The findings from the studies of the Nile countries confirm that flooding is a potential hazard in the larger Nile basin and hence the same is true in the Lake Victoria basin that includes the Yala river basin. Flood mitigation measures are hence a requirement to reduce the flood risk in the downstream inhabitants of the Yala river basin. The M-C streamflow routing technique has been applied by Macchione (2009); Craig and Boroughs (2004); Jasem and Ismail (2006); Tewolde and Smithers, (2006); Shrestha and Franz (2007) and Rolando *et al.* (1994) but none of these applications have attempted to verify the M-C model. This wide spectrum of the utilization of the M-C technique indicates its universal acceptability as a flood routing tool. This study did not estimate flood levels but instead, streamflow rate was generated in addition to the flood wave travel time.

1.1 Objectives of the Study

The general objective was to develop a flood early warning system to mitigate potential flood hazard risk from the Yala river basin. To achieve the general objective, the following were the specific objectives:

(i) To perform the sensitivity analysis, calibration and verification of the GeoSFM system.
(ii) To simulate streamflow at Yala at Bondo streamflow gauging station (1FG02) using the GeoSFM system.
(iii) To route the simulated streamflow from the Yala at Bondo streamflow gauging station (1FG02) to Yala at Kadenge streamflow gauging station (1FG03) using the M-C streamflow routing technique.

2.0 Research Design and Methods

2.1 Data for the Study

Several data sets (Table 1 and Figures 1-3) were used to model streamflow using the GeoSFM and M-C models.

Table 1: Data types, period, category and sources

Data Type	*Period*	*Category*	*Data Sources*
Rainfall data	1975-2005	Secondary data	Kenya Meteorological Department, Nairobi
Evaporation data	1975-2005	Secondary data	Kenya Meteorological Department, Nairobi
Streamflow data	1975-2005	Secondary data	Water Resources Management Authority
Soils data	1997	Secondary data	Digital Soil Map of the World developed by Food and Agricultural Organization
Land cover data	2006	Secondary data	United States Geological Survey
Digital elevation model (DEM)	2009	Secondary data	International Centre for Research in Agro-forestry
River channel hydrologic characteristics	2009	Primary data	Measured using the River Discharge Measurement System (Qliner) at 1FG02 and 1FG03 sub-reaches

Rainfall, evaporation and streamflow gauging stations from the Yala river basin were as shown in Figure 1.

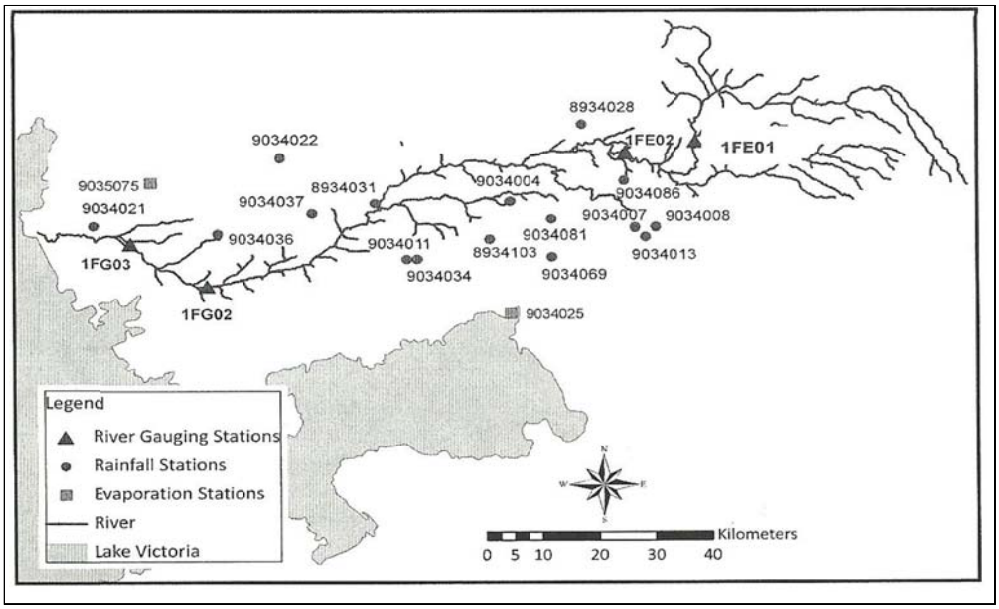

Figure 1: Rain gauges, streamflow gauges and evaporation stations used for modeling the Yala River basin

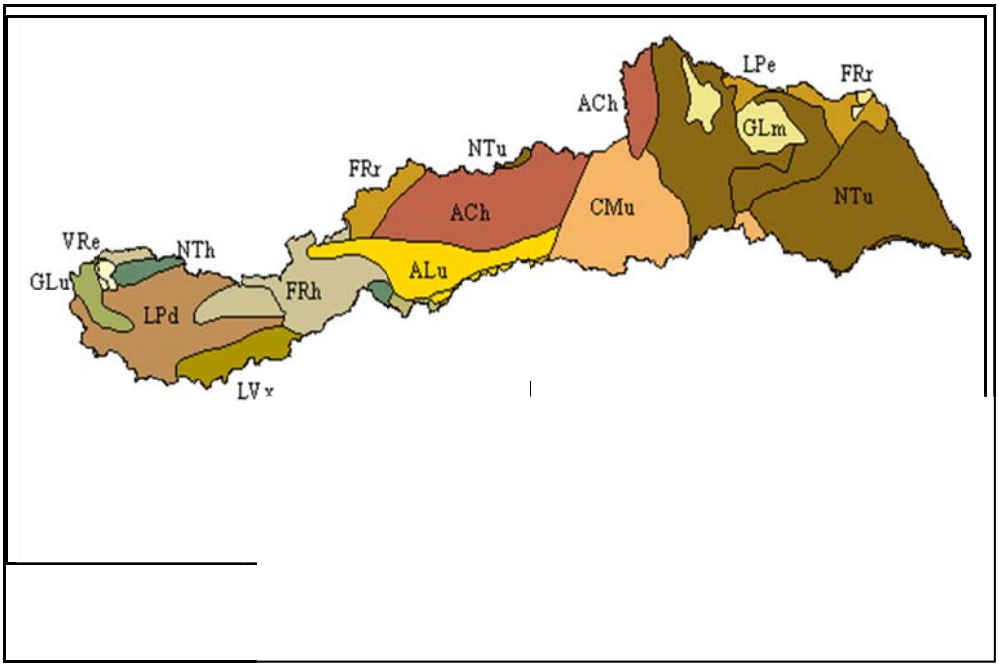

Figure 2: Category of soils in the Yala river basin (FAO, 1997)

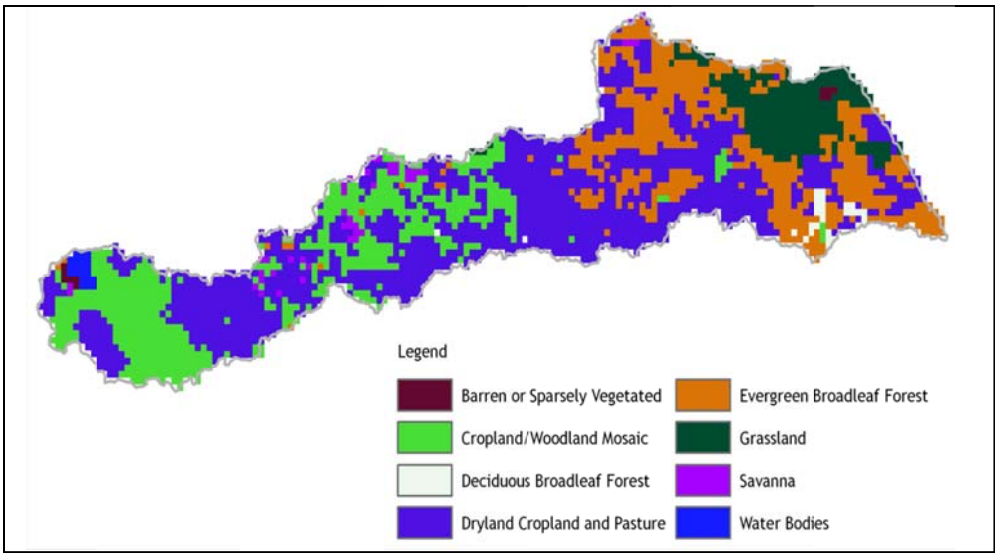

Figure 3: Land cover for Yala river basin (Source: USGS continent data sets)

2.1.1 Split Record Analysis

Split record analysis (Table 2) was done on the daily series datasets of rainfall, evaporation and streamflow for the purposes of model calibration, verification and flow routing. This split record analysis represented the diverse weather and climatic conditions and hence fully characterized the features and the dynamic nature of the catchment.

Table 2: An illustration of split record analysis on the hydro-meteorological datasets

Modeling phase	*Record considered*	*Duration (years)*
GeoSFM calibration	1980-1985	6
GeoSFM verification	2000-2005	6
M-C streamflow routing	1975-2005	31

2.2 Parameter Sensitivity Analysis

In order to guide the calibration process, parameter sensitivity analysis was done to identify which parameters had much impact in the model's generated streamflow. Rainfall from the sampled 20 raingauges and evaporation from the two evaporation gauges in the Yala river system were used to perform the parameter sensitivity analysis. Initially, interpolation of station data to grid was done to equally spread and distribute the rainfall and evaporation over the entire river basin. The major model parameters are the river Manning's coefficient (n), the Runoff Curve Number (RCN), Active Soil Depth (ASD) and the Water Holding

Capacity (WHC) of the soil (McCuen, 1998; Guleid et al., 2007 and Asante et al., 2007).

2.3 Model Calibration

The calibration of the GeoSFM computer code was automatically done using the Multi-Objective Shuffled Complex Evolution Metropolis (MOSCEM) Algorithm (Vrugt et al., 2003). The hydrologic datasets for the Yala river system were divided into two sets to create a set used for model calibration (period 1980-1985) and another set used for validation (period 2000-2005). This period was considered suitable for it had the least number of missing values in daily observed streamflow data. An agreement between the observed and simulated streamflow was made in terms of coefficient of determination (R^2 value) and a visual examination was done on the input data, recorded and simulated streamflow to determine any discrepancies from the regression charts.

2.4 Model Validation

To validate the GeoSFM, the already calibrated model should be able to make sufficient accurate predictions. Daily rainfall and evaporation data for the period of 2000-2005 were used. This period was specifically chosen for the validation exercise because high streamflow values or floods were known to have occurred in Yala river system during this time, 2003 in particular, hence a good test period for the GeoSFM computer code performance. The resulting streamflow was compared to the observed values, and the goodness of fit evaluated.

2.5 Streamflow Routing

The main purpose of calibrating the GeoSFM computer code was to use it in forecasting streamflow for the Yala river basin at 1FG02 situated at Yala at Bondo bridge in readiness for applying the M-C streamflow routing technique. This was done so that in the case of an impending flood, the people living in the floodplains areas could be warned in advance of the impending flood hazard.

2.6 Simplifications/Assumptions Adopted in the Study

When modeling the hydrology of the Yala river channel using the M-C model, the following assumptions were made:

(i) When routing streamflow from station 1FG02 to 1FG03, it was assumed that the hydrologic and channel characteristics did not change but only varied at 1FG03 station

(ii) That there was no lateral inflow of water from the surrounding area into the river channel.

2.7 Overview of the GeoSFM Hydrologic Modeling System and the M-C Model

2.7.1 The GeoSFM Hydrologic Modeling System

The GeoSFM is a semi-distributed hydrologic model developed by the United States Geological Survey's Earth Resources Observation System (EROS) Data Centre. The GeoSFM simulates the dynamics of runoff processes by using remotely sensed and widely available global datasets. The GeoSFM model assimilates spatially distributed data to simulate streamflow on a daily basis. The model is a physically-based catchment scale hydrologic computer code. It consists of a Geographical User Interface (GUI) and a rainfall-runoff simulation component. The GeoSFM GUI component runs within the GIS for model input, data preparation and visualization of the model outputs. Topographic, land cover and soil information are the basic inputs to derive and parameterize the hydrologic modeling units.

The GeoSFM uses a linear reservoir concept to route overland flow. The integral equation of continuity for an unsteady, constant density overland flow is used to route the overland flow and is expressed as Eq. 1.

$$\frac{\delta s}{\delta t} = I(t) - Q(t) \quad \text{.....(1)}$$

where, (*S*) is the volume of fluid stored in control volume,

($\frac{\delta s}{\delta t}$) is the change in storage,

{*I (t)*} is the inflow,

{*Q (t)*} is the outflow.

The GeoSFM utilises the modification of Eq. 1 to determine the overland flow, as in Eq. 2.

$$S_j = S_0 + \sum_{i=1}^{j} (I_i - O_i) \quad \text{.....(2)}$$

Where, (S_0) is the initial storage at time (*0*),

(S_j) is the storage after time (*j*).

(I_i) is the inflow after time (*i*).

(O_i) is the outflow after time (*i*).

2.7.2 The M-C Model

The Muskingum Cunge (M-C) model is applied in the streamflow routing module of the GeoSFM. Mathematically, the M-C model is expressed using the conventional original Muskingum Eqs. 3 and 4.

$$\frac{\Delta S}{\Delta t} = I - Q \quad \text{.....(3)}$$

$$S = K[XI + (1 - X)Q] \quad \text{.....(4)}$$

The Muskingum K and X coefficients are estimated using Eqs. 5 and 6.

$$K = \frac{\Delta x}{\bar{c}} \quad \text{.....(5)}$$

$$X = \frac{1}{2} - \left(\frac{\bar{Q}}{2\bar{c}\bar{B}S_e \Delta x} \right) \quad \text{.....(6)}$$

where, ($\bar{Q}$) is the streamflow (m^3/s),

(K) is the Muskingum K coefficient (seconds),

(X) is the Muskingum X coefficient (dimensionless),

($\bar{c}$) is the average flood wave celerity corresponding to the streamflow ($\bar{Q}$) in meters per second,

($\bar{B}$) is the average channel width associated with the streamflow ($\bar{Q}$) in meters,

(S_e) is the dimensionless friction or the channel bed slope,

(Δx) is the length of the channel (meters),

(S) is the storage in the channel at time (t) in meters per second,

(I) is the inflow (m^3/s).

The GeoSFM was calibrated, verified and subsequently applied on the Yala river basin based on a split record analysis (Table 2) to model streamflow at 1FG02 station which was then routed by the M-C model to 1FG03 station to generate flood early warning system for the river basin downstream inhabitants.

3.0 Results and Discussions

Daily series of the rainfall, evaporation together with the soils, land use and topographical information modeled streamflow. Daily series of observed streamflow data compared with the model's generated streamflow to assess the correlation between the two for model performance testing. All hydro-meteorologic variables spanned within the period 1975 to 2005 that defined and incorporated climate change aspects. A digital elevation model of the study area guided and routed the generated streamflow to the downstream region guided by the terrain of the catchment. The hydro-meteorological datasets used in this study included streamflow data records of the streamflow gauging stations 1FE01, 1FE02, 1FG02 and 1FG03, rainfall data records for 20 rain gauging stations and the evaporation data records for Kisumu and Kadenge evaporation stations. The results from sensitivity analysis, calibration, verification and routing are presented in the sub-sections that follow.

3.1 Parameter Sensitivity Analysis

The most sensitive parameters (Table 3) obtained after parameter sensitivity analysis were soil water holding capacity with a standard deviation (SD) value of

0.489mm, total soil depth with a sd value of 0.443cm, excess rainfall with a SD value of 0.421 mm, river channel roughness coefficient (Manning n) with a sd value of 0.314 and scs runoff curve number with a sd value of 0.223.

Table 3: Parameter sensitivity analysis results of the GeoSFM system

S. No.	***Sensitivity parameters category***	***Maximum value***	***Mean value***	***Standard deviation (SD) value***
1	SoilWhc [soil water holding capacity (mm)]	1.790	0.550	0.489
2	Depth [total soil depth (cm)]	1.822	0.402	0.443
3	Texture [soil texture]	0.255	0.031	0.043
4	Ks [saturated hydraulic conductivity (cm/hr)]	0.775	0.061	0.144
5	Interflow [interflow storage residence time (days)]	0.014	0.009	0.003
6	HSlope [average sub-basin slope]	0.050	0.006	0.011
7	Baseflow [baseflow reservoir residence time (days)]	0.026	0.009	0.009
8	CurveNum [SCS runoff curve number]	0.654	0.157	0.223
9	MaxCover [permanently impervious cover fraction]	0.895	0.171	0.250
10	BasinLoss [fraction of soil water infiltrating to ground water]	0.000	0.002	0.000
11	PanCoeff [pan coefficient for correcting PET readings]	0.849	0.275	0.262
12	TopSoil [fraction of soil layer that is hydrologically active]	0.504	0.078	0.099
13	RainCalc [excess rainfall (mm)]	1.229	0.278	0.421
14	RivRough [river channel roughness coefficient (Manning n)]	0.384	0.100	0.314
15	RivSlope [average slope of the river]	0.013	0.000	0.001
16	RivWidth [average channel width]	0.010	0.000	0.001
17	RivLoss [fraction of the flow lost within the river channel]	0.035	0.002	0.003
18	RivFPLoss [fraction of the river flow lost in floodplain]	0.267	0.019	0.037
19	Diffusion [flow attenuation coefficient (m^3/sec)]	0.000	0.000	0.000
20	Celerity [flood wave celerity (m/sec)]	0.022	0.000	0.001

3.2 Calibration phase of the GeoSFM

The GeoSFM performed better during the verification phase than during the calibration phase. At the verification phase, the R^2 value obtained was 87.3% while a the calibration phase, it yielded a R^2 value of 80.6%. Figure 4 shows the mean rainfall (mm), observed and simulated streamflow (m^3/sec) for the period 1980 to 1985 during the model calibration phase in the Yala River basin.

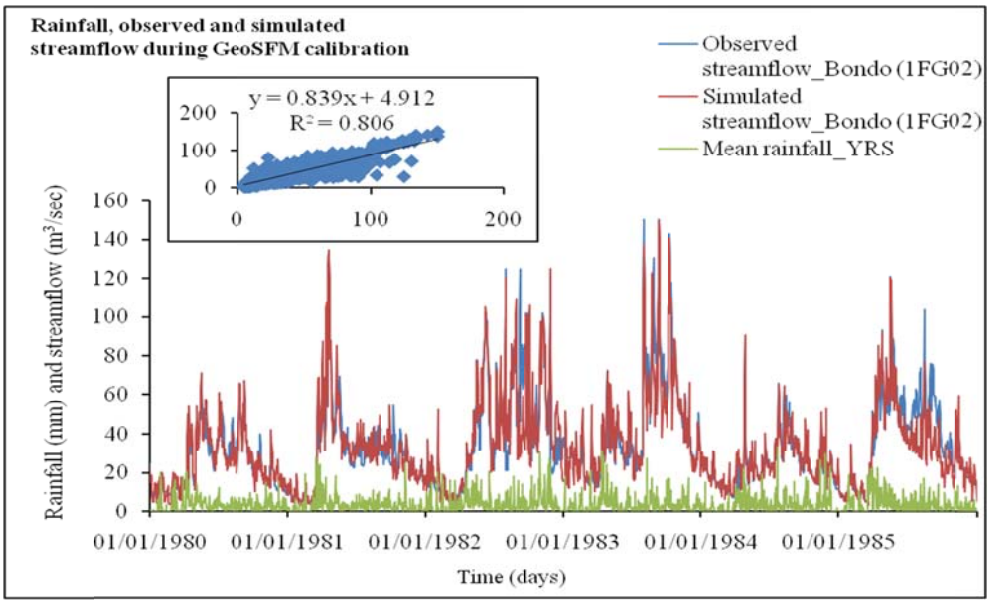

Figure 4: A hydrograph showing rainfall, observed and modeled streamflow for station 1FG02 in the Yala River basin during the calibration phase

3.3 Verification/validation phase of the GeoSFM

The calibrated GeoSFM was applied on the mean rainfall of the period 2000-2005 to verify the ability of the model to reproduce well fitted and accurate hydrographs. In general, at the verification phase, the GeoSFM proved to very well simulate the streamflow at the 1FG02 station with a R^2 value of 87.3%. The hydrograph for the period 2000-2005 was selected for presentation as in Figure 5 which shows the mean rainfall (mm), observed and simulated streamflow (m^3/sec) obtained during the model verification phase in the Yala river basin.

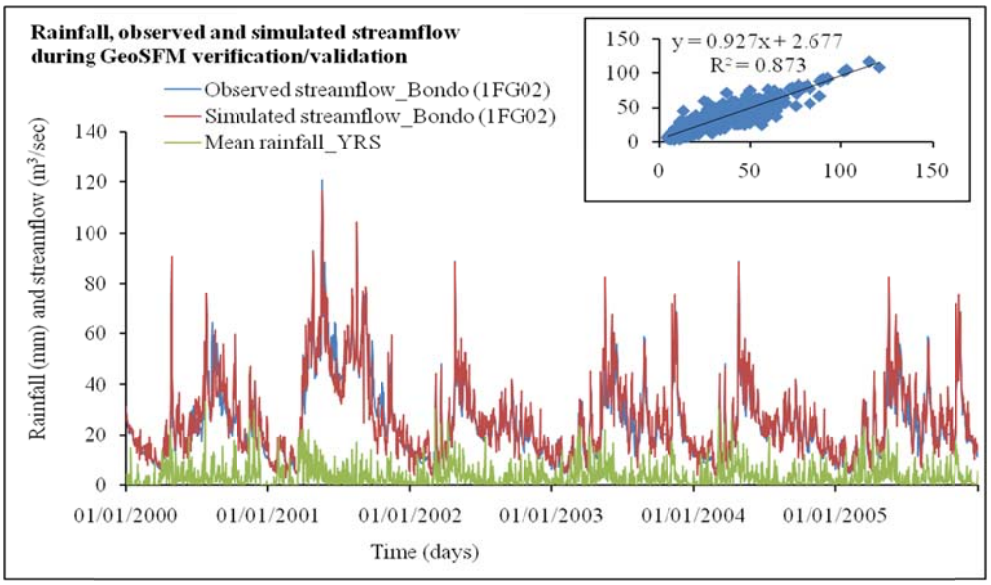

Figure 5: A hydrograph showing rainfall, observed and modeled streamflow for station 1FG02 in the Yala river basin during the verification phase

3.4 Streamflow Routing Phase using the Muskingum Cunge Model

Figure 6 shows the correlation between the observed and the routed streamflow at 1FG03 streamflow gauging station as was routed by the M-C model.

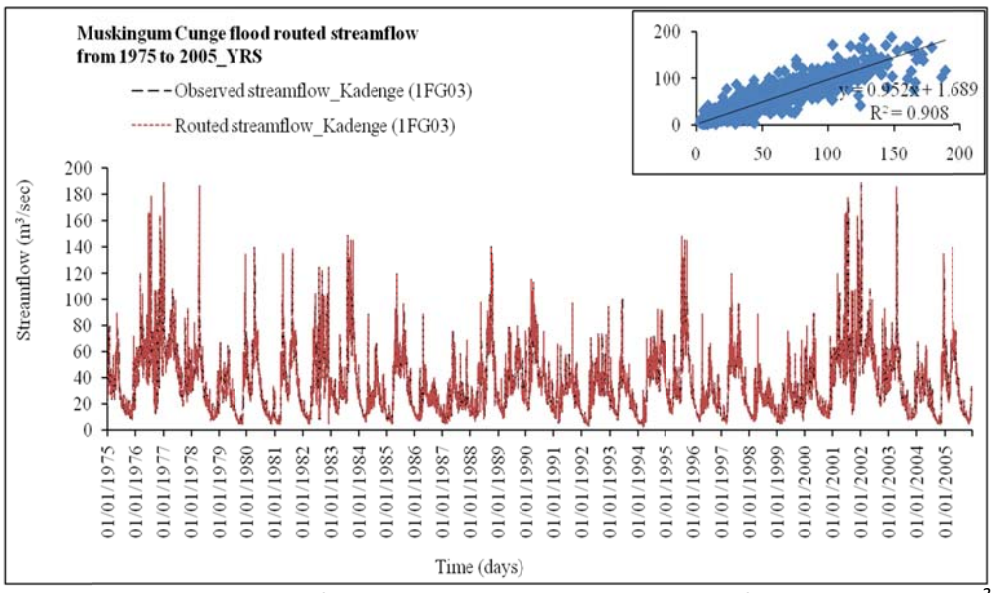

Figure 6: A hydrograph of the observed and routed streamflow showing the R^2 value at station 1FG03 for the period 1975-2005 in Yala river basin

From Figure 6, the highest flood peak values were identified in the years 1978, 1989, 1997, 2002 and 2003. As indicated by historical flood records, these years recorded flood incidents downstream of the Yala river basin. In general, streamflow was routed using the M-C streamflow routing method from the station 1FG02 to the station 1FG03 for the period 1975-2005 at a R^2 value of 90.8%. The lack of fit with the rising and falling limbs of the measured outflow hydrograph that made the R^2 value not to yield 100% was probably due to out-of-bank floodplain inundation. The M-Cunge K and X parameter values obtained on routing the flood from 1FG02 station to 1FG03 station were as shown in Table 4.

Table 4: Muskingum Cunge K and X parameter values obtained during the streamflow routing phase

Streamflow Routing Phase (1975-2005)	
Muskingum Cunge parameters and channel length	River sub-reach
	1FG02 to 1FG03 gauging station
Channel length Δx (Kilometers)	14.00
Computational time Δt (seconds)	7200
Muskingum K (seconds)	9953
Muskingum K (hours)	2.76
Muskingum X (ratio)	0.4609

Based on the derived M-C parameter values in Table 4, it meant that a drop of water that was released from 1FG02 station at time zero seconds took 9953 seconds, which was equivalent to 2.76 hours, to propagate along the river channel to 1FG03 station. The inhabitants of the downstream region of the 1FG03 station in the Yala river basin hence needed to be warned 2.76 hours in advance of an impending flood disaster originating from the Yala river basin when streamflow monitoring was based at 1FG03 station.

3.5 Application of the Results

The downstream zone of the Yala river basin is not protected from riverine flooding. Flood mitigation can be achieved by either utilizing structural measures (include dykes and dams among others) or non-structural measures (include early warning and awareness creation among others). The generated 2.76 hours of early warning forms a non-structural flood mitigation strategy when it is communicated to the inhabitants downstream of the Yala river basin. In the event of an impending flood, the inhabitants of the downstream zone are able to evacuate the area to safer areas within a period of 2.76 hours. This evacuation will save both their lives and livelihoods from the flood inundation. This lead-time is also important to decision makers who administer flood mitigation measures in the floodplain.

4.0 Conclusions

This study concludes that:

(i) The sensitivity analysis, calibration, verification and flow routing applications using the GeoSFM and M-C models on the hydro-meteorologic and geospatial datasets were able to model streamflow in the river channel sub-reaches with high R^2 values. Decision makers could then administer flood mitigation measures in the Yala river floodplain on an informed foundation.

(ii) The modeled streamflow was able to generate the flood wave travel time. This provided a non-structural solution to the flood problem in the Yala river floodplain.

(iii) The GeoSFM and M-C models were applied to predict and route floods using variables in the Yala river and it was postulated that the methods could be used to model floods in other ungauged rivers in Kenya and in other countries experiencing riverine flooding.

Acknowledgements

The authors would like to thank Masinde Muliro University of Science and Technology for approving the study and awarding the partial scholarship to undertake the same study.

References

Asante K. O., Artan G. A., Pervez S., Bandaragoda C. and Verdin J. P., (2007). Technical Manual for the Geospatial Streamflow Model (GeoSFM). Open file Report Series of 2007-1440 U.S. pp 25.

Bashar K. E., Mutua F., Mulungu D. M., Deksyos T. and Shamseldin A. (2006). Appraisal study to select suitable Rainfall-Runoff model(s) for the Nile River Basin. pp 23.

Berhane M.(2005). Western Kenya Ecosystem Management. GEF Project Document, Africa Regional Office AFTS2, pp 50, Date: January 25, 2005.

Chow V. T., Maidment D. R. and Mays L. W. (1988). Applied Hydrology. McGraw-Hill, New York, **201**, pp 584.

Chow V. T., Maidment D. R. and Mays L. W. (1994). Applied Hydrology. McGraw-Hill, New York, **203,** pp 200-240.

Craig B. and Boroughs P. E. (2004). Daily Flow Routing With Muskingum-Cunge Method in the Pecos Riverware Model. In the Center for Advanced Decision Support for Water and Environmental Systems, University of Colorado, Boulder, CO. pp 8-9.

DMCN-UNEP- United Nations Environment Program (2004). Strategy for Flood Management in Lake Victoria Basin, Kenya. Prepared under Associated Programme on Flood Management (APFM), Geneva, 25th August 2003, Available on website: http://www.apfm.info/pdf/strategy-Kenya-e.pdf.

FAO, (1997). A Digital Soil Map of the World. CDROM. In Rome, Italy.

Gorbrecht J. and Brunner G. (1991a). Hydrologic Channel-Flow Routing for Compound Sections. In the Journal of Hydraulic Engineering, Vol. 117, No. 5, May 1991, **103**, pp 629-642.

Gorbrecht J. and Brunner G. W. (1991b). A Muskingum-Cunge Channel Flow Routing Method for Drainage Networks. pp 29-39.

Guleid A. A., Kwabena A., Jodie S., Shahriar P., Debbie E., James V., and James R., (2007). Users Manual for the Geospatial Stream Flow Model (GeoSFM). pp 91-100.

Jasem M. and Ismail I. E. (2006). Approximate Methods for the Estimation of Muskingum Flood. In the Journal of Water Resources Management Publisher Springer

Netherlands ISSN 0920-4741. Issue Volume 20, Number 6/December, 2006. pp 1573-1650. Available on website: http://www.springerlink.com/content/.

Kiluva V. M. (2007). Development of a Sustainable Low-cost Non-structural flood Mitigation Strategy. Master of Science Thesis. pp 56-57.

Kiluva V. M. (2010). A Multi-system Approach to Modeling of Floods in the Budalang'i Floodplains of Western Kenya. Doctor of Philosophy Thesis. pp 46-50.

Kiluva V. M., Oteng'i S.B.B. and Miima J.B. (2007). Development of a Sustainable Low-cost Non-structural flood Mitigation strategy for Nzoia River basin - Kenya. In the J-STEM (Journal of Science Technology Education and Management). pp 28-30.

Macchione F. (2009). Application of the Muskingum-Cunge method for dam break flood routing. In the Transactions of the Wessex Institute collection. pp 99-109.

McCuen R. H., (1998). Hydrologic Design and Analysis. Prentice Hall, New Jersey. pp 814.

Mutua F. M. and Radwan A. (2006). Rainfall-Runoff Modeling in Selected Catchments in the Lake Victoria Basin. Nile Initiative 2006 513RAB2042_finalreport. pp 10-15.

Mutua F. M., Mtalo F. and Bauwens W. (2006). Challenges of Modeling the Flows of the Nile River. Nile Initiative 2006 513RAB2042_finalreport. pp 20-21.

NBCBN-RE (2004a). Floods and their influence on the Nile River System. Nile Basin Capacity Building Network Report. pp 78.

NBCBN-RE (2004b). Flood and catchment management. Nile Basin Capacity Building Network Report. pp 89-90.

NBCBN-RE (2004c). Flood and draught forecasting and early warning program (for the Nile Basin). NBCBN-RE-Nile Basin Capacity Building Network Report- River Engineering. pp 95-100.

Ogallo L. A., Mutua F. and Ayayo O. (2004). Coping with Floods in Kenya: Vulnerability, Impacts and Adaptation Options for the Flood Prone Areas of Western Kenya. Final Draft Report (DMCN-UNEP Project) - March, 2004, pp 79-89.

Rolando B., David A. D. and Jerry R. R. (1994). Parameter Determination for the Muskingum-Cunge Flood Routing Method. Issue: Volume 30, Number 5, October 1994, 1020, pp 891-899. Available on website: http://www.awra.org/jawra/toc.

Seki K. (1989). Comprehensive flood loss prevention and management in Japan. In the Proceedings of the Japan-China (Taipei) Joint Seminar on Natural Hazard Mitigation, Kyoto, Japan, July 16th-20th, 1989., **608**, pp 9.

Shrestha R. R. and Franz N. (2007). River Water Level Prediction Using Physically Based and Data Driven Models. pp 89-90.

Tewolde M. H. and Smithers J. C. (2006). Flood routing in ungauged catchments using Muskingum methods. Vol. 32 No. 3 July 2006. pp 93 Available on website: http://www.wrc.org.za.

Todini E. (1978). Using a Desk-Top Computer for an On-Line Flood Warning System. BM. Develop., **22(5),** pp 464-471.

Todini E. (2007). A mass conservative and water storage consistent variable parameter Muskingum-Cunge approach. Department of Earth and Geo-Environmental Sciences, University of Bologna, Italy. pp 9-12.

Vrugt J. A., Gupta H. V., Bastidas L. A., Bouten W. and Sorooshian S., (2003). Effective and efficient algorithm for multi-objective optimization of hydrologic models. pp 8.

Wang Z. Y. (1996). UNDP Project: Support for the Sustainable Development of the Yellow River Delta. In the International Journal of Sediment Research, Vol. 11, No. 3. 109. pp 40-48.

Young P. C. (2001). Data-based mechanistic modeling of environmental systems. Presented at the International Federation on Automatic Control (IFAC) Workshop on Environmental Systems, Tokyo, Japan, August 21st 2001, pp 189-196.

EMERGING AZOLE RESISTANCE AMONG *CANDIDA ALBICANS* FROM CLINICAL SOURCES IN NAIROBI, KENYA

M. C. Kangogo[1], W. Wanyoike[2], G. Revathi[3], J. G. Wakibia[4] and C. Bii[5]
[1,2,4]Department of Botany, Jomo Kenyatta University of Agriculture and Technology.
[5] Mycology Laboratory, Centre for Microbiology Research, Kenya Medical Research Institute.
[3] Department of Microbiology, Aga Khan University Hospital
E-mail: wanjiru_wanyoike@yahoo.com

Abstract
In the recent years the number of serious opportunistic yeast infections, particularly in immunocompromised patients has increased significantly. The increased incidence of these infections has paralleled the emergence of HIV/AIDS pandemic that result in lowered resistance of the host. Azole antifungal agents has been extensively used in the management of these yeast infections. *Candida albicans* is one of the most frequently isolated yeasts in clinical laboratories and accounts for up to 80 % of the yeasts recovered from sites of infection. The study was set out to determine antifungal susceptibility of clinical isolates of *Candida albicans* and to establish the Minimum Inhibitory Concentrations (MIC) to Fluconazole, Clotrimazole, Nystatin and Amphotericin B. Laboratory based experiment were conducted at Mycology Laboratory, Kenya Medical Research Institute, Nairobi, Kenya. One hundred and thirty clinical isolates of *Candida albicans* were subjected to antifungal susceptibility testing. Susceptibility to Fluconazole, Clotrimazole, Nystatin and Amphotericin B was done using Broth Microdilution Technique with reference to Clinical laboratory Standard Institute (CLSI). The investigations showed that 16/130 (12.3 %) of the *Candida albicans* isolates were resistant (MIC ≥ 64 µg/ml) to fluconazole, 121/130 (93.1 %) of the isolates had an MIC ≤ 1 µg/ml to Amphotericin B. Of the isolates 51/130 (39.2 %) had MIC> 1 µg/ml to clotrimazole whereas 109/130 (83.8 %) of the isolates had MIC ≤ 1 µg/ml to nystatin. The study showed elevated MICs among *Candida albicans* isolates to fluconazole and clotrimazole and calls for constant antifungal resistance surveillance especially in the context of fluconazole maintenance treatment for opportunistic infections in HIV/AIDS.

Key words:

1.0 Introduction

The last two decades have seen a steady increase in the incidence of systemic opportunistic fungal infections especially in sub-Sahara Africa (Selik *et al.,* 1987). This rise is associated with Acquired Immunodeficiency Syndrome (AIDS) pandemic, prolonged antimicrobial therapy, invasive procedures and immunosuppressive therapy (Frye *et al*., 1988; Hazen, 1995; Reef and Mayer, 1995). Invasive fungal infections, particularly those caused by *Candida* and Cryptococcus species are emerging significant opportunistic organisms that have increased over the past few decades (Kremery and Barnes, 2002). These infections are major complications in immunocompromised patients as well as those with profound neutropenia due to hematological malignancies or chemotherapy usually associated with high mortality (Hikey, 1983; Harvey and Myres 1987).

The available treatment for fungal infections includes azoles (fluconazole, ketoconazole, voriconazole and clotrimazole) and polyene antifungals such as Nystatin, and Amphotericin B. In the recent past, there have been reports of emerging resistance among *Candida* species to some of the antifungal drugs (Bii *et al*., 2002; Seibold and Tintelnot 2003; Bii *et al*., 2006). This has made it necessary to isolate, identify yeasts from clinical sources and to determine and monitor antifungal resistance. The present study aimed at determining the current levels of MICs to the four commonly used antifungal drugs that are essentially used for clinical management of patients susceptible to opportunistic pathogens.

2.0 Materials and Methods

A total of 150 isolates of *Candida* species recovered from blood, sputum, swabs, urine and catheter tips isolated between 1997 - 2004 were used. The isolates were culture collections at Mycology Laboratory, Kenya Medical Research Institute from various health Institutions in Nairobi, Kenya. Azole resistance in yeasts is estimated at 11.0 % (Bii *et al.,* 2006). 1t was therefore necessary that a sample size expected to detect 89 % of non-azole resistant *Candida* be used. The formula according to Fischers *et al.*, (1998) was used to calculate and arrive at a sample size of 150 isolates.

Isolation of *Candida albicans* was done using Sabouraud Dextrose Agar (SDA, Oxoid LTD Basingstoke, Hampshire, England) supplemented with 2 % Chloramphenicol. The Germ Tube Test (GTT) was used for presumptive identification of *Candida albicans.* GTT negative yeasts were further identified on slide culture using chlamydospore formation on Corn Meal Agar incorporated with Tween 80 and ChromAgar Candida (Johnson and Nickson, 1970; Pfeller, 1996). Confirmation of the isolates was done using Analytical profile index (API 20 C aux). The procedures were done according to the manufacturers instructions. The susceptibility tests and Minimum Inhibitory Concentration (MIC) were determined as recommended by Clinical Laboratory Standards (CLSI) and (NCCLS, 2002). The MIC was scored as

the lowest concentration that significantly inhibited fungal growth. MIC_{50} was calculated as the minimum inhibitory concentration reached by 50 % and MIC_{90} as the manimum inhibitory concentration reached by 90 %.

3.0 Results

C. albicans susceptibility to fluconazole (MIC ≤ 8 µg/ml) was 95/130 (73.1 %), susceptible dose-dependent (MIC 16-32 µg/ml) 14.6 % and resistant (MIC ≥ 64 µg/ml) 12.3 %. The MIC_{50} and MIC_{90} to fluconazole were 4 µg/ml and 64 µg/ml respectively. At 1 µg/ml of Amphotericin B, 121/130 (93.1 %) of the isolates were inhibited by only 9/130 (6.9 %) showing MIC of ≤ 1 µg/ml. The MIC_{50} and MIC_{90} to Amphotericin B were 0.25 µg/ml and 1.0 µg/ml respectively. The MIC_{50} and MIC_{90} of clotrimazole were 1 and 16 µg/ml and nystatin 0.25 and 2 µg/ml respectively.

Table: Results of the response of 130 Clinical isolates of Candida albicans to common antifungals

Class of antifungal compounds	**Drug**	**Tested Concentration range (ug/ml) and number of isolates inhibited (%)**				
Azoles		0.03-0.25	0.5-1	2-8	16-32	≥64
	Clotrimazole	39(30)	40(30.8)	35(27.0)	16(12.2)	-
	Fluconazole	40()	35()	20()	19(14.6)	16(12.3)
Polyenes						
	Nystatin	76(58.3)	33(26.9)	14(10.8)	5(3.8)	-
	Amphotericin B	89(68.5)	32(24.6)	6(4.6)	3(2.3)	-

-Beyond tested concentration

4.0 Discussion

In the recent years the number of opportunistic yeast infections, particularly in immunocompromised patients has dramatically increased (Richardson and Warnock, 2003). Among them are *Candida* species especially *Candida albicans*. The higher incidence of fungal infections in hospitalized patients has resulted to the use of systemic antifungal agents especially fluconazole, which remains a first line antifungal agent of choice (Redding et *al*., 1994). Another reason for the increased Candida infections is due to more aggressive cancer and post-transplantation chemotherapy and the use of antibiotics, cytotoxins, immunosuppressives, corticosteroids and other macro disruptive procedures that result in lowered resistance of the host leaving the opportunistic *Candida albicans* to flourish.

Out of the 130 *Candida albicans* isolates sampled in this study, 73.1 % of *Candida albicans* were susceptible to fluconazole (MIC ≤ 8 µg/ml) and 12.3 % were resistant. This is in agreement with previous studies whereby fluconazole resistant *C. albicans* accounts for 9-12 % of the isolates from HIV-Positive patients (Newman, 1994; Wheat, 1998). Since *C. albicans* is a natural part of the intestinal and vaginal flora, drugs that keep candidiasis at its check may never completely eradicate it. The continued presence of the organism during treatment makes the emergence of drug resistant fungal organisms more likely. As the prophylactic use of azoles increases so is the likelihood of increased azole resistant *Candida* (Smith and Aronson, 1992; Hazen, 1995).

This study revealed that 39 % of *Candida albicans* had an MIC of ≥ 1 µg/ml to clotrimazole which is an indication of resistance to the drug. Clotrimazole has been shown to inhibit all the major fungi causing systemic infection, at a concentration of 1µg/ml, with efficacy against *Candida, Histoplasma and Aspergillus* species (Nyst *et al.*, 1992). Although favorable results from systemic treatment of candidiasis and aspergillosis have been described, most *C. albicans* still show high MICs to clotrimazole. Induction of low blood pressure and toxicity are some of the draw backs for its systemic use. Despite the high MIC to clotrimazole, the drug is extensively used in Kenya for management of vaginal candidiasis and for dermatological conditions. Azole antifungal agents have five membered organic rings that contain either two or three nitrogen molecules (imidazole and triazoles respectively) and are thought to inhibit cytochrome P_{450} dependent enzyme involved in the biosynthesis of all membrane sterols. The clinically useful imidazoles are clotrimazole, miconazole and ketoconazole. Two important triazoles are itraconazole and fluconazole. Similar mode of action implies that if *Candida* becomes resistant to one antifungal, cross resistance is possible with related antifungals with the same mode of action (Krcmery and Barnes, 2002).

Majority of the *Candida albicans* isolates were susceptible to Amphotericin B with only 6.9 % of the isolates having an MIC ≥ 1 µg/ml. Amphotericin B is still widely used as the drug of choice for most fatal disseminated fungal infections. However the high cost of the drug makes it unaffordable to the majority of patients especially in the developing world. It should also be noted that amphotericin B can only be administered in low doses due to its toxicity. Its perenteral administration in poor resource setting is also a challenge.

Most of the *Candida albicans* isolates tested were susceptible to nystatin with 80 % of isolates having an MIC range of 0.07-1.15 µg/ml. Nystatin has been considered effective against *Candida* oesophangitis. However a cure rate of only less than 10 % has been reported in Zaire and 21.6 % in Uganda (Nyst *et al.*, 1992; Ravera *et al.*, 1999). Amphotericin B and nystatin belong to polyene antifungal drugs. Polyene compounds interact with sterols to form channels through the membrane causing the cells to leak. However the toxicity of these compounds

limits their use and also the correlation between *in vitro* and *in vivo* studies (Seibold and Tintelnot, 2003).

5.0 Conclusion

The study revealed increased MICs to azoles among *Candida albicans* species which is an indication of resistance. This calls for regular monitoring of resistance levels of *Candida* species to the antifungals particularly azoles. This is particularly important given the increased prophylactic use of fluconazole among the rising numbers of HIV/AIDS infections. Additionally, management of *Candida albicans* using antifungals with different modes of action is recommended especially with HIV/AIDS patients.

References

Bii C. C., Ouko T. T., Amukoye E. and Githinji L. W. (2002) Antifungal drug susceptibility of *Candida albicans*. East African Medical Journal. 79, **3**, pp 143 - 145.

Bii C. C., Makimura K. Abe S. Taguchi H., Mugasia O. M. Revathi G., Wamae C. N., Kamiya S. (2006) Serotypes and azole resistance in Cryptococcus neoformans MATα from clinical sources in Nairobi Kenya. Mycoses., **450**, pp 25 - 30.

Fisher A. A., Laing J. E. and Townsend J. W. (1998) A handbook for family planning operations research design. Second edition, population council New York. pp 280.

Frye K. R., Donovan J. M. and Drach G. W. (1988). *Torulopsis glabrata* urinary tract infection. J. Urol., **139**, pp 1245 - 1249.

Harvey R. L. and Myers J. P. (1987). Nosocomial fungemia in a large community teaching hospital. Arch. Intern. Med., **147**, pp 2117 - 2120.

Hazen K.C. (1995). New and emerging yeast pathogens. Clin. Microbio., **8**, pp 462 - 478.

Hickey W. F., Sommerville L. H and Schoen F. J. (1983) Disseminated *C. glabrata*: Report of a uniquely severe infection and literature review. Amer. J. Clin. Pathol. ,**80**, pp 724 - 727.

Johnson V. K. and Nickson W. J. (1970). Introduction morphogenesis and germination of chlamydospores of *C. albicans*. J. Bacteriol., **104**, pp 910 - 921.

Krcmery V. and Barnes A. J. (2002) Non-Albicans spp. causing fungaemia: pathogenicity and antifungal resistance. J. Hosp. Infect., **50**: pp 243 - 260.

National Committee for Clinical Laboratory Standards (NCCLS) (2002) Reference methods for Broth Dilution Antifungal Susceptibility Testing of Yeasts. Approved Standard NCCLS document M27-A2.

Newman S. I. (1994). Clinically significant mucosal candidiasis resistant to fluconazole treatment in patients with AIDS. Clin. Infect Dis, **19**, pp 684 - 686.

Nyst M. J., Perriens J. H., Kimputu L., Lumbila M., Nelson A. M., Piot P. Gentian V. (1992). Ketaconazole and Nystatin in Orophangyeal and esophageal candidiasis in Zairean AIDS patients. *Annales de la Societ'e Belge de madecine Tropicale,* **72**, pp 45 - 52.

Pfeller M. A. (1996) Application of CHROMAgar *Candida* for rapid screening of clinical specimens for *Candida albicans*, *Candida tropicalis Candida krusei*, and *Candida (Torulopsis) glabrata*. J. clin. Microbiol., **34**, pp 58 - 61.

Ravera M., Reggiori A., Anliata A. M. and Rocco R. P. (1999) Evaluating diagnosis and treatment of oral and esophageal candidiasis in Ugandan AIDS patients. Emerg. Infect. Dis. **5**, pp 274 - 277.

Redding S. Smith J. Farinacci G. Rinaldi M. Forthegill A. Rhine-Chalberg J. and Pfaller M. (1994) Development of resistance to fluconazole by *Candida albicans* during treatment of oropharyngeal candidiasis in AIDS: Documentation by *invitro* susceptibility testing and DNA subtype analyses. Clin. Infect. Dis., **18**, pp 240 - 242.

Reef S. E. and Mayer K. H. (1995). Opportunistic Candida infections in patients infected with human immunodeficiency virus: prevention issues and priorities. Clin. Infect. Dis., **21**, pp 99 - 102.

Richardson M. D. and Warnock D. W. (2003) *Fungal infection, Diagnosis and treatment*, 3rd ed, Blackwell Publishing UK. pp 366.

Seibold M. and Tintelnot K. (2003) Susceptibility testing of fungi - Current status and Open questions. Prog. Drug. Research, pp 191 - 241.

Selik R. M., Starcher E. T., Curran J. W. (1987). Opportunistic disease reported in AIDS patients: frequencies, associations, and trends. AIDS., **1**, pp 175 - 182.

Smith D. G. and Arsonson J. K. (1992). *Oxford textbook of clinical pharmacology and drug therapy*. 2nd edition. New York: Oxford University Press. Inc. pp. 559.

Wheat L. J. (1998) Fluconazole treatment for histoplasmosis in patients with the Acquired immunodeficiency syndrome. AIDS Clinical Trial Group. Am J Med., **98**, pp 336 - 342.

IMPLEMENTING A REAL ESTATE MANAGEMENT SYSTEM USING OPEN SOURCE GIS SOFTWARE

E. K. Mwangi and D. N. Kuria
Department of Geomatic Engineering and Geospatial Information Systems, Jomo Kenyatta University of Agriculture and Technology, Kenya
E-mail:

Abstract
Developing real estate in Kenya today has become a profitable business that is growing day by day. Many Kenyans living in towns and cities buy, build or rent a house. The aim of this project is to create a GIS system that can be used as a tool for those people who want to buy, sell or let their home in a fast, cheap and convenient way. By just looking at the GIS based site on the Internet, the interested buyer already gets most of the information without having to leave home or work. A topographic map of the area is acquired and then georeferenced to provide the background on which the parcels of land (plots) are displayed. Major roads and other important features and institutions in the area are captured and displayed alongside the plots and houses. The system is then put on the internet using Mapguide open source and then tested using Mozilla Firefox web browser.The research creates an online GIS system that allows users to search for land parcels (plots) for sale and houses to rent in Kasarani area. Users can run searches that suit their needs, e.g. search for a plot costing 500,000 Kenya shillings or a house costing 10,000 Kenya shillings per month in the area.All the land parcels satisfying this search criterion will be displayed for the user to select one that satisfies their needs. Conditional searches providing a range of results can also be performed e.g. one bedroom houses costing less than KSH10, 000 in the area. All houses satisfying the criteria will be displayed for the user to select one that satisfies their needs and then zoom into the area surrounding that house. This allows for closer analysis of the desired features. Spatial queries such as buffering, distance and area measuring can also be performed by the user.The system produced can be used by the realtor and the developers to help display choices available and easily make decisions using the map before making the physical visits on the ground. The use of open source software makes the system available to Kenyans realtors who may not afford expensive proprietary software based systems.

Key words:

1.0 Introduction

Urban growth is recognized as physical and functional changes due to the transition of rural landscape to urban forms. It occurs when the population distribution changes from being village to town and city (Rajesh and Yuji, 2009). Many regions of the developing countries are experiencing rapid urban growth. The urban growth rate in Nairobi is the highest in Kenya. As the world population increases every second, our urban areas are increasingly being faced with the problems of inadequacies of basic facilities such as good housing as a result of over population, rural-urban migration, etc. Hence, there is an increase in demand for the construction/setting up of new houses.

The majority of the people in Kenya that want to sell a property or house rely entirely on a real estate companies, individual brokers, newspapers or, more recently but to a lesser degree, the Internet. Unfortunately these sources do not provide an effective way to transmit all the necessary information that a customer needs in order to make an informed decision. For instance the newspaper provides the price, the size, the number of rooms and the exact location's name. However information such as, whether it is close to my work place, if there is any principal road access nearby will not be available on the newspaper advertisement.

The World Wide Web with the help of GIS facilities and the proper information background can give a customer exactly what they need in a fast and convenient way. Moreover the integration of GIS and the web allows easy access to useful GIS information and data without necessarily using any specific GIS software (Tyler, 2005). An Internet GIS server usually combines a standard Web (HTTP) server and a GIS application server, and the GIS databases and functionality reside completely on the server(s) (Daniel and Jinglan, 2009). Using GIS and the Web, it is possible to put the developer on the exact location of any property on sale anywhere on the region and get a pretty good idea of what this place is like. The surrounding area can also be easily examined for desired features. This information can then be used to identify those properties that are most likely to meet customers' needs (Ayalew, 2007). The focus of the system is to provide the potential buyers with enough information that makes them feel as if they have already been to the property. This allows property preselecting on the computer screen. The system will therefore save time for the seller and buyer.

Currently on the Internet there are many websites that offer some information on selling or renting homes in the country. They include: photos of the property, general location, price guide, size and general description. While this is useful information, for potential buyers it doesn't allow them to see it in a graphical way.

From the foregoing it is therefore a good idea to use the WEBGIS (Web based geographical information systems) as a tool to show the exact position of the plot and by querying any feature that involves the surrounding area to inform a client.

For instance, determine in a graphical way how many supermarkets, stores, churches, police stations are in surrounding area, simply by querying all of these features and setting the program to identify them within a specific radius of say 500m or more depending on the preferences of the client. The net effect is a more educated and more informed buyer, who is able to inspect many more attributes that can't normally be seen in the newspaper or ordinary Internet sites. In this method the buyer is not only persuaded by the houses appearance but also by its residential commodities and convenient location.

1.1 Real estate management systems

1.1.1 GIS for Real Estate

To a large extent location/geography drives the real estate industry (Atteberry and Rutherford, 2003). Effective real estate management involves not just finding any site but finding the best site possible (Tanakorn, 2007). Customers are not just interested in getting a site; they have preferences that the site must satisfy. To satisfy their customer's needs real estate companies rely heavily on GIS technology to deliver the results they need. By analyzing data around locations such as accessibility to major roads, electricity, clean water etc. GIS helps to find properties that match specifications for each client. GIS helps the real estate industry to analyze, report, map, and model the merits of one seemingly good site or location over another (Tanakorn, 2007). From identifying the best fit for new commercial development or matching a homebuyer's decision criteria to managing a property portfolio, a well designed GIS system delivers the required answers needed to make the best choice in real estate business.

"Users can walk through" the whole area viewing the different types of plots before settling on their preferred one. They can choose the type of environment to live in or to put up rental houses. (Chengda, 2001)

1.1.2 Application of GIS in Real Estate in other Countries

Real estate professionals are increasingly using maps in their property Web sites to create a more user-friendly and more fulfilling experience for consumers looking for homes. Examples of such sites include the Google Maps Miami Real Estate (http://www.miamibeach411.com). It provides users with the option of browsing a street map, a satellite image or a hybrid of the two. It assists to connect real estate developers, and buyers searching for investments anywhere in Miami, in a valuable way. The system provides an easy to use navigation tool that allows the user to just drag the map with their mouse, and use the slider to zoom in and out.
Another example is the New York real estate (www.citycribs.com); this site integrates Google maps with its real estate database to provide its users with a rich and enjoyable search experience. It applies "mash-ups" to allow the home seeker to search for New York City apartments and homes on a map (complete with property information), then link to receive full details for each listing. Users are able to filter their CribsMap™ results by selecting a borough, property type, price

and desired number of bedrooms. Once a request is entered, each apartment or house location is then overlaid onto a Google map. Each listing is displayed as a pushpin, and by clicking on the pushpin, a small window pops up with the property details, price and a thumbnail image.

The systems described above make use of expensive proprietary GIS software. This pushes them way out of reach for many realtors in developing nations. Thus there is need to explore the option of basing such technology on open source GIS software whenever possible. As explained in the next section there exist many free and open source GIS software today which can readily be used for such endeavors.

1.1.3 Open Source Geospatial Software

Open Source Software (OSS) refers to programs with licenses that give users the freedom to run the program for any purpose, to modify it and even to freely redistribute it. Open Source Software can be defined as separate from open standards and open Application Programming Interface (API) technologies. Web-based mapping tools such as the services offered by Google, Yahoo and Microsoft have open APIs that can be accessed by anyone on the Web, but they use only some open standards, and end-users have no access to the source code.

By its nature, OSS has open APIs and it must follow open standards. The defining characteristics that differentiate OSS from proprietary tools are that anyone with a computer and an Internet account can download the source code of an OSS application and use it with no further licenses. With the advance of the Internet technology, open source software is becoming increasingly popular. As Mohammad Firuz (2004) asserts, there are several open source GIS software in the Internet such as Mapguide open source Quantum GIS etc.

OSS is crucial for the developing world. They enable poorer countries to develop their own technology instead of having to import it (Rafael, 2005). It is therefore necessary for developing nations and their donor partners to review policies for procurement of computer software, with a view to ensuring that options for using low-cost and/or open-source software products are properly considered and their costs and benefits carefully evaluated.

1.1.4 Study Area

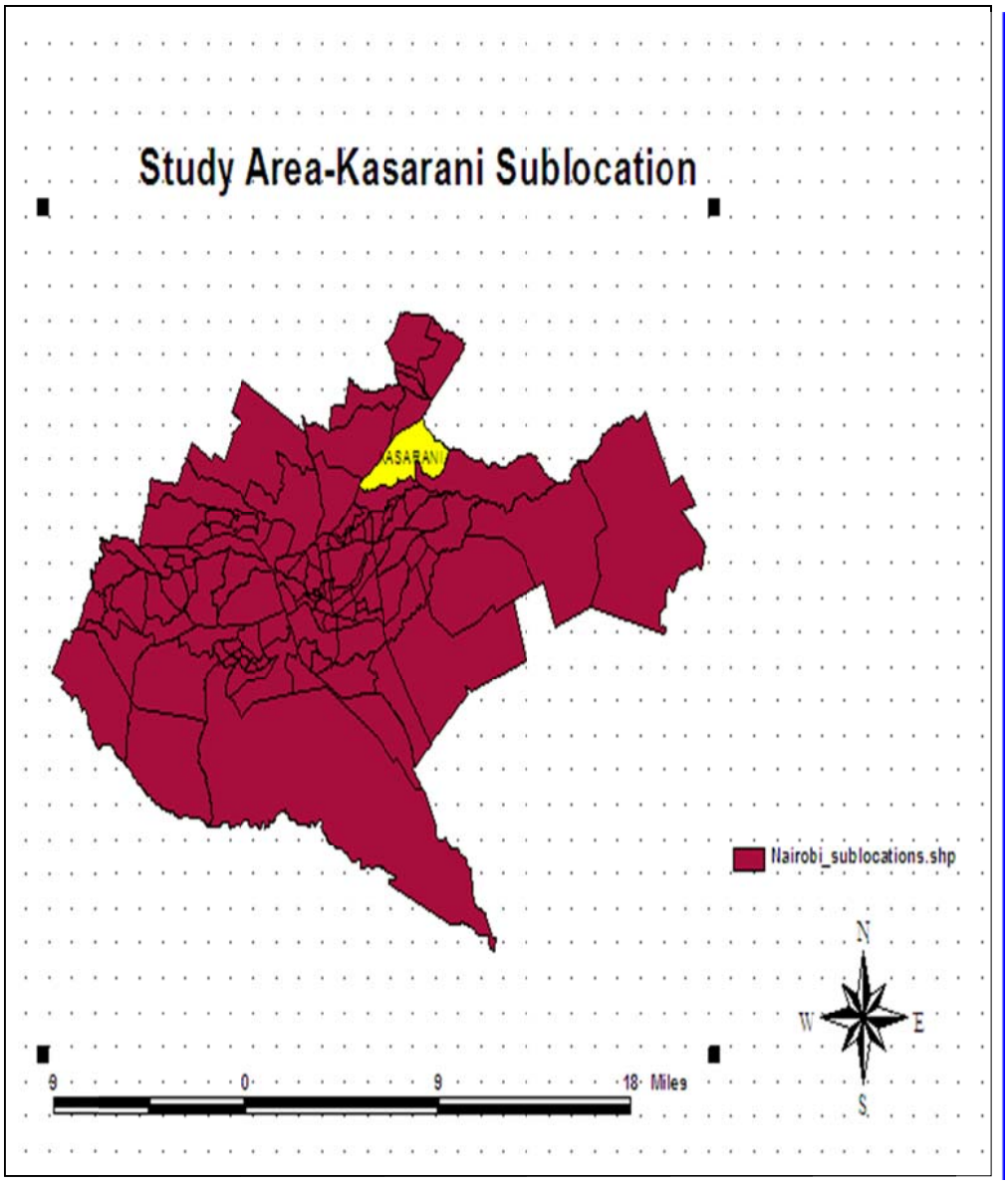

Figure 1: location of Kasarani area within Nairobi province in Kenya

The study area (Kasarani Estate) Figure 1 represents the face of the fast growing Nairobi suburbs. About 10 years ago much of it was plain grassland. Today it has been converted to a densely populated estate with both commercial and residential houses coming up all the time. Being on the outskirts it still has great potential for expansion especially towards the eastern side. It is located 10 km from Nairobi City centre.

2.0 Methodology and Data

2.1 Data

This research aims at building up a GIS based webpage which can help people in Kasarani to "advertise", in the case of a seller or, "find" in the case of a buyer plots and houses through the help of Internet in a professional, convenient, and less costly way. GIS techniques are used to allow for preselecting of desire property before actual visitation on the ground. The user should be able to perform some GIS queries about a property of interest eg measure distance from a feature of interest such as a road, a dumping site, etc. The data used is given in Table1.

Table1: Data used in the research

Data	**characteristics**	**source**
Nairobi area topographic map	Scale 1: 5000	Survey of Kenya
Nairobi administrative boundaries (sub locations)	Scale 1:251239	ILRI
Land parcels	Scale 1:2500	Survey of Kenya

2.2 Methodology

The methodology adopted in this research is as follows:

Step1: Coordinate Transformation (Georeferencing) to WGS 84 UTM 37 South

The Nairobi topographic map was georeferenced prior to digitization. Kasarani sub location boundary map acquired from ILRI website in UTM was overlaid on the map to demarcate the study area.

Land parcels (plots) were acquired from (Survey of Kenya) SOK. The parcels were in Cassini soldier projection. Thus they needed to be projected in (Universal Transverse Mercator) UTM. The transformation was done using Microsoft Excel.

Step2: Data capture

Quantum GIS is used to digitize the parcels and other features on the map like roads, police station, police post, power supply lines, swamps and other important land marks in the area.

MYSQL DBMS was used to develop attribute tables for the data needed in this project such as type of house available for rent, cost, owner contacts etc

Step 3: Selecting Tools for Website Creation

Some quick trials (explorations) emphasizing mainly on ease of use ended in favour of Mapguide open source. This is a web-based platform that allows users to quickly develop and deploy web mapping applications and geospatial web services. It provides a powerful viewer that includes support:

- For feature selection,
- Property inspection,
- Map tips
- Buffering,
- Select within, and
- Measuring.

Thus Mapguide open source was selected for the task of putting the maps on the web. Mapguide open source was downloaded from the internet and then installed using the bundled configuration option which installs and configures the Apache HTTP Server, and PHP. Then a port for the Apache HTTP Server was selected. By default, the port is 8008, so that it won't conflict with any existing web servers that listen on port 80. The service name for Apache is ApacheMapGuide. The development environment is then selected as PHP.

Step 4: Selecting The Authoring Tool

Mapguide Maestro is the authoring tool for Mapguide open source. Its equivalent to Mapguide studio in the commercial version of Mapguide (Autodesk Mapguide). Map guide Maestro allows us to upload data, make layers, define the layers (symbology, labels, scale dependencies, etc.), and create maps.

Step 5: Creating a Folder Structure

In this step, the recommended folder structure for a new project is created. Folders for data, layers, maps, and layout were created for the project.

Step 6 Loading Shapefiles

The next step was loading SHP files. This is done by first connecting the data provider corresponding to the data to be loaded directly into a folder in the shape file folder.

Step 7: Making Layers

After connecting and loading the shape files the layers for the shape files were made.

Step 8: Connect to an MYSQL Database

In this section, a connection to the MYSQL database for the Kasarani plots and houses data was established and saved as a resource.

Step 9: Setting The Style for Layer

The basic style for a polygon, lines and point feature layers were edited by selecting a fill color and a border color for each layer in the project.

Step 10: Create a New Map

This involves creating new map and setting its properties. The basic description, of the map was entered here leaving the Coordinate System section blank (the map used the coordinate system of the first layer that was added to it). For Background Color, a light colour was selected (white).

The various Layers were then added to the map.

Step 11: Organize the layers in a map

Layers were organized in appropriate order starting with point features then lines and finally polygons so that viewers can see all the features clearly.

Layers that have not yet been edited were edited so that the layers in the map are displayed in color and at the appropriate scales. Labels were also generated on the map.

Step 12: Adding Tooltips

To improve on the usability of the system tooltips were included on the map

Tooltips are pop-up boxes that contain information about the features in the map. users will be able to view the tooltips in the Web browser. When a user points the mouse to a given feature a tool tip appears describing, briefly, the specific feature under scrutiny. Whenever a user places the mouse cursor on a feature the information set on the tool tips appears automatically.

Step 13: Setting up The Map Legend

Some layers were initially turned on while others are turned off. Labels for the various layers are also set here.

3.0 Results and Discussions

3.1 Viewing the Map

A new layout was created and the map was embedded on it finally, the map was previewed in a Web browser as shown by Figure 2.

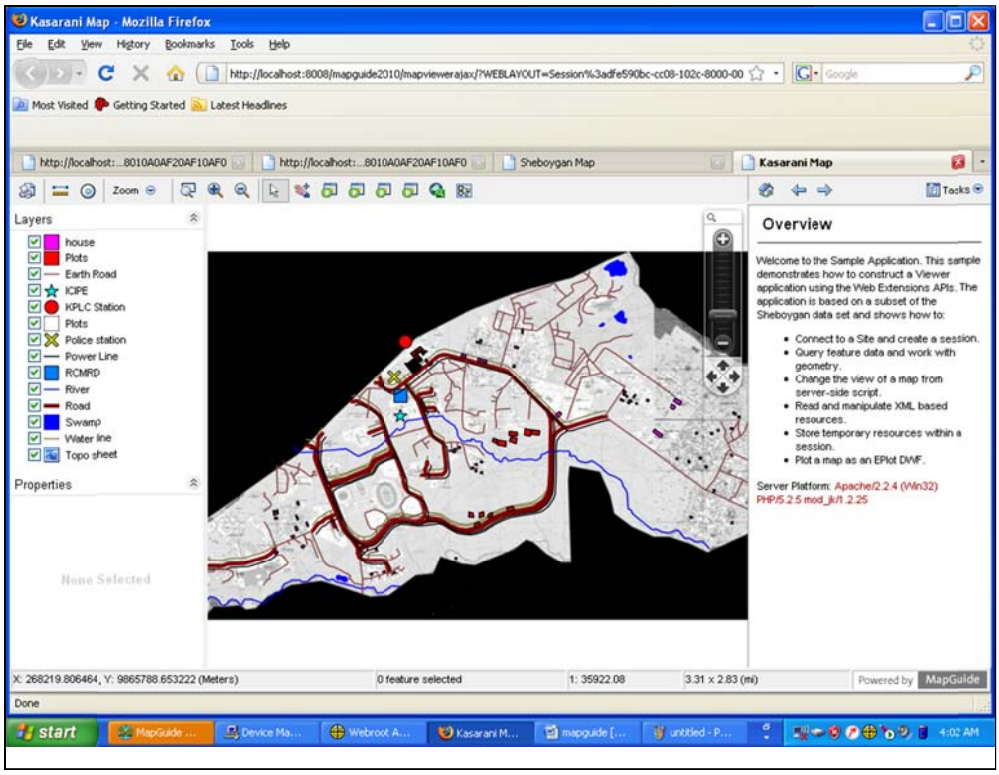

Figure 2: Final map on Mozilla Firefox

The content of toolbar, context menu and task menu was edited to include functions meant for this system as shown in Figure 3

Tool for searching plots and houses based on size and cost was added to the layout. Customers can search for a desired property simply by inputting the property or condition in the search tool. Figure 3 shows a customer searching for a plot costing 500,000 Kenyan shillings.

The results of the search are displayed on the right pane. All plots on sale that cost 500,000 Kenyan shillings are displayed on the map. The user then can select the one that satisfy their needs by inspecting their various positions on the map

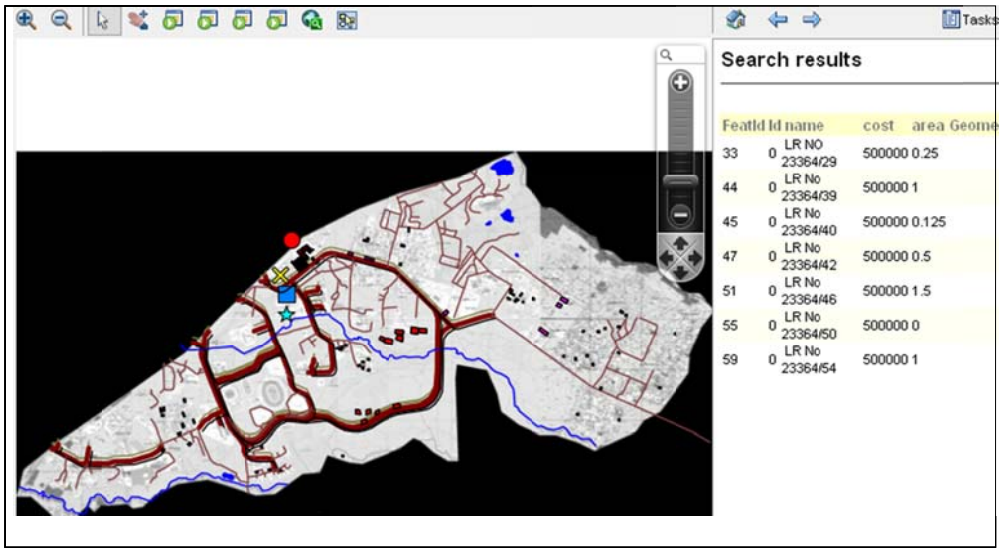

Figure 3: Search results on the site showing all plots costing 500,000 Kenyan shillings

A conditional search can also be performed so that one can get a range of results. For example one may be interested in houses that are costing less than a given amount eg 10,000 Kenyan shillings. Figure 4 demonstrates such a search, where the customer is interested in houses costing more than 10,000

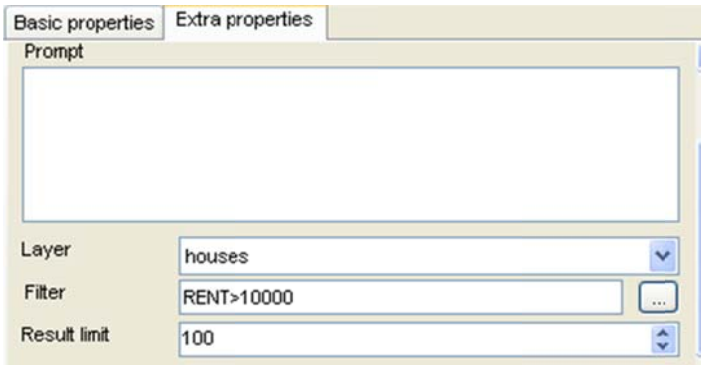

Figure 4: Searching for a house of rent more than 10,000 Kenyan Shillings

The results of the search are shown on Figure 5

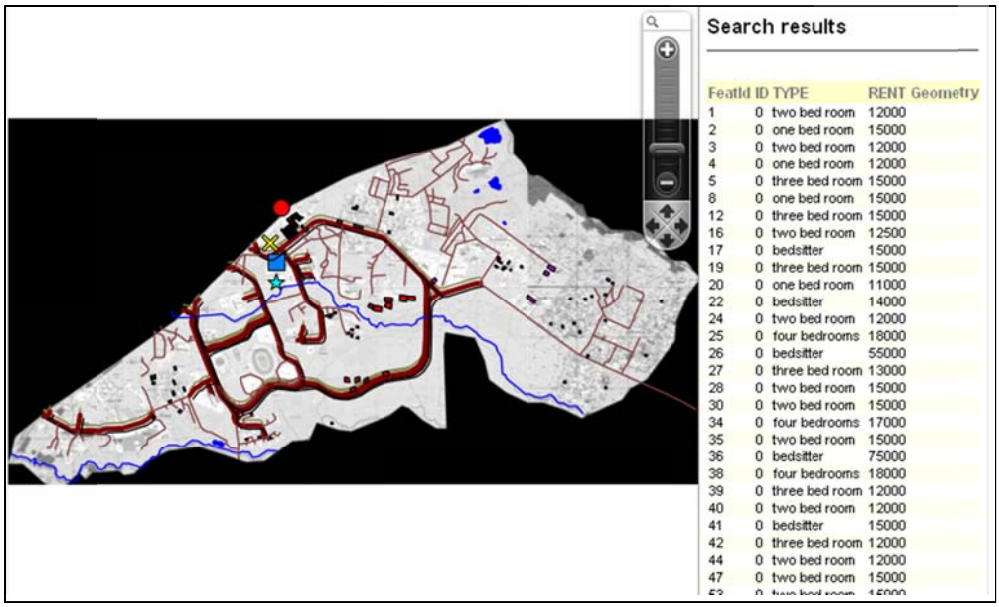

Figure 5: Results of conditional search

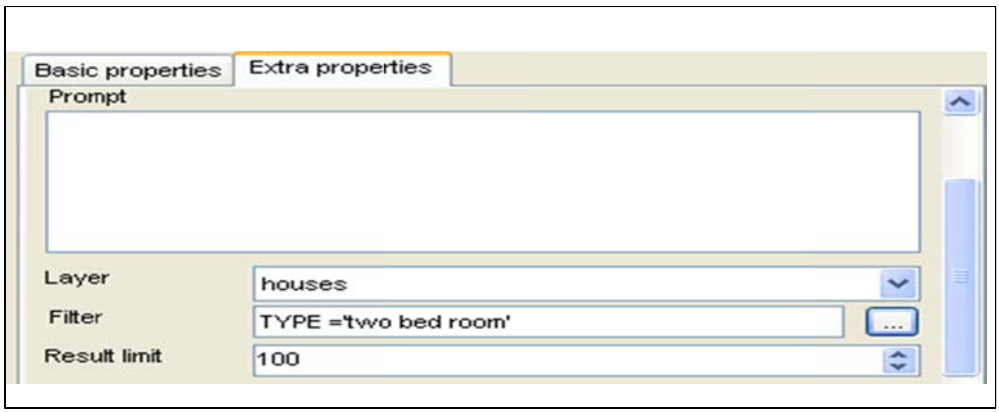

Figure 6: Searching all two bedroom houses in the area that are available for rent

To create a search one needs to define the layer and the filter condition as shown in Figure 6.

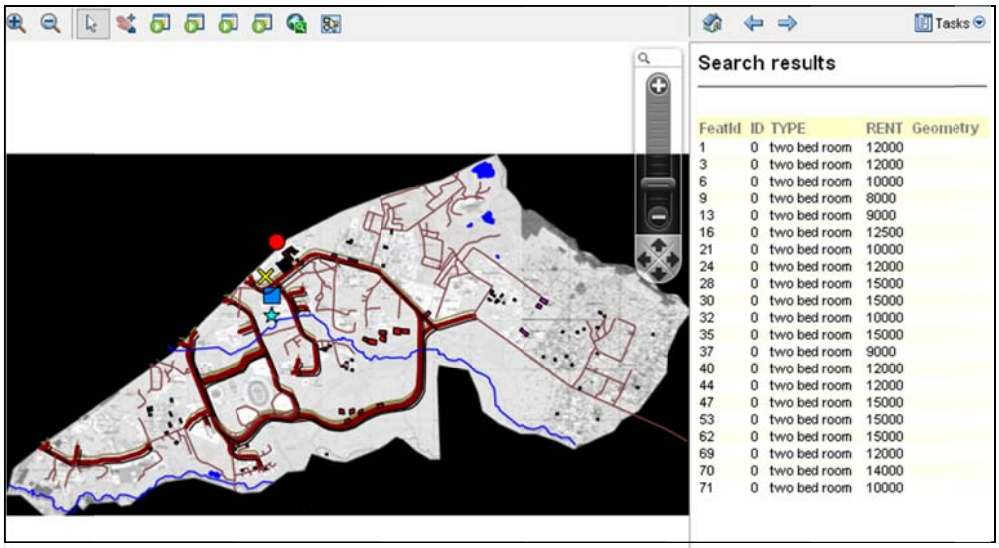

Figure 7: Results of the search for all two bed roomed houses and their cost on the website

When the search is run, all the results are displayed on the browser as shown on Figure 6. To move to the area and zoom on a parcel or house, one only needs to click on the selected house. The focus moves to that area allowing for a close examination on the feature in question, as figure 7 shows below.

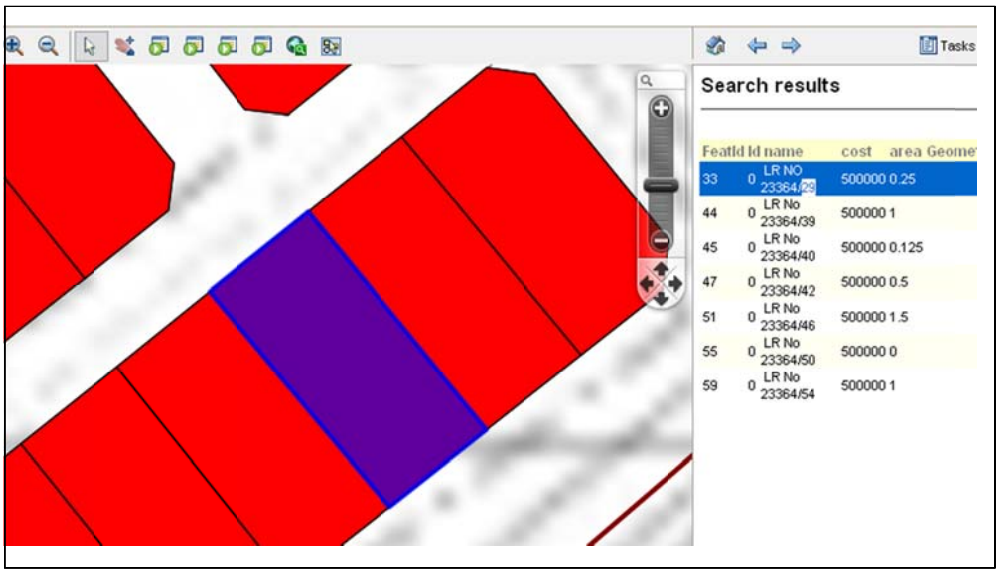

Figure 8: clicking a selected feature to zoom to it

The particular parcel is shown in different color. In Figure 8 above, the one in colour blue. The site also allows for carrying out spatial queries in the area such as buffering or measuring as described below.

3.2 Buffering

A user may be interested in ensuring that the area they rent or built their house is far or near certain features. For instance people will not want to live near garbage dumps or noisy night clubs. On the other hand some people may want to be near features such as roads or schools for the convenience of their school going children. It's easy to buffer on the site, just set the distance from the feature of interest. The results of the buffer just show the feature of interest and the desired features in the surrounding area. This assists in decision making without necessarily going to the field to observe the features.

3.3 Measuring

Customers may be interested in determining how far features of interest are from their homes. One feature of interest is more often than not the main road and the shopping center. The measuring tool can assist in determining the distance from any feature of interest.

4.0 Discussion

The open source GIS software selected for this project proved adequate for the desired tasks. One objective of the project was to show that open source GIS software can be used to produce a system to support real estate agents. This has been shown to be true, through the use of Quantum GIS to perform the GIS work; this is a powerful desktop GIS software providing most typical GIS functionalities. To cater for any unavailable functionality Quantum GIS provides a powerful user interface for GRASS tools (Gary, 2007). Mapguide open source as the map server, apache as the web server and MYSQL as the database management system, Firefox is used as the browser. All these are open source software available free for any interested developer.

Quantum GIS would at times crash especially when a lot of data is loaded. It would simply say it has to close down. In addition digitizing was not very easy using Quantum GIS. These are very minor draw backs as compared to the cost of proprietary software, especially considering that it is not clear whether the difficulties are due to software deficiencies or due to inadequate user training.

Proprietary GIS software is quite expensive especially for cash strapped third world economies and small to medium organizations (Christopher, 2006). Open GIS

software provides excellent alternatives to their GIS needs. The budgets for purchasing one proprietary solution for these organizations would by far surpass the amount required to train internal staff on open source GIS software use.

5.0 Conclusion and Recommendations

5.1 Conclusion

The Internet and World Wide Web is gaining popularity as the revolutionary medium of communication for the new millennium. Thus the integration of Internet and GIS for information dissemination has provided a new opportunity for GIS Industries to exploit.

Map data will normally be transmitted to a Web client in standard HTML formats. This implies that they can be accessed through any Web browser.

Furthermore the use of Open Source GIS software application makes the software available to people who would otherwise not have afforded it. Selling real estate in Kenya is becoming an important business. It is because of its vital importance that creative and sustainable ways to keep this profitable industry on track must be found. Users must not only adjust with what is on the market now but find new ways to promote what we already have in our hands. Open source software such as Quantum GIS and Mapguide open source are free platforms that provide facilities that can be used for many applications. Putting the system on the web means that the user does not have to possess any special software to display it. It is as simple as opening a web page.

With that incredible quality users can reach more people and let them know about

their products; in this particular case plots and houses for rent. The Internet as a search tool does, in fact, reduce search costs. The Web allows buyers to quickly and cheaply locate and learn about houses and plots on the market. This information can then be used to identify those properties that are most likely to meet their needs. The main focus of the system is to provide the potential buyers with enough information that makes them feel as if they have already been to the property. Furthermore it offers the customer additional information about the property which may be the enticement needed to make the purchase/rent instead of only relying on the appearance of the property.

5.2 Recommendations

This system can be improved to cover the whole city or the whole country or even the whole world. Such a system would then allow buyers and sellers all over the

world to interact, buy and sell property from anywhere in the world. The integration of the system with Google maps would assist to provide a more natural experience to customers. Just like the CityCribs.com for New York real estate system which integrates Google maps with its real estate database to provide its users with a rich and enjoyable search experience. In addition the application of tool tips can be improved further by including "mash-ups" to allow the home/plot seeker to search for plots and homes on a map (complete with property information),then link to receive full details for each listing.

As regards apartments for rent, the system can be improved by including virtual tours like the Honduras real estate system which allow the user some preview of the house interior for better decision making. Thus, in order to keep the cost down, there is need to investigate the open source or other cheap software alternatives to allow for the inclusion of desired features, without making the system too expensive for real estate agents in Kenya. In addition, a user needs assessment would go a long way to making the system more responsive to the specific user needs in this industry.

References

Atteberry and Rutherford (2003), *Industrial Real Estate Prices and Market Efficiency*, *Journal of Real Estate Research*, 2003, **8(3)**, pp 377–85.

Ayalew B. (2007). Internet-GIS: An application to Real Estate and Housing Management in the City Government of Addis Ababa (CGAA) master's thesis

Chengda Lin (2001). Application and research on GIS for real estate Wuhan University china.

Christopher J. (2006). Open Source Geospatial Software Provides an Enterprise Alternative for Small Agencies. Autodesk, Inc

Daniel and Jinglan (2009). OpenCIS—Open Source GIS-based web community information system**,** a School of Software Engineering & Data Communications, b Faculty of Information Technology, Queensland University of Technology (QUT), Brisbane, QLD 4000, Australia. International Journal of Geographical Information Science.

Gary W. (2007). Introduction to Quantum GIS Florida University centre for ocean-atmospheric prediction studies GN U free documentation license.

Mohammad F. (2004) open source geographical resources analysis support system (GRASS) for landslide hazard assessment in disaster prevention and management ,**14,** pp 522-532. emald group publishing limited.

Rafael M. S. (2005). Building Web-Based Spatial Information solutions around Open specifications and Open Source Software Geoffrey Anderson Cloudshadow Consulting, Inc Boulder, Colorado Department of Geography University of Colorado at Denver.

Rajesh and Yuji (2009). Drivers of urban growth in the Kathmandu valley, Nepal: Examining the efficacy of the analytic hierarchy process 1 Division of Spatial Information Science, Graduate School of Life and Environmental Sciences, University of Tsukuba, 1-1-1 Tennodai, Tsukuba, Ibaraki 305-8572, Japan journal of applied geography Applied Geography 30 (2010) pp 70–83.

Tanakorn J. (2007). A Web-based Electrical GIS MapServer via Open Source GIS Software Geographic Information System University of Texas at Dallas Tanakorn10@hotmail.com

Tyler M. (2005). Web Mapping Illustrated. O'Reilly Publisher Bil Kropla. 2005. Beginning MapServer: Open Source GIS Development. A press Publisher

Google Maps Miami Real Estate system
(http://www.miamibeach411.com).accessed 12/1/2010, 12.30pm

New York real estate system (www.citycribs.com) accessed 10/1/2010, 10.00am

THE USE OF SATELLITE IMAGES TO MONITOR THE EFFECT OF SAND DAMS ON STREAM BANK LAND COVER CHANGES IN KITUI DISTRICT

H. K. Manzi[1] and D. N. Kuria[2]
[1]Ministry of Agriculture, Nyeri, Kenya
[2]Geomatic Engineering and Geospatial Information Science department, Kimathi University College of Technology, Kenya
E-mail:

Abstract
A study was carried out to investigate the effect of sand dam construction on land cover changes along the stream bank during the dry season using satellite images. Two water catchments namely Kiindu and Mbusyani in Kitui district that have similarities in topographical features were chosen for the study. Land cover change detection analysis was done by use of Landsat ETM+ 2001 and Landsat TM 1986 satellite images for Kiindu and Mbusyani catchment for the period 1995- 2001 (after sand dam construction) and 1986 (before sand construction) respectively. Based on the reference data collected from the field two land cover types were of significance importance for the research study i.e. vegetation and bare land.
The classification involved identifying areas of vegetation existence and non-existence during the dry season along the stream banks. Following the classification a change detection analysis was carried out between 2001 and 1986 whose results indicated an increase in vegetation as result of sand dam construction. Kiindu catchment vegetation increased by 52% whilst Mbusyani increased by 43% in 2001 i.e. The relative change in area (ha) from bare land to vegetation was 1356.5 ha and 1218.8 ha compared to vegetation in 1986 which was 229.7 ha and 264.3 ha respectively. The overall accuracies of the classification maps for the two catchments were; Kiindu 90% in 2001 and 87% in 1986 with Kappa Statistics of 0.74 in 2001 and 0.67 in1986. Mbusyani on the other hand had 89% in 2001 and 87% in 1986 with Kappa Statistics of 0.78 in 2001 and 0.66 in 1986. The results from the analysis therefore indicated that sand dam did have a significant influence on land cover changes along stream bank channels during the dry period.

Key words: sand dam, land cover, remote sensing, GIS, water catchment, landsat ETM+

1.0 Introduction

Over the years the arid and semi-arid areas in Kenya have experienced land degradation largely due to multiplicity of interacting environmental and socio economic factors. The degradation process has been aggravated by deforestation, overgrazing, increased demand for agricultural land with poor agricultural practices, increased evapotranspiration and reduced annual rainfall. It is projected according to studies that annual rainfall is about (450-900) mm on average (FAO, 1987) leading to poor land cover especially in the dry season. The result of this is increased rates of runoff, decreased infiltration rates and increased wind and water erosion.

Land cover along stream channels is a prerequisite to high water infiltration and aquifer recharge in the dry season. It enhances the stream capacity to accumulate and store water underground that is useful to the people and the environment during the dry spell. It averts high levels of sediment accumulation which are as a result of extreme levels of soil erosion during the rain period.

Sand dams are concrete structures, whose location in ephemeral sand-river beds demands detailed surveys, preferably with thorough ground truth (Munyao J.N. *et al.* 2004). The potential of sand dams in an area is a function of the availability of sand on streams, topography that allows construction of weirs, geology to suit storage structures and the presence of a population to make use of the water. (Nissen-Petersen, 1997), Sand dams effectively increase the volume of groundwater available for abstraction as well as prolonging the period in which groundwater is available for abstraction (Nissen-Perterson E**.,** 1982). Sand dam construction is associated with land cover change due to the lateral movement of water as result of aquifer water recharge. The amount of extractable water from a river stretch in between two sand dams is 8372 m^3 per year, (Borst L., De Haas S**,** 2006). Changes in land cover alter both runoff behavior and the balance that exists between evaporation, groundwater recharge and stream discharge in specific areas and in entire watersheds, with considerable consequence for all water users (Sahin, V., and Hall, M. J., 1996), (Defries, R. and Eshleman, K. N., 2004). Sand dams are fully functional within a period of 5-8 years after construction. The research draws inferences through comparing land cover before and after sand dam construction during the dry month.

Remote sensing technology has enhanced land cover assessment through the increased availability and improved quality of multi-spatial and multi-temporal remote sensing data as well as new analytical techniques. (Rogan, J. and Chen. D.M, 2004), Land cover assessment involves change detection which is defined as a process of “identifying differences in the state of an object or phenomenon by observing it at different times” (Rogan, J. and Chen. D.M, 2004). A change-detection technique such as Post-classification comparison method used in this research determines the difference between independently classified images from

each of the dates in question (Deer P., 1995). The assessment provides essential requirements for the sustainable management of natural resources, environmental protection and food security.

1.1 Study Area

The study area consists of two catchments, namely Kiindu and Mbusyani in Kitui District as shown in figure 1. The District in the Eastern Province of Kenya is a semi-arid region under agro-ecological zone iv and v situated 150 km East of Nairobi. The total land area is approximately 20,402 km^2 and is characterized by hilly ridges, separated by low lying areas between 600 and 900 meters above sea level, about 1^o 22' south and 38^o1'East. The rainfall amount is (450-900) mm on average. Soils in these areas are sandy, dry and therefore prone to soil erosion by wind and sporadic torrential rains.

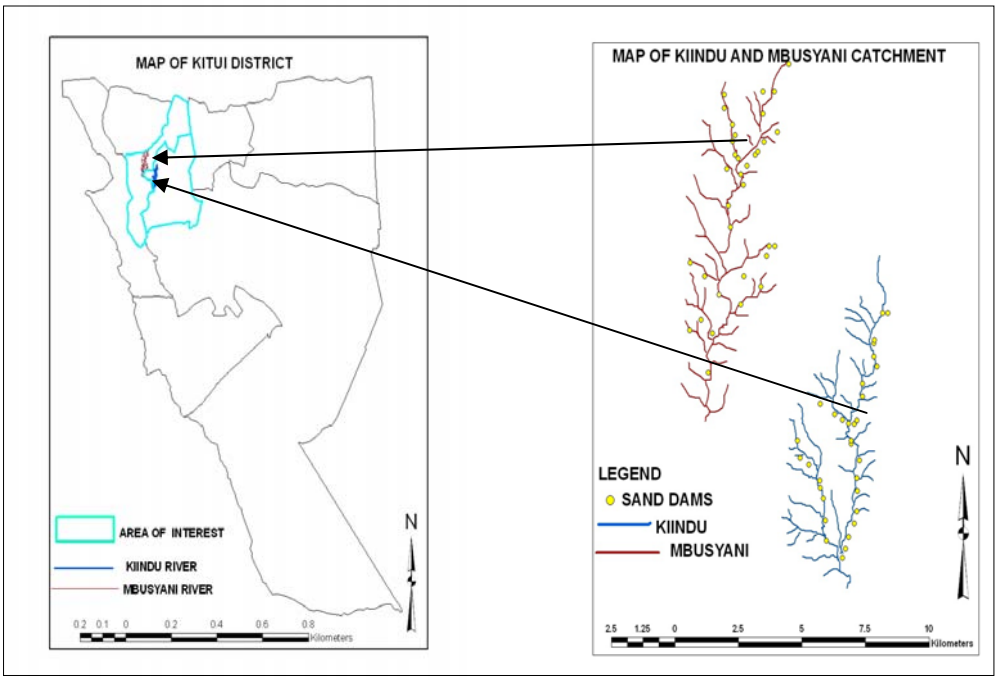

Figure 1: map of study area

Notable vegetation in the area includes deciduous woodlands such as *Acacia tortillis, Hpaenae ventricosa, Salvadora persica, Acacia Nubica* and *Acacia commiphora*. (Gooding J.R, and Northington J.K, 1985). Ephemeral rivers in Kitui District experience high flow in April-May and November-December rains while becoming dry immediately after one month. The water catchments are characterised by metamorphic and igneous basement covered with weathered rocks.

1.2 Rainfall Data

The rainfall data shown in Figure 2 was significant in establishing the rainfall trends and fluctuations between the two periods; before sand dam construction (1986) and after sand dam construction (1995 to 2001). Rainfall has a great influence on the vegetation and similar rainfall trends were significant for the study.

The other importance of rainfall data was to serve as an aid in the selection of the most appropriate month for the research study, a dry month in the year.

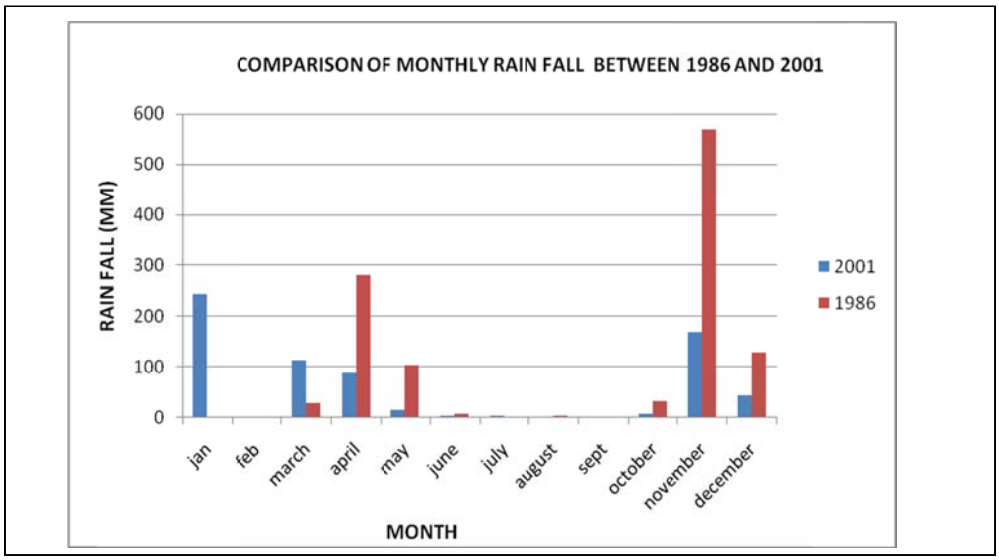

Figure 2: Monthly rainfall data

Vegetation in the semi arid areas is characteristics of tall shrubs and other thorny Bushes, e.g. *Acacia clavigera, Acacia nilotica, Acacia seyal, Terminalia combretum* and *Commiphora* sp. (Katumo V., 2001) succumbs to drought after 3 months dry period. The vegetation sheds off its leaves as drought escaping mechanism and hence would appear as bare land on a satellite image, (Bunn S. E., and Arthington A. H., 2002).

2.0 Methodology

2.1 Data Sources and Specification

There are various data sources used in the research, the GPS location of sand dams and training areas for the vegetation type obtained from the field, digital topographical map at a scale of 1:50,000 for Kitui area from the department of Geomatic Engineering and Geospatial Information Systems of Jomo Kenyatta University of Agriculture and Technology. Finally satellite imageries from the Landsat TM for 26th August 1986 and Landsat ETM+ for 14th October 2001 were acquired from the Regional Centre for Mapping of Resources for Development at Kasarani, Nairobi.

2.2 Tools Used for Data Capture

The reference/ field data was collected from the field through a GPS survey of the water catchment area. The reference data was significant in validating the classification results of the satellite images, with GPS survey used to establish the location of sand dams. During the survey the various land cover types prevalent in the area were identified namely, bare land, grassland, short and tall shrubs, tall trees and irrigated agricultural land. For the purpose of the research study the grassland, short, tall shrubs, tall trees and irrigated land were merged as one land cover type i.e. vegetation. Other tools involved in data capture and its storage and analysis included computer software ArcGIS 9.3 and ERDAS IMAGINE 8.6.

2.3 Data Preparation/Geo-Referencing

Scanned topographical map at a scale of 1:50,000 were georeferenced to Clarke 1880 UTM zone 37 South, and subsequently used for digitizing the catchments used for the study. The satellite images obtained for the study were also georeferenced using ERDAS IMAGINE 8.6 to the same projection system.

2.4 Data Processing

Digitization of the field data using ArcGIS 9.3 was done in order to enable the classification of the satellite images. Water catchments i.e. Kiindu and Mbusyani were extracted from digitized topographical map of Kitui using ArcGIS 9.3 and a buffer of 400m created. Buffering was for identification of the stream bank area of interest. Overlaying of the water catchments onto the satellite images was done using ERDAS IMAGINE and a subset of the region of interest for the study created. The subset images for Kiindu and Mbusyani catchments were 2631.2ha and 2812 ha respectively. Cloud cover effect in the Landsat ETM+ 2001 image was evident and hence a shape file was created using ArcGIS 9.3 which was used in masking out clouds on the all the images (coinciding areas on all images) using ERDAS IMAGINE.

2.5 Image Classification

A supervised land cover classification was carried out based on the ground truthing data/field data using ERDAS IMAGINE. The classification was performed, using a maximum likelihood classifier. Figure 3 shows, the land cover classifications for the year 1986 and 2001 respectively. The classification of the two Landsat images was geared towards separating two prominent classes with reference to the field data obtained and with relevance to the research study.

2.6 Change Detection Analysis

This encompasses the quantification of temporal phenomena from multi-date imagery that is most commonly acquired by satellite-based multi-spectral sensors (Coppin, P.I *et. al.*, 2004).

The method used in the change detection analysis was post classification that produces spectral classification results from each end of the time interval of

interest, followed by a pixel by pixel or segment by segment comparison to detect changes in land cover types (Bunn S. E., and Arthington A. H., 2002). The two land cover maps were compared pixel by pixel with the final results showing both change and no-change information as well as 'from to' land cover change information.

3.0 Results

3.1 Results of Supervised Classification

The objective of the research study was to use satellite image to deduce the significance influence of sand dams on land cover types along stream banks. The study hence narrowed down to two land cover types based on the reference data collected from the field. The two land cover types were vegetation (tall and short shrubs, irrigated agricultural land, grasses and trees) and bare land (roads, dry vegetation and fallow land).The results indicated a visible land cover change between the two periods. Vegetation and bare land did exist in both periods with a difference in the area covered. Concentration of vegetation is evident closer to the stream channel but expand gradually for the period after dam construction. Bare land is sparsely distributed along the stream channel as captured in Figure 3.

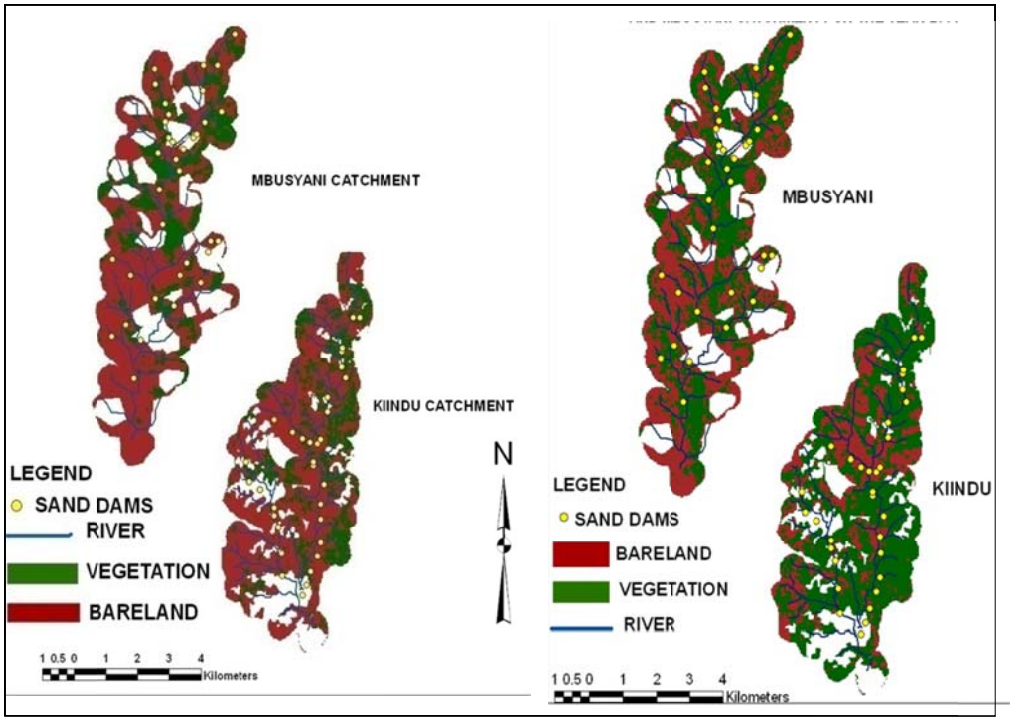

Figure 3: Map of land cover types for Kiindu and Mbusyani catchment for the year 1986 and 2001

Studies carried out by (Vogelmann J.E. *et al*. 2001) have indicated a higher similarity of occurrence in the ability of Landsat TM and Landsat ETM+ to measure

land cover changes accurately. An increase in vegetation in the 2001 satellite image can be associated with inter-annual fluctuations in vegetation occurrence as well as vegetation productivity (Wezel, A., and Schlecht, E., 2004). Such fluctuations in vegetation occur with changes in soil moisture. (Rogan, J., *et. al*. 2008) chose a supervised land cover classification method and the resulting classification averaged an overall accuracy assessment of 84% and hence considered an indicative of the potential for Landsat TM data in land cover assessment over a diverse area. Comparing the findings of the above studies to the results of the supervised classification of Landsat images used in this study together with the accuracies therein it is evident that the accuracy results for the classification are comparable and hence reliable. The prior knowledge of the research area and reference data used during the classification enhanced confidence in the accuracy of the classification results.

Supervised classification works best when it involves the identification of relatively few classes, when the training sites can be verified with ground-truthed data, and/or when the user can identify distinct, homogeneous regions that represent each desired class (Lillesand T. M., and Kiefer R. W., 1994). This is the reason for merging various vegetation classes into one class in order to improve on the classification.

3.2 Results of Accuracy Tests for Land Cover Classification for 1986 and 2001

The overall accuracy of the land cover classification in 2001 for Kiindu and Mbusyani catchment was 90% and 89% respectively with kappa statistics being 74% and78% as shown in tables 1 and 3. In the 1986 overall accuracy test were 87% for both catchment and a kappa statistics of 67% and 66% respectively as shown in tables 2 and 4. These slight differences in the accuracy results from the two Landsat sensors (TM and ETM+) while not very significant can be attributed to the differences in the sensor characteristics, especially their radiometric ranges with ETM+ being able to allow finer radiometric resolution in contrast to that by TM.

Table 1: Error matrix accuracy statistics for Landsat ETM+ 2001 for Kiindu catchment

Classified data	**Reference data**				
	Vegetation	Bare land	Total possible	**Producers accuracy %**	**Users accuracy %**
Vegetation	257	12	269	91.79	95.54
Bare land	23	70	93	85.37	75.27
Totals	280	82	362		
overall accuracy %	**90.33**				
Kappa	**0.7366**				

Statistics					

Table 2: Error matrix and accuracy statistics for Landsat TM 1986 for Kiindu catchment

Classified data	**Reference data**				
	Vegetation	Bare land	Total possible	**Producers accuracy %**	**Users accuracy %**
Vegetation	38	9	47	71.7	80.85
Bare land	15	136	151	93.79	89.47
Total	53	145	198		
Overall Accuracy	**87.44**				
Kappa Statistics	**0.6699**				

Table 3: Error Matrix and accuracy assessment for Landsat ETM+ 2001 for Mbusyani catchment

Classified data	**Reference data**				
	vegetation	Bare land	Total possible	**Producers accuracy %**	**Users accuracy %**
Vegetation	90	13	103	89.11	87.38
Bare land	11	109	120	89.34	90.83
Total	101	122	223		
Overall Accuracy %	**89.24**				
Kappa Statistics	**0.7832**				

Table 4: Error Matrix and accuracy statistics for Landsat TM 1986 for Mbusyani catchment

Classified data	**Reference data**				
	vegetation	Bare land	Total possible	**Producers accuracy %**	**Users accuracy %**
Vegetation	51	10	61	94.65	87.62
Bare land	25	177	202	68.92	83.61
Total	76	187	263		
Overall Accuracy %	**86.69**				
Kappa Statistics	**0.6576**				

A standard overall accuracy for land-cover mapping studies has been set between 85 percent (Anderson, J.R., 1976) and 90 percent (Lins, K. S.,1996) The accuracy results therefore fall within the acceptable ranges that define quality in classification.

3.3 Results of Change Detection Accuracy Assessment for Kiindu and Mbusyani Catchment Respectively

The accuracies of the change detection were computed based on visual interpretation of the image data. The reference visual random points were generated using ERDAS IMAGINE and used for the accuracy assessment.

Table 5: Change detection accuracy assessment for Kiindu catchment

Classified data	**Reference data**				
	To bare land	To vegetation	Total possible	**Producers accuracy %**	**Users accuracy %**
To bare land	7	2	**9**	**77.78**	**70**
To vegetation	3	115	**118**	**97.46**	**98.29**
Classified Totals	**10**	**117**	**261**		
Overall accuracy %	**96.06**				
Kappa statistics %	**71.56**				

Table 6: Change detection accuracy assessment for Mbusyani catchment

Classified data	**Reference data**				
	vegetation	Bare land	Total possible	**Producers accuracy %**	**Users accuracy %**
Vegetation	90	13	103	89.11	87.38
Bare land	11	109	120	89.34	90.83
Total	101	122	223		
Overall Accuracy %	**89.24**				
Kappa Statistics	**0.7832**				

The classification had only two land cover types therefore the visual analysis was not as intensive hence an appropriate tool for the interpretation as shown in tables 5 and 6. [11] Examined the use of different accuracy indices, including overall, average and combined accuracies and the Kappa coefficient of agreement to determine an optimal threshold level for change detection images. They recommended the Kappa coefficient because it considers all elements of the confusion matrix. The accuracy of a post classification method depends on the accuracy of the independent satellite images (9).

3.4 Results of Change Detection Analysis

Changes in land cover were established through the changes in pixel counts in both 1986 and 2001 respectively and computed into percentage and total area in ha as shown in table 7. A relative change of 60% and 57% for Kiindu and Mbusyani respectively was evident. This covered an area of 1581ha and 1622ha for the two catchments respectively. Therefore a significant land cover change between vegetation and bare land occurred for the period (before) and (after) sand dam construction. To further deduce this, a change detection analysis was carried out.

Table 7: Showing change in land cover classes from 1986 to 2001

Land cover types	**Kiindu catchment land cover change**						**Mbusyani catchment land cover change**					
	1986		**2001**		**Relative change**		**1986**		**2001**		**Relative change**	
	Area (Ha)	Proportion (%)	Area (Ha)	Proportion (%)	**Area (Ha)**	**Proportion (%)**	Area (Ha)	Proportion (%)	Area (Ha)	Proportion (%)	Area (Ha)	Proportion (%)
Vegetation	229.7	9	1810.5	69	**1580.8**	**60**	264.3	26	1357.7	48	**1622**	**57**
Bare land	2401.5	91	820.4	31	**-1581.1**	**-60**	2549.7	74	1456.3	52	**-1622**	**-57**

A change detection analysis for all land cover types was computed using ERDAS IMAGINE as shown in table 8 and figure 4 on change detection analysis. The results obtained were compared to percentage pixel counts and area (ha) for each land cover type. The percentage change for each land cover type i.e. increases; decreases and area that remained unchanged were deduced. The focus for the

research study was on the increases and decreases on the land cover types. The land cover changes were compared to the presence of the sand dams along the catchment.

Table 8 shows that bare land decreased by 52 %(1357ha) and 43 %(1219ha) to vegetation for Kiindu and Mbusyani respectively. The vegetation decreased by 8 %(224ha) and 14 %(403ha) for Kindu and Mbusyani catchment to bare land. This can be associated with area of land cleared for cultivation (fallow land). About 40% and 43% of the area for Kiindu and Mbusyani remained unchanged respectively.

Figure 4 shows the increase in vegetation associated with the decrease in bare land, (see the decrease in green color). There is also a decrease in vegetation which leads to an increase in bare land, (see the red color). The areas in white are those where there was no significant change.

In north China, (Xiao, J., *et. al*, 2006) evaluated urban expansion and land use change with 1987 Landsat TM and 2001 Landsat ETM+ data. Successful land use and land cover classification allowed (Xiao, J., *et. al*, 2006) to identify a relationship between land use and land cover change and urban expansion using post classification change detection technique.

The accuracy test in the research are indicative of accurate results obtained from the change detection analysis i.e. Overall accuracy of 96.06% and Kappa Statistic of 71.56% for Kiindu catchment and overall accuracy of 94.44% and kappa statistics of 85.78% for Mbusyani catchment. It is evident that there is a positive change in vegetation for the two catchments.

Table 9: change detection analysis between 1986 and 2001 for Kiindu and Mbusyani Catchment

	Kiindu catchment change analysis						**Mbusyani catchment change analysis**					
land cover type	**bare land**		**Vegetation**		**Relative change**		**bare land**		**Vegetation**		**Relative change**	
	Area (Ha)	Proportion (%)	Area (Ha)	Proportion (%)	**Area (Ha)**	**Proportion (%)**	Area (Ha)	Proportion (%)	Area (Ha)	Proportion (%)	**Area (Ha)**	**Proportion (%)**
Bare land			1356.5	52	**1356.5**	**52**			**1218.8**	**43**	**1218.8**	**43**
Vegetation	224.3	8			**224.3**	**8**	**403.2**	**14**			**403.2**	**14**
Total	**224.3**	**8**	**1356.5**	**52**	**1580.8**	**60**	**403.2**	**14**	**1218.8**	**43**	**1622**	**57**

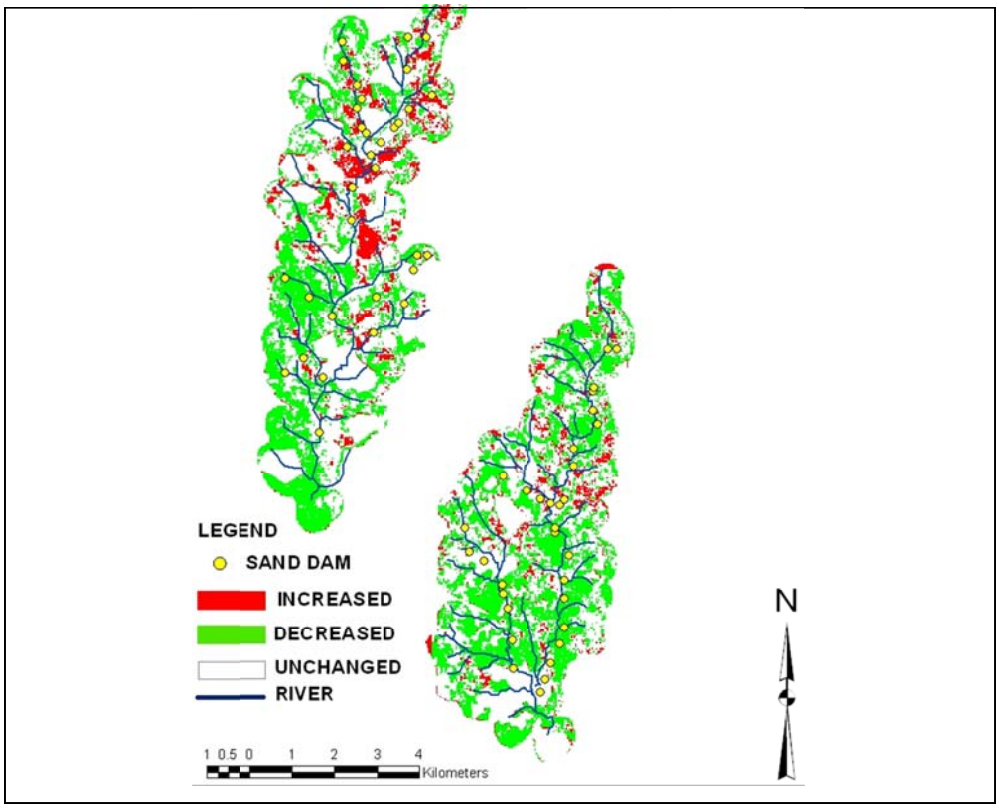

Figure 4.0: Change detection analysis for Kiindu and Mbusyani

4.0 Discussion

The change is evident in 28 out of the 32 sand dams on Kiindu catchment. 4 sand dam did not show any change in land cover type. This could be associated with the lateral abstraction of water due to rocks on the banks of the river. In Mbusyani catchment 34 sand dams were featured in the research study and 2 out of these did not show any change in land cover type whilst 4 were affected by clouds since these areas were masked out. In total 28 sand dams showed a significant change in land cover.

The research was conducted during the dry period in the month of August and October respectively when the relative vegetation present is very low in the semi-arid areas. The increase in vegetation in the dry period with respect to the presence of sand dams in the two water catchment is explained by (Borst L., De Haas S, 2006) through a hydrological study that quantified the ability of a sand dam to increase underground water recharge.

This can be interpreted as the reason for the vegetation to remain green through the dry period and also the upsurge of vegetation that normally would be non-existence during the same period e.g. short shrubs such as lantana camara and grassland characteristic of couch grass. (Jacobson, P. J., *et al.* 1995) describes sand

dams as being able to create artificial aquifers which are responsible for vegetation change along river banks. Looking at (3) summary of dam's ecological impacts, he mentions the modification of river systems through a change in existing species and the manner in which they may occur. Alterations in soil moisture regimes which under natural factors would be due to rainfall (3) usually cause plants to respond in terms of germination, growth, and reproduction. Similarly then according to this study sand dams cause a shift in soil moisture regimes(increases) and therefore would sustain vegetation during the dry period in the catchments where they have been constructed.
(Bunn S. E., and Arthington A. H., 2002) The green vegetation response to change in soil moisture may not have been primary in this study but include such response as;

(i) Increase in green vegetation matter (leaves).
(ii) New species of vegetation that do not occur during dry period up surging.
(iii) Increase in extent of vegetation i.e. area covered.

The unique response of the vegetation towards change in soil moisture regimes can be established through NDVI and soil moisture studies for these catchments where sand dams have been constructed.
The use of remote sensing satellite imagery of medium resolution plays a significant role in trend analysis of land cover change. The period before sand dam construction 1986 and after sand dam construction 2001 has been significantly compared using the Landsat ETM+ and Landsat TM. 1986. Studies by (Vogelmann J.E., et al., 2001) as discussed earlier have shown similarity in the measurements of land cover changes by use of Landsat TM and Landsat ETM+ without any major effects.

A shorter period for comparison i.e. before and after sand dam construction would have been preferred for the study but the use of satellite imagery for 1995 was not possible due to cloud cover effect of above 50% for the specific dry months in the area of interest. A series of epochs before and after sand dams could also have been preferred but the cloud cover effect of above 50% in the area of interest for most of the years before and after sand dam construction made it difficult. These epochs would have been able to establish the land cover change trend with the maturity of a sand dam since as earlier indicated a sand dam becomes fully functional after 5-8 years of construction.

Other years namely (1994 to 1987) were also affected by cloud cover effect of above 50%. Evidently research study was still able to show that a significant relationship did in fact exist between sand dam construction and land cover change along the stream channels.

5.0 Conclusion

Accurate land cover assessment and monitoring of its dynamics is possible using remote sensing medium resolution satellite imagery. Land cover alters evaporation, ground water recharge and stream discharge and therefore prerequisite for sustainable management of natural resources, environmental protection and food security. The effect of sand dam on land cover along stream banks shows the significance of spatial scale data in the development of regional estimates of land cover changes and hence improving the ability to estimate land use and ecosystem interactions with global climate change. The resulting spatial data yielded from these study shows, a significant presence of vegetation during the dry period due to sand dam construction.

Acknowledgement

The authors sincerely express their gratitude to Jomo Kenyatta University of Agriculture and Technology and Sahelian Solutions (SaSol) Foundation for their support in research facilities used to carry out the study, and the anonymous reviewers who through their positive reviews helped improve the final version of this paper.

References

Anderson J. R., Hardy E., Roach J. and Witmer R. (1976). A Land Use and Land Cover Classification System for Use with Remote Sensor Data, U.S. Geological Survey Professional Paper 964, Reston, VA: U.S. Geological Survey, pp 28.

Borst L., De Haas S. (2006). Hydrology of Sand Storage Dams – *A case study in the Kiindu catchment, Kitui District, Kenya.* VU University, Amsterdam.

Bunn S. E. and Arthington A. H. (2002). Basic principles and ecological consequences of altered flow regimes for aquatic biodiversity. *Environmental Management,* **30**, pp 492-507.

Cihlar J. and Jansen J. M. (2001). From Land cover to land Use: A Methodology for Efficient Land Use Mapping Over large Areas. *Professional Geography*, **53(2)**, pp 275-289.

Collins J. B. and Woodcock E. C (1996). An Assessment of Several Linear Change Detection Techniques for Mapping Forest Mortality Using Multi temporal Landsat TM Data. *Remote Sensing of Environment,* **56**, pp 66-77.

Congalton R. and Green K. (1993). A practical look at the sources of confusion in error matrix generation. *Photogrammetric Engineering and Remote sensing,* **59(5)**, 641-644

Coppin P. I., Jonckheere K. and Nackers B.M. (2004). Digital change detection in ecosystem monitoring: a review. *International journal of remote sensing*, **25(9)**, pp 1565 -1596.

Deer P. (1995). Digital Change Detection techniques: civilian and military applications, in International symposium for spectral Sensing Research.

Defries R. and Eshleman K. N. (2004)**.** Land-use change and hydrologic processes: a major focus for the future. *Hydrological Processes*, **18,** pp 2183-2186.

FAO, (1987)**.** Soil and water conservation in semi-arid areas. Soils bulletin, **57**, FAO, Rome.

Fung T. and Ledrew E. (1988). The determination of optimal threshold levels for changes detection using various accuracy indices. *Photogrammetric Engineering and Remote Sensing*, **10,** pp 1449- 1454.

Gijsbertsen C. (2007). A research to up scaling of the sand storage dam principle and sedimentation processes behind sand storage dam. VU University, Amsterdam.

Gooding J. R. and Northington J. K. (1985). Plant resources of arid and semi-arid lands; global perspective Orlando, FL (USA), Academic Press, pp *338.*

Jacobson P. J., Jacobson K. N. and Seely M. K. (1995). *Ephemeral Rivers and their Catchment*, Desert Research Foundation of Namibia. Windhoek, Namibia. ISBN No 99916-707-4-7.

Jansen J. (2007). The influence of sand dams on rainfall-runoff response and water availability in the semi-arid Kiindu catchment, Kitui District, Kenya*.* VU University, Amsterdam.

Leica Geosystems GIS and Mapping, LLC, 2005. ERDAS Field Guide. Norcross, GA: Leica Geosystems Geospatial Imaging, LLC.

Lillesand T. M., and Kiefer R. W. (1994). *Remote sensing and image interpretation.* John Wiley and Sons, Inc. New York.

Lins K. S. and Kleckner R. L. (1996). Land cover mapping: An overview and history of the concepts, *Gap Analysis: A Landscape Approach to Biodiversity Planning* (J.M. Scott T. H., Tear and Davis F. editors), American Society for Photogrammetry and Remote Sensing, Bethesda, Maryland, pp. 57–65.

Katumo V. (2001)**.** *Environmental Impact assessment of Kiindu and Kyuusi rivers, Kitui District, 5th annual report 2000.* SASOL and the Department of Range Management, University of Nairobi, pp 106 .

Munyao J. N., Munywoki J. M., Kitema M. I., Kithuku D. N., Munguti J. M., Mutiso S. M, (2004). *Kitui sand dams: Construction and operation.* SASOL foundation, Kitui Town, Kenya.

Nissen- Perterson E. (1982). Rain water catchment and water supply in rural Africa; A manual Hodder, and strought SUB.

Nissen-Petersen, (1997). *Water from sand-rivers*. 23rd WEDC Conference Durban, Water and sanitation for all: Partnerships and innovations, South Africa.

Rogan J. and Chen D. M. (2004). Remote sensing technology for mapping and monitoring land-cover and land-use change. Progress in Planning*,* **43***,* pp 56-59.

Rogan J., Franklin J., Stow D., Miller J., Woodcock C., and Roberts D., (2008). "Mapping land-cover modifications over large areas: A comparison of machine learning algorithms." Remote Sensing of Environment, pp 2272-2283.

Sahin V., and Hall M. J., (1996). The effects of afforestation and deforestation on water yields. *Journal of Hydrology*, **178**, pp 293-309.

Vogelmann J. E., Helder D., Morfitt R., Choate M. J., Mercant J. W., and Bulley, H., (2001). Effects of Landsat 5 Thematic Mapper and Landsat 7 Enhanced Thematic Mapper Plus radiometric and geometric calibrations and corrections on landscape characterization, Remote Sensing of Environment, **78**, pp. 55-70.

Wezel A. and Schlecht E. (2004). Inter-annual variation of species composition of fallow vegetation in semi-arid Niger, Journal of Arid Environments, **56***,* pp. 265-282

Xiao J., Shen Y., Ge J., Tateishi R., Tanga C., Liang Y., and Huang Z. (2006). Evaluating urban expansion and land use changes in Shijiazhuang, china, by using GIS and Remote sensing. Landscape and Urban Planning,**75**, pp 69–80.

EVALUATING PERFORMANCE OF WRP AND AODV MANETS ROUTING PROTOCOLS UNDER MOBILITY

E. W. Mureu[1], S. Musyoki[2] and P. Kihato[3]
[1, 2]Department of Telecommunication and Information Engineering, Jomo Kenyatta University of Agriculture and Technology, Kenya
[3]Department of Electrical and Electronic Engineering, Jomo Kenyatta University of Agriculture and Technology, Kenya
E-mail: ewmureu@yahoo.com

Abstract
The Mobile *ad hoc* networks (MANET) is a wireless networks which have no central bridge, and where each node acts as a destination as well as a router. The MANETs are dynamic networks because the network topology keeps on changing because of the mobility of the nodes. There are many protocols that have been developed to aid in routing in these types of networks. Each of these protocols is designed with some certain mobility scenarios in mind. To achieve effective routing in a given scenario, the right protocol must be chosen. Choosing the right protocol involves evaluating many interdependent performance metrics that define the effectiveness of a routing protocol, and this often poses a challenge to application designers. This research endeavored to model a simulation platform on which various protocols could be evaluated under various mobility scenarios to determine their suitability. The GloMoSim was used as the simulation platform and two MANET protocols namely wireless routing protocol (WRP) and *ad hoc* on-demand distance vector (AODV) evaluated. Our results demonstrated the usefulness of this modeled platform as it was able to establish that the AODV outperformed WRP in four out of the five of the measured performance metrics. The AODV is thus a better protocol for MANETs compared to WRP. The same simulation platform could be used test other protocols.

Key words: MANET, WRP, AODV, Simulation, GloMoSim

1.0 Introduction

Mobile *ad hoc* networks (MANETs) (Macker and Corson 1997) are networks composed of a set of communicating nodes able to spontaneously interconnect without any pre-existing infrastructure. These nodes generally have a limited transmission range and, so, each node seeks the assistance of its neighboring nodes in forwarding packets. In addition to that, these devices are generally mobile.

In order to establish routes between nodes which are further than a single hop, specially designed routing protocols are engaged. The unique feature of these protocols is their ability to trace routes in spite of a dynamic topology. These protocols can be categorized into two main types: reactive and proactive. In this research work we have chosen one protocol from each of these two categories for purposes of evaluating and comparing their performances. In the category of proactive protocols we have chosen WRP and in the category of reactive protocols we have chosen AODV. The Reactive routing protocols discover routes only when they are essentially required. This has an advantage of reducing the messaging overhead but has a disadvantage of increasing the end to end delay as it takes time before a route could be established. In contrast, the proactive routing protocols establish and maintain routes at all instants of time. This has an advantage of reducing the end to end delay but it increases the messaging overhead which could lead less to congestion.

Some of the applications of MANETs are as follows (Jeroen *et al.* 2003):

(i) Military vehicles on a battlefield with no existing infrastructure.
(ii) A fleet of ships at sea.
(iii) Emergency workers at an earthquake that destroyed the infrastructure
(iv) A gathering of people with notebook computers in an area lacking 802.11 (Wi-Fi).

Selecting a particular protocol for an application or deployment environment involves evaluating many inter-dependent metrics and can be an overwhelming task for an application designer. However, this decision can have a significant impact on the success of a system in terms of performance. Hence, there is need to analyse and compare the performances of various available protocols to determine their suitability in a given network scenario.

Evaluating performance of MANETs routing protocols is achieved by resorting either to experimentation networks (test-beds) or to the software-based simulators (Furqan and Thomas 2005). In our case we resorted to the use of a software based network simulator. What hindered the use of a test-bed is its implementation cost and its inherent lack of flexibility and repeatability. This becomes particularly impeding as the size of the experimented network grows.

The software based network simulator used in this research work is called GloMoSim (Zeng, Bagrodia and Gerla1998).
This research paper consists of five sections which are organized as follows: Section one has served as an introduction to the MANETs and need to analyze performance of the MANETs routing protocols. Section two surveys the theory behind the two mobile ad hoc network routing protocols under investigation and the performance metrics used. Section three details the simulation set-up. Section four presents the simulation results and discussion. Section five concludes the paper by describing various conclusions and the future research areas.

2. 0 Theory

2.1 The MANETs Routing Protocols under Investigation

2.1.1 Wireless Routing Protocol (WRP)

WRP is a proactive routing protocol and was proposed by (Murthy and Gracia 1996). The WRP eliminates the possibility of routing loops. Nodes in a network using WRP maintain a set of four tables:

(i) *Link cost table.* This table contains the cost of the link to each immediate neighbor node and information about the status of the link to each immediate neighbor.
(ii) *Distance table.* The distance table of a node contains a list of all the possible destination nodes and their distances beyond the immediate neighbors.
(iii) *Routing table.* The routing table contains a list of paths to a destination via different neighbors. If a valid path exists between a source and a destination node, its distance is recorded in the routing table along with information about the next-hop node to reach the destination node.
(iv) *Message Retransmission List (MRL).* The MRL of a node contains information about Acknowledgement (ACK) messages from its neighbors. If a neighbor does not reply with an ACK to a hello message within a certain time, then this information is kept in its MRL and an update is sent only to the non-responding neighbors.

The WRP works by requiring each node to send an update message periodically. This update message could be new routing information or a simple 'hello' if the routing information has not changed from the previous update. After sending an update message to its all neighbors, a node expects to receive an ACK from all of them. If an ACK message does not come back from a particular neighbor, the node will record the non-responding neighbor in MRL and will send another update to the neighbor node later. The nodes receiving the update messages look at the new information in the update message and then update their own routing table and link cost table by finding the best path to a destination. This best-path information is then relayed to all the other nodes so that they can update their routing tables.

WRP avoids routing loops by checking the status of all the direct links of a node with its direct neighbors each time a node updates any of its routing information.

2.1.2 *ad hoc* On-demand Distance Vector Routing (AODV)

The ad hoc on-demand distance vector routing (AODV) as described by (Perkins, Belding and Das 2003) is an improvement of the destination-sequenced distance-vector (DSDV) algorithm. It is a reactive protocol and constructs routes on demand and aims to reduce routing load. It uses a table driven routing framework and destination sequence numbers for routing packets to destination mobile nodes and has location independent algorithm. It sends messages only when required and it has bi-directional route from the source and destination. When it has packets to send from source to destinations mobile node then it floods the network with route request (RREQ) packets. When a node receives an AODV control packet from a neighbor, or creates or updates a route for a particular destination or subnet, it checks its route table for an entry for the destination. All mobile nodes that receive the RREQ checks its routing table to find out that if it is the destination node or if it has fresh route to the destination then it unicast route reply (RREP) which is routed back on a temporary reverse route generated by RREQ from source node, or else it re-broadcast RREQ.

Five performance metrics were used to analyse and compare the two protocols.

2.2 Performance Metrics

To analyse and compare the performances of protocols, standard performance metrics are used as described by (Jayakumar and Gopinath 2008) . In our case we have used five metrics namely; packet delivery ratio, mean end-end delay; messaging overhead; energy consumption and throughput. The five metrics used in our experiments are defined as follows:

2.2.1 Packet Delivery Rate

Packet delivery rate (PDR) is the number of received packets divided by the number of sent packets, computed at the application layer. It reflects the routing protocol reliability which is a very important issue. It is expressed as a percentage. The higher the value of the PDR, the better the performance of the protocol. High values of this metric reflect a good reliability, i.e low packet loss.

2.2.2 Consumed Energy

Because energy resources of devices used in MANETs are limited, energy consumption is an important issue related to routing protocols. A routing protocol is better if it causes less energy consumption compared with others in the same conditions. The consumed energy is measured in milliwatt hour (mwHr).

2.2.3 Messaging Overhead

Messaging overhead is the number of control packets generated by the routing protocol during the simulation. The generation of high number of control packets would decrease the protocol performance as more network resources are taken up by these control packets leaving fewer resources for the actual data packets delivery. Although control packets are essential to ensure protocol functionality, their number should be as low as possible. The messaging overhead is expressed in terms of the number of control packets generated.

2.2.4 Mean End-End Delay

The mean end-end delay is the average time it takes for a data packet to move from the source node to the destination node. This metric is very important to study the quality of service, especially in real-time applications. The lower the value of mean end-end delay the better the protocol in-terms of its performance. The mean end-end delay is expressed in second(s).

2.2.5 Throughput

Throughput refers to how much data can be transferred from one location to another in a given amount of time. It is used to measure the performance of network connections. A high throughput value is desirable as it ensures maximum delivery of data packets. The throughput is expressed as bits per second (bps).

2.3 Mobility Models

To evaluate the performance of a protocol for an ad-hoc network, it is necessary to test the protocol under realistic conditions, especially including the movement of the mobile nodes. This is achieved by the use of a mobility model. Several mobility models exist for use in MANETs (Davies 2000). In this work we have chosen to use the random waypoint mobility model because we found it to be more realistic in-terms of modeling the movement of the nodes.

In random waypoint mobility model, each node remains stationary for the duration of its 'pause time'. At the end of a pause time, a node starts moving in a randomly selected direction in the network terrain at a fixed speed. Once a node reaches its new location, it remains stationary during its next pause time. At the end of the new pause time, a node again starts moving in another randomly selected direction in the network. This movement process is continued during a simulation experiment. Therefore a shorter pause time denotes high mobility and vice versa.

3.0 Simulation

3.1 Simulation Environment

To evaluate the performances of the two routing protocols, a parallel discrete event-driven simulator, global mobile simulator (GloMoSim), was used. Our

simulation experiments were executed on a Compaq Presario CQ60 notebook Personal Computer (PC) with a Pentium IV processor@ 2.16 MHz with 2GB random access memory (RAM).

3.1.1 Global Mobile Simulator (GloMoSim)

GloMoSim as described by (Zeng, Bagrodia and Gerla1998) is developed at UCLA (California, USA). It is widely used as wireless network simulator. GloMoSim is written in Parsec and hence benefits from the latter's ability to run on shared-memory symmetric processor (SMP) computers. New protocols and modules for GloMoSim must be written in Parsec too. GloMoSim conforms to the OSI standard.

3.2 Simulation Experiments

To compare the performance of the two routing protocols described in the previous sections, simulation experiments were performed.

3.2.1 Experimental Modeling

In setting up our experimental model for purposes of simulation, we used the Nodes' mobility as the control parameter. Three different levels of nodes' mobility were used as described as below:

(i) High mobility- pause time 30s;
(ii) Medium mobility- pause time 120s and
(iii) Low mobility- pause time 240s.

For each of the two protocols under investigation, the five performance metrics were then measured for each of these three levels of nodes' mobility and results tabulated in Table 1 and Table 2.

The movement of the nodes was modeled using the Random Waypoint mobility model.

Traffic load generated by each source node was modeled by a constant bit rate data stream, whose transmission rate is defined by packet transmission interval for fixed-size packets. In our case one packet was sent every 1s. The network terrain size was fixed for 2000m x 2000m. The radio signal transmission range was fixed at 175m (radius of 175m). The transmission data rate of each link was fixed at 2Mbps and the simulation time was 15 Minutes for all the experiments. In every experiment, there were 30 randomly selected pairs of a sender and a receiver nodes.Data packet size was fixed at 512 bytes. The above parameters were used for both of our simulation experiments.

4.0 Results and Discussion

The data obtained from the simulations is as contained in Table 1 and Table 2.

Table 1: WRP simulation data

Nodes mobility	***Energy (mwHr)***	***Control Packets***	***Throughput***	***Delay (s)***	***Packet Delivery Ratio(PDR)%***
High	225.16	912	1530	0.01	34.61
Medium	225.15	831	2519	0.008	46.14
Low	225.14	797	2532	0.007	50.0

Table 2: AODV simulation data

Nodes mobility	**Energy (mwHr)**	**Control Packets**	**Throughput**	**Delay (s)**	**Packet Delivery Ratio(PDR)%**
High	225.023	120	1771.	0.0356	54.20
Medium	225.015	80	2383	0.0339	68.21
Low	225.01	50	2664	0.032	78.05

The analysis of the results is done using graphs shown in Figures 1 to Figure 5. Each Figure denotes a particular performance metric evaluated against the three different levels of nodes' mobility.

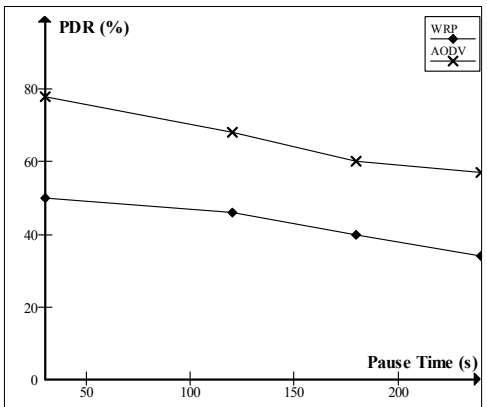

Figure 1: Packet Delivery Ratio (PDR) versus nodes' mobility

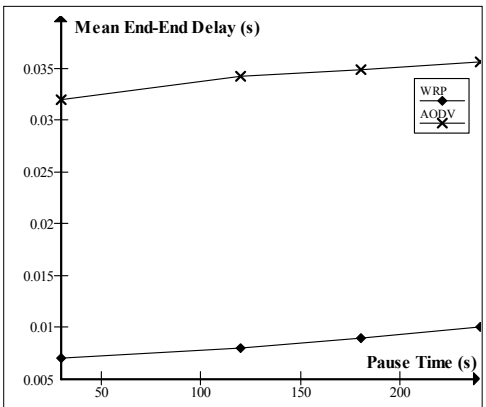

Figure 2: Mean End-to-End Delay versus nodes' mobility

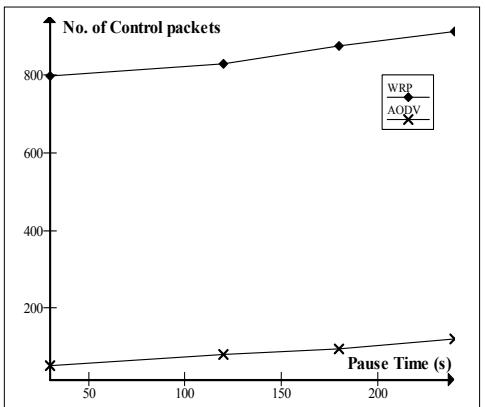

Figure 3: Messaging Overhead versus nodes' mobility

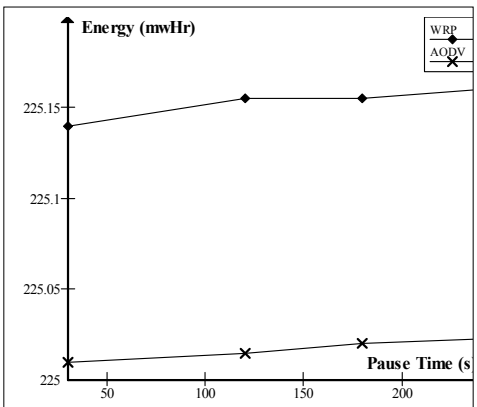

Figure 4: Consumed Energy versus nodes' mobility

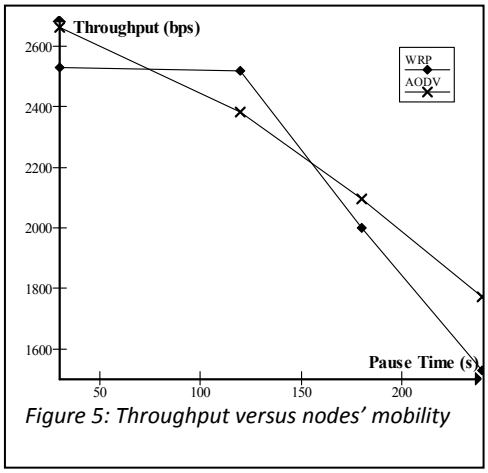

Figure 5: Throughput versus nodes' mobility

4.1 Packet Delivery Ratio

In Figure 1, we see that the AODV has a higher packet delivery ratio **(**PDR) compared to WRP in all mobility speeds which implies a better performance. The reason for this is that AODV being a reactive protocol responds more quickly to link failures by each node sending an error packet to all its active neighbors as soon as it detects a link failure thus avoiding excessive packet losses. On the other hand WRP being a proactive protocol sends packets before routing tables converge to a stable state, which leads nodes to take failed routes supposed to be valid and thus suffer from increased packet losses. For both protocols, PDR decreases when the mobility increases.

4.2 Mean End-to-End Delay

Looking at Figure 2, we remark that WRP has low mean end-end delay compared to the AODV protocol which implies a better performance. This is because WRP being a proactive protocol constructs and maintains routing tables permanently, which eliminates the route discovery time as opposed to AODV which constructs routes on demand. In both protocols, the delay is not significantly affected by mobility

4.3 Messaging Overhead

We can see in Figure 3 that WRP generates the most overhead of the two protocols by a factor of 80. This is because WRP being a proactive protocol generates periodic messages whereas AODV do not generate overhead unless there is a need for a route or when a route is failed.

The messaging overhead in both protocols increases slightly with increase in mobility. This is because mobility rise implies route failure rise, which causes the

generation of more route discovery packets. So as far as this performance metric is concerned the AODV performs better than the WRP.

4.4 Energy Consumption

We remark that consumed energy plots (Figure 4), shows that WRP consumes more energy than AODV. The reactive protocols consumed less energy than the proactive ones, because the latter, generated more control packets that led to consumption of more battery power. Therefore the AODV performed better than the WRP as far as this metric is concerned.

4.5 Throughput

It can be seen from Figure 5 that the throughput of both protocols is heavily adversely affected by mobility. This is because mobility increases the chances of link failures, which in turn decreases the throughput as more packets end up not reaching their destinations. But of the two, the AODV has a higher throughput and hence a better performance.

5.0 Conclusion

In this paper, we have conducted a GloMoSim based simulation study, to investigate the mobility effects on the performance of two MANETs' routing protocols; A reactive (AODV), and a proactive (WRP). This study is performed by measuring different performance metrics at different mobility levels.

From the study it was seen that the AODV outperformed the WRP in four out of the five measured performance metrics namely Packet Deliver Ratio, Messaging Overhead, Energy consumption and Throughput. Its only in Mean End-End Delay that the WRP outperformed the AODV. We could therefore conclude that the AODV is a better MANET routing than the WRP especially under the considered three levels of nodes' mobility. Hence the AODV protocol could be used in network scenarios where nodes' mobility is relatively highly and where the packet end to end delay is not a critical parameter. On the other hand, the WRP protocol could be used in network scenarios of relatively low mobility but where end to end delay is a critical parameter especially in real time applications.

We also realize from this study that the mobility, which characterizes MANETs, has negative effects on routing protocols. This is because of the broken links caused by the nodes' mobility. This in turn causes more energy consumption, more Mean End-End Delay, more packet loss, and more congestion (due to the increasing overhead).

The results obtained also showed that our modeled platform that used the GloMoSim is a good tool for use in determining the right protocol for a given network scenario.

As work for future research area, it would be interesting if someone was able to carry out this study but now using a test-bed in order to compare results.

Acknowledgements
The authors would like also to appreciate the Jomo Kenyatta University of Agriculture and Technology for funding this research work.

References

Perkins C., Belding-Royer E. and Das S. Ad hoc on-demand distance vector (aodv) routing,. in *Internet Engineering Task Force (IETF) draft*,July 2003.

Haq F. and Kunz T. (2005). Simulation vs. Emulation:Evaluating Mobile Ad Hoc Network Routing Protocols. Systems and Computer Engineering Carleton University Ottawa, Canada.

Jayakumar G. and Gopinath G., (2008) "Performance Comparison of MANET protocols based on Manhattan Grid Mobility Model": Journal of Mobile Communications,**2,** (1) pp 18-26.

Macker J. and Corson S., "Mobile Ad Hoc Networks (MANET)," IETF WG Charter., http://www.ietf.org/html.charters/manet-charter.html, 1997.

Hoebeke J., Moerman I., Dhoedt B. and Demeester P.(2003). An Overview of Mobile Ad Hoc Networks: Applications and Challenges. Department of Information Technology (INTEC), Ghent University, Belgium.

Murthy S., Gracia-Luna-Aceves J. J. (1996). An efficient routing protocol for wireless networks. *ACM Mobile Networks and Applications Journal*, Special Issue on Routing in Mobile Communications Networks. pp 183–197.

Davies V. (2000). Evaluating mobility models within an ad hoc network, Master's thesis, Colorado School of Mines, pp. 24-37.

Zeng X., R. Bagrodia and Gerla M., Glomosim (1998). A library for parallel simulation of large-scale wireless networks, in: Workshop on Parallel and Distributed Simulation, pp. 154–161.

CLOSED-LOOP TRANSMIT DIVERSITY (TRANSMIT BEAMFORMING) FOR MITIGATION OF INTERFERENCE AND MULTIPATH FADING IN WIRELESS COMMUNICATION SYSTEMS

M. Rugara[1], D. B. O. Konditi[2] and S. Musyoki[3]
[1]Department of Electrical and Electronics Engineering, Jomo Kenyatta University of Agriculture and Technology
[2]Multimedia University College of Kenya
[3]Department of Telecommunication and Information Engineering, Jomo Kenyatta University of Agriculture and Technology
E-mail: muigarugara@gmail.com

Abstract
The wireless communication channel suffers from many impairments such as the thermal noise often modeled as Additive White Gaussian Noise (AWGN), the path loss in power as the radio signal propagates, the shadowing due to the presence of fixed obstacles in the radio path, and the fading which combines the effects of multiple propagation paths and the rapid movement of mobile units reflectors. Deploying multiple antennas at the transmitter has been shown to increase diversity and therefore improve signal quality with increased throughput. This paper proposes a transmit diversity scheme, where multiple transmit antennas are used at the transmitter. A feedback path is provided from the receiver to communicate the channel seen by the receiver to the transmitter (closed-loop). When closed-loop transmit diversity is applied, the symbol from each transmit antenna is multiplied with a complex number corresponding to the inverse of the phase of the channel so as to ensure that the signals add constructively at the receiver. From this research it was found that sending the same information on multiple transmit antenna does not always provide diversity gain. However if the transmitted symbols are multiplied by a complex phase to ensure that the phases align at the receiver, there is diversity gain though the bit error rate performance seems to be slightly poorer than the maximal ratio combining case.

Key words: Closed-loop, transmit diversity, transmit beamforming, single-input single-output, multipath fading, mmaximal ratio combining

1.0 Introduction

The performance of a communication system depends on the received signal energy. Higher energy signals are detected more reliably (with fewer errors) than are lower energy signals. In other words, the received signal does the work. On the other hand power, is the rate at which energy is delivered. An electrical signal can be represented as a voltage *v(t)* or a current *i(t)* with instantaneous power *p(t)* across the load (resistor) defined by. (Hourani, 2004).

$$p(t) = \frac{v(t)}{R} = i^2(t)R \quad \text{.....(1)}$$

In communication systems, power is often normalized by assuming the load resistor (R) to be *1Ω,* therefore regardless of whether the signal is a voltage or a current waveform, the normalized convention allows instantaneous power to be expressed as

$$p(t) = v^2(t) = i^2(t) \quad \text{..... (2)}$$

$$p(t) = x^2(t) \quad \text{.....(3)}$$

Where *x(t)* is either a voltage or a current signal (Tarokh *et al*, 1998).

The performance of a communication system is generally measured by the bit error rate (BER), which is a function of the signal-to-noise ratio (SNR). Due to unknown location of the mobile station and the unknown medium between the transmitter and the receiver, the wireless channel is best characterized as random. A wireless communication system is fundamentally limited by the random nature of the channel. (Sklar, 2001).

1.1 Challenges in wireless signal transmission.

The wireless communication channel suffers from many impairments such as the thermal noise often modeled as Additive White Gaussian Noise (AWGN), the path loss in power as the radio signal propagates, the shadowing due to the presence of fixed obstacles in the radio path, and the fading which combines the effects of multiple propagation paths and the rapid movement of mobile units reflectors. (Zheng, 2003).

In communications, the additive white Gaussian noise (AWGN) channel model is one in which the information is given a single impairment: a linear addition of wideband or white noise with a constant spectral density and a Gaussian distribution of noise samples. The model does not account for the phenomena of fading, frequency selectivity, interference, nonlinearity or dispersion. However, AWGN produces simple and tractable mathematical models which are useful for gaining insight into the underlying behavior of a system before these other phenomena are considered. (Proakis, 1995).

The wideband Gaussian noise comes from many natural sources, such as the thermal vibrations of electrons in atoms (referred to as thermal noise or Johnson-Nyquist noise), shot (schottky) noise (which arises in an electric current due to discontinuous nature of conduction by electrons), black body radiation from the earth and other warm objects, and from celestial sources such as the sun.

The AWGN channel is represented by a series of outputs Y_i at discrete time event. Y_i is the sum of the input x_i and noise, n_i, where n_i is independently and identically distributed (i.i.d.) and drawn from a zero mean normal distribution with variance ***v.*** The n_i are further assumed not to be correlated with the x_i i.e. $n_i \sim N(0,v)$.

$$Y_i = x_i + n_i \quad \text{..... (4)}$$

Physical channels such as under water acoustic channels and ionospheric radio channels result in time-variant multipath propagation of the transmitted signal which may be characterized mathematically as time-variant linear filter i.e.

$$y(t) = x(t) * c(\tau; t) + n(t)$$
$$= \int_{-\infty}^{+\infty} c(\tau; t)x(t-\tau)\delta\tau + n(t) \quad \text{..... (5)}$$

where $c(\tau; t)$ is the impulse response of the linear time-variant filter and * denotes convolution.

A good model for multipath signal propagation through physical channels such as the mobile cellular radio channels, is a special case of the above equation in which the time-variant impulse response has the form

$$c(\tau; t) = \sum_{k=1}^{L} a_k(t)\delta(\tau - \tau_k) \quad \text{..... (6)}$$

where the $a_k(t)$ represent the time variant attenuation factor for the L multipath propagation paths and τ_k are the corresponding time delays. If equation (6) is substituted into equation (5) the received signal has the form

$$y(t) = \sum_{k=1}^{L} a_k\, x(t-\tau_k) + n(t) \quad \text{..... (7)}$$

Hence the received signal consists of L multipath components, where each component is attenuated by $a_k(t)$ and delayed by τ_k.

Shanon formulated the basic problem of reliable transmission of information in statistical terms, using probabilistic models for information sources and communication channels (Proakis, 1995). He also demonstrated that the effect of a transmitter power constraint, bandwidth (W) constraint and additive noise can be associated with the channel and incorporated into a single parameter called the channel capacity (C).

$$C = W\, log_2\left(1 + \frac{P}{WNo}\right) bits/sec \quad \text{..... (8)}$$

Where *P* is the average transmitted power and N_o is the power spectral density of the additive noise. Therefore if the information rate (R) from the source is less than channel capacity (C), i.e. (R < C) then it is theoretically possible to achieve

reliable (error free) transmission through the channel by an appropriate coding. On the contrary, if R > C, reliable transmission is not possible regardless of the amount of signal processing performed at the transmitter and receiver.

2.0 Interference and Multipath Fading in Wireless Communication Systems

2.1 Multipath propagation of wireless signals

In a typical wireless communication environment, multiple propagation paths often exist from a transmitter to a receiver due to scattering by different objects as shown in figure 2.0.

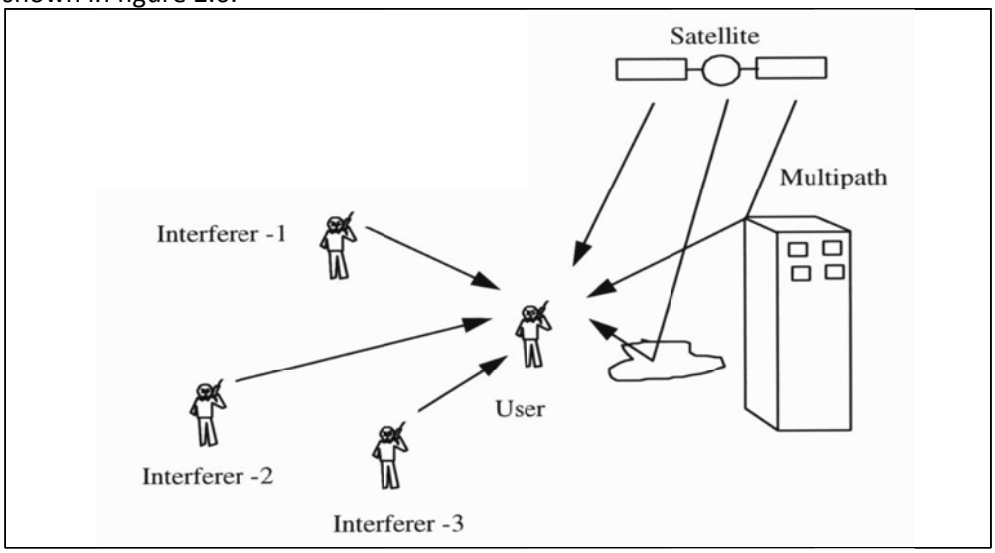

Figure 2: Mobile user in the presence of multipath and interference

Upon the signal transmission, different signal copies following different paths undergo different attenuation, distortion, delays and phase shifts. Multipath fading is known to arise due to the non-coherent combination of signals arriving at the receiver. Interference is caused by deep-fades that occur at a particular point in space, or at a particular time or frequency, and results in severe degradation of the quality of signals at the receiver making it impossible to detect or decode. (Rappaport, 1996).

Several mathematical models have been developed to describe such channels, taking into account, the phenomenon of multipath fading and correlation between sub-channels. Common models employ Rayleigh, Rice and Nakagami-m distributions to approximate actual channel conditions. (Rappaport, 1996). The Rayleigh flat fading channel is commonly used to describe multipath fading channels when there is no line-of-sight (LOS) component. (Proakis, 1995; Nakagami, 1960).

The performance of the systems (in terms of error rate) can be severely degraded by fading. In mobile communications, multiple propagation paths exist, and are time-varying. The result is a time-varying fading channel. Communication through these channels is difficult and special techniques may be required to achieve satisfactory performance. (Hourani, 2004).

2.2 Overcoming Challenges in Wireless Signal Transmission

Equalisation, diversity, and channel coding are the three techniques which can be used independently or in tandem to improve received signal quality and link performance over small scale times and distances. Equalisation compensates for intersymbol interference (ISI) created by multipath propagation within time dispersive channels. Channel coding improves the small-scale link performance by adding redundant data bits in the transmitted message so that if an instantaneous fade occurs in the channel, the data may still be recovered at the receiver. Diversity technique is used to compensate for fading channel impairments, and is usually implemented by using two or more transmitting and/or receiving antennas. (Rappaport, 1996).

Diversity technique is a widely known technique in combating channel impairments arising due to multipath fading. In diversity, several replicas of the same information carrying signal are received over multiple channels with comparable strengths and exhibit independent fading. (Zheng, 2003). Diversity techniques improves the quality of a wireless communications link without altering the common air interface, and without increasing the transmitted power or bandwidth. (Rappaport, 1996). Diversity is usually employed to reduce the depth and duration of the fades experienced by a receiver. Diversity techniques are often employed at both the transmitter (Transmit Diversity) and/or the receiver (Receive Diversity). For a broad class of interference-dominated wireless systems including mobile, personal communications, and wireless LAN networks, a significant increase in systems capacity can be achieved by use of multiple antennas. (Winters, 1998). Use of diversity is made more compelling by decrease in the cost of digital signal processing hardware and the advances in adaptive signal processing. There are different kinds of diversity commonly employed in wireless communication systems; frequency diversity, time diversity, and space diversity. (Winters, 1998).

In frequency diversity, the information signal is modulated through different carriers. Each carrier should be separated from the others by at least the coherence bandwidth $(\Delta f)c$ as shown in figure 2.1 below, so that different copies of the signal undergo independent fading. The fact that waves transmitted on different frequencies induce different multipath structure in the propagation media is exploited. Thus replicas of the transmitted signal are provided to the receiver in the form of redundancy in the frequency domain.

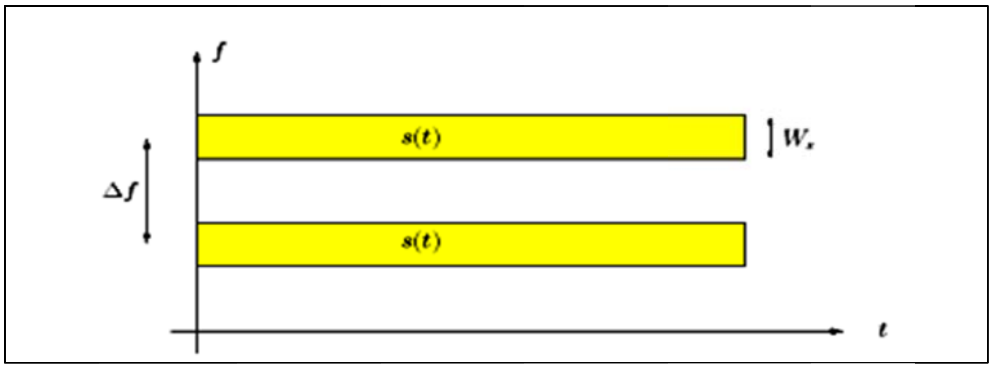

Figure 2.1 Frequency Diversity

Time diversity is achieved by transmitting the desired signal through different periods of time i.e. each symbol is transmitted ***m*** times. The interval between transmissions of the same symbol should be at least the coherence time ***(Δt)c*** as shown in figure 2.2 below so that different copies of the same symbol undergo independent fading. Thus replicas of the transmitted signal are provided to the receiver in the form of redundancy in time domain. (Hourani, 2004).

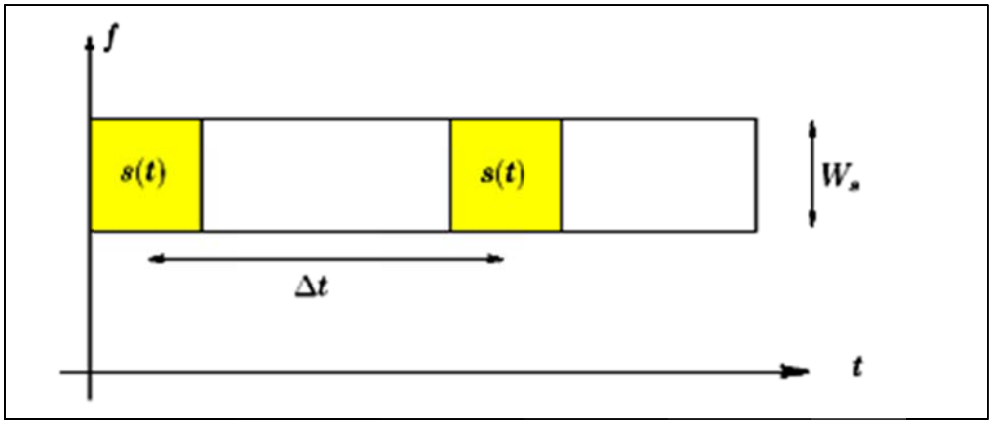

Figure 2.2: Time diversity

2.3 Spatial Diversity Techniques

Spatial diversity is the most common diversity technique. In space diversity, multiple antennas are strategically spaced and connected to a common transmitting and/or receiving system. Spatial diversity provides an attractive means for improving the performance of wireless communication systems. Spatial diversity can be employed to combat both frequency selective fading and time selective fading. (Hourani, 2004; Rappaport, 1996).

Unlike frequency diversity where additional bandwidth may be required and time diversity where additional time may be required, in spatial diversity no additional bandwidth or transmission time is required. Spatial diversity can be implemented

at the receiver (Receive diversity) and/or the transmitter (transmit diversity). Transmit and receive diversity have emerged as effective means of achieving higher throughput in wireless communication systems. (Winters, 1998).

3.0 Theoretical Analysis

Multiple antenna systems have been known to increase diversity to combat channel fading. Each pair of transmit and receive antennas provides a signal path from the transmitter to the receiver. By sending signals that carry the same information through different paths, multiple independently faded replicas of the data symbol can be obtained at the receiver end; hence more reliable reception is achieved. (Alamouti, 1998). In a slow Rayleigh fading environment with one transmit and n receive antennas, the transmitted signal is passed through n different paths. If the fading is independent across antenna pairs, a maximal diversity gain of n can be achieved. (Rappaport, 1996; Foschini). The average error probability is known to decay by $1/SNR^n$ at high (Signal to Noise Ratio) SNR in contrast to SNR^{-1} for the single input single output (SISO) system. With multiple transmit antennas, m and one receive antenna, the underlying idea is still averaging over multiple path gains to increase the reliability. It has been shown that with m transmit antennas and one receive antenna, a diversity gain within 0.1dB that of n receive antennas with one transmit antenna can be achieved. (Zheng, 2003).

3.1 Closed-loop Transmit Diversity (CLTD) Scheme

In closed-loop Transmit diversity scheme, the transmitter has the knowledge of the channel as there is a feedback path required from the receiver to communicate the channel seen by the receiver to the transmitter. The channel experienced by each receive antenna is randomly varying in time. For the i^{th} receive antenna, each transmitted symbol gets multiplied by a randomly varying complex number $\boldsymbol{h_i}$ The channel is a flat fading Rayleigh channel, the real and imaginary parts of $\boldsymbol{h_i}$ are Gaussian distributed having mean $\boldsymbol{\mu_{h_i} = 0}$ and variance $\boldsymbol{\sigma^2_{h_i}} = \frac{1}{2}$. The channel experienced by each transmit antenna to receive antenna is independent from the channel experienced by other transmit antennas. On the receive antenna, the noise $\boldsymbol{n}$ has the Gaussian probability density function with $\boldsymbol{\mu = 0}$ and $\boldsymbol{\sigma^2} = \frac{N_o}{2}$.

A 2 transmit 1 receive antenna case is depicted in figure 3.0 below.

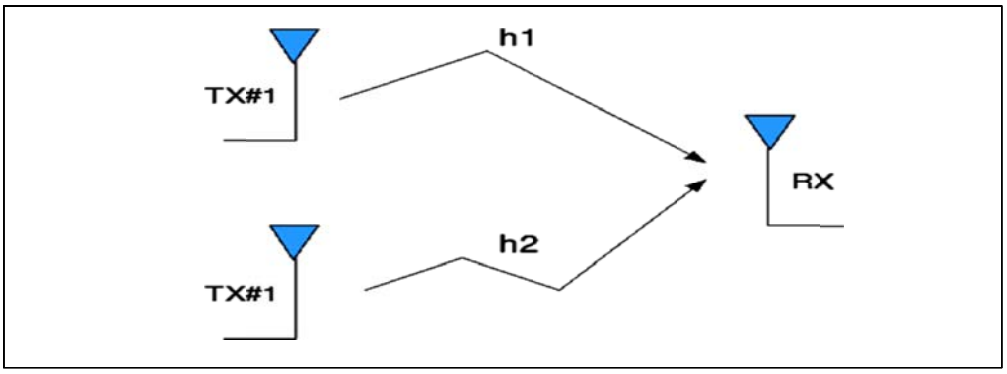

Figure 3.2: Transmit 1 receive beam steering

On the receive antenna RX, the received signal is,

$$\boldsymbol{y_i} = [\boldsymbol{h_1}\ \boldsymbol{h_2}]\begin{bmatrix}\boldsymbol{x}\\ \boldsymbol{x}\end{bmatrix} + \boldsymbol{n} = (\boldsymbol{h_1} + \boldsymbol{h_2})\boldsymbol{x} + \boldsymbol{n} \quad \text{..... (9)}$$

where $\boldsymbol{y}_i$ is the received symbol, $\boldsymbol{h_i}$ is the channel on the i^{th} transmit antenna, $\boldsymbol{x}$ is the transmitted symbol and $\boldsymbol{n}$ is the noise on the receive antenna. When transmit beamforming (closed-loop) is applied, the symbol from each transmit antenna is multiplied by a complex number corresponding to the inverse of the phase (the channel effect are reversed) of the channel so as to ensure that the signals add constructively at the receiver. In this scenario, the received signal is,

$$\boldsymbol{y} = [\boldsymbol{h_1}\ \boldsymbol{h_2}]\begin{bmatrix}\boldsymbol{e}^{-j\theta_1}\\ \boldsymbol{e}^{-j\theta_2}\end{bmatrix}\boldsymbol{x} + \boldsymbol{n} \quad \text{..... (10)}$$

where,

$$\boldsymbol{h_1} = |\boldsymbol{h_1}|\,\boldsymbol{e}^{j\theta_1} \quad \text{and} \quad \boldsymbol{h_2} = |\boldsymbol{h_2}|\,\boldsymbol{e}^{j\theta_2}$$

In this case, the signal at the receiver is,

$$y = \underbrace{(|h_1| + |h_2|)}\, x + n \quad \text{.....(11)}$$

For equalization, we need to divide the received symbol $\boldsymbol{y}$ with the new effective channel, i.e.

$$\breve{y} = \frac{\boldsymbol{y}}{[|\boldsymbol{h_1}|\ \ |\boldsymbol{h_2}|]} = \boldsymbol{x} + \frac{\boldsymbol{n}}{[|\boldsymbol{h_1}|\ \ |\boldsymbol{h_2}|]} \quad \text{..... (12)}$$

4.0 Discussion and Conclusion

From this research, it was found that sending the same information on multiple transmit antenna does not provide diversity gain. This is depicted in figure 4.0 by the graphs for *1tx – 1rx* (theory) and *2tx – 1rx* (no beamforming – simulated). Intuitively, this is due to the fact that the effective channel $h_1 + h_2$ in a 2 transmit antenna case is again a Rayleigh channel; hence the Bit Error Rate (BER) performance is identical to 1 transmit 1 receive Rayleigh channel case. However if the transmit symbols are multiplied by a complex phase (closed loop) to ensure that the phases align at the receiver, there is diversity gain though the BER

performance seems to be slightly poorer than the 1 transmit (tx) 2 receive (rx) Maximal Ratio Combining (MRC) case as in figure 4.0 (*1tx-1rx* mrc theory and *2tx-1rx* beamforming simulated graphs). This is because the noise is scaled by $|h_1| + |h_2|$ in the case of transmit beamforming.

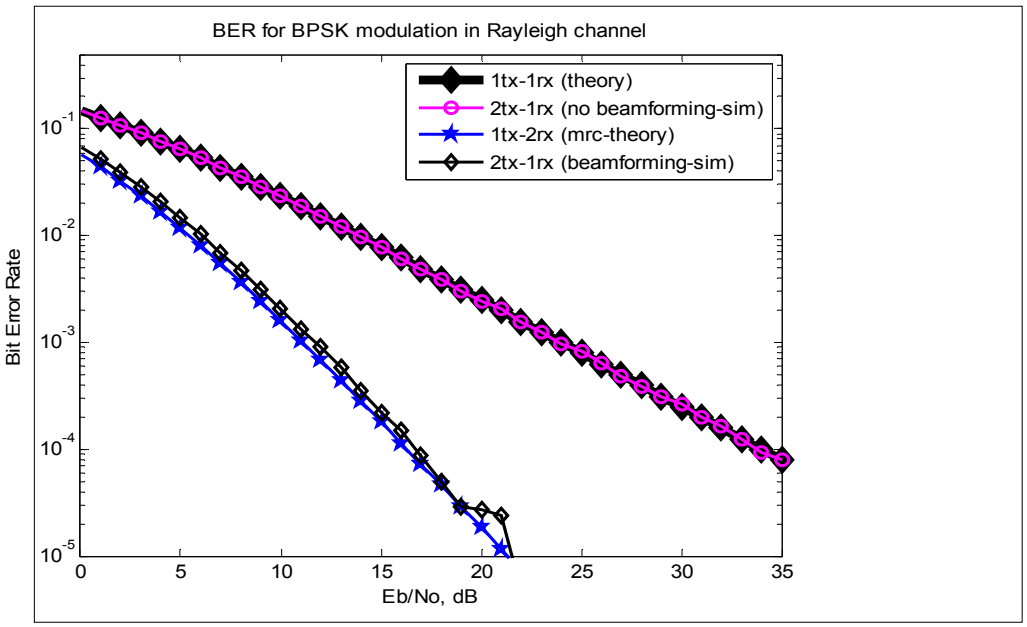

Fig. 4: BER plot for 2 transmit 1 receive CLTD for Binary Phase Shift Keying (BPSK) in Rayleigh channel

Acknowledgement

The authors wish to acknowledge the valuable contributions of Mr. Kanai, Mr. Mureu, Mr. Kidegho and Mr. Ombati of Jomo Kenyatta University of Agriculture and Technology.

References

Alamouti (1998), *A Simple Transmit Diversity Technique for Wireless Communications,* IEEE Journal on Selected Areas in Communications, **6**(8), pp. 1451-1458.

Sklar (2001). *Digital Communication Fundamentals and Application,* 2nd Edition Prentice Hall PTR.

Foschini, *Layered space-time architecture for wireless in a fading environment when using multi-element antennas.*

Hourani (2004). *An overview of diversity techniques in wireless communication systems*, Communications Lab, Helsinki University of Technology.

Winters (1998). *The diversity gain of transmit diversity in wireless systems with Rayleigh fading,* IEEE, **47, (1)**.

Proakis, (1995). *Digital Communication,* McRAW- Hill International Editions.

Zheng (2003). *Diversity and Multiplexing: A fundamental Tradeoff in Multi-Antenna Channels,* IEEE Journal on Information Theory, Vol. 49, No 5, pp 1073 – 1096.

Nakagami (1960). *The m-distribution - A general formula of intensity distribution of rapid fading in Statistical Methods in Radio Wave Propagation*, Oxford, U.K.: Pergamon Press, pp. 3–36.

Rappaport (1996). *Wireless Communications: Principles and Practice,* Prentice Hall, New Jersey.

Tarokh *et al.,* (1998), *Space-Time Codes for High Data Rate Wireless Communications: Performance Criterion and Code Construction,* IEEE Trans. Of Inf. Th., **44(2)**, pp. 744-765.

Appendices

Appendix A

Script for computing the BER for BPSK modulation in a Rayleigh fading channel with and without transmit beamforming.

```
clear
N = 10^6 % number of bits or symbols

% Transmitter
ip = rand(1,N)>0.5; % generating 0,1 with equal probability
s = 2*ip-1; % BPSK modulation 0 -> -1; 1 -> 0
nTx = 2;

Eb_N0_dB = [0:35]; % multiple Eb/N0 values

for ii = 1:length(Eb_N0_dB)

  n = 1/sqrt(2)*[randn(1,N) + j*randn(1,N)]; % white gaussian noise, 0dB variance
  h = 1/sqrt(2)*[randn(nTx,N) + j*randn(nTx,N)]; % Rayleigh channel

  sr = (1/sqrt(nTx))*kron(ones(nTx,1),s);

  % Channel and noise Noise addition
  hEff = h.*exp(-j*angle(h));
  y1 = sum(h.*sr,1) + 10^(-Eb_N0_dB(ii)/20)*n;
  y2 = sum(hEff.*sr,1) + 10^(-Eb_N0_dB(ii)/20)*n;

  % equalization
  y1Hat = y1./sum(h,1);
  y2Hat = y2./sum(hEff,1);

  % receiver - hard decision decoding
  ip1Hat = real(y1Hat)>0;
  ip2Hat = real(y2Hat)>0;

  % counting the errors
  nErr1(ii) = size(find([ip- ip1Hat]),2);
  nErr2(ii) = size(find([ip- ip2Hat]),2);

end

simBer1 = nErr1/N; % simulated ber (no beam forming)
```

```
simBer2 = nErr2/N; % simulated ber (with beam forming)
theoryBerAWGN = 0.5*erfc(sqrt(10.^(Eb_N0_dB/10))); % theoretical ber
EbN0Lin = 10.^(Eb_N0_dB/10);
theoryBer = 0.5.*(1-sqrt(EbN0Lin./(EbN0Lin+1)));
p = 1/2 - 1/2*(1+1./EbN0Lin).^(-1/2);
theoryBer_nRx2 = p.^2.*(1+2*(1-p));

close all
figure
semilogy(Eb_N0_dB,theoryBer,'bp-','LineWidth',2);
hold on
semilogy(Eb_N0_dB,simBer1,'ys-','LineWidth',2);
semilogy(Eb_N0_dB,theoryBer_nRx2,'gp-','LineWidth',2);
semilogy(Eb_N0_dB,simBer2,'mx-','LineWidth',2);
axis([0 35 10^-5 0.5])
grid on
legend('1tx-1rx (theory)','2tx-1rx (no beamforming-sim)','1tx-2rx (mrc-theory)','2tx-
1rx (beamforming-sim)');

xlabel('Eb/No, dB');
ylabel('Bit Error Rate');
title('BER for BPSK modulation in Rayleigh channel');
```

AN INVESTIGATION OF THE UTILITY SCALE WIND ENERGY FOR NORTH-EASTERN KENYA REGION

J. N. Kamau[1], R. Kinyua[2] and J. K. Gathua[3]
[1, 2]Department of Physics, Jomo Kenyatta University of Agriculture and Technology, Kenya
[3]Department of Physics, Kenyatta University, Kenya
E-mail: jngugikamau@yahoo.com

Abstract
In the present study, the wind energy potential for Garissa (0°28'S, 39°38'E) and Marsabit (2° 19'N, 37° 58'E), both rural towns in north-eastern Kenya have been statistically analyzed on a 6-year measured hourly time series wind speed data. The probability distribution parameters are derived the time series data and the distributional parameters are identified and fitted annually on the basis of Weibull model. Garissa's average wind speeds were found to range between 2.5 and 3.5 m/s giving power densities of between 74 and 190 W/m^2 at a height of 50 m. The yearly value of Weibull's shape parameter k ranged from 1.26 to 1.38, whilst the values of the scale parameter c ranged between 2.92 and 3.90 m/s. In the case of Marsabit average wind speeds greater than 11 m/s are prevalent. The available power density at a height of 50 m is between 1776 and 2202 W/m^2 which is in the wind class range of 7 and 8. Values of Weibull parameters k and c ranged between 2.5-3.05 and 11.86-12.97 m/s, respectively. From the analysis, the Marsabit site was found suitable for grid connected power generation while the Garissa site was found suitable for non-grid uses such as water pumping and battery charging.

Key words: Wind speed, power law, Weibull parameters, wind class, wind rose, energy potential

Nomenclature

v	wind speed (m/s)
$\bar{v}$	average wind speed (m/s)
c	Weibull scale parameter (m/s)
k	Weibull shape parameter (dimensionless)
$f(v)$	- probability of observing wind speed, v
$F(v)$	cumulative probability distribution function
$f(x)$	Gumbel probability density function
$F(x)$	Gumbel cumulative probability density function
σ^2	Variance
ρ	density of air (kg/m^2)
Γ	gamma function

1.0 Introduction

Energy utilisation has continued to rise globally over the years as technologies expand in the developed countries and as Third World countries experience growth in industrialization and population. Primary energy sources include fossil fuels such as oil, coal, natural gas; and renewable sources such as solar, wind, tidal, geothermal and hydropower. While energy consumption and demand will continue to grow there is fear of depletion of the non renewable sources, with estimates suggesting that the world's oil supply may fail to meet demand by year 2015 (Kumar, 2000).

Most developing nations, Kenya included, rely on fossil fuels for most of their energy; but clean renewable energy is becoming increasingly important as the world faces the threat of global warming and the realization that the fossil fuels will eventually run out or become to expensive to retrieve. International conventions such as The Intergovernmental Panel on Climate Change (IPCC) in its Second Assessment Report (SAR) noted that the average global temperatures are likely to rise between 1.4 and 5.8^{o}c over the current century leading to average sea-level rises of between 0.09 to 0.88m by 2100 (IPCC, 2001). This might cause severe climate change precipitating drought and flooding in most parts of the world. It is therefore becoming increasingly evident that renewable energy technologies have a strategic role to play in the achievement of the goals of sustainable economic development and a good mitigation measure for clean environment and the reduction of the greenhouse gases (GHGs) (Mathur *et al.,* 2002).

In Kenya, the cost of oil based imports has increased by over 1000% in the past three decades. The cost of electricity alone has more than doubled in the past one year rising from Ksh.3.92 in June 2009 to Ksh. 9.0 by August 2011. Generation of electricity has been growing steadily in Kenya. Of the installed capacity of about 1200MW, 79% is hydropower, 16% geothermal, 4% thermal while the rest comes from other sources like fossil fuel, wind and solar. Most people in Kenya live in the rural areas, and only about 10% have access to electricity. Due to unreliability in the rain patterns leading to persistent drought (1999-2002), (2005/6) and more recently year 2008, Kenya cannot continue to rely on hydropower generation for most of its electricity needs. Therefore there is need for using alternative renewable sources such as solar and wind to make country globally competitive and prosperous in line with Kenya's Vision 2030.

Wind energy is world's fastest growing energy source, expanding at annual rates of between 25 to 35% (Shikha *et al.,* 2004). In 2007 alone world wide wind capacity increased by 26% to reach the 100 GW mark (IEA, 2007)**.** Recent interest in wind energy technology has resulted in bigger turbines, larger rotor diameters and

reduced costs that are quite competitive with other resources, such as hydro and coal. Currently, Kenya has only 5.5 MW of wind power connected to the grid.

This paper examines the wind energy potential for Garissa (0^o 28'S, 39^o 38'E) and Marsabit (2^o 19'N, 37^o 58'E) in Kenya with possibilities of feeding the power obtained into the national grid and also for pumping water for domestic use, irrigation and for pasture in the surrounding areas.

The specific objectives include, determining the average wind speeds (diurnal, monthly and annual) for the sites, characterising the various wind parameters (average speed, Weibull shape parameter *k* (dimensionless) and Weibull scale parameter *c* (m/s)), performing Wind rose analysis to determining the available power density and to model the extreme wind speeds to determine the 'return period' for the sites.

2.0 Materials and Methods

The data used in this study consists of averaged time series 6-year wind speeds for the period between 2001 and 2006. The wind speed data was recorded at the standard height of 10m by the Kenya Meteorological Department (KMD). Wind direction and air density were also recorded for the same period.

Wind energy resource is highly variable both in space and time; therefore, to understand the characteristics of the resource various parameters were considered.

2.1 Mean Wind Speeds

Mean wind speed, $\bar{v}$ is the most commonly used indicator of wind production potential **(**Manwell *et al,* 2002).
The mean wind speed is defined as

$$\bar{v} = \frac{1}{N}\sum_{i=1}^{N} v_i \quad \text{.....(1)}$$

where N is the sample size and v_i is the wind speed recorded for the i^{th} observation.
Where the sample size is large, the probability of the observed wind speed being within an interval can be written as

$$P(v_j) = \frac{n_j}{N} \quad \text{..... (2)}$$

where v_j is the median value and n_j is the number of observations in the j^{th} interval.
The mean wind speed can then be calculated as

$$\bar{v} = \sum_{j=1}^{m} P(v_j) v_j \quad \text{..... (3)}$$

where *m* is the number of intervals, or:

$$\bar{v} = \int_0^{\infty} v.f(v)dv \quad \text{..... (4)}$$

where *f (v)* is the non-cumulative probability distribution function.
The variance σ^2 is given by

$$\sigma^2 = \int_0^{\infty} (v - \bar{v})^2 f(v)dv \quad \text{..... (5)}$$

2.2 Probability Distribution Function (PDF)

Due to the variability of the wind speed it is found useful to plot the wind speed probability distribution function (the percentage of time that the wind spends at each speed) to understand the character of the variation. One of the commonly used functions for this purpose is the Weibull distribution given by (Seguro and Lambert, 2000; Akpinar and Akpinar, 2004)

$$f(v) = \left(\frac{k}{c}\right)\left(\frac{v}{c}\right)^{k-1} \exp\left[-\left(\frac{v}{c}\right)^{k}\right] \quad \text{..... (6)}$$

where $f(v)$ is the probability of observing wind speed *v*, *c* (m/s) is the Weibull scale parameter and *k* is the dimensionless shape factor.

The cumulative probability function of the Weibull distribution is given by

$$F(v) = 1 - \exp\left[-\left(\frac{v}{c}\right)^{k}\right] \quad \text{..... (7)}$$

To determine *k* and *c* requires a good fit of equation (7) to the recorded discrete cumulative frequency function (Mikhail and Justus, 1986). By taking the natural logarithm of both sides of equation (7) twice gives

$$\ln\langle -\ln[1 - F(v)]\rangle = k \ln(v) - k \ln c \quad \text{..... (8)}$$

Plotting $\ln\langle -\ln[1 - F(v)]\rangle$ against $\ln(v)$ presents a straight line whose gradient is *k* and the y-intercept is $-k \ln c$ from which *c* was calculated.

2.3 Wind Direction

A wind rose is a polar plot that represents the percentage of the time that the wind direction falls within the sector of the compass. Where the wind direction is shown over a period, the value represents the vector sum for the period. The

direction shown on the pie graphs in the results section are for standard anemometer height of 10m.

2.4 Wind Speed Variation with Height

As stated before, the standard anemometer height is 10m. However, in order to harvest wind energy, wind speeds at heights greater than 10 m are required for better results. Therefore, equations that predict the wind speeds at one height in terms of the measured speed at another height are required. We applied the power law model (Oludhe and Ogallo, 1990; Lun and Lam, 2000) which takes the form

$$\frac{v_2}{v_1} = \left(\frac{z_2}{z_1}\right)^a \quad \text{..... (9)}$$

where v_2 is the extrapolated wind speed at height z_2 and v_1 is the measured speed at z_1.

The exponent a depends on such factors as nature of terrain (surface roughness), wind speeds and temperature. For neutral stability the exponent value of $\frac{1}{7}$ has widely been chosen as a good representative of the prevailing conditions (Damarais, 1959). We used the power law to predict the wind speeds at the various heights.

2.5 Wind Power Density

The power in the wind can be computed by using the concept of kinetics. The wind turbine works on the principle of converting kinetic energy of the wind into mechanical energy.

The maximum power (P) available from the wind is given by

$$P = \frac{1}{2}\rho A v^3 \quad \text{..... (10)}$$

where ρ is the density of air , A is the cross-sectional area swept by the rotor and *v* is the average wind speed. The actual amount would be less since all available energy is not extractable.

To calculate the monthly or annual wind power density per unit area, P_w, of a site based on Weibull probability density function, the following equation as reported by Akpinar and Akpinar (2004) can be used

$$P_w = \frac{1}{2}\rho\, c^3\left(1+\frac{3}{k}\right) \quad \text{..... (11)}$$

The two significant parameters k and c have been shown to be related to the mean value of the wind speed $\bar{v}$ (Mayhoub and Azzam, 1997) as

$$\bar{v} = c\Gamma\left(1+\frac{1}{k}\right) \quad \text{..... (12)}$$

where Γ is the gamma function.

The maximum extractable power P_E (W/m^2), by a system working at its optimum efficiency, is limited by the power coefficient called the Betz limit whose value is $\frac{16}{27}$ or 0.593 (John and Antony, 1987) and is therefore given by

$$P_E = 0.593P \quad \text{..... (13)}$$

This capacity factor makes the maximum extractable power approximately 59.3 % of the theoretical power density.
Equation 11 was used to calculate the power densities.

2.6 Gumbel Distribution

It is necessary to know the return period of extreme winds in a locality. The Gumbel distribution is useful for modeling the probability of extreme wind speeds. The probability distribution function f(x) and the cumulative probability distribution function F(x) of the Gumbel distribution are given respectively by (Stevens and Smulders, 1979)

$$f(x) = \exp\left\langle -\exp\left[-\frac{(x-\mu)}{B}\right]\right\rangle .\exp\left\langle -\exp\left[-\frac{(x-\mu)}{B}\right]\right\rangle .\frac{1}{B}$$

..... (14)

$$F(x) = \exp\left\langle -\exp\left[-\frac{(x-\mu)}{B}\right]\right\rangle \quad \text{.....}$$

(15)

Where *x* is the extreme value of the wind speed, μ is the mode parameter and B, the scale parameter.
The return period (R) of the extreme winds is the reciprocal of the probability of Exceedence given by

$$x = \mu - B\ln\left[-\ln\left(1-\frac{1}{R}\right)\right] \quad \text{..... (16)}$$

3.0 Results and Discussion

In this study, wind speed data for Garissa and Marsabit, both rural towns in north-eastern, Kenya, for the six year period from 2001 to 2006 was analyzed. Based on this data, wind speeds, altitudes, wind directions and densities for the site were processed using statistical software programs to generate distribution curves and Wind Rose plots. Calculations were then made to obtain Weibull distribution parameters in terms of the shape parameter k (dimensionless) and the scale

parameter c (m/s), the average (diurnal, monthly, annual) wind speeds and the mean power density. The summary of the results are presented in Tables 1a, 1b, 2a and 2b.

Table1a: Monthly average wind speeds v (m/s) and standard deviation σ (m/s) for Garissa, Kenya 2001-2006

Garissa	Parameters	2001	2002	2003	2004	2005	2006
Jan	v	1.690	1.655	1.138	1.219	1.501	2.007
	σ	1.822	1.479	1.398	1.468	1.596	1.811
Feb	v	2.458	2.080	1.624	1.942	2.453	2.132
	σ	2.151	1.811	1.549	1.807	2.151	1.697
Mar	v	2.653	2.596	2.242	1.997	2.655	2.555
	σ	2.130	1.830	1.991	1.809	2.129	2.184
April	v	3.253	2.606	3.156	2.604	3.251	3.119
	σ	2.281	2.155	2.264	2.155	2.284	2.053
May	v	4.246	3.202	2.583	4.674	4.251	3.573
	σ	2.665	2.235	2.057	2.163	2.661	2.346
Jun	v	5.050	4.031	3.209	4.333	5.047	5.725
	σ	3.400	2.550	2.108	2.589	3.403	3.657
Jul	v	5.267	3.782	3.898	5.017	5.273	5.696
	σ	3.189	2.129	2.491	2.773	3.186	3.124
Aug	v	5.895	4.521	3.206	4.157	5.897	4.630
	σ	2.847	2.521	1.831	2.397	2.847	2.910
Sep	v	4.454	3.402	3.691	4.020	4.447	4.769
	σ	2.690	2.202	1.988	2.119	2.690	2.628
Oct	v	4.461	3.122	3.371	3.468	4.460	4.009
	σ	2.948	1.914	2.011	1.918	2.949	2.932
Nov	v	1.751	1.591	1.192	1.900	1.749	1.479
	σ	1.804	1.412	1.281	1.918	1.806	1.334
Dec	v	1.191	1.419	1.444	0.839	1.192	0.872
	σ	1.231	1.352	1.336	1.332	1.231	1.134
All Year	v	3.539	2.839	2.568	3.018	3.522	3.387
	σ	2.925	2.227	2.125	2.491	2.925	2.885

Table 1b: Monthly average wind speeds v (m/s) and standard deviation σ (m/s) for Marsabit, Kenya 2001-2006

Marsabit	Parameters	2001	2002	2003	2004	2005	2006
Jan	v	8.530	9.140	8.240	9.420	10.130	10.850
	σ	4.253	3.071	3.094	4.662	4.773	4.261
Feb	v	12.860	10.590	9.880	10.910	11.640	11.730
	σ	3.993	3.192	3.940	5.708	4.460	4.655
Mar	v	12.630	8.600	10.760	10.870	11.400	10.890
	σ	4.959	3.973	3.542	4.744	4.150	3.665
April	v	9.750	8.640	10.290	9.200	11.480	9.820
	σ	4.583	3.830	4.054	4.423	3.833	3.419
May	v	11.220	9.730	12.250	10.100	9.980	11.100
	σ	4.226	4.856	5.335	4.896	4.180	3.197
Jun	v	11.290	11.350	11.050	13.380	12.510	12.150
	σ	3.807	4.032	4.989	4.310	3.974	3.400
Jul	v	12.080	13.060	11.480	12.590	13.040	12.110
	σ	3.622	3.855	3.775	3.856	4.033	2.260
Aug	v	12.680	14.490	10.890	13.160	12.170	10.840
	σ	4.272	4.131	3.611	3.476	3.710	3.861
Sep	v	12.370	13.930	13.160	12.960	11.790	12.270
	σ	4.313	4.470	4.003	4.223	4.507	3.485
Oct	v	10.920	11.280	10.470	11.640	12.430	9.540
	σ	3.886	4.168	3.432	4.176	3.262	3.669
Nov	v	9.430	9.170	10.340	8.890	9.640	8.460
	σ	3.131	3.425	2.556	4.284	3.682	3.101
Dec	v	10.150	7.440	9.550	8.720	10.400	8.160
	σ	3.303	3.725	3.092	3.920	3.665	3.744
All Year	v	11.150	10.620	10.700	10.990	11.380	10.650
	σ	4.286	4.487	4.038	4.718	4.171	3.837

The monthly average wind speeds, v (m/s) and the standard deviations, σ (m/s) calculated for the available time series data are presented in Table 1a and 1b and the inter-annual monthly variations of the average speeds are presented in Figs. 1a and1b for Garissa and Marsabit respectively. It can be seen from the plots that in the case of Garissa the months of June through October have the highest wind speeds for all the six years, having average wind speeds greater than 4 m/s, except year 2003 whose average speeds were between 3.2 and 3.9 m/s. These high wind speeds may be influenced by the northern hemisphere summer which occurs

between June and August. The months of November, December, January and February registered the lowest average wind speed of less than 2.5 m/s corresponding to the northern hemisphere winter season (December-February).

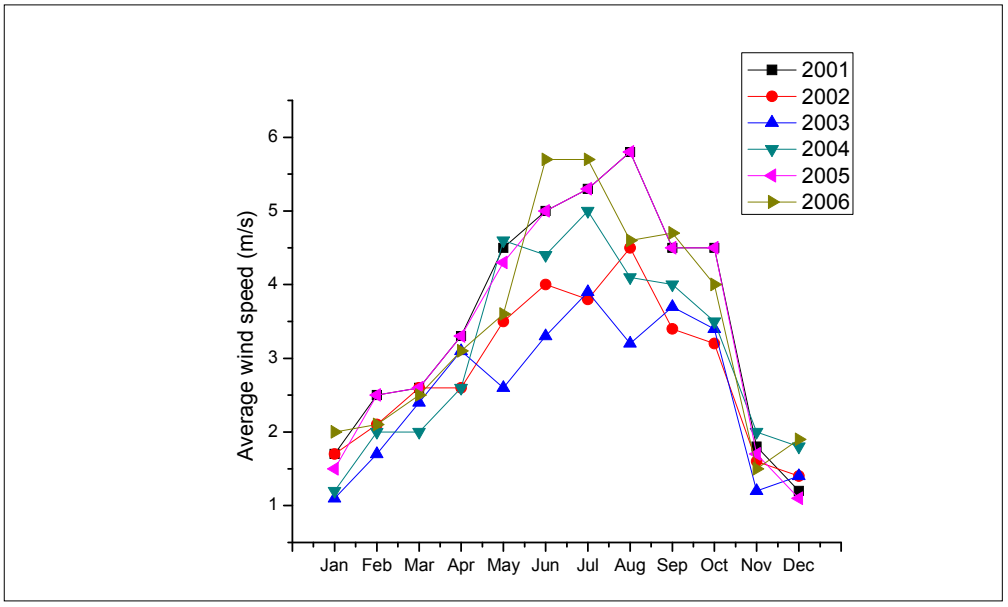

Figure 1a: Inter-annual variability of the monthly average wind speeds, Garissa 2001-2006

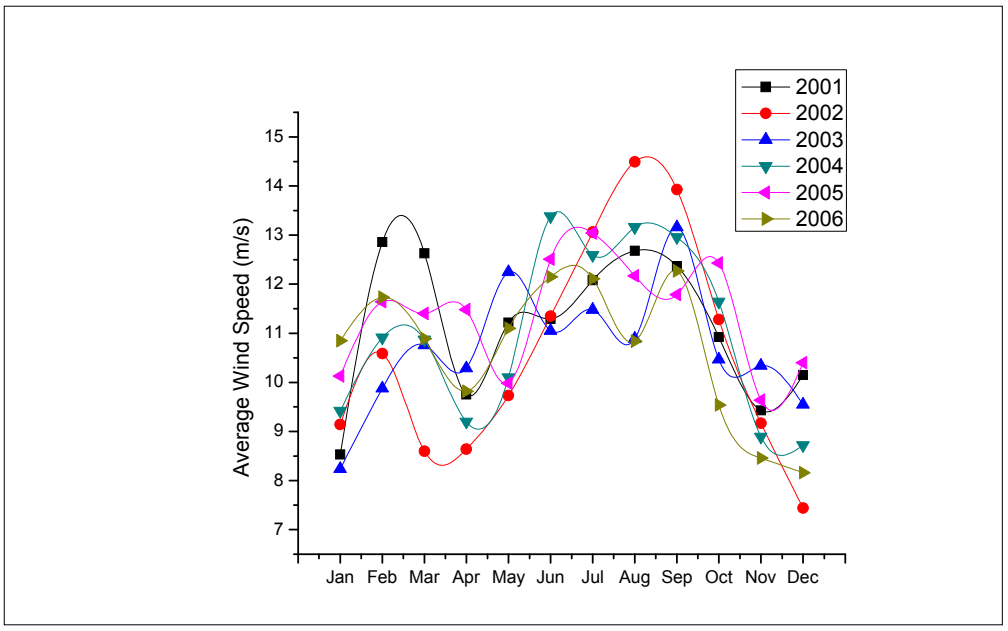

Figure 1b: Inter-annual variability of the monthly average wind speeds, Marsabit 2001-2006

The month to month variation for Marsabit exhibited in Figure 1b may be attributed to channeling effects of wind due the many hills around this area. The inter-annual variability in the wind speeds could be associated with the inter-annual variation in the monsoonal wind characteristics. Figure 2a and 2b illustrates the inter-annual variability of the average wind speed by hour of day. It is clear that for Garissa (Figure 2a) that the peak wind speeds trend is bimodal for all the six years. It depicts high speeds between 11 am and 4 pm, and then between 9 pm and 12 midnight. The early morning hours between 4 am and 8 am depicts the lowest speeds of below 2 m/s. In the case of Marsabit all the years under consideration show a similar profile (Fig. 2b) with the lowest average speed of 7.5 m/s occurring between 15 and 16 hrs (GMT). This corresponds to the sunset hours in Kenya. High wind speeds of above 11 m/s are prevalent during the nighttime hours and peaking to speeds of above 13 m/s during the early morning hours. This enhanced nocturnal resource may be attributed to the reduced vertical mixing of low momentum near-surface air due to the large thermal stability during the night hours (Kamau *et al.,* 2010).

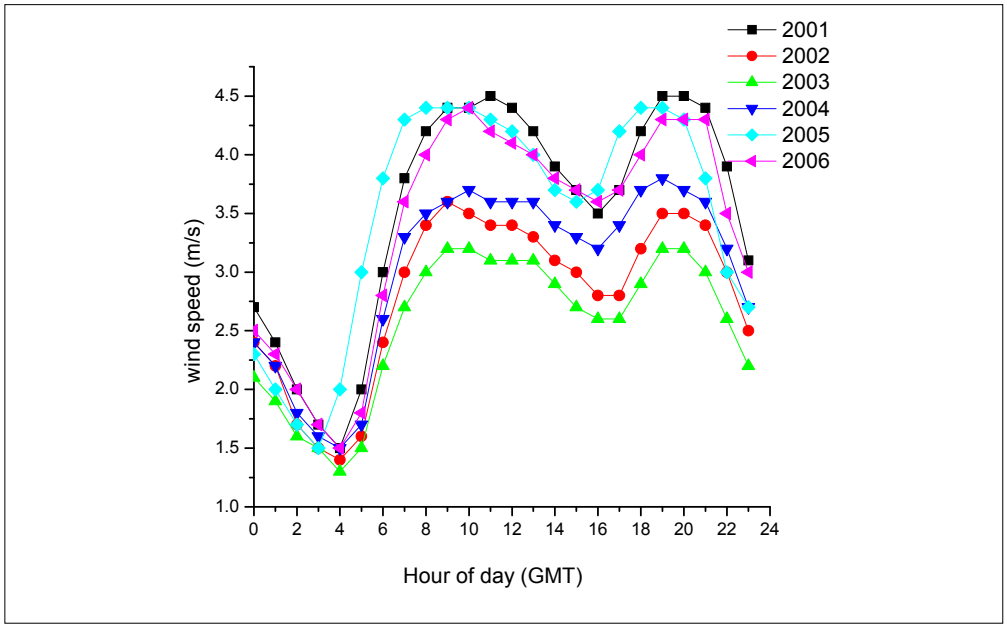

Figure 2a: Inter-annual variability of the average wind speed by hour of day Garissa, Kenya 2001-2006

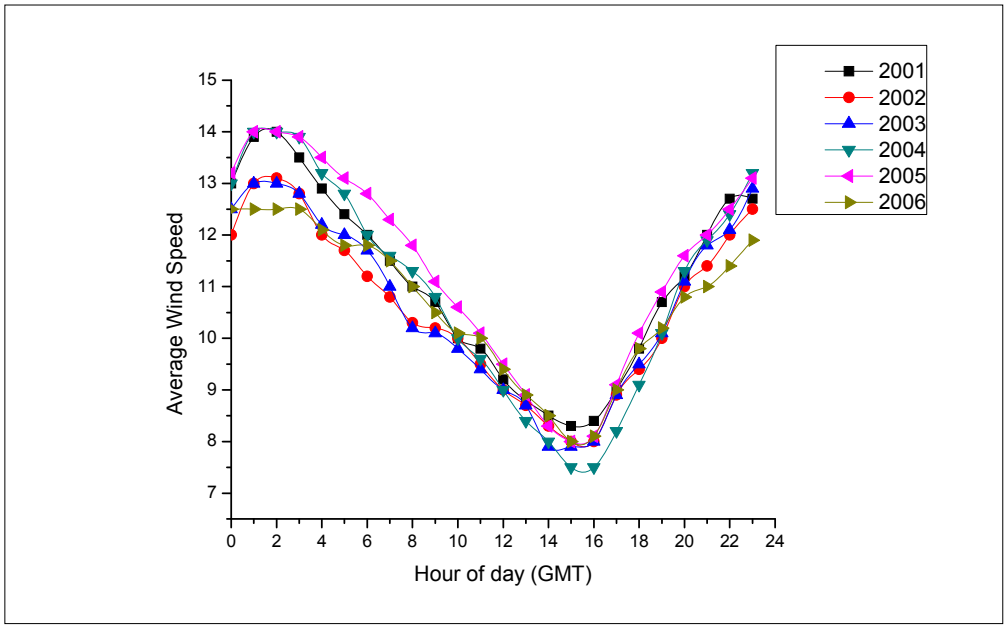

Figure 2b: Inter-annual variability of the average wind speed by hour of day Marsabit, Kenya 2001-2006

Figures 3a and 3b show the probability distribution for the wind speeds for the six year period between 2001and 2006 for Garissa and Marsabit respectively. For Garissa, it can be seen that year 2001 and year 2005 return a similar probability distribution in both shape and scale. Both years have the highest average wind speed of 3.5 m/s. Years 2003 and 2002 had the narrowest distribution owing to their relatively high k values of 1.36 and 1.38 respectively. All the plots for Marsabit show a similar profile of a near normal distribution around the modal value of 11 m/s. The mean annual values of wind speeds range between10.6 and 11.4 m/s whilst the *k* values range between 2.50 and 3.10 showing very small spatial variation.

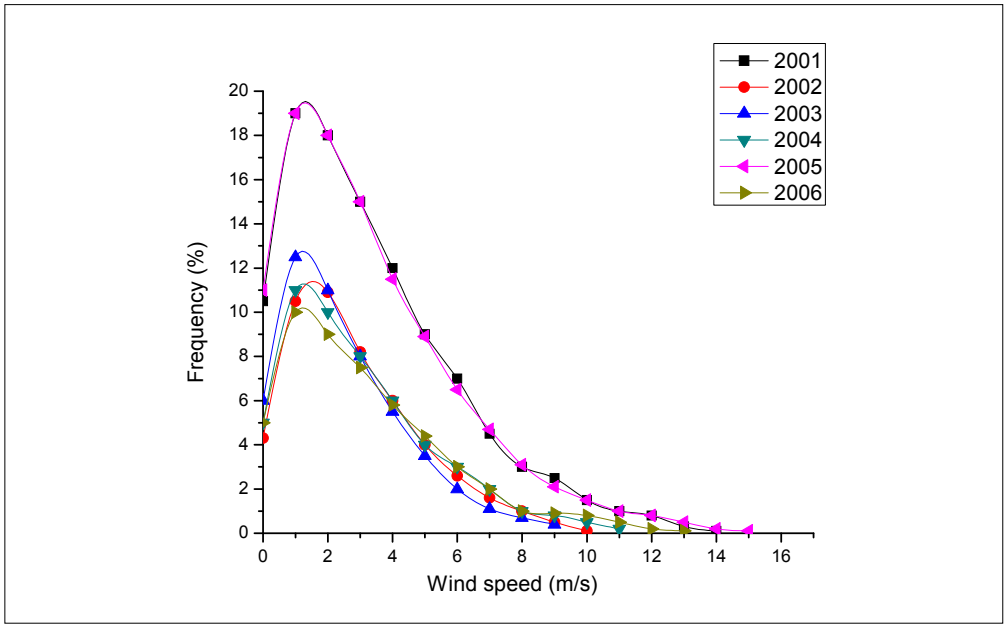

Figure 3a: Probability distribution functions, Garissa 2001-2006

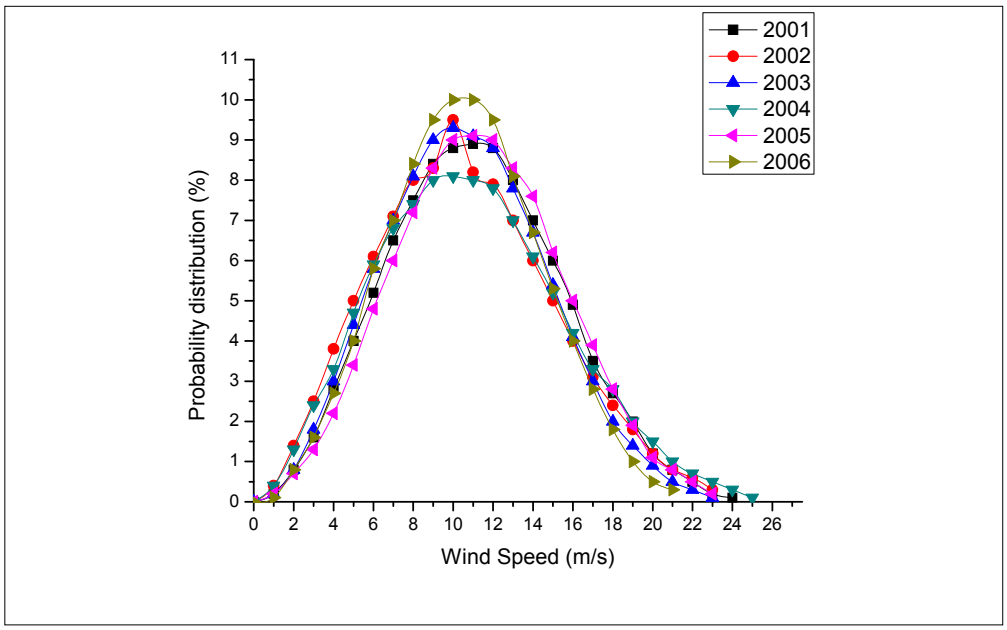

Figure 3b: Probability distribution functions, Marsabit 2001-2006

Table 2a and 2b present the values of Weibull dimensionless shape parameter *k* and the scale parameter *c* (m/s). For Garissa, the monthly values of *k* range between 0.74 and 2.33 both values in year 2004 while the monthly values of *c*

ranged between 1.0 and 6.4 m/s. The yearly values of *k* range between 1.27 and 1.39 while the yearly values of *c* range between 2.9 m/s and 3.9 m/s. Clearly the parameter k has a much smaller spatial variation than *c*. The k value for Marsabit ranges from 2.50 to 3.05, while the values of c range between 11.9 and 12.7. In this case the value of k has a higher spatial variation than c. For most wind conditions, values of *k* typically range between 1.5 and 3.0 whilst the values of c are proportional to the wind speed (Akpinar and Akpinar, 2004).

Table 2a: Monthly shape parameter, k (dimensionless) and scale parameter, c (m/s) for Garissa, Kenya 2001-2006

Garissa	**Parameters**	**2001**	**2002**	**2003**	**2004**	**2005**	**2006**
Jan	k	1.133	1.460	0.895	0.742	0.920	1.001
	c	1.979	2.025	1.177	1.124	1.536	2.077
Feb	k	1.186	1.354	1.356	1.281	1.175	1.486
	c	2.654	2.406	1.969	2.272	2.637	2.498
Mar	k	1.433	1.460	1.134	1.351	1.440	1.319
	c	3.036	2.891	2.402	2.367	3.043	2.899
April	k	1.586	1.346	1.156	1.385	1.571	1.768
	c	3.732	2.965	3.301	2.986	3.720	3.630
May	k	1.591	1.431	1.302	2.331	1.586	1.656
	c	4.727	3.544	2.839	5.298	4.726	4.048
Jun	k	1.561	1.573	1.539	1.778	1.555	1.658
	c	5.665	4.487	3.577	4.910	5.656	6.463
Jul	k	1.669	1.823	1.484	1.961	1.678	1.973
	c	5.889	4.254	4.300	5.711	5.901	6.479
Aug	k	2.158	1.863	1.846	1.865	2.165	1.719
	c	6.634	5.093	3.621	4.730	6.640	5.246
Sep	k	1.748	1.695	1.922	2.048	1.759	1.996
	c	5.029	3.887	4.159	4.568	5.030	5.448
Oct	k	1.552	1.811	1.739	1.965	1.548	1.325
	c	4.971	3.578	3.793	3.948	4.967	4.368
Nov	k	1.192	1.485	1.364	1.141	1.183	1.479
	c	2.055	1.967	1.569	2.184	2.050	1.842
Dec	k	0.965	1.415	1.453	0.860	0.974	1.237
	c	1.274	1.791	1.805	1.012	1.281	1.252
All Year	k	1.274	1.386	1.357	1.287	1.270	1.268
	c	3.908	3.203	2.926	3.378	3.888	3.757

Table 2b: Monthly average values of Weibull shape parameter k (dimensionless) and scale parameter c (m/s) for Marsabit, Kenya 2001-2006

Marsabit	Parameters	2001	2002	2003	2004	2005	2006
Jan	k	2.077	3.155	2.896	2.112	2.190	2.783
	c	9.590	10.180	9.240	10.610	11.380	12.180
Feb	k	3.486	3.610	2.708	1.884	2.894	2.694
	c	14.300	11.760	11.110	12.180	13.040	13.080
Mar	k	2.739	2.315	3.390	2.453	3.107	3.364
	c	14.180	9.720	11.970	12.220	12.750	12.080
Apr	k	2.278	2.427	2.741	2.204	3.316	3.184
	c	11.040	9.760	11.550	10.380	12.770	10.930
May	k	2.909	2.063	2.428	2.175	2.520	3.800
	c	12.590	10.940	13.790	11.390	11.180	12.270
Jun	k	3.278	3.038	2.367	3.459	3.416	4.042
	c	12.600	12.700	12.480	14.870	13.900	13.360
Jul	k	3.769	3.610	3.278	3.717	3.572	6.113
	c	13.370	14.470	12.810	13.950	14.420	13.030
Aug	k	3.379	3.768	3.363	4.260	3.708	3.149
	c	14.140	16.030	12.140	14.430	13.460	12.080
Sep	k	3.176	3.392	3.605	3.365	2.909	4.180
	c	13.830	15.520	14.600	14.420	13.250	13.510
Oct	k	3.072	2.866	3.297	3.047	4.229	2.795
	c	12.220	12.670	11.670	13.020	13.610	10.640
Nov	k	3.310	2.902	4.446	2.182	2.805	3.056
	c	10.510	10.290	11.330	10.030	10.770	9.440
Dec	k	3.310	2.114	3.348	2.391	3.098	2.274
	c	11.310	8.400	10.620	9.840	11.540	9.140
All	k	2.817	2.533	2.835	2.502	2.984	3.053
	c	12.510	11.970	12.000	12.360	12.720	11.860

The average power density by direction for Garissa's year 2001 and Marsabit's year 2006 is illustrated in Figure 4a and 4b respectively. Year 2001 returned the highest average power density of 97 W/m^2 at 10 m in the case of Garissa, the mean direction of the wind speed being 165^o with a standard deviation of 70.7^o. Year 2006 returned the lowest power density of 903 W/m^2 in the case of Marsabit, the mean wind speed being between 150^o and 160^o with a standard deviation of 33.5^o.

It is clear from the foregoing and from figs. 4a and 4b that the wind speeds are more dispersed for the Garissa site than the Marsabit site for the years considered.

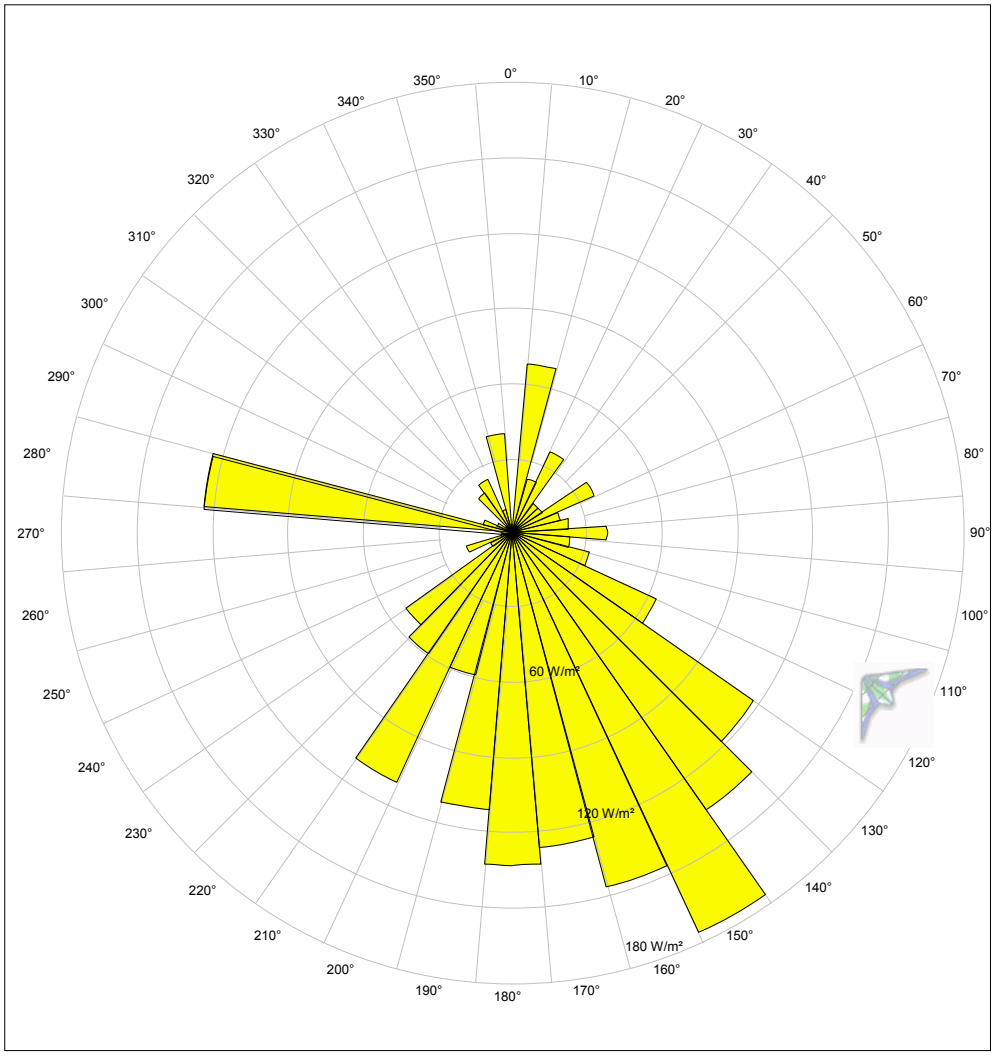

Figure 4a: Average power density by direction, Garissa 2001

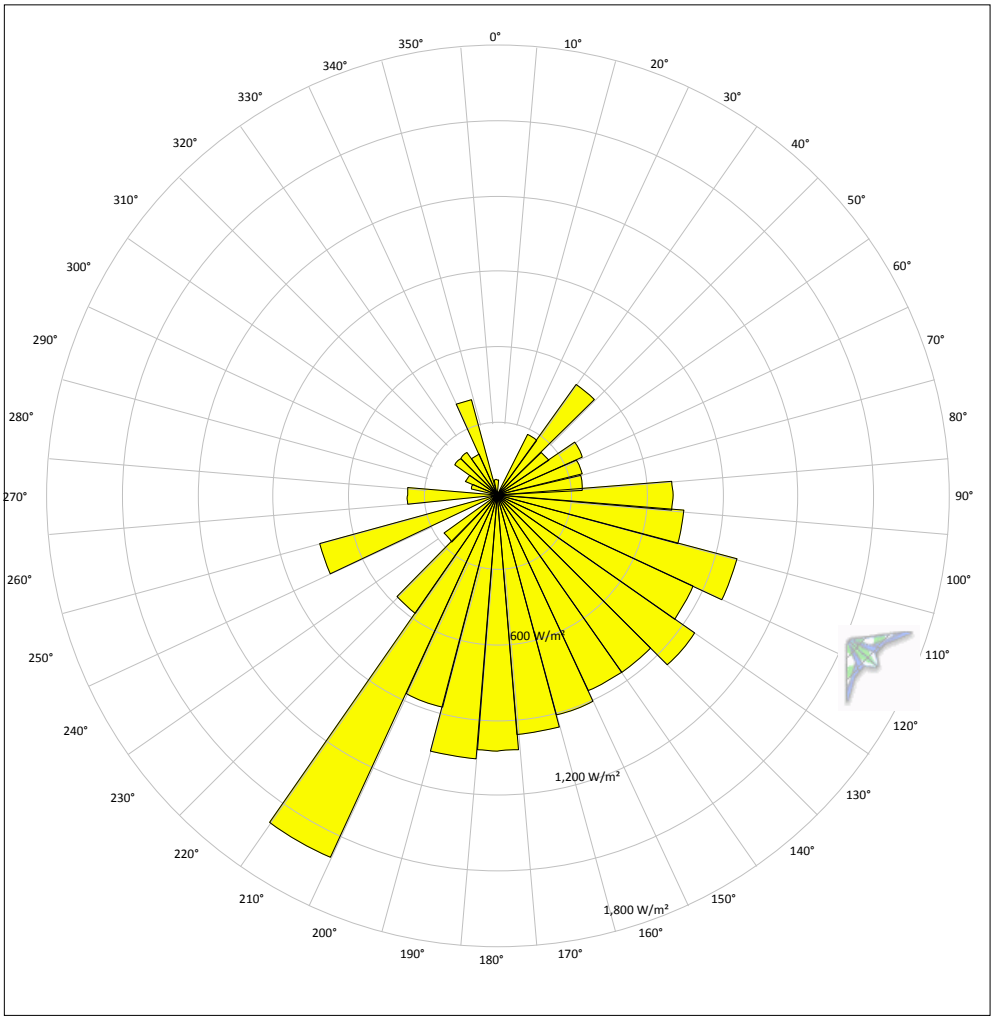

Figure 3b: Probability distribution functions, Marsabit 2001-2006

Table 3 shows a summary of the annual results. Garissa site had a wind class of 1 while the Marsabit site had high power densities with a wind class > 7. Details on wind class can be obtained from reference (Bailey and MacDonald, 1997).

Table 3: Summary of the annual results for Garissa and Marsabit

Garissa **Year**	**Av. Speed (m/s)**	**Weibull,k**	**Weibull, c (m/s)**	**Power density at 10m, W/m^2**	**Power density at 50m W/m^2**	**Wind class**
2001	3.54	1.27	3.90	97	190	1
2002	2.84	1.38	3.20	46	90	1
2003	2.54	1.36	2.92	37	74	1
2004	3.02	1.29	3.38	58	114	1
2005	3.52	1.27	3.89	97	190	1
2006	3.39	1.26	3.75	91	178	1
Marsabit						
2001	11.15	2.81	12.51	1097	2157	8
2002	10.62	2.53	12.97	1021	2007	8
2003	10.70	2.83	12.00	967	1901	7
2004	10.99	2.50	12.36	1119	2199	8
2005	11.38	2.99	12.72	1121	2202	8
2006	10.65	3.05	11.86	903	1776	7

Figures 5a and 5b show respectively the graph of the probability of exceedence plotted against the recorded extreme winds for Garissa and Marsabit in the six years under study. The best Gumbel curve was fitted and the return period calculated for 20, 25 and 50 years period. The extreme wind speeds were found to be 24, 24.5 and 50 m/s respectively for Garissa, and 32, 32.4 and 33.8 respectively in the case of Marsabit.

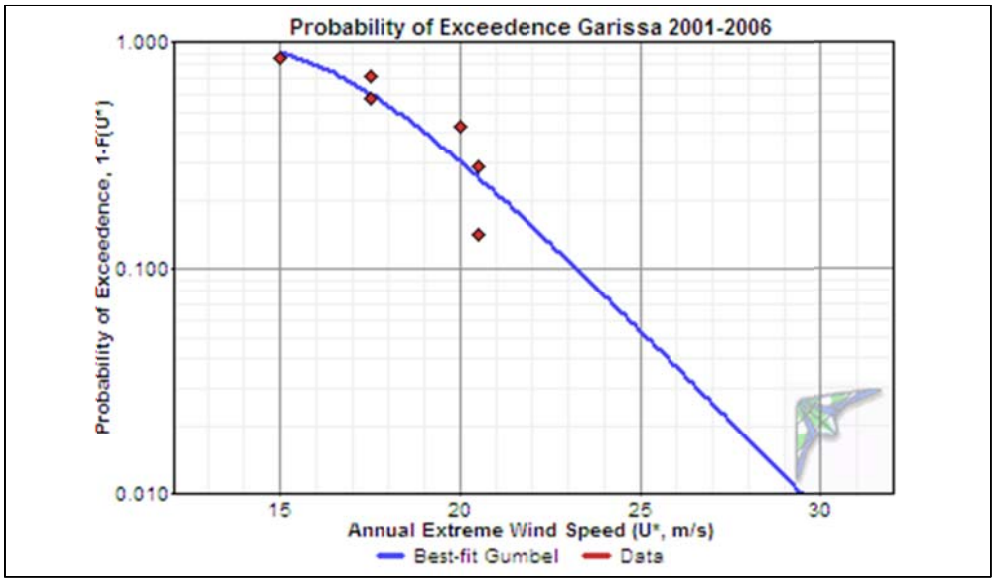

Figure 5a: Best Gumbel fit of the extreme wind speeds, Garissa 2001-2006

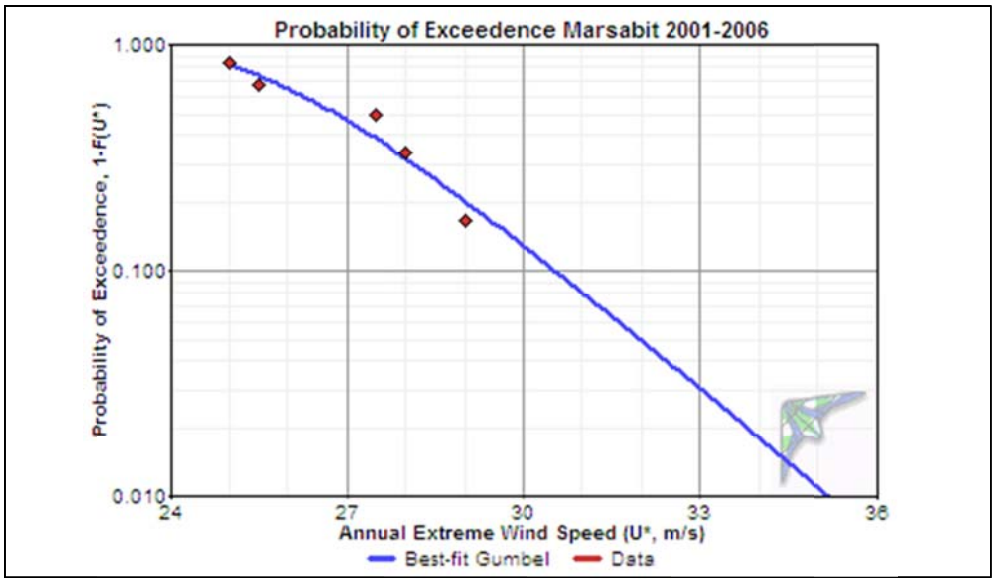

Figure 5b: Best Gumbel fit of the extreme wind speeds, Marsabit 2001-2006

4.0 Conclusions

The following conclusions can be drawn from this study:

(i) The Garissa site had an annual average wind speed of between 2.5 and 3.5 m/s, while that of Marsabit ranged from 10.62-11.38 m/s. The highest monthly wind speed for any year was recorded in the months of June-October. The Garissa site depicted mixed diurnal variation for both day

and night hours while the Marsabit site showed enhanced nocturnal speeds.

(i) The Weibull dimensionless shape parameter *k* had a smaller spatial variation ranging between 1.26 and 1.38 than the scale parameter *c* which ranged between 2.92 m/s and 3.90 m/s for Garissa. For Marsabit the yearly values of k and c ranged from 2.05-3.05 and 11.86-12.96 m/s respectively.

(ii) The maximum theoretical power density obtained for the Garissa site was 190 W/m^2 at 50m, corresponding to a wind class of 1. This site was found unsuitable for grid- connected applications. The power in the wind can however be used for non-connected mechanical and electrical applications such as water pumping and battery charging. The high wind speeds in Marsabit throughout the six years gave power densities of between 903-1119 W/m^2 at 10 m. Power law calculation gave available power densities of between 1776-2202 W/m^2 at a height of 50 m with a wind class greater than 7. The maximum theoretical extractable power was found to be between 1053 and 1306 W/m^2

(iii) Since most commercial wind turbines have a claimed cut-off speed > 35 m/s, the sites are suitable for turbine operation since the extreme wind return period of 25 years is 24.5 m/s in the case of Garissa and 32.4 m/s for Marsabit which falls below the cut-off threshold.

References

Akpinar E. K. and Akpinar S.(2004). Statistical analysis of wind energy potential on the basis of the Weibull and Rayleigh distributions for Agin-Elazig, Turkey. In Pro.Instn. Mech.Engrs, *J. Power and Energy*, 2004, **218** Part A, pp 557-565.

Bailey H. B., MacDonald S. L., ***(Eds)*** (1997). Fundamentals for conducting a successful monitoring program, In *Wind Resource Assessment Handbook*, AWS Scientific Inc., **14**, 1997.

Damarais A. G.(1959). Wind speed profiles at Brookhaven National Laboratory, *J. of applied Met.*, 1959, **16**, pp 181-190.

Intenational Energy Agency (IEA), Wind (2007). www.ieawind.org

Intergovernmental Panel on Climate change (IPCC) (2001). *Second Assessment Report (SAR*), 2001

John W. T., and Antony D. W., (1987). *Renewable energy resources*, The University press, Cambridge London, 1987.

Kamau J. N., Kinyua R. and Gathua J. K. (2010). 6 years of wind data for Marsabit, Kenya average over 14 m/s at 100 m hub height; An analysis of the wind energy potential. *Renewable Energy*, **35**, (2010), pp 1298-1302.

Kumar A. (2000). Sustainable energy technologies: a case study of biomass gasification. *Industry and environment*, 2000, **23 (3**), pp 28-30.

Lun I. Y. F. and Lam J. C., (2000). **A** study of Weibull parameters using long term wind observations, *Renewable Energy*, 2000, **20**, pp 145-153.

Manwell J. F., MacGowan J. G. and Rogers A. L. (2002). *Wind energy explained*. John Wiley and Sons Limited.

Mathur J., Bansal N. K., and Wagner H. J. (2002). Energy and Environment Correlation for Renewable Energy Systems in India, 2002, *Energy Sources* **24**, pp 19-26.

Mayhoub A. B., and Azzam A. (1997). A survey on the assessment of wind energy potential in Egypt, *Renewable Energy*, **119(2)**, pp 235-247

Mikhail A. S. and Justus C. G. (1986). Comparison of height extrapolation models and sensitivity analysis, *Physical climatology for solar and wind energy*, World Scientific, Singapore, pp 377-397.

Oludhe C. and Ogallo L. J. (1990). Vertical variation of wind power. *J. of discovery and innovation,* 1990*,* **2**, pp 73-80.

Seguro J. V. and Lambert T. W. (2000). Modern estimation of the parameters of the Weibull wind speed distribution for wind energy analysis*.* J. Wind Engineering and Ind. Aerodynamics, 2000, **85**, pp 75-84.

Shikha S., Bhatti T. S. and Kothari D. P. (2004). Wind Energy in India, Shifting Paradigms and Challenges Ahead. *J. Energy Engineering.,* pp 67-74.

Stevens M. J. M. and Smulders P. T. (1979). The estimation of the parameters of the Weibull distribution for wind energy utilization purposes, Wind Engineering, **3**, pp 132-145.

List of Figures

List of Tables